Medical Radiology · Diagnostic Imaging
Series Editors: H.-U. Kauczor · P. M. Parizel · W. C. G. Peh

Sebastian Ley · Julia Ley-Zaporozhan *Editors*

Congenital Heart Diseases in Adults

Imaging and Diagnosis

Springer

Medical Radiology

Diagnostic Imaging

Series Editors

For further volumes:
http://www.springer.com/series/4354

Sebastian Ley • Julia Ley-Zaporozhan
Editors

Congenital Heart Diseases in Adults

Imaging and Diagnosis

Springer

Editors
Sebastian Ley
Diagnostic and Interventional Radiology
Chirurgisches Klinikum München Süd
Munich
Germany

Radiology
Internistisches Klinikum München Süd
Munich
Germany

Julia Ley-Zaporozhan
Department of Radiology
Pediatric Radiology
Ludwig-Maximilians-University
of Munich
Munich
Germany

ISSN 0942-5373 ISSN 2197-4187 (electronic)
Medical Radiology
ISBN 978-3-319-61886-9 ISBN 978-3-319-61888-3 (eBook)
https://doi.org/10.1007/978-3-319-61888-3

Library of Congress Control Number: 2019935168

This Springer imprint is published by the registered company Springer Nature Switzerland AG
The registered company address is: Gewerbestrasse 11, 6330 Cham, Switzerland

Preface

Congenital heart diseases are a complex and heterogeneous group of diseases mostly becoming obvious shortly after birth. Other forms can already be detected intrauterine and on the other end of the spectrum diseases may only become obvious later in life. This broad spectrum of disease severity brings together many clinical disciplines, mainly (pediatric) cardiology, (pediatric) heart surgeon, and radiology. Some congenital heart diseases can be corrected with one interventional or surgical intervention; others need multiple surgeries as the anatomy grows. Due to the tremendous scientific and clinical improvement of the whole team, more and more small patients survive and reach adulthood. These patients require regular follow-up of their anatomic and functional status.

For this reason, all clinical disciplines caring about this group of patients should know about the basics of congenital heart diseases and the required follow-up examinations. Therefore, each chapter outlines the basic anatomical findings and anomalies, covers the surgical correction technique, and presents results on the outcome.

Given the various experts involved in the follow-up, especially cardiology and radiology, it was important for this book to cover the respective imaging modalities like echocardiography, invasive catheterization, magnetic resonance imaging, and computed tomography. At various stages of the patient's life, different follow-up recommendations exist. However, as some diseases are quite rare, no standardized recommendations for follow-up exist and the expert authors were asked to share their institutional experience.

For us, as the editors of this book, it was an enormously invigorating experience bringing together renowned experts and the publisher, Springer, to provide this well-illustrated and comprehensive textbook *Congenital Heart Diseases in Adults*. It provides an extensive overview of the various forms of congenital cardiovascular malformations and the different treatment options. Special emphasis is placed on the long-term results and the required imaging strategies and answers the clinician needs to know for optimal patient care. For this purpose, the authors have been selected throughout the imaging disciplines covering all imaging aspects and thus providing a most complete imaging guide.

We hope the book will be of great assistance to all who are caring for patients with congenital heart diseases on the long term.

Munich, Germany — Sebastian Ley
Munich, Germany — Julia Ley-Zaporozhan

Contents

Technical Considerations for ACHD Imaging

Andrew M. Crean

Contents

1 Introduction

There are now more adults alive with congenital heart disease than children (Marelli et al. 2007), and many will have ongoing problems despite surgical repair. Surgery is never a cure—merely a fix—and in some cases directly introduces new problems that were not present previously (Celermajer and Greaves 2002). ACHD patients therefore generally require lifelong follow-up in specialized institutions where the technical and clinical expertise exists to recognize and deal with issues as they arise.

Imaging lies at the heart of this follow-up process. Today we have so many advanced modalities to choose from that a nonimager may be bewildered by the options available and uncertain about what test would best answer the clinical problem facing him or her. The purpose of this chapter is to review briefly the strengths and weaknesses of the major cardiac imaging modalities and propose a few principles to help guide the selection of most appropriate modality in each case. It should be recognized that this is a single author opinion, and—as with everything else in medicine—there is more than one way to skin a cat! Nevertheless the principles here are expected to be non-contentious and largely self-evident.

A.M. Crean, M.R.C.P., F.R.C.R.
Sanghvi Endowed Chair in Cardiovascular Imaging
Professor of Cardiology and Pediatrics, University of Cincinnati Medical Center and Cincinnati Children's Hospital Medical Center,
Cincinnati, OH, USA
e-mail: andrewcrean@gmail.com

Med Radiol Diagn Imaging (2018)
DOI 10.1007/174_2017_169, © Springer International Publishing AG
Published Online: 05 April 2018

2 What Information Do We Want?

In imaging the key question to the referrer should always be: 'what do you want to know?'. An uncertain or unfocussed question is unlikely to result in a lucid and helpful report. Lack of clarity in the request may also lead to incorrect selection of modality. Clear communication between the referrer and the imager is therefore vital for appropriate triage and protocolling of requests. The imager cannot however entirely rely on the referrer to provide all essential knowledge, and it is incumbent upon an ACHD imager to review prior imaging and—on occasion—the hospital notes as the underlying anatomy and physiology (and even the patient's personality) may dictate the most appropriate imaging technique to use.

In general terms, however, the commonest type of information required in ACHD patients pertains to anatomy, function and flow. These and other potential requirements are summarized in Table 1.

Table 1 Areas of potential interest in an ACHD imaging examination

Anatomy
Cardiac anatomy
Bronchial anatomy
Visceral situs
Anomalies of systemic and/or pulmonary venous return
Anomalies of the aorta and/or branch vessels
Physiology
Ventricular volumes
Ventricular function
Flow
Peak velocity across stenoses
Volume of forward and regurgitant flow
Direction of flow
Quantification of shunts
Perfusion
Reimplanted coronary arteries
Compressed or stenosed coronary arteries
Aneurysmal coronary arteries
Assessment of functional reserve prior to major surgery
Tissue characterization
Ischaemic scar
Myocardial oedema
Subclinical fibrosis
Calcium
Metal
Thrombus
Within cardiac chambers
Within aneurysmal coronary arteries
Within pulmonary arteries
Postsurgical complications
Anatomic distortion
Infection
Leakage
Resolving conflicting information

3 Imaging Anatomy

Understanding the anatomy of the patient is fundamental to ACHD care. Many conditions have seen era-based variations in surgical repair, leading to very different anatomic appearances—for example, a *d*-TGA patient repaired 40 years ago by a Mustard or Senning procedure has quite different anatomy to the same patient repaired by the arterial switch operation which is the standard of care today (Roche et al. 2011).

Basic anatomy can be inferred to some degree from the plain CXR with PA and lateral views. Heart size and bronchial situs, great vessel anatomy and pulmonary arterial and venous anomalies may all be recognized by plain film. Inferences about physiology may even be made based on atrial chamber enlargement, pulmonary venous distension and lung parenchymal lymphatic engorgement. However it is hard to argue that a two-dimensional representation of the chest represents the standard of reference in first-world countries any longer. One useful feature of the CXR remains its ability to depict small stainless steel devices, clips or coils that may have been used in childhood to close holes or embolize vessels. Many of these devices cause substantial disturbance to the uniformity of a magnetic field and result in large signal voids on CMR images (Fig. 1). Recognition of these in advance is useful so that limited magnet time is not wasted.

Although echocardiography is usually the first imaging test experienced by the ACHD patient, it is in fact probably the least well suited to questions of pure anatomy. Image quality is both operator and patient dependent. Obesity, in particular, challenges the echocardiographer in a way that is rarely

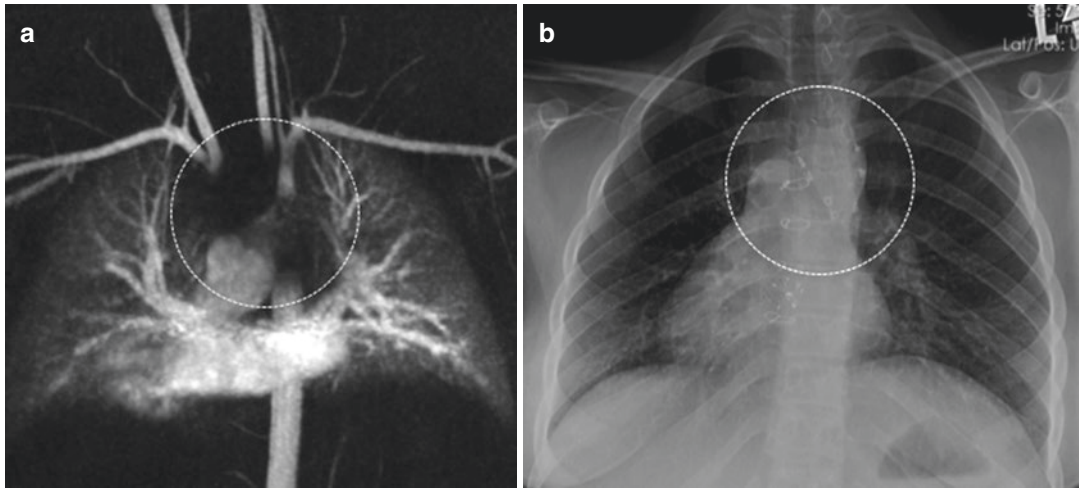

Fig. 1 Artefact due to stainless steel coils. (**a**) MR angiogram in a patient with a Fontan circuit shows a large central area (dotted circle) where the underlying anatomy is obscured. (**b**) CXR in same patient (note incidental dextrocardia) reveals multiple metallic densities in the central mediastinum (dotted circle) from venous embolization with stainless steel coils

a problem for CT or CMR (assuming the patient does not exceed the maximum table weight and can physically fit into the scanner). Although image acquisition is usually standardized, this is in the form of selective 2D tomographic views selected by the operator at the time of the scan. There is no possibility to return to the data and reconstruct further views desired after the fact. This limitation of standard 2D echo has only partially been overcome by 3D techniques (Yang 2017). These remain cumbersome, imperfect (Crean et al. 2011) and far from routine in the majority of laboratories. The other major limitation of echo pertains to its inability to visualize more than the proximal portions of the vascular structures of the thorax or to interrogate the lung parenchyma beyond basic recognition of pleural fluid and lung collapse/consolidation. Therefore, although echocardiographic assessment is vital in ACHD for other reasons, assessment of anatomy alone is rarely its forte.

What then should we use to determine the thoracic anatomy of the ACHD patient with confidence? If anatomy is the sole or primary question, there is little doubt that computed tomography (CT) is the test of choice in many patients (Han et al. 2015a). Advances in technology have been so profound that imaging of the chest by CT now takes only a few seconds. Images can be acquired in most ACHD patients at trivial doses of radiation. Low-dose imaging is possible for two reasons. Firstly, many complex ACHD patients are well below mean adult size due to chronic illness, and a relative lack of obesity means that images contain less noise. Secondly—as a corollary to the first point—low body mass index means that tube voltage may usually be reduced down to 80 kV rather than the standard 120 kV resulting in an exponential decrease in radiation exposure (Han et al. 2015b). The additional noise created by this approach is usually tolerable for all but the smallest structures and can be smoothed out by both iterative reconstruction techniques or simply by reconstructing at thicker slice thickness than that acquired (Fig. 2).

There are additional benefits of anatomic imaging by CT. Many of the peculiarities of ACHD can be relatively subtle—small communications between structures, anomalous vessels including aorta-pulmonary and veno-venous collaterals, pulmonary arteriovenous malformations, etc. may all be missed without high spatial resolution. This is an inherent advantage of CT where it is possible to acquire volumes of isotropic data with a voxel size of 0.5 mm^3 at still acceptable radiation exposure levels. Such high-resolution data sets have the further advantage of potential reconstruction in any non-standard imaging plane required to best demonstrate the abnormality, long after the patient has departed the CT suite. The ability to synchronize

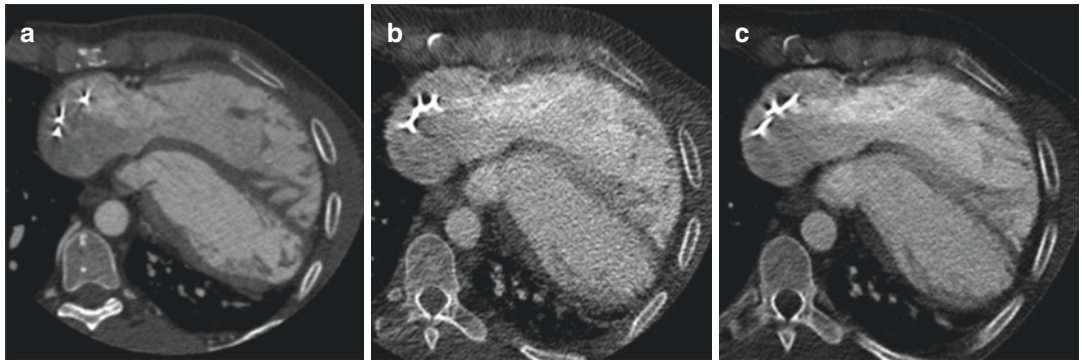

Fig. 2 Decreasing dose in cardiac CT through kV manipulation. (**a**) Axial cross section by CT in 2008 in a patient with tetralogy of Fallot acquired at 0.5 mm, **120 kV**, multiphase. Image quality is excellent with little noise but the total effective dose was 25 mSv. (**b**) Same patient reimaged in 2010 at 0.5 mm, **80 kV**, multiphase. The image is significantly noisier but still interpretable. (**c**) Same data set as in (**b**) but this time the slice *has been thickened post acquisition to 5 mm rather than the native 0.5 mm*. Note how much of the image noise is reduced by this manoeuvre with little change in diagnostic quality for the major cardiac structures

CT image acquisition to the ECG also makes it particularly suitable for anatomical assessment of the aortic root and coronary arteries which are otherwise obscured by cardiac motion. The principal disadvantage of anatomic imaging by CT is the need for administration of intravenous contrast. This slows the workflow and may be contraindicated in patients with reduced renal function or severe contrast allergy.

CMR anatomic imaging is usually performed as part of any cardiac study. Sequences may use bright blood techniques in which the blood pool is seen as higher signal intensity than surrounding myocardium or black blood techniques in which the signal from flowing blood is suppressed. Compared to CT, anatomic CMR imaging incurs a considerable time penalty (10–15 min for bright blood imaging of the thorax by CMR versus under 5 s by CT) and is obtained at significantly lower spatial resolution. Despite this, many centres employ CMR as the primary tool for assessment of the ACHD patient. This is not because it is a better anatomic test than CT but because other information (particularly ventricular size and function) is usually also desired.

However there are rare situations when CMR may be used principally for anatomy. The most common indication for this at our centre usually involves a pregnant woman with a known aortopathy (Marfan syndrome, coarctation patch aneurysm) who develops chest pain—rapidly leading to similar symptoms in the responsible clinician! Although CT may be the most logical test for patients in the second trimester or beyond, the spectre of unproven 'risk' to the foetus almost invariably results in both patient and physician insisting upon CMR. This may not be a trivial undertaking in a heavily pregnant woman who may need to lie partially elevated to prevent IVC compression and who is usually uncomfortable and restless. Limited diaphragmatic excursion results in poor breath holding and frequently suboptimal images. Furthermore, gadolinium is relatively contraindicated in pregnancy (Garcia-Bournissen et al. 2006; Sundgren and Leander 2011). Here, however, one advantage of CMR over CT emerges. Steady-state free precession (SSFP) pulse sequences generate intrinsic contrast within the blood pool without the need to inject exogenous agents (Fig. 3). Furthermore, the use of free-breathing navigated SSFP sequences can obviate concerns about poor breath holding (Stehning et al. 2005).

Cardiac catheterization should not be forgotten as a method for determining anatomy. Indeed in the early days of congenital heart disease, it was the principal if not the only way to assess complex intracardiac anatomy. Whilst that role has largely been usurped by echo and other cross-sectional techniques, it remains useful for assessment of vascular structures particularly where intervention is contemplated (e.g. delivery of coarctation or pulmonary artery stent, collateral embolization). The direct injection into collateral

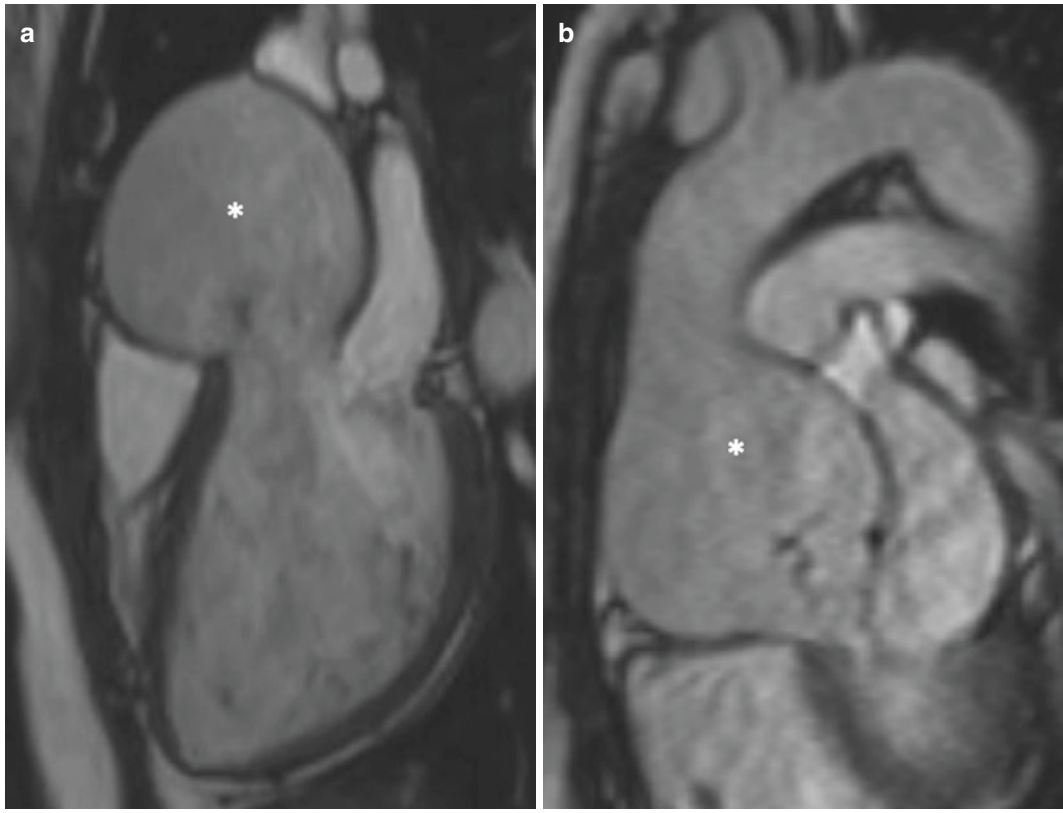

Fig. 3 Examples of severe aortic root dilatation in two different pregnant patients with Marfan syndrome. To avoid administering gadolinium—and limit heating of the foetus by radiofrequency deposition—single-shot steady-state free precession imaging has been used. In both cases the aortic root (asterisk) measured almost 6 cm across (normal is less than 4 cm; 5 cm is the usual operative threshold in Marfan syndrome)

vessels may also reveal the course and extent of these more clearly than simply relying upon passive filling by contrast as happens at CT or CMR.

We close this section with nuclear medicine, only to comment that the limited spatial resolution of this technique results in little or no role for anatomical imaging of the ACHD patient. It may still have some limited role in physiologic imaging which will be discussed subsequent sections.

	Echo	Nuclear	CT	CMR	Cath
Spatial resolution	++	+	++++	++	++++
Temporal resolution	++++	+	++	+++	++++
Suitability in obese	++	+	++++	++++	+++
Multiplanar reformats possible	–	++	++++	+++	–
3D reconstructions possible	–	++	++++	+++	–
Limited by metal	++	+++	+	+++	–
Limited by calcium	+	+	+	++	–
Speed of assessment	++	++	++++	+	+++
Requires exogenous contrast injection	–	++++	+++	+	++++
Availability	++++	++++	++++	++	++++
Claustrophobia	–	+	++	+++	–
Radiation	–	+++	+/++	–	++/+++

4 Imaging Ventricular Function

One of the most frequently asked questions of an ACHD imager pertains to the size and function of the ventricles. Accurate assessment is vital since serial follow-up is often performed in order to determine the most appropriate time to intervene on lesions which are responsible for ventricular enlargement or impairment of ventricular function. Although 2D echo is most frequently used for this purpose, its accuracy and interobserver variability leave much to be desired. Endocardial definition is often poor, and, since a volume of data is not acquired, size and function are estimated in ways that make assumptions about the shape of the ventricles. Such assumptions are frequently untrue in normal hearts and are quite unreliable in malformed or repaired hearts. 3D echo has been shown to be more accurate and precise in the paediatric population, but the size of enlarged ventricles (particularly the RV) in adults often results in incomplete coverage of the ventricle within the sector field of view and can lead to quite significant underestimation of ventricular volume (Crean et al. 2011).

CMR is generally regarded as the standard of reference for functional and volumetric assessment of the ventricles, notwithstanding occasional dissenters (DeFaria Yeh and Foster 2014; Geva 2014). Sequential slices are acquired in a 2D fashion, and then the resulting stack of discs is contoured offline and provides measurements derived from Simpson's rule. Since the precise geometry of the ventricle is accounted for in the image acquisition, there are no geometric assumptions made. Values derived in this way are usually highly reproducible both within and between observers (Mooij et al. 2008; Moody et al. 2015). Nonetheless there are several technical considerations of which to be aware. CMR cine images, as conventionally acquired, do not in fact reflect real-time motion data—in other words the image as seen is not constructed from motion data pertaining to a single cardiac cycle. Instead, using a process of 'segmented acquisition', the cine data required to build a moving cine image at any one slice location is acquired over multiple temporally sequential cardiac cycles. In practice this means that each moving image is usually the result of a data acquisition process over 10–15 heartbeats. There are several implications of this: (a) the temporal resolution (i.e. frame rate) of each cine image is a function of how many heartbeats are used to acquire data, better temporal resolution can be achieved by collecting more data over more heartbeats but at a cost of a longer breath hold; (b) since the image data is derived from sequential beats, stable sinus rhythm is a prerequisite for clear images free of the temporal blurring which can make contouring unreliable. Although there are methods for acquiring a cine slice in a single heartbeat ('single-shot imaging'), the resulting image is often low in both spatial and temporal resolution, and since each slice is acquired from beats of different cycle length, the varying number of cardiac phases per cycle means that conventional contouring packages (which require each slice to have the same number of phases) cannot load the data for quantitative measurement. Finally, published normal ranges exist with different values—how is this possible? The answer for the LV depends on whether the papillary muscles are ignored ('left in the blood pool') or included when drawing the endocardial contour (Alfakih et al. 2003a; Buechel et al. 2009; Hudsmith et al. 2005; Cain et al. 2009; Salton et al. 2002; Lorenz et al. 1999; Sievers et al. 2004). Novel planes of acquisition may also affect the ideal normal range (Childs et al. 2011; Clay et al. 2006).Values may differ for the RV according to whether the ventricle was contoured from the axial, short axis or some other plane (Maceira et al. 2006; Alfakih et al. 2003b; James et al. 2013; Fratz et al. 2009; Strugnell et al. 2005; Winter et al. 2008). It is therefore important that each CMR lab maintain a consistent approach to contouring and use of the appropriate normal range. Very recently, work produced from the UK Biobank project has provided normal sex and age-defined ranges in over 5000 healthy individuals, and this is likely to become the standard reference paper in this area—at least for Caucasian populations (Petersen et al. 2017).

Cardiac CT is being utilized at most ACHD centres with volumetric and functional assessment an increasingly common indication. Usually

this is requested in patients who are either claustrophobic or have implanted devices and thus contraindicated for CMR. There have been several reports suggesting comparable accuracy to CMR for volumetric assessment (Fuchs et al. 2016; Koch et al. 2004; Juergens et al. 2004; Mahnken et al. 2003; Singh et al. 2014). Caveats relate not only to the nature of the populations studied which were invariably small and free of congenital heart disease but also to the CT equipment employed in the majority of studies frequently involving dual-tube technology resulting in a potential temporal resolution considerably superior to many other types of scanner. It is necessary to understand that the ability to construct a time-volume ventricular filling curve accurately is a function of not only the patient's heart rate but also the effective temporal resolution of the scanner used. This latter itself can vary according to the scan mode selected. As usual in cardiac imaging, there is no substitute for understanding how image acquisition occurs.

Nonetheless, there is no doubt that cardiac CT provides measurements of end diastolic volume that are usually highly reliable. End systolic volume (and therefore ejection fraction) measurement accuracy depends on sufficient temporal resolution. Therefore an apparently impaired ventricle may be either genuinely impaired or apparently so because true end systolic images have not been acquired. Distinction between genuine and artificial ventricular impairment may be difficult unless the other ventricle demonstrates entirely normal function. Since it is difficult to overestimate ejection fraction (EF) by CT, normal function on one side makes it more likely that true end systole has been captured and therefore that the abnormal function on the other side is more likely to be genuine. One final caveat is that since most CT scanners acquire cine data by segmentation, they are as vulnerable to irregular cardiac cycles as CMR.

In cases where CMR is not possible and CT and echo give conflicting results, use of radionuclide angiography should not be forgotten (Schelbert et al. 1975; Harel et al. 2007; Navare et al. 2003; Johnson and Lawson 1996; Hesse et al. 2008). This is a simple and reliable technique for either ventricle. Since images are acquired by averaging over hundreds of heartbeats, the technique is also relatively independent of cycle length variations. Careful attention must be paid to correctly defining the boundary of the ventricle. This may be difficult for technologists unfamiliar with congenital hearts, particularly if there are abnormalities of situs or looping. It is often wise for the ACHD imager to directly inspect the raw data to ensure ventricles have been correctly identified and encircled.

Finally, visual assessment of ventricular function by conventional angiography is still a valid approach even if it appears to lack the rigour of cross-sectional imaging. The temporal resolution of angiography is so high that reliable visual estimates of function can be made even in the presence of arrhythmia in most cases.

5 Imaging Pressure and Flow

Abnormalities of flow are fundamental to many of the conditions seen in congenital heart disease. Reliable methods are required to measure both velocity and volume of flow (Lotz et al. 2002). On occasion it may be useful to additionally have information about direction of flow. The commonest requirement is for flow assessment across a valvular lesion where varying degrees of stenosis and regurgitation may coexist. Not infrequently there may also be questions regarding the flow across conduits—which often calcify and stenose with time—as well as differential flow into branch pulmonary arteries. Aortic flow may be requested in the setting of aortic coarctation. In cases of multiple sources of pulmonary blood flow (i.e. some or all of the blood flow being derived from collateral sources and not simply the pulmonary arteries), then summed flow of all four pulmonary veins may be required in order to calculate total pulmonary resistance according to the equation: **PVR = 80 * (Mean Pulmonary Artery Pressure - Left Atrial Pressure)/ Pulmonary Flow.** Calculation of pulmonary arterial and aortic flows is also required in the setting of shunt lesions where the shunt fraction has to be calculated.

Echo is once again on the front line for these requests but usually only manages to provide partial answers. There are a number of reasons for this including the previously mentioned problems with poor visualization in a proportion of patients. For isolated valvular stenosis in patients with suitable body habitus, echo estimates peak and mean gradients with a high degree of reliability and reproducibility. Regurgitant lesions are typically more difficult to quantify since all available echo methods are surrogates for the true regurgitant volume which echo cannot measure directly. Echo also struggles with conduit stenosis since the Bernoulli assumptions break down often leading echo to overestimate gradients.

CMR is complementary to echo in many cases. Its strengths are the mirror image of echo in that direct measurement of aortic and pulmonary regurgitant fractions is straightforward and reliable (Mercer-Rosa et al. 2012). Atrioventricular regurgitation may also be directly calculated although is not routinely performed. Net forward flow measurements in the main pulmonary artery and aorta permit calculation of the shunt ratio (Q_p:Q_s) in shunt lesions such as atrial septal defect or patent ductus arteriosus. CMR is also the only available method for measuring total pulmonary blood flow in conditions where some of the arterial supply to the lungs is not derived from the pulmonary arteries. In this circumstance, the total blood supply *to* the lungs is equivalent to the total blood volume returning *from* the lungs (Grosse-Wortmann et al. 2007). Thus measurements of blood flow in each of the pulmonary veins may be summated to provide a rough assessment of total pulmonary flow, which is required for the calculation of pulmonary vascular resistance (see above) in these challenging cases.

CMR is inferior to echo generally for the assessment of stenotic lesions. This is because the velocity profile across a stenosis is rapidly changing and a high temporal resolution is required to catch peak velocity. Although there are technical tricks possible to improve CMR temporal resolution (by decreasing 'views per segment'), this comes at the expense of longer breath holds, and a move to free breathing with multiple averages may be necessary. Since this can produce rather blurred images, many centres refrain from doing this. As a consequence the peak velocity across a stenosis (and therefore the derivative, peak gradient) is often underestimated by CMR compared to echo. Both CMR and echo may also underestimate the severity of a stenosis due to collateral run-off. A classic example of this is tight coarctation of the aorta where the peak gradient may be lower than expected due to the presence of large collateral vessels, which circumvent the obstruction and reduce the measured gradient (Fig. 4). Here, the presence of multiple large collaterals and direct inspection of the severity of the stenosis may be a better guide to its true significance than relying upon a number produced by any technique! Technical factors relating to correct implementation of phase-contrast CMR techniques are nicely reviewed by Nayak et al. (2015).

Fig. 4 Underestimation of coarctation gradient due to collateral flow. In cases of significant coarctation, it is possible for echocardiography to underestimate the severity of coarctation if run-off down large collateral vessels (arrows) means that the volume of flow across the coarct segment (asterisk), and therefore its velocity, is reduced. One way of recognising this is by using phase-contrast imaging to measure the flow in the aorta at two levels—firstly, just beyond the coarct and, secondly, at the level of the diaphragm. A significant increase in measured flow between these two points implies that there is significant collateral return to the descending aorta

There is a limited role for nuclear techniques particularly for the calculation of relative pulmonary flow in the setting of pulmonary artery stenosis. A ratio of greater than 70:30 between the two sides is usually regarded as an indication to intervene. Although this could be easily measured by CMR, there may be situations where claustrophobia or device contraindications preclude this (Roman et al. 2005). Prior stent implantation would also make direct measurement of branch flow impossible as the presence of metal disturbs the homogeneity of the magnetic field and leads to inaccurate values. CT has little or no role since flow measurement is not possible, but it may be useful to delineate areas of potential narrowing invisible to MRI—for example, within stents in the aorta or pulmonary arteries. CT may also be relevant to reveal the underlying cause of stenosis—for example, calcified homograft conduits where the obstructing calcium is low signal and difficult to recognize by CMR but readily apparent on CT (Fig. 5).

Cardiac catheterization remains the standard of reference for stenotic lesions (McLaughlin et al. 2006). The ability to measure simultaneous pressures at two distinct ends of a stenosis provides the most accurate assessment of stenosis severity. As mentioned above, lesions which appear severely stenotic on CMR or echo may be less impressive at catheterization. Many surgical decisions are still made primarily on the basis of catheter-derived gradients, and relatively few

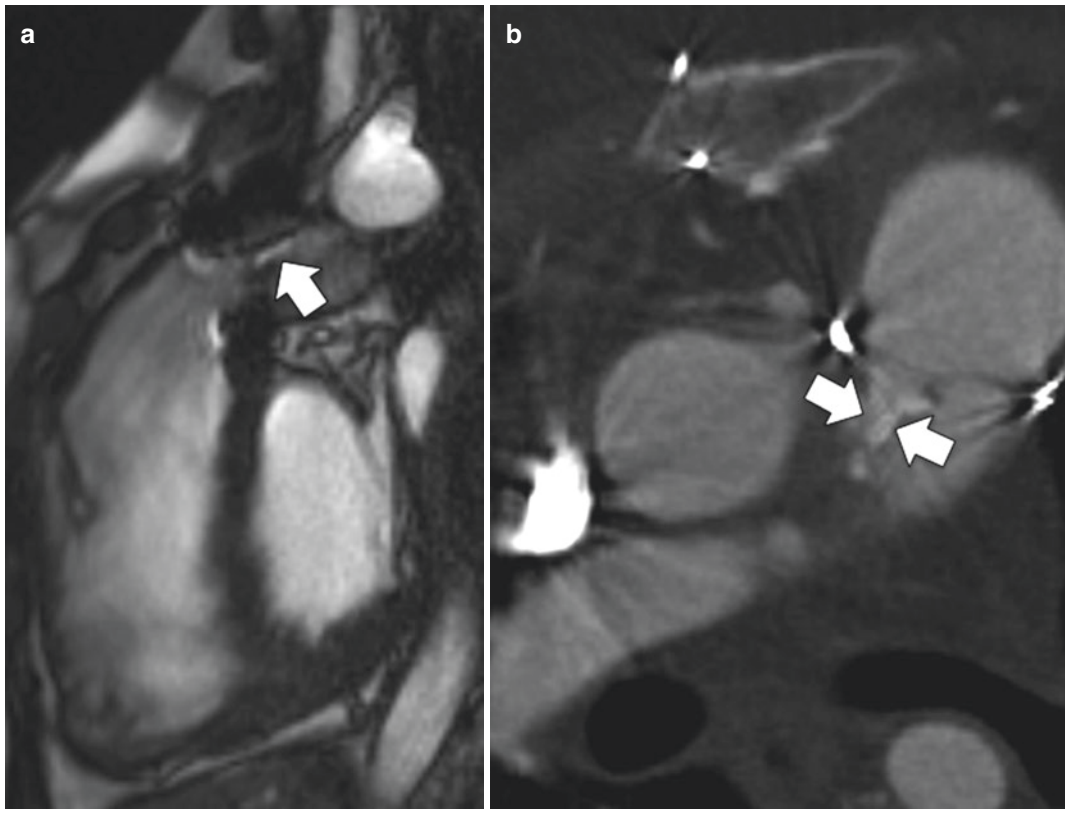

Fig. 5 Outflow tract obstruction across a homograft conduit in tetralogy of Fallot recognized by complementary imaging modalities. This patient with prior insertion of a pulmonary valve homograft conduit was noted to have increased velocities across the RVOT at echocardiography, but the exact level of obstruction could not be determined with certainty. (**a**) Sagittal cine SSFP CMR image demonstrates flow acceleration (arrow) which appears to be arising just above the level of the conduit valve. (**b**) Axial cardiac CT slice confirms that the obstruction is at valve level and is due to dystrophic calcification of both valve leaflets (arrows)

cardiologists would feel comfortable sending a patient for surgery on the basis of echo or CMR measurements alone. Measurement of shunt fraction may also be made by catheterization using the Fick principle. This assumes that flow can be derived from oxygen consumption divided by the arteriovenous difference in oxygen content of the blood. Although this is commonly done—and is reasonably accurate—it is important to understand one potential source of error is the term for oxygen consumption which is routinely *assumed* for convenience based on gender, age and body surface area rather than being directly *measured* which is preferable but more complex. Use of catheterization for assessment of regurgitant lesions is purely visual and rather dependent on operator experience.

6 Imaging Perfusion

Assessment of the coronary circulation is more commonly required than might be expected in young people in the congenital clinic. Although there are only a number of patients with coronary anomalies who present to congenital clinics each year, there are also significant numbers of patients with either inflammatory coronary disease (Kawasaki, Takayasu, Behcet) or surgical procedures which have necessitated detachment then reimplantation of the coronary arteries during surgery. Aortic root replacement, the Ross procedure and the arterial switch operation are all good examples of the latter and consequently require long-term coronary surveillance. Similarly, late presentations of coarctation are often associated with hypertension and an accelerated risk of coronary atherosclerosis which will need to be excluded prior to decision about the best treatment for the coarctation itself (Fig. 6).

There is really no consensus about the optimum approach to this sort of patient. The guidelines are vague and unhelpful in this regard. There is lack of clarity and agreement as to frequency of surveillance and modality to be used. In the absence of clear guidelines, choice of strategy may depend mainly on local imaging availability and expertise. The principal decision for the clinician is whether to seek to reassure him/herself that the myocardium is properly perfused under stress or whether to undertake direct inspection of the coronary vessels. The decisions are often—but not always—mutually exclusive as we review below.

Stress echo is an excellent modality for providing reassurance—especially when combined with treadmill stress. Most young adults are capable of reaching target heart rate, and additional prognostic data is derived from the ECG and exercise capacity portions of the test as well as the principal focus on wall motion. The test is widely available and the equipment required is inexpensive. Furthermore the lack of ionizing radiation makes it ideal for repeated examinations in a young population. The principal disadvantage stems as always from the requirement for an adequate echo window, which is variable from subject to subject. With good windows, however, a negative exercise echo can be highly reassuring.

Nuclear cardiology perfusion techniques have dominated the assessment of ischaemia in congenital patients until relatively recently. Single-photon computed emission tomography (SPECT) cameras are commonplace, and stress perfusion of the heart is easy to perform and well tolerated by patients. The main drawbacks of the technique include the associated radiation dose, which currently is in the range of 10–15 mSv using technetium isotopes (but historically was much higher with thallium isotopes). The other principal limitation of SPECT imaging is that of relatively poor spatial resolution, often in the region of 8–10 mm, which contrasts unfavourably with the 1.5–2 mm resolution achievable by CMR.

Recent advances in camera technology continue to reduce the expected dose, and with the advent of rubidium positron emission tomography (PET) imaging, doses as low as 2–4 mSv can be expected. Heavy water PET has been used on occasion and is an ideal tracer because of a linear relationship between uptake and perfusion (Yoshinaga et al. 2003; Furuyama et al. 2003, 2002). PET technology is currently limited to major academic centres however.

As PET becomes more widespread, it is likely to play a major role in the assessment of all forms of coronary disease including congenital problems. This is because of the ability to image the coronary

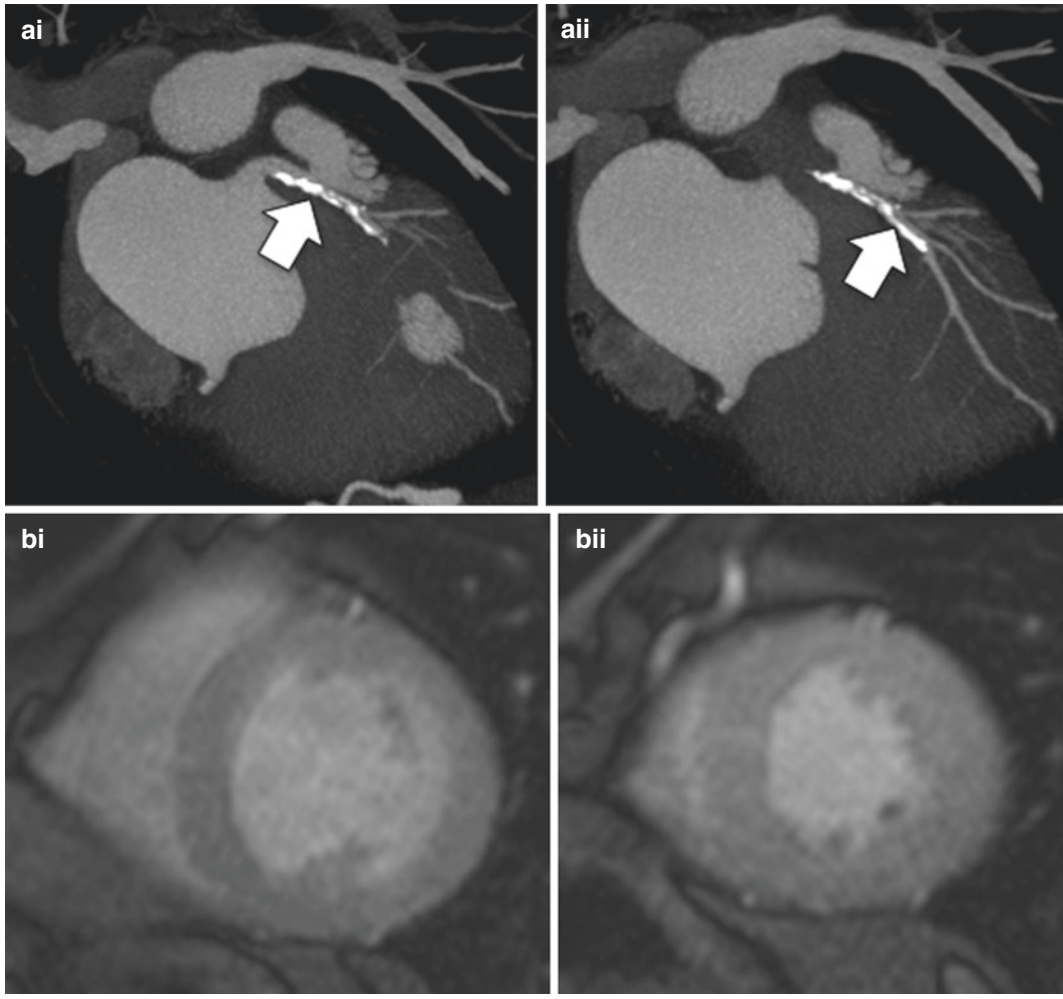

Fig. 6 Multimodality coronary imaging in a 35-year-old man with unrepaired coarctation. (**a**i–ii) Thin-slice maximum intensity projection images from cardiac CT show evidence of severe calcification of the left main and left anterior descending coronary arteries (arrows), raising concern for significant underlying stenosis. (**b**i–ii) Basal and mid-ventricular short axis slices acquired during vasodilator stress perfusion CMR, however, demonstrate normal perfusion in all coronary territories. Conventional angiography confirmed the absence of any flow-limiting coronary lesion

anatomy directly (most PET now is performed on integrated PET-CT systems) and superimpose regional flow onto three models of the vascular territories. Furthermore, software packages now allow for derivation of fully quantitative myocardial perfusion in mL/min/g of tissue, improving the specificity of the test (Hagemann et al. 2015).

PET therefore is arguably the ideal test for congenital coronary imaging despite the modest associated radiation burden. However its limited availability means that, in most large ACHD centres, CMR is regarded as the current non-invasive gold standard for perfusion assessment. The technique of vasodilator stress perfusion CMR is quick, easy and safe and has been validated extensively in adult ischaemic disease (Greenwood et al. 2009, 2012, 2014, 2016; Foley et al. 2017) and to a lesser degree in congenital heart disease. Furthermore, the use of free-breathing SSFP sequences has made it possible to acquire high-resolution images of the coronary arteries and their pathology. This has been particularly successful when applied to Kawasaki disease and congenital coronary anomalies (Fig. 7) (Tobler et al. 2014; Deva et al. 2014).

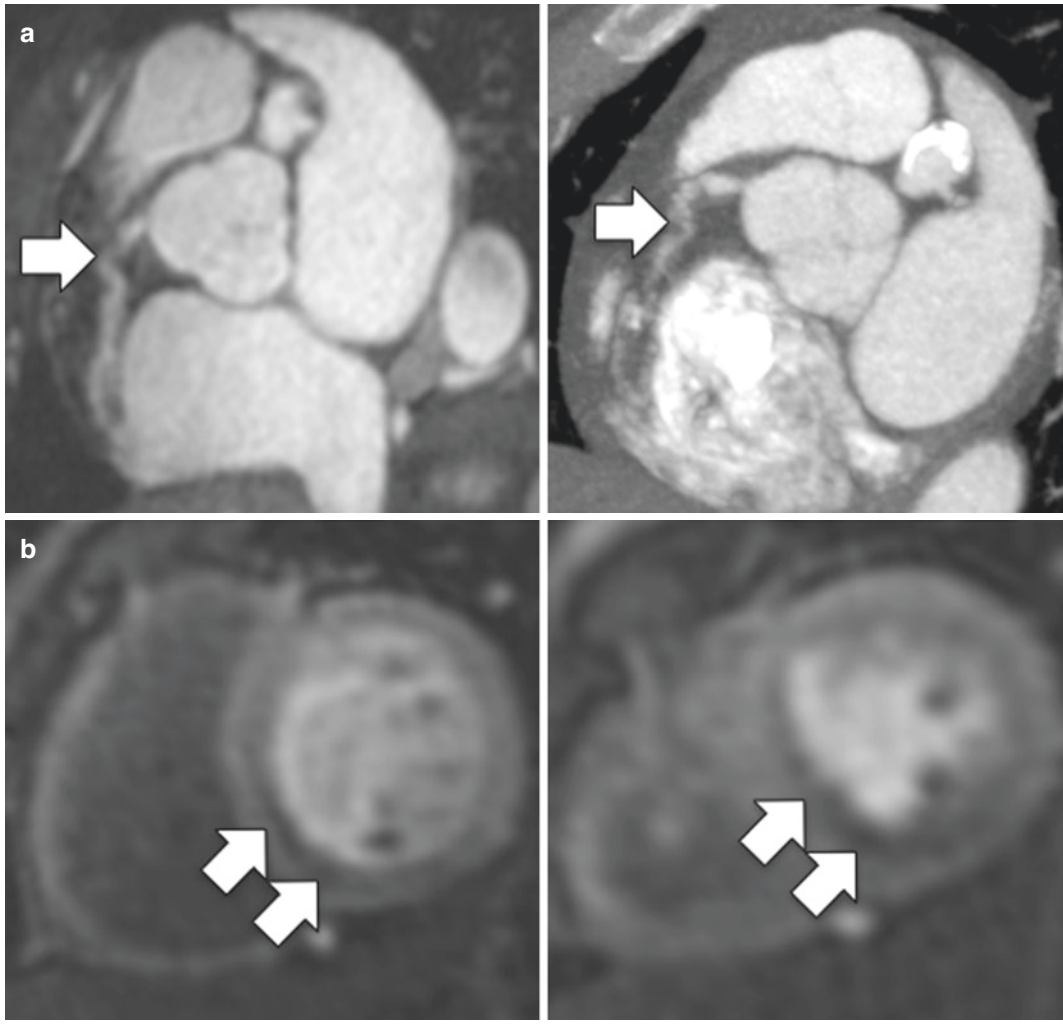

Fig. 7 Kawasaki disease with RCA occlusion. (**a**) Short axis view of the RCA (arrow) on MR angiography (left panel) and cardiac CT (right panel)—the vessel does not look entirely normal on MRA, but the extent of disease is more easily recognized on CT due to inherently higher spatial resolution. (**b**) Basal and mid-ventricular frames from vasodilator stress perfusion CMR demonstrate a zone of hypoperfusion in the inferior septum (arrows)

7 Imaging Myocardial Substrate

Patients with congenital heart disease often have abnormal myocardium. This may be congenital, for example, left ventricular non-compaction (Vermeer et al. 2013; Stähli et al. 2013; Bagur et al. 2008); or it may be acquired, for example, after chronic ischaemia or chronic volume loading. The ability to recognize and categorize abnormal myocardium has been relatively under-explored in the past in ACHD cohorts; however recent developments in the field of both molecular and CMR imaging indicate that greater attention to this area is warranted.

Substrate imaging in the nuclear world is limited by lack of clinical development although many interesting tracers have been developed for preclinical work. In practical terms SPECT-MIBI is the main tool for myocardial imaging. Persistent defects at stress and rest are usually indicative of scar—here, the absence of tracer acts as a 'negative signal' to identify abnormality. Unfortunately the limited spatial resolution of the technique means that important but limited or dispersed degrees of scarring may be missed entirely.

Conversely both diaphragmatic motion and body habitus may result in false positive defects that are misconstrued as real areas of scar (Fig. 8).

CMR has emerged as the primary method for assessing myocardial structure and composition. The technique of late gadolinium enhancement (LGE) imaging (Jimenez Juan et al. 2015) has been mainstream for 15 years and has revolutionized management of cardiomyopathies in particular. When performed with care it is exquisitely sensitive and can detect as little as 1 g of scar within the heart. In congenital work it may be used to identify areas of myocardium that have been scarred by ischaemic, mechanical or inflammatory insult (Fig. 9). It is therefore a fundamental part of any imaging protocol where coronary

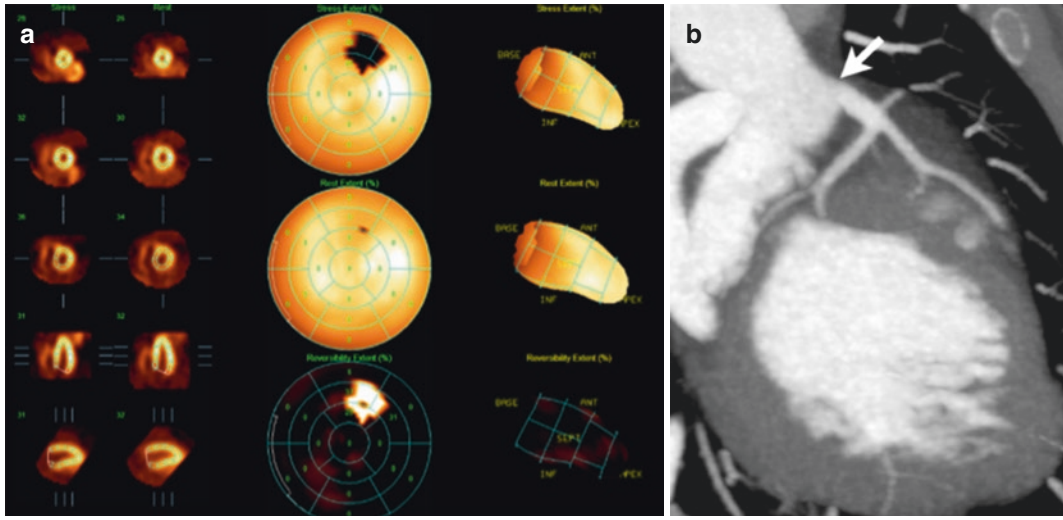

Fig. 8 False positive SPECT MIBI study in a patient following the arterial switch procedure. (**a**) Bullseye plot from stress-rest MIBI demonstrates an area of apparent reversible ischaemia in the basal to mid-anterior wall. (**b**) MIP reconstruction of the proximal to mid-left coronary tree from CT coronary angiogram demonstrates an entirely normal reimplantation site (arrow) and more distal coronary branches

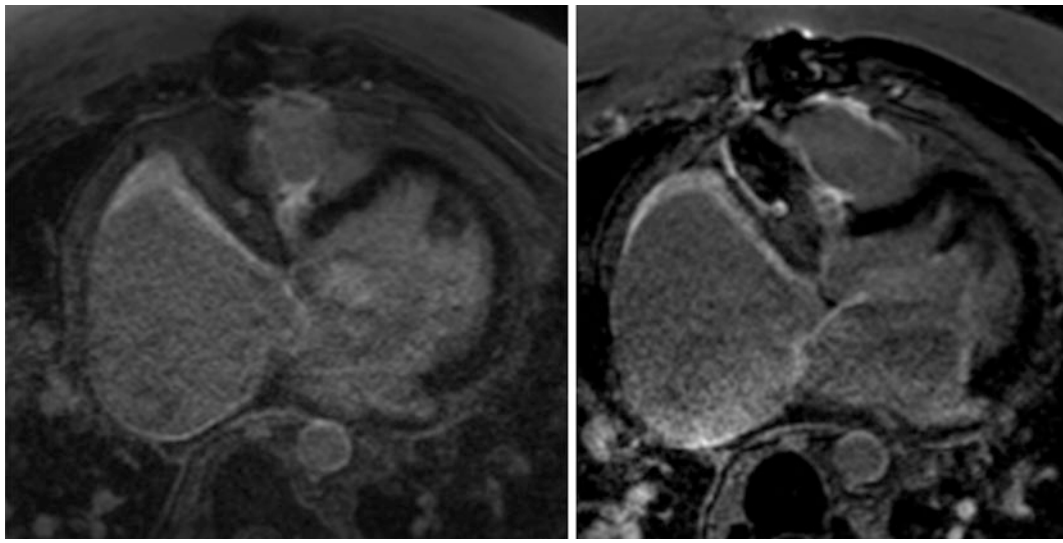

Fig. 9 Atrial fibrosis and enhancement in an atriopulmonary Fontan connection. Axial LGE images demonstrating intense enhancement in the wall of the hugely dilated right atrium. Scar in the atrial wall is common in Fontan patients but often goes unrecognized

abnormality is suspected. The very high achievable spatial resolution also makes it possible to see pathology that previously was only identifiable at surgery, for example, endocardial fibroelastosis in chronically pressure-overloaded or ischaemic ventricles (Fig. 10).

One limitation of the LGE technique, however, is the necessity for there to be some recognizable normal myocardium in the slice acquired. This is because the technique works by suppression of signal from (operator recognized) normal myocardium so that scar may be highlighted. This works well in conditions of regionality where scar is, for example, confined to a vascular territory; however it fails when there is a field change with diffuse increase in interstitial fibrosis throughout the myo-

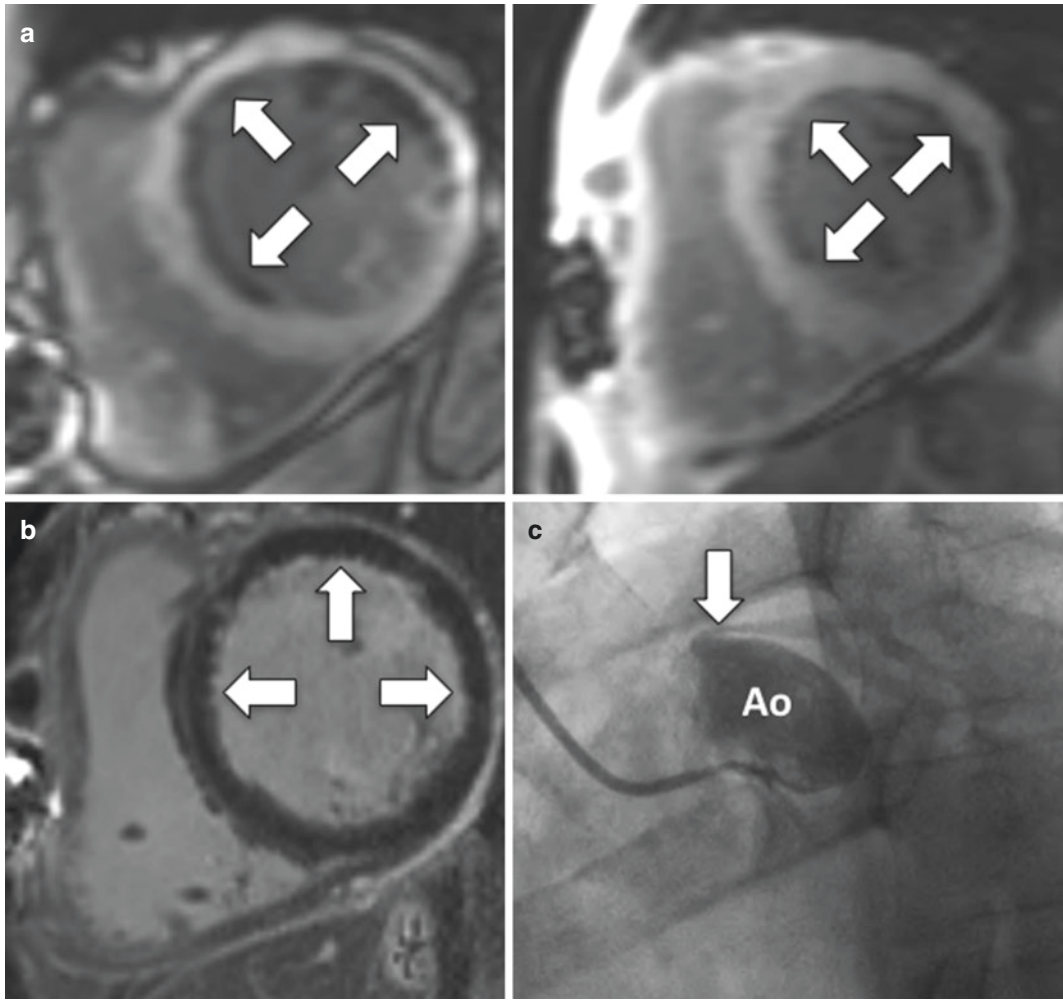

Fig. 10 Endocardial fibroelastosis (EFE) in setting of chronic ischaemia. (**a**) Basal and mid-ventricular short axis slices from an inversion time scout sequence. The majority of the myocardium is grey/white, but note the subendocardial dark rim (arrows) which has a different inversion time since it is composed of fibroelastic tissue rather than myocardium. (**b**) Short axis LGE image demonstrating a subtle inner rim of enhancing tissue (arrows) which represents the fibroelastic membrane. Very high-quality imaging is required to identify this finding—both high spatial resolution and appropriately timed image acquisition. Had LGE images been acquired even a few minutes earlier after contrast injection, the blood pool signal would have been sufficiently high to conceal the increased subendocardial signal. (**c**) Aortic root (Ao) angiogram in a man with chronic severe stenosis of the left main coronary artery (arrow) following earlier complicated reinsertion. Chronic ischaemia was believed to be the cause of the endocardial fibroelastosis in this case

cardium. More recently the technique of T1 mapping has been proposed to overcome this limitation. The details are beyond the scope of this chapter, and several useful reviews are provided (Messroghli et al. 2017; Radenkovic et al. 2017). In essence however it is possible to derive a T1 value for every pixel in the image—where the shortening of T1 post gadolinium generally reflects a local increase in fibrosis concentration. As such, a 'map' of the fibrosis content and distribution may systematically be created (Fig. 11). There are a number of assumptions made by T1 mapping, and in an attempt to reduce the influence of these, the field has lately turned towards using measured T1 values pre- and post-contrast, corrected for haematocrit, to produce instead a map of the extracellular volume (ECV) (Cameron et al. 2017; Haaf et al. 2016). In chronic conditions, the ECV corresponds mainly to the degree of interstitial fibrosis, and the normal range is 20–30% with most normal volunteers lying around 25%. Limited initial work suggests that this concept may translate to the ACHD population although it remains unclear as yet precisely how it might affect management (Hanneman et al. 2017). One possibility, however, is that subclinical heart failure—a growing problem in ACHD populations—might be detected earlier through an ECV biomarker than by conventional measures such as ejection fraction (Riesenkampff et al. 2015; Schelbert et al. 2015).

8 Imaging Thrombus

Thrombus is usually a result of derangement of one or more of the three principal components of Virchow's triad:

- Altered coagulability
- Altered wall
- Altered flow

This is not a trivial issue in adult congenital heart disease as many patients will have two if not three of these conditions. Fontan patients are peculiarly vulnerable to developing thrombus particularly if they have one of the older right atrium to pulmonary artery type connections (RA-PA Fontan) (Fig. 12). These—often very dilated—chambers with swirling flow provide ideal conditions for thrombus to form and possibly embolize more distally within the circulation (Fig. 13). Atrial arrhythmias may compound the thrombotic tendency. This kind of event may be life-threatening in a Fontan patient, and prompt recognition and treatment of this complication are vital.

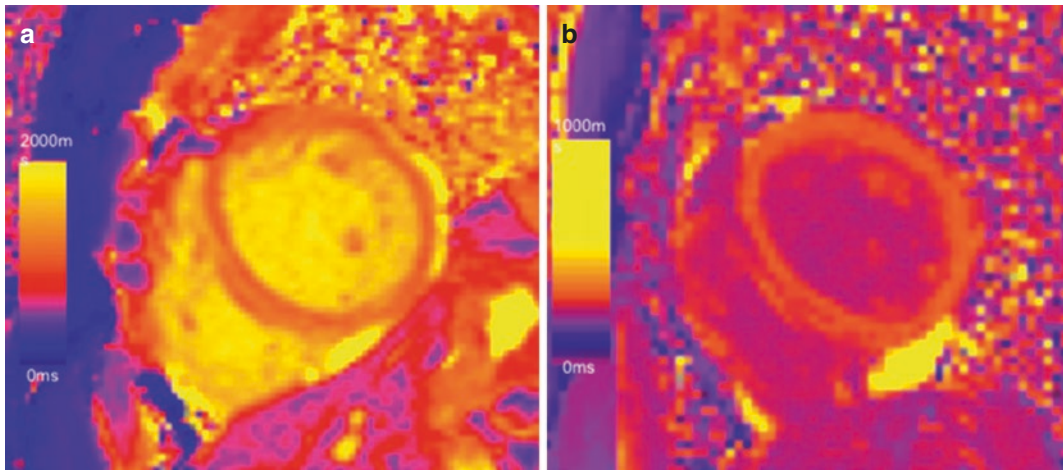

Fig. 11 T1 mapping in congenital heart disease. Adult patient with unrepaired anomalous left coronary artery from the pulmonary artery. (**a**) Native (pre-contrast) T1 map. (**b**) Post-contrast T1 map. Combined, these maps allow generation of an extracellular volume (ECV) map which—in the chronic situation—reflects the degree of underlying diffuse tissue fibrosis. Normal ECV is 20–30%. This patient has an ECV of about 32% even though the LGE imaging was unremarkable—and as such may be a more sensitive marker for diffuse tissue changes

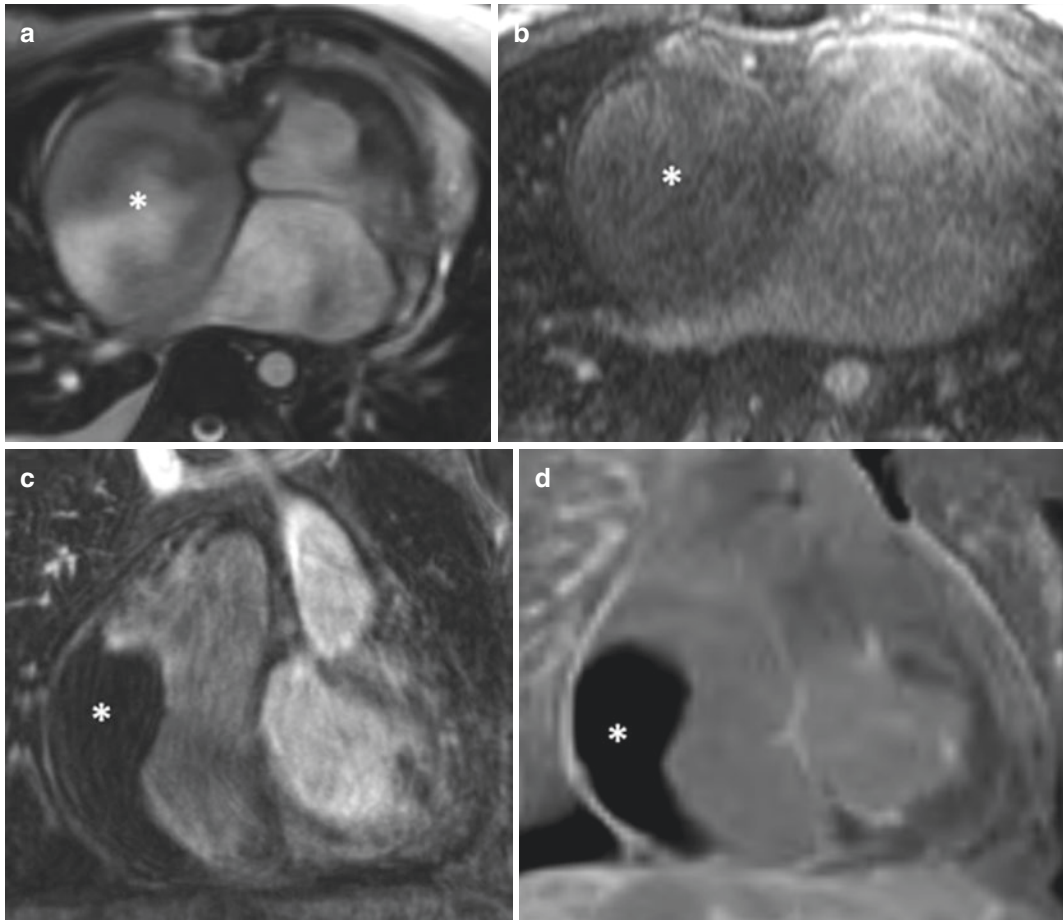

Fig. 12 The challenges of identifying thrombus in ACHD patients. (**a**) Axial cine SSFP image demonstrates mixed intensities suspicious for thrombus in the right atrium (asterisk) in this patient with a Fontan circuit. (**b**) Same patient following contrast—no thrombus is present. The appearances in (**a**) were due to swirling slow flow only. (**c**) Same patient several years later with thrombus (asterisk) visible in the right atrium on coronal view from MR angiogram. (**d**) This is made even more obvious by using phase-sensitive inversion recovery LGE sequences—with thrombus (asterisk) appearing uniformly low signal

Echo is usually the first-line examination for such a patient. In our experience transthoracic echo rarely allows confident exclusion of thrombus within a Fontan circuit. More surprising is how often transesophageal echocardiography leads to an equivocal 'unable to definitively rule out thrombus'. Why does echo find it so difficult? The answer lies in the appearance of slow-moving twisting patterns of blood flow giving rise to what echocardiographers refer to as 'smoke' within the atrium. In places this smoke may be sufficiently dense and slow moving as to be indistinguishable from fully formed thrombus. A similar phenomenon can be seen in the giant aneurysms of Kawasaki patients in whom swirling flow is problematic and can even confuse at the time of coronary angiography.

CMR suffers from the same limitation when only cine imaging is used for assessment. However, after administration of gadolinium, the use of LGE imaging invariably allows confident detection or exclusion of thrombus (Srichai et al. 2006; Goyal and Weinsaft 2013). This is because LGE imaging is usually performed 8–10 min after the administration of contrast by which time even the slow-moving currents of flow within the right atrium have had chance to distribute the gadolinium evenly throughout the chamber (Fig. 12).

Patients who are unwell and unstable or who have a contraindication to CMR may be alternatively

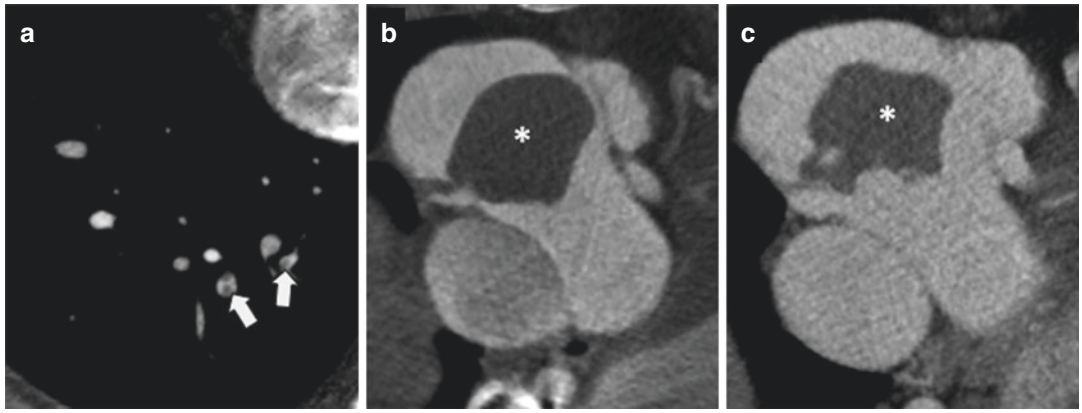

Fig. 13 Cardiac CT to identify thrombus in a Fontan patient. (**a**) The patient presented with acute breathlessness, and CT pulmonary angiogram demonstrated right lower lobe filling defects (arrows) consistent with pulmonary emboli. (**b**) Axial CT image with large low attenuation mass (asterisk) in the right atrium, consistent with thrombus and attached by a thin stalk to the posterior atrial wall. (**c**) Same patient 1 month later after anticoagulation. The thrombus is still present (asterisk) but has reduced in size. Cardiac CT is a very rapid method for identifying thrombus in the heart and can be performed at very low radiation doses by use of a low-kilovoltage technique

investigated by cardiac CT (Fig. 13). This is an excellent modality for thrombus detection aided by best-in-class spatial resolution and unlimited multiplanar reconstruction abilities (Choi et al. 2017). Many modern scanners have dual-energy capability which may further enhance discrimination between slow-flowing blood and genuine thrombus (Hur et al. 2012). Although dose has been a concern in the past, an examination of diagnostic quality can be carried out at a dose of only 1–2 mSv or even less if dose factors are aggressively modulated. Since we see many patients with atrial arrhythmias related to a variety of underlying lesions, it would be challenging to arrange CMR rapidly in each case prior to cardioversion. Over the years we have increasingly moved away from pre-cardioversion transesophageal echo and now perform cardiac CT instead in many cases—transforming both the workflow and the patient experience—with no adverse outcomes.

9 Imaging Infection

Imaging infection in ACHD usually means imaging endocarditis, which is unfortunately not a rare occurrence in this population (Li and Somerville 1998). Here there is no doubt that echocardiography—both transthoracic and transesophageal—comes into its own (Greaves et al. 2003). Detection of vegetations may be challenging if small and rapidly moving and only echo really has sufficient spatial and temporal resolution to do this reliably. There is little role for CMR here, except perhaps occasionally to confirm embolism from an aortic valve vegetation—by demonstration of new oedema and scar in a coronary territory or by revealing acute cerebral embolic lesions.

CT, however, has a more relevant role. Right-sided (tricuspid, pulmonary) lesions should routinely undergo periodic surveillance to ensure that silent pulmonary embolism is not occurring with risk for empyema and mycotic aneurysm formation. Left-sided lesions—particularly aortic—should probably undergo baseline screening once the diagnosis is established with imaging of the brain, chest, abdomen and pelvis to establish the event of embolic disease in case there is later deterioration, which might then favour surgery. Infection that is slow to respond with persistent fever and/or elevation of inflammatory markers should prompt a search for occult sources (Fig. 14).

A more recent addition to the imaging armamentarium for endocarditis is FDG PET imaging (Pizzi et al. 2015). This has been shown to be effective in whole-body screening of patients to

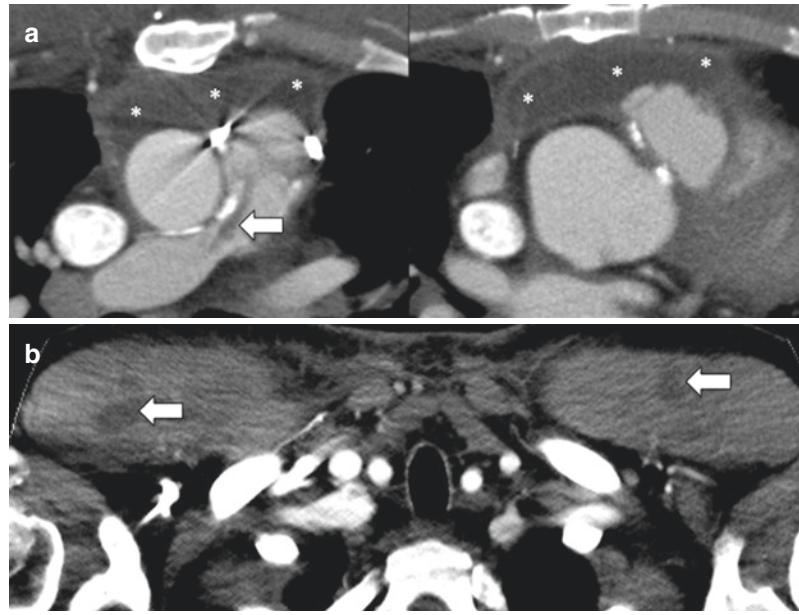

Fig. 14 Detection of disseminated infection in endocarditis. (**a**) Axial post-contrast CT image in a patient with pulmonary valve homograft endocarditis (arrow) and an anterior mediastinal collection (asterisks) with a thickened enhancing wall. (**b**) Incidental detection of multiple pectoral muscle abscesses (arrows) in the same patient

look for evidence of unsuspected embolism to various vascular beds (Amraoui et al. 2016; Bonfiglioli et al. 2013; Van Riet et al. 2010). It also enables early reclassification from possible endocarditis to a definite or rejected diagnosis of endocarditis. Although available literature is principally confined to non-ACHD patients, there are early data suggesting that this might be equally valuable in congenital heart patients, many of whom have prosthetic valves and devices (Pizzi et al. 2017). Since FDG imaging may be performed even on standard SPECT cameras equipped with appropriate collimators, this may become a more widespread approach in the future.

10 Imaging Surgical Complications

Complications following surgery for ACHD are an unfortunate fact of life. Prompt recognition of a problem by a surgeon is usually followed by an equally prompt request for imaging! There is no substitute for talking directly to the surgeon in order to find out what (s)he did at the operation and what (s)he feels may have gone wrong. This is essential in order to tailor the examination to the precise question of concern. Failure to do this usually results in requests for additional imaging in subsequent days.

No specific guidance can be given in this section since the imaging required varies according to situation. A few general comments may be made. Cardiac MR is usually poorly tolerated in the immediate post-operative period, and image quality is often poor. It may be useful however if there are concerns about myocardial damage. Cardiac CT is a very rapid and well-tolerated examination even in quite sick patients and may provide a lot of information above and beyond what may be obtained by echocardiography (although the two are usually complementary). If a surgeon is concerned about coronary artery compromise (ECG or wall motion abnormality or unexpected troponin rise), it is rare that anything other than a conventional coronary angiogram will reassure. However, following a normal angiogram, CMR may reveal the cause for chest pain.

11 Imaging by Invasive Coronary Angiography

Despite the bias towards non-invasive imaging in this chapter, it should be recognized that coronary catheterization is neither outdated nor irrelevant. Imaging in its broader sense also includes physiologic imaging, and the determination of intracardiac pressures is of vital importance both for diagnosis and management. Likewise for an experienced operator, there is little substitute for an angiographic roadmap and measurements derived from catheter images. Conventional angiographers are increasingly interested in seeing how the 3D data derived from CT and CMR may be integrated with the angiographic data to plan procedures such as coarctation stenting and pulmonary valve implantation. Coronary angiography remains the gold standard for the assessment of chest pain in general ACHD patients and is specifically indicated in most congenital patients with coronary anomalies of origin, course and termination—particularly when associated with symptoms. Direct arterial injection permits the visualization of flow within coronary arteries, fistulae and aneurysms in a way that remains impossible for CT and CMR. For coronaries with an intramural proximal course, the possibility of physiologic assessment by fractional flow reserve and intravascular ultrasound arises. More recently optical coherence tomography has also been employed to look at the structure of the coronary wall in conditions such as Kawasaki disease.

Conclusion

Adult congenital heart disease is a challenging area in which to work. No two patients are alike—even those who appear to share a common underlying lesion. The temporal evolution of surgery and intervention means that patients born 40 years ago may look quite different from those born 20 years ago even if they share the same diagnosis. The variety and complexity amongst the ACHD population argues for a personalized rather than dogmatic approach to imaging. Flexibility of approach—and sometimes more than one approach—is needed to fully characterize the challenging lesions and problems seen in this population.

References

Alfakih K, Plein S, Thiele H, Jones T, Ridgway JP, Sivananthan MU (2003a) Normal human left and right ventricular dimensions for MRI as assessed by turbo gradient echo and steady-state free precession imaging sequences. J Magn Reson Imaging 17(3):323–329

Alfakih K, Plein S, Bloomer T, Jones T, Ridgway J, Sivananthan M (2003b) Comparison of right ventricular volume measurements between axial and short axis orientation using steady-state free precession magnetic resonance imaging. J Magn Reson Imaging 18(1):25–32

Amraoui S, Tlili G, Sohal M, Berte B, Hindié E, Ritter P et al (2016) Contribution of PET imaging to the diagnosis of septic embolism in patients with pacing lead endocarditis. JACC Cardiovasc Imaging 9(3):283–290

Bagur RH, Lederlin M, Montaudon M, Latrabe V, Corneloup O, Iriart X et al (2008) Images in cardiovascular medicine. Ebstein anomaly associated with left ventricular noncompaction. Circulation 118(16):e662–e664

Bonfiglioli R, Nanni C, Morigi JJ, Graziosi M, Trapani F, Bartoletti M et al (2013) ^{18}F-FDG PET/CT diagnosis of unexpected extracardiac septic embolisms in patients with suspected cardiac endocarditis. Eur J Nucl Med Mol Imaging 40(8):1190–1196

Buechel EV, Kaiser T, Jackson C, Schmitz A, Kellenberger CJ (2009) Normal right- and left ventricular volumes and myocardial mass in children measured by steady state free precession cardiovascular magnetic resonance. J Cardiovasc Magn Reson 11:19

Cain PA, Ahl R, Hedstrom E, Ugander M, Allansdotter-Johnsson A, Friberg P et al (2009) Age and gender specific normal values of left ventricular mass, volume and function for gradient echo magnetic resonance imaging: a cross sectional study. BMC Med Imaging 9:2

Cameron D, Vassiliou VS, Higgins DM, Gatehouse PD (2017) Towards accurate and precise T1 and extracellular volume mapping in the myocardium: a guide to current pitfalls and their solutions. MAGMA. https://doi.org/10.1007/s10334-017-0631-2

Celermajer DS, Greaves K (2002) Survivors of coarctation repair: fixed but not cured. Heart 88(2):113–114

Childs H, Ma L, Ma M, Clarke J, Cocker M, Green J et al (2011) Comparison of long and short axis quantification of left ventricular volume parameters by cardio-

vascular magnetic resonance, with ex-vivo validation. J Cardiovasc Magn Reson 13:40

Choi YR, Kim H-L, Kwon H-M, Chun EJ, Ko SM, Yoo SM et al (2017) Cardiac CT and MRI for assessment of cardioembolic stroke. Cardiovasc Imaging. Asia 1(1):13

Clay S, Alfakih K, Radjenovic A, Jones T, Ridgway JP, Sinvananthan MU (2006) Normal range of human left ventricular volumes and mass using steady state free precession MRI in the radial long axis orientation. MAGMA 19(1):41–45

Crean AM, Maredia N, Ballard G, Menezes R, Wharton G, Forster J et al (2011) 3D Echo systematically underestimates right ventricular volumes compared to cardiovascular magnetic resonance in adult congenital heart disease patients with moderate or severe RV dilatation. J Cardiovasc Magn Reson 13:78

DeFaria Yeh D, Foster E (2014) Is MRI the preferred method for evaluating right ventricular size and function in patients with congenital heart disease?: MRI is not the preferred method for evaluating right ventricular size and function in patients with congenital heart disease. Circ Cardiovasc Imaging 7(1):198–205

Deva DP, Torres FS, Wald RM, Roche SL, Jimenez-Juan L, Oechslin EN et al (2014) The value of stress perfusion cardiovascular magnetic resonance imaging for patients referred from the adult congenital heart disease clinic: 5-year experience at the Toronto General Hospital. Cardiol Young 24(5):822–830

Foley JRJ, Kidambi A, Biglands JD, Maredia N, Dickinson CJ, Plein S et al (2017) A comparison of cardiovascular magnetic resonance and single photon emission computed tomography (SPECT) perfusion imaging in left main stem or equivalent coronary artery disease: a CE-MARC substudy. J Cardiovasc Magn Reson 19(1):84

Fratz S, Schuhbaeck A, Buchner C, Busch R, Meierhofer C, Martinoff S et al (2009) Comparison of accuracy of axial slices versus short-axis slices for measuring ventricular volumes by cardiac magnetic resonance in patients with corrected tetralogy of fallot. Am J Cardiol 103(12):1764–1769

Fuchs A, Mejdahl MR, Kühl JT, Stisen ZR, Nilsson EJP, Køber LV et al (2016) Normal values of left ventricular mass and cardiac chamber volumes assessed by 320-detector computed tomography angiography in the Copenhagen General Population Study. Eur Heart J Cardiovasc Imaging 17(9):1009–1017

Furuyama H, Odagawa Y, Katoh C, Iwado Y, Yoshinaga K, Ito Y et al (2002) Assessment of coronary function in children with a history of Kawasaki disease using (15)O-water positron emission tomography. Circulation 105(24):2878–2884

Furuyama H, Odagawa Y, Katoh C, Iwado Y, Ito Y, Noriyasu K et al (2003) Altered myocardial flow reserve and endothelial function late after Kawasaki disease. J Pediatr 142(2):149–154

Garcia-Bournissen F, Shrim A, Koren G (2006) Safety of gadolinium during pregnancy. Can Fam Physician 52:309–310

Geva T (2014) Is MRI the preferred method for evaluating right ventricular size and function in patients with congenital heart disease?: MRI is the preferred method for evaluating right ventricular size and function in patients with congenital heart disease. Circ Cardiovasc Imaging 7(1):190–197

Goyal P, Weinsaft JW (2013) Cardiovascular magnetic resonance imaging for assessment of cardiac thrombus. Methodist Debakey Cardiovasc J 9(3):132–136

Greaves K, Mou D, Patel A, Celermajer DS (2003) Clinical criteria and the appropriate use of transthoracic echocardiography for the exclusion of infective endocarditis. Heart 89(3):273–275

Greenwood JP, Maredia N, Radjenovic A, Brown JM, Nixon J, Farrin AJ et al (2009) Clinical evaluation of magnetic resonance imaging in coronary heart disease: the CE-MARC study. Trials 10:62

Greenwood JP, Maredia N, Younger JF, Brown JM, Nixon J, Everett CC et al (2012) Cardiovascular magnetic resonance and single-photon emission computed tomography for diagnosis of coronary heart disease (CE-MARC): a prospective trial. Lancet 379(9814):453–460

Greenwood JP, Motwani M, Maredia N, Brown JM, Everett CC, Nixon J et al (2014) Comparison of cardiovascular magnetic resonance and single-photon emission computed tomography in women with suspected coronary artery disease from the Clinical Evaluation of Magnetic Resonance Imaging in Coronary Heart Disease (CE-MARC) Trial. Circulation 129(10):1129–1138

Greenwood JP, Herzog BA, Brown JM, Everett CC, Nixon J, Bijsterveld P et al (2016) Prognostic value of cardiovascular magnetic resonance and single-photon emission computed tomography in suspected coronary heart disease: long-term follow-up of a prospective, diagnostic accuracy cohort study. Ann Intern Med. https://doi.org/10.7326/M15-1801

Grosse-Wortmann L, Al-Otay A, Goo HW, Macgowan CK, Coles JG, Benson LN et al (2007) Anatomical and functional evaluation of pulmonary veins in children by magnetic resonance imaging. J Am Coll Cardiol 49(9):993–1002

Haaf P, Garg P, Messroghli DR, Broadbent DA, Greenwood JP, Plein S (2016) Cardiac T1 Mapping and Extracellular Volume (ECV) in clinical practice: a comprehensive review. J Cardiovasc Magn Reson 18(1):89

Hagemann CE, Ghotbi AA, Kjær A, Hasbak P (2015) Quantitative myocardial blood flow with Rubidium-82 PET: a clinical perspective. Am J Nucl Med Mol Imaging 5(5):457–468

Han BK, Rigsby CK, Hlavacek A, Leipsic J, Nicol ED, Siegel MJ et al (2015a) Computed tomography imaging in patients with congenital heart disease Part I: Rationale and utility. An Expert Consensus Document of the Society of Cardiovascular Computed Tomography (SCCT): Endorsed by the Society of Pediatric Radiology (SPR) and the North American

Society of Cardiac Imaging (NASCI). J Cardiovasc Comput Tomogr 9(6):475–492

Han BK, Rigsby CK, Leipsic J, Bardo D, Abbara S, Ghoshhajra B et al (2015b) Computed tomography imaging in patients with congenital heart disease, Part 2: Technical Recommendations. An Expert Consensus Document of the Society of Cardiovascular Computed Tomography (SCCT): Endorsed by the Society of Pediatric Radiology (SPR) and the North American Society of Cardiac Imaging (NASCI). J Cardiovasc Comput Tomogr 9(6):493–513

Hanneman K, Crean AM, Wintersperger BJ, Thavendiranathan P, Nguyen ET, Kayedpour C et al (2017) The relationship between cardiovascular magnetic resonance imaging measurement of extracellular volume fraction and clinical outcomes in adults with repaired tetralogy of Fallot. Eur Heart J Cardiovasc Imaging. https://doi.org/10.1093/ehjci/jex248

Harel F, Finnerty V, Ngo Q, Grégoire J, Khairy P, Thibault B (2007) SPECT versus planar gated blood pool imaging for left ventricular evaluation. J Nucl Cardiol 14(4):544–549

Hesse B, Lindhardt TB, Acampa W, Anagnostopoulos C, Ballinger J, Bax JJ et al (2008) EANM/ESC guidelines for radionuclide imaging of cardiac function. Eur J Nucl Med Mol Imaging 35(4):851–885

Hudsmith LE, Petersen SE, Francis JM, Robson MD, Neubauer S (2005) Normal human left and right ventricular and left atrial dimensions using steady state free precession magnetic resonance imaging. J Cardiovasc Magn Reson 7(5):775–782

Hur J, Kim YJ, Lee H-J, Nam JE, Hong YJ, Kim HY et al (2012) Cardioembolic stroke: dual-energy cardiac CT for differentiation of left atrial appendage thrombus and circulatory stasis. Radiology 263(3):688–695

James SH, Wald R, Wintersperger BJ, Jimenez-Juan L, Deva D, Crean AM et al (2013) Accuracy of right and left ventricular functional assessment by short-axis vs axial cine steady-state free-precession magnetic resonance imaging: intrapatient correlation with main pulmonary artery and ascending aorta phase-contrast flow measurements. Can Assoc Radiol J 64(3):213–219

Jimenez Juan L, Crean AM, Wintersperger BJ (2015) Late gadolinium enhancement imaging in assessment of myocardial viability: techniques and clinical applications. Radiol Clin N Am 53(2):397–411

Johnson LL, Lawson MA (1996) New imaging techniques for assessing cardiac function. Crit Care Clin 12(4):919–937

Juergens KU, Grude M, Maintz D, Fallenberg EM, Wichter T, Heindel W et al (2004) Multi-detector row CT of left ventricular function with dedicated analysis software versus MR imaging: initial experience. Radiology 230(2):403–410

Koch K, Oellig F, Kunz P, Bender P, Oberholzer K, Mildenberger P et al (2004) Assessment of global and regional left ventricular function with a 16-slice spiral-CT using two different software tools for quantitative functional analysis and qualitative evaluation of wall motion changes in comparison with magnetic resonance imaging. Röfo 176(12):1786–1793

Li W, Somerville J (1998) Infective endocarditis in the grown-up congenital heart (GUCH) population. Eur Heart J 19(1):166–173

Lorenz CH, Walker ES, Morgan VL, Klein SS, Graham TP (1999) Normal human right and left ventricular mass, systolic function, and gender differences by cine magnetic resonance imaging. J Cardiovasc Magn Reson 1(1):7–21

Lotz J, Meier C, Leppert A, Galanski M (2002) Cardiovascular flow measurement with phase-contrast MR imaging: basic facts and implementation 1. Radiographics 22(3):651–671

Maceira AM, Prasad SK, Khan M, Pennell DJ (2006) Reference right ventricular systolic and diastolic function normalized to age, gender and body surface area from steady-state free precession cardiovascular magnetic resonance. Eur Heart J 27(23):2879–2888

Mahnken AH, Spuentrup E, Niethammer M, Buecker A, Boese J, Wildberger JE et al (2003) Quantitative and qualitative assessment of left ventricular volume with ECG-gated multislice spiral CT: value of different image reconstruction algorithms in comparison to MRI. Acta Radiol 44(6):604–611

Marelli AJ, Mackie AS, Ionescu-Ittu R, Rahme E, Pilote L (2007) Congenital heart disease in the general population: changing prevalence and age distribution. Circulation 115(2):163–172

McLaughlin P, Benson L, Horlick E (2006) The role of cardiac catheterization in adult congenital heart disease. Cardiol Clin 24(4):531–556, v

Mercer-Rosa L, Yang W, Kutty S, Rychik J, Fogel M, Goldmuntz E (2012) Quantifying pulmonary regurgitation and right ventricular function in surgically repaired tetralogy of Fallot: a comparative analysis of echocardiography and magnetic resonance imaging. Circ Cardiovasc Imaging 5(5):637–643

Messroghli DR, Moon JC, Ferreira VM, Grosse-Wortmann L, He T, Kellman P et al (2017) Clinical recommendations for cardiovascular magnetic resonance mapping of T1, T2, T2* and extracellular volume: a consensus statement by the Society for Cardiovascular Magnetic Resonance (SCMR) endorsed by the European Association for Cardiovascular Imaging (EACVI). J Cardiovasc Magn Reson 19(1):75

Moody WE, Edwards NC, Chue CD, Taylor RJ, Ferro CJ, Townend JN et al (2015) Variability in cardiac MR measurement of left ventricular ejection fraction, volumes and mass in healthy adults: defining a significant change at 1 year. Br J Radiol 88(1049):20140831

Mooij CF, de Wit CJ, Graham DA, Powell AJ, Geva T (2008) Reproducibility of MRI measurements of right ventricular size and function in patients with normal and dilated ventricles. J Magn Reson Imaging 28(1):67–73

Navare SM, Wackers FJT, Liu Y-H (2003) Comparison of 16-frame and 8-frame gated SPET imaging for determination of left ventricular volumes and

ejection fraction. Eur J Nucl Med Mol Imaging 30(10):1330–1337
Nayak KS, Nielsen J-F, Bernstein MA, Markl M, Gatehouse PD, Botnar RM et al (2015) Cardiovascular magnetic resonance phase contrast imaging. J Cardiovasc Magn Reson 17(1):71
Petersen SE, Aung N, Sanghvi MM, Zemrak F, Fung K, Paiva JM et al (2017) Reference ranges for cardiac structure and function using cardiovascular magnetic resonance (CMR) in Caucasians from the UK Biobank population cohort. J Cardiovasc Magn Reson 19(1):18
Pizzi MN, Roque A, Fernández-Hidalgo N, Cuéllar-Calabria H, Ferreira-González I, Gonzàlez-Alujas MT et al (2015) Improving the diagnosis of infective endocarditis in prosthetic valves and intracardiac devices with 18F-fluordeoxyglucose positron emission tomography/computed tomography angiography: initial results at an infective endocarditis referral center. Circulation 132(12):1113–1126
Pizzi MN, Dos-Subirà L, Roque A, Fernández-Hidalgo N, Cuéllar-Calabria H, Pijuan Domènech A et al (2017) (18)F-FDG-PET/CT angiography in the diagnosis of infective endocarditis and cardiac device infection in adult patients with congenital heart disease and prosthetic material. Int J Cardiol 248:396–402
Radenkovic D, Weingärtner S, Ricketts L, Moon JC, Captur G (2017) T1 mapping in cardiac MRI. Heart Fail Rev 22(4):415–430
Riesenkampff E, Messroghli DR, Redington AN, Grosse-Wortmann L (2015) Myocardial T1 mapping in pediatric and congenital heart disease. Circ Cardiovasc Imaging 8(2):e002504
Roche SL, Silversides CK, Oechslin EN (2011) Monitoring the patient with transposition of the great arteries: arterial switch versus atrial switch. Curr Cardiol Rep 13(4):336–346
Roman KS, Kellenberger CJ, Farooq S, MacGowan CK, Gilday DL, Yoo S-J (2005) Comparative imaging of differential pulmonary blood flow in patients with congenital heart disease: magnetic resonance imaging versus lung perfusion scintigraphy. Pediatr Radiol 35(3):295–301
Salton CJ, Chuang ML, O'Donnell CJ, Kupka MJ, Larson MG, Kissinger KV et al (2002) Gender differences and normal left ventricular anatomy in an adult population free of hypertension. A cardiovascular magnetic resonance study of the Framingham Heart Study Offspring cohort. J Am Coll Cardiol 39(6):1055–1060
Schelbert HR, Verba JW, Johnson AD, Brock GW, Alazraki NP, Rose FJ et al (1975) Nontraumatic determination of left ventricular ejection fraction by radionuclide angiocardiography. Circulation 51(5):902–909
Schelbert EB, Piehler KM, Zareba KM, Moon JC, Ugander M, Messroghli DR et al (2015) Myocardial fibrosis quantified by extracellular volume is associated with subsequent hospitalization for heart failure, death, or both across the spectrum of ejection fraction and heart failure stage. J Am Heart Assoc 4(12):e002613
Sievers B, Kirchberg S, Bakan A, Franken U, Trappe H-J (2004) Impact of papillary muscles in ventricular volume and ejection fraction assessment by cardiovascular magnetic resonance. J Cardiovasc Magn Reson 6(1):9–16
Singh RM, Singh BM, Mehta JL (2014) Role of cardiac CTA in estimating left ventricular volumes and ejection fraction. World J Radiol 6(9):669–676
Srichai MB, Junor C, Rodriguez LL, Stillman AE, Grimm RA, Lieber ML et al (2006) Clinical, imaging, and pathological characteristics of left ventricular thrombus: a comparison of contrast-enhanced magnetic resonance imaging, transthoracic echocardiography, and transesophageal echocardiography with surgical or pathological validation. Am Heart J 152(1):75–84
Stähli BE, Gebhard C, Biaggi P, Klaassen S, Valsangiacomo Buechel E, Attenhofer Jost CH et al (2013) Left ventricular non-compaction: prevalence in congenital heart disease. Int J Cardiol 167(6):2477–2481
Stehning C, Börnert P, Nehrke K, Eggers H, Stuber M (2005) Free-breathing whole-heart coronary MRA with 3D radial SSFP and self-navigated image reconstruction. Magn Reson Med 54(2):476–480
Strugnell WE, Slaughter IR, Riley RA, Trotter AJ, Bartlett H (2005) Modified RV short axis series—a new method for cardiac MRI measurement of right ventricular volumes. J Cardiovasc Magn Reson 7(5):769–774
Sundgren PC, Leander P (2011) Is administration of gadolinium-based contrast media to pregnant women and small children justified? J Magn Reson Imaging 34(4):750–757
Tobler D, Motwani M, Wald RM, Roche SL, Verocai F, Iwanochko RM et al (2014) Evaluation of a comprehensive cardiovascular magnetic resonance protocol in young adults late after the arterial switch operation for d-transposition of the great arteries. J Cardiovasc Magn Reson 16:98
Van Riet J, Hill EE, Gheysens O, Dymarkowski S, Herregods M-C, Herijgers P et al (2010) (18)F-FDG PET/CT for early detection of embolism and metastatic infection in patients with infective endocarditis. Eur J Nucl Med Mol Imaging 37(6):1189–1197
Vermeer AMC, van Engelen K, Postma AV, Baars MJH, Christiaans I, De Haij S et al (2013) Ebstein anomaly associated with left ventricular noncompaction: an autosomal dominant condition that can be caused by mutations in MYH7. Am J Med Genet C: Semin Med Genet 163C(3):178–184
Winter MM, Bernink FJ, Groenink M, Bouma BJ, van Dijk AP, Helbing WA et al (2008) Evaluating the systemic right ventricle by CMR: the importance of consistent and reproducible delineation of the cavity. J Cardiovasc Magn Reson 10:40
Yang HS (2017) Three-dimensional echocardiography in adult congenital heart disease. Korean J Intern Med 32(4):577–588
Yoshin aga K, Katoh C, Noriyasu K, Iwado Y, Furuyama H, Ito Y et al (2003) Reduction of coronary flow reserve in areas with and without ischemia on stress perfusion imaging in patients with coronary artery disease: a study using oxygen 15-labeled water PET. J Nucl Cardiol 10(3):275–283

Venoatrial Abnormalities

Chantale Lapierre

Contents

Abstract

Congenital anomalies of thoracic veins can be subdivided into systemic and pulmonary anomalies. This group of pathologies is not uncommon. The most common systemic thoracic venous anomalies are: persistent left superior vena cava, retroaortic left brachiocephalic vein, and azygos continuation of inferior vena cava. The pulmonary venous anomalies can be separated into partial and total anomalous returns. They have a broad spectrum of presentations and can be associated with other congenital heart malformations. Most systemic venous anomalies are incidental findings whereas pulmonary venous malformations can have a relatively benign course like partial anomalous pulmonary venous return to a more severe critical disease like an obstructed pulmonary venous return. Also, total anomalous pulmonary venous return induces cyanosis and should be corrected surgically as soon as possible. Although echocardiography remains the initial noninvasive imaging modality, an accurate characterization and diagnosis of these anomalies can be obtained by CT or MR imaging. However, MRI stays the cross-section modality of choice because, in addition to providing a comprehensive assessment of the cardiac anatomy, it can accurately quantify shunts, ventricular size, and function.

Keywords

Pulmonary • Systemic • Thoracic congenital vein

C. Lapierre, M.D.
Medical Imaging Department, CHU Sainte-Justine,
3175, Cote-Sainte-Catherine
Montreal, QC, Canada H3T 1C5
e-mail: chantal_lapierre@ssss.gouv.qc.ca

Med Radiol Diagn Imaging (2017)
DOI 10.1007/174_2017_82, © Springer International Publishing AG
Published Online: 01 September 2017

1 Introduction

Congenital anomalies of the thoracic veins may go unnoticed until adulthood. Most of the time, they are recognized incidentally as part of an examination for a totally unrelated indication. However, these abnormalities require characterization as they may be associated with other malformations and have important clinical or surgical implications.

The chapter reviews and illustrates the normal and abnormal anatomy/venoatrial connections of the thoracic veins, which are separated into systemic and pulmonary anomalies. It also covers the postsurgical sequelae and imaging strategies.

1.1 Imaging Strategies

Patients with congenital anomalies of the thoracic veins can be evaluated using catheter angiography, echocardiography, computed tomography (CT), or magnetic resonance (MR) imaging. Despite the fact that echocardiography permits a noninvasive evaluation, this modality of investigation has limitations such as poor acoustic window and poor depiction of extravascular structures. In the past, catheter angiography played a major role, but nowadays it is currently reserved for vascular interventions and hemodynamic evaluations. Presently, the anomalies are assessed using CT or MRI with well-known advantages and limitations for each modality (Türkvatan et al. 2017; Hellinger et al. 2011; Ruano et al. 2015; White 2000; Rahmani and White 2008; White et al. 1997; Mueller et al. 2015).

Multidetector contrast-enhanced CT with reconstructions can be realized with or without cardiac gating. Acquisitions without gating permit a good evaluation of both systemic and pulmonary thoracic veins anatomy. However, the intracardiac anatomy, for example, associated with atrial (ASD) or ventricular (VSD) septal defects, is less precise on CT. The counterpart of that technique is the higher radiation dose.

MRI evaluation of the thoracic veins can be done with different sequences, with and without gadolinium (Table 1). MRI is a good imaging modality to assess both the venous anatomy and the associated cardiac anomalies. By both cardiac function and flow assessment, MRI can precise the pulmonic-to-systemic flow ratio (QP/QS) and the eventual effect of the anomalies on the cardiac chambers size and function. In addition to be time consuming, MRI have well-known contraindications that preclude that technique (Mueller et al. 2015).

Table 1 Institutional cardiovascular MRI protocol for thoracic venous assessment

1. Localizers through the thorax images
2. Anatomic examination with half Fournier shot turbo spin echo (HASTE) or balanced steady state free precession (SSFP) according to heart rate in axial and coronal plane of the thorax
3. Four-chamber SSFP cine stack views including the atrial septum
4. Short axis SSFP cine stack views including the atrial septum
5. Multiplanar oblique SSFP cine views on the abnormal veins (perpendicular views on each selected structure)
6. Qp/Qs evaluation by flow mapping on:
(a) Left pulmonary artery
(b) Right pulmonary artery
(c) Main pulmonary artery
(d) Ascending aorta
7. Gadolinium enhanced 3D MRA acquisition of the thorax in coronal plane, with multiple phases acquisition

2 Systemic Thoracic Venous Anomalies

2.1 Normal Anatomy

Normal systemic thoracic venous anatomy for the upper part of the body consists of bilateral subclavian and brachiocephalic veins draining into the right atrium via the right superior vena cava (RSVC). The RSVC courses along the right mediastinum. The azygos vein, its major tributary, travels along the right anterior borders of the thoracic vertebrae up to the level of the carina and then arches over the right tracheobronchial angle to drain posteriorly into the RSVC. The coronary sinus travels in the left atrioventricular groove, receives mainly the great cardiac veins, and drains into the right atrium. The inferior vena

cava (IVC) receives systemic venous drainage from the legs, retroperitoneal viscera, and the hepatic circulation, and drains into the inferior surface of the right atrium.

2.2 Congenital Anomalies

Many anomalies of the systemic veins are asymptomatic but can co-exist with other more serious congenital heart diseases (CHD).

2.2.1 Persistent Left Superior Vena Cava (LSVC)

A persistent LSVC, the most common congenital thoracic venous anomaly, is described in 0.3% of the general population with prevalence increasing to 4.3% in patients with congenital heart disease (Gonzalez-Juanatey et al. 2004; Biffi et al. 2001). The commonly associated anomalies include septal defects, aortic coarctation, and anomalous pulmonary venous return (Cha and Khoury 1972). It is frequently an incidental finding in an asymptomatic patient. Documentation of the anatomy is necessary because it can interfere with the placement of several devices such as central venous catheters, cardiac pacemakers, and defibrillator leads. It may have some surgical implications, namely artery bypass surgery (Gonzalez-Juanatey et al. 2004; Biffi et al. 2001).

In most patients (92%), the LSVC drains normally into the right atrium through an enlarged coronary sinus (Gonzalez-Juanatey et al. 2004). No RSVC is detected in 10–18% of cases (mirror image) (Fig. 1). A dilated coronary sinus, especially with an absent RSVC,

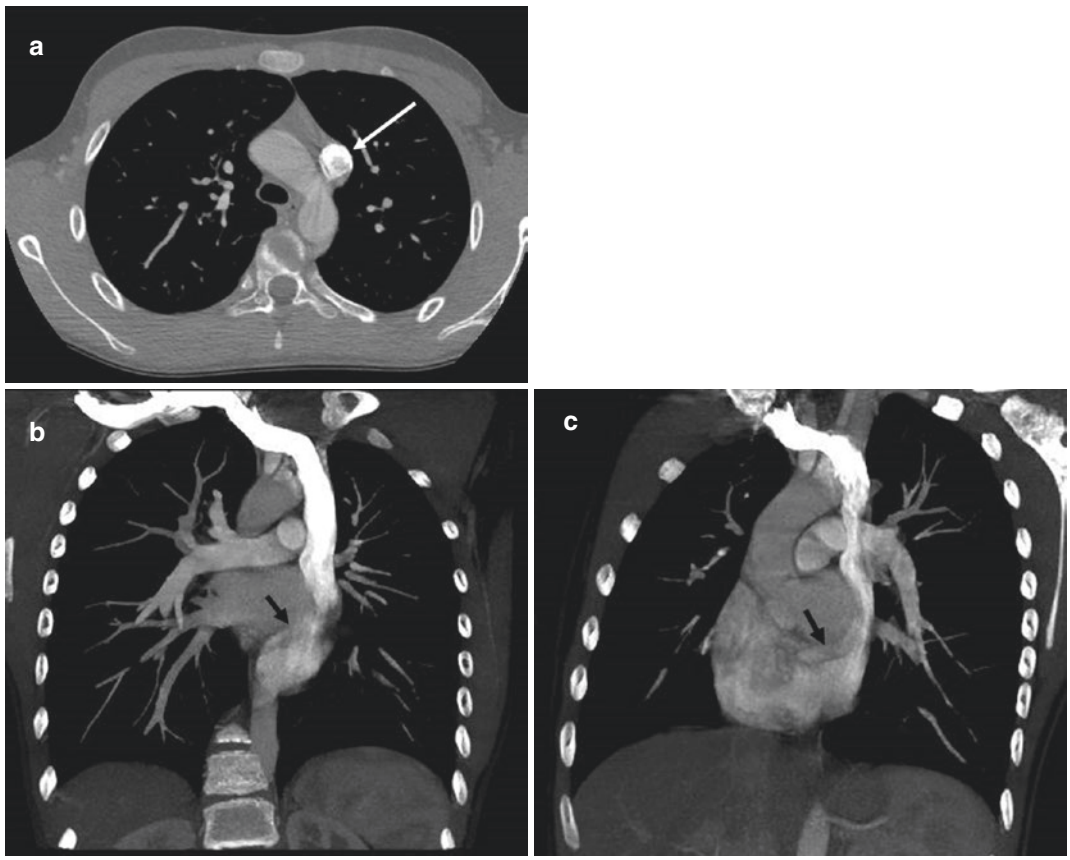

Fig. 1 Persistent left superior vena cava (mirror image) at CT angiography. (**a**) Axial, (**b**) coronal oblique, and (**c**) sagittal oblique thin maximum intensity projection images demonstrate a persistent left superior vena cava (*white arrow*) draining into an enlarged coronary sinus (*black arrows*) and an absence of right superior vena cava

can cause stretching of the atrioventricular node and the bundle of His; cardiac arrhythmias have been reported (James et al. 1976). In 65% of patients with persistent LSVC, the left brachiocephalic vein is absent (Fig. 2). Even if both vena cava are present, the caliber of the RSVC is reduced (Pretorius and Gleeson 2004). When isolated, the finding of LSVC has no

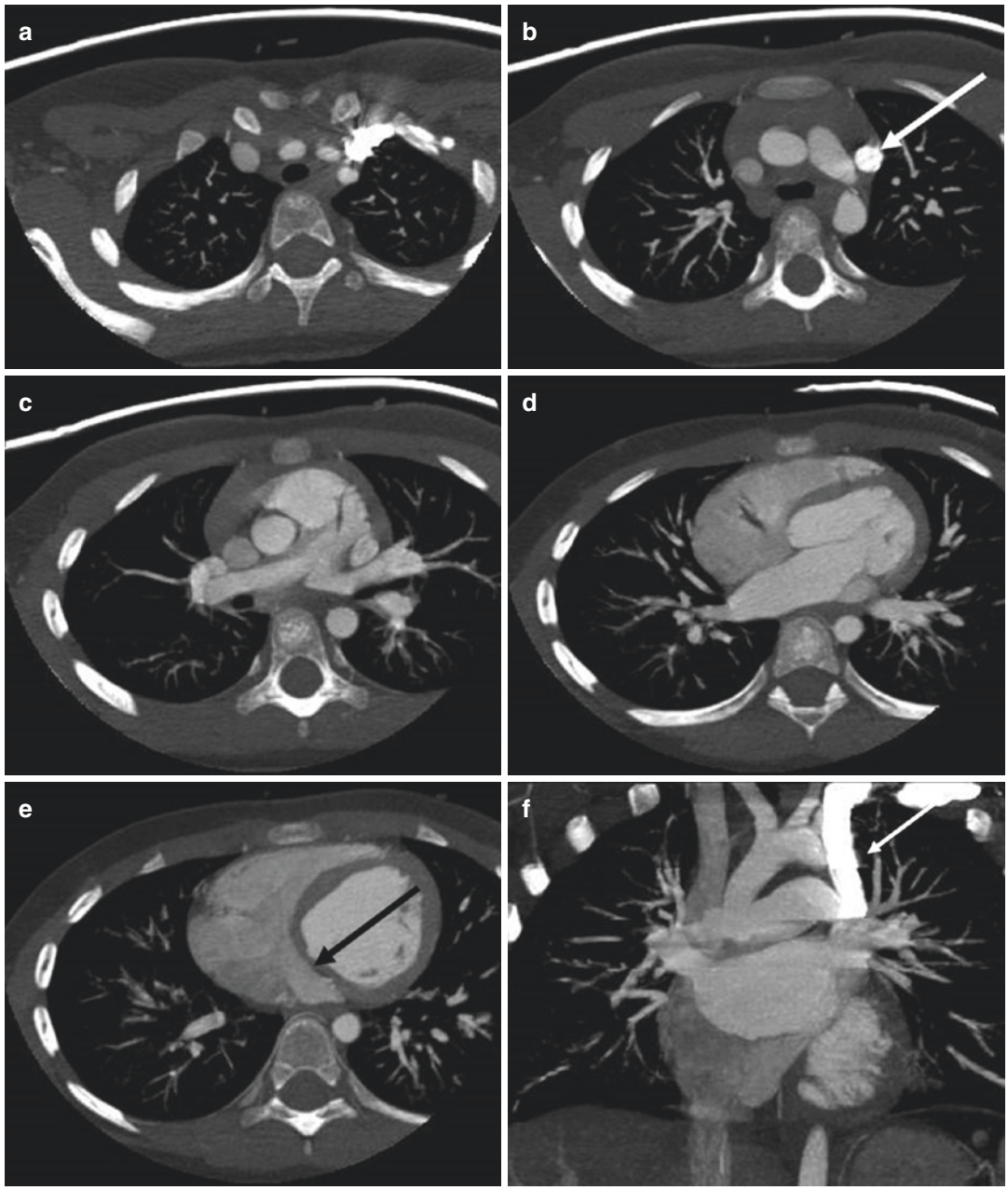

Fig. 2 Persistent left superior vena cava at CT angiography. (**a**)–(**e**) Axial thin maximum intensity projection (MIP), (**f**) coronal MIP, and (**g**) sagittal oblique MIP images demonstrate a persistent left superior vena cava (*white arrows*) draining into an enlarged coronary sinus (*black arrows*), a right superior vena cava, and an absence of left brachiocephalic vein

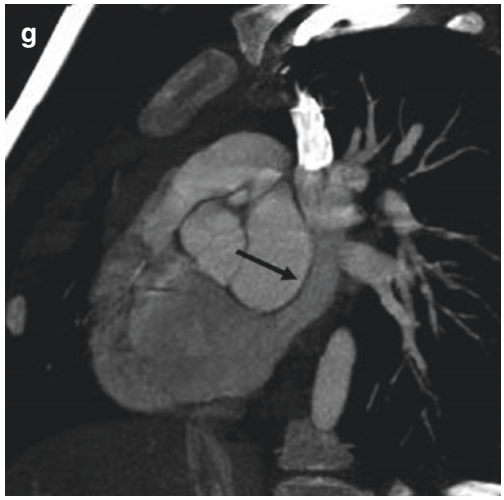

Fig. 2 (continued)

physiologic consequence and is detected incidentally.

Drainage of LSVC into the left atrium is rare but creates a right-to-left shunt and is associated with significant increased incidence of CHD. Patients are usually asymptomatic but are at risk of right-to-left shunting complications including paradoxical emboli, brain abscess, strokes, and death (Geva and Van Praagh 2008a).

The unroofed coronary sinus can be included in this category because it is almost always associated with a LSVC. In this entity, the common wall between the left atrium and the coronary sinus is partially or completely absent (Fig. 3). The orifice of the unroofed coronary sinus is enlarged and functions like an interatrial communication (Raghib syndrome). Such a left-to-right shunt results in systemic arterial desaturation created by the mixing of LSVC blood with pulmonary venous flow blood to the left atrium. The degree of arterial desaturation is proportional to the net right-to-left shunt, which, in turn, depends on the amount of systemic venous blood carried by the LSVC and the proportion of systemic venous flow that crosses the atrial septum and reaches the pulmonary circulation. Patients with this anomaly are at risk of right-to-left shunting complications like patients with LSVC draining into the left atrium (Geva and Van Praagh 2008a). Treatment of unroofed coronary sinus and LSVC into the left atrium, if needed, is surgical or through percutaneous correction. The type of treatment is based on the anatomy and associated abnormalities. Few postsurgical complications are described, usually either stenosis or residual shunt. Given the limited number of published cases, no standardized posttreatment follow-up recommendations are available.

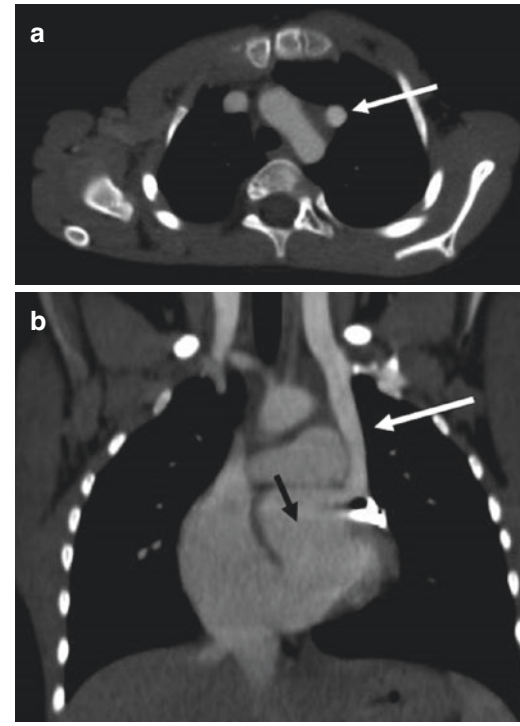

Fig. 3 Totally unroofed coronary sinus and persistent left superior vena cava at CT angiography. (**a**) Axial and (**b**) coronal thin maximum intensity projection images demonstrate an absence of wall between the coronary sinus and the left atrium (*black arrow*), a persistent left superior vena cava (*white arrows*), a right superior vena cava, and an absence of left brachiocephalic vein. The orifice of the coronary sinus is enlarged

To summarize, the most frequent conditions associated with a LSVC are:

- Single LSVC draining into the coronary sinus (mirror image)
- Single LSVC draining into the left atrium
- Dual SVC with or without left brachiocephalic vein
- Dual SVC or single LSVC with unroofed coronary sinus

2.2.2 Anomalies of Right SVC (RSVC)

Isolated anomalies of RSVC are rare. RSVC can drain into the left atrium, have low insertion into the right atrium, or be congenitally dilated (Cormier et al. 1989; Freedom et al. 1982; Modry et al. 1980; Park et al. 1983). Drainage of RSVC into the left atrium results in a right-to-left shunt and can occur without any associated anomalies. Accordingly, patients are at risk of right-to-left shunting complications. An aneurysmal dilatation is an incidental finding and a low insertion is associated to complex CHD.

2.2.3 Anomaly of Left Brachiocephalic Vein (LBCV)

Normally, the LBCV joins the RSVC anteriorly to the aorta. With retroaortic LBVC, the vein courses posteriorly to the ascending aorta, underneath the aortic arch, and anteriorly to the main pulmonary artery (Fig. 4). The prevalence of this finding is 0.5–0.6%, and is usually associated with CHD such as Tetralogy of Fallot, truncus arteriosus (Cormier et al. 1989). When isolated, this anomaly does not cause physiologic modifications, but can have some clinical implications at the time of insertion of central venous lines and pacemakers (Hellinger et al. 2011).

2.2.4 Anomalies of IVC

The azygos continuation of the IVC, also described as the absence of hepatic segment of the IVC with azygos continuation, occurs in 0.6% of the general population (Ruano et al. 2015) (Fig. 5). The hepatic veins drain directly into the right atrium. This entity is a classical finding in heterotaxia syndrome with polysplenia (Geva and Van Praagh 2008a). Rarely, the continuation is through the hemiazygos vein with three possible paths of drainage: (1) the azygos vein, (2) a LSVC, and (3) a RSVC (coursing through the accessory hemiazygos vein and LBCV) (Dudiak et al. 1991) (Fig. 6). These venous anomalies do not have any consequences on physiologic circulation but may have clinical implications such as IVC filter placement. Since the advent of cross-sectional imaging, anomalies of IVC are being increasingly found in asymptomatic patient.

Other anomalies like bilateral IVC and IVC drainage into the left atrium are rare.

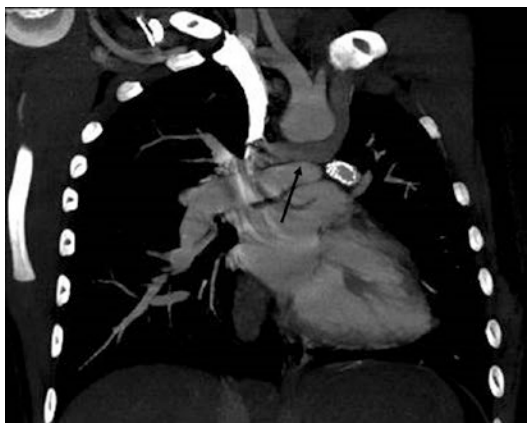

Fig. 4 Retroaortic left brachiocephalic vein at CT angiography. Coronal maximum intensity projection image demonstrates the left brachiocephalic vein (*black arrow*) projective under the aortic arch

2.3 Postsurgical Sequelae

2.3.1 Atrial Switch

Prior to the establishment of the arterial switch procedure to treat patients with d-transposition of the great arteries (D-TGA), many patients have been palliated using a Mustard or Senning procedure (atrial switch) (Fig. 7). These surgeries consist of rerouting systemic and pulmonary venous return to the ventricles that were associated with the appropriate great vessels. So, oxygenated blood from the pulmonary veins is redirected to right ventricle, aorta, and systemic circulation. Conversely, the systemic blood from the systemic veins is redirected to left ventricle, pulmonary arteries, and lungs for oxygenation. Persistent and progressive functional cardiac abnormalities have long been recognized following repair and included: residual intra-atrial shunts, caval and pulmonary venous obstructions, right ventricular dysfunction, tricuspid regurgitation, and arrhythmia (Wernovsky 2008).

Residual intra-atrial baffle shunts occur most commonly at the superior right atrial baffle suture lines and may cause either

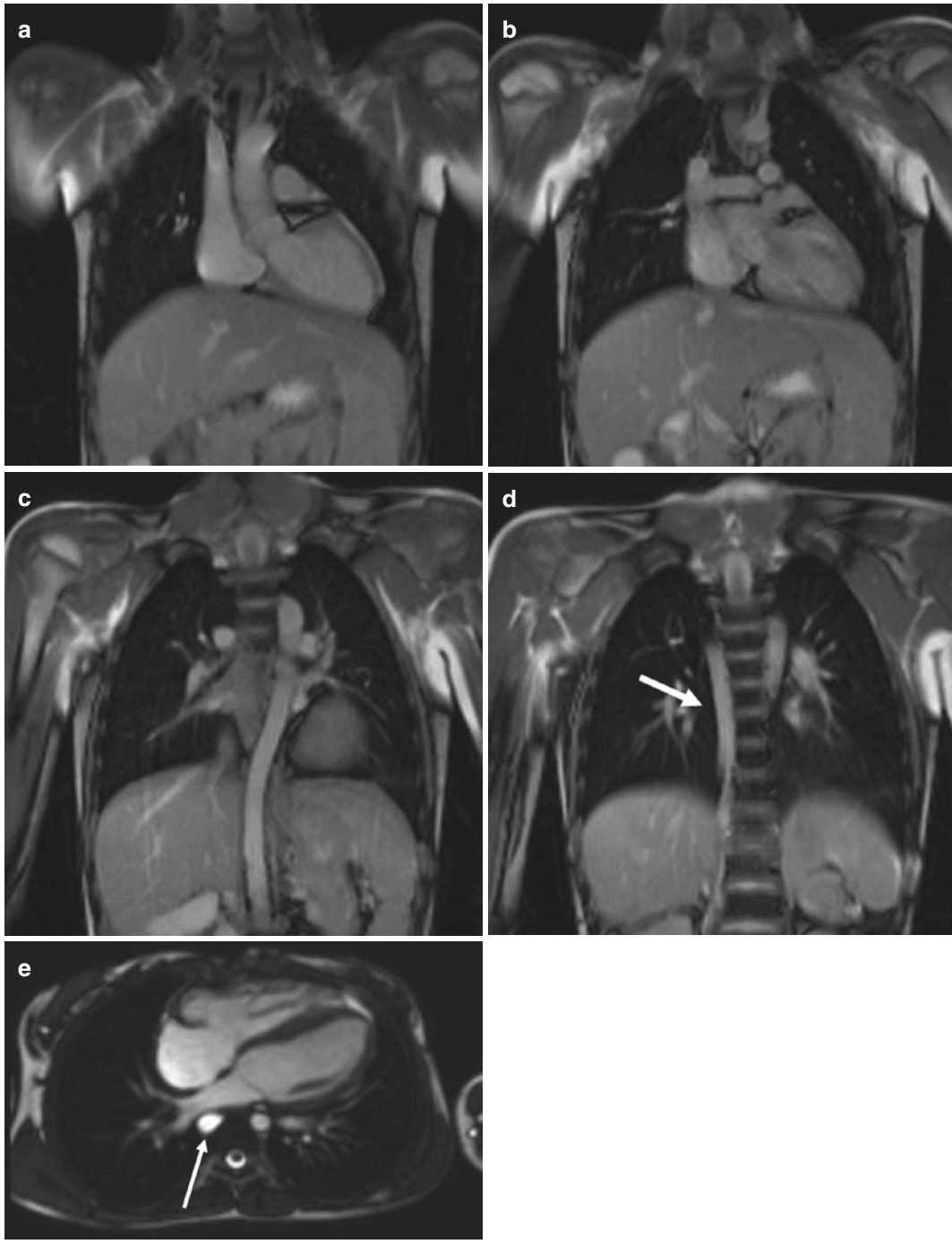

Fig. 5 Interruption of inferior vena cava with azygos continuation (*white arrows*) on (**a**)–(**d**) coronal TruFISP and (**e**) on four-chamber view cine TruFISP MRI sequence images

systemic-to-pulmonary or pulmonary-to-systemic venous shunting. Although trivial leaks have been observed at late postoperative angiography in 10–20% of patients, significant leaks requiring re-intervention have been uncommon (1–2%) (Wernovsky 2008).

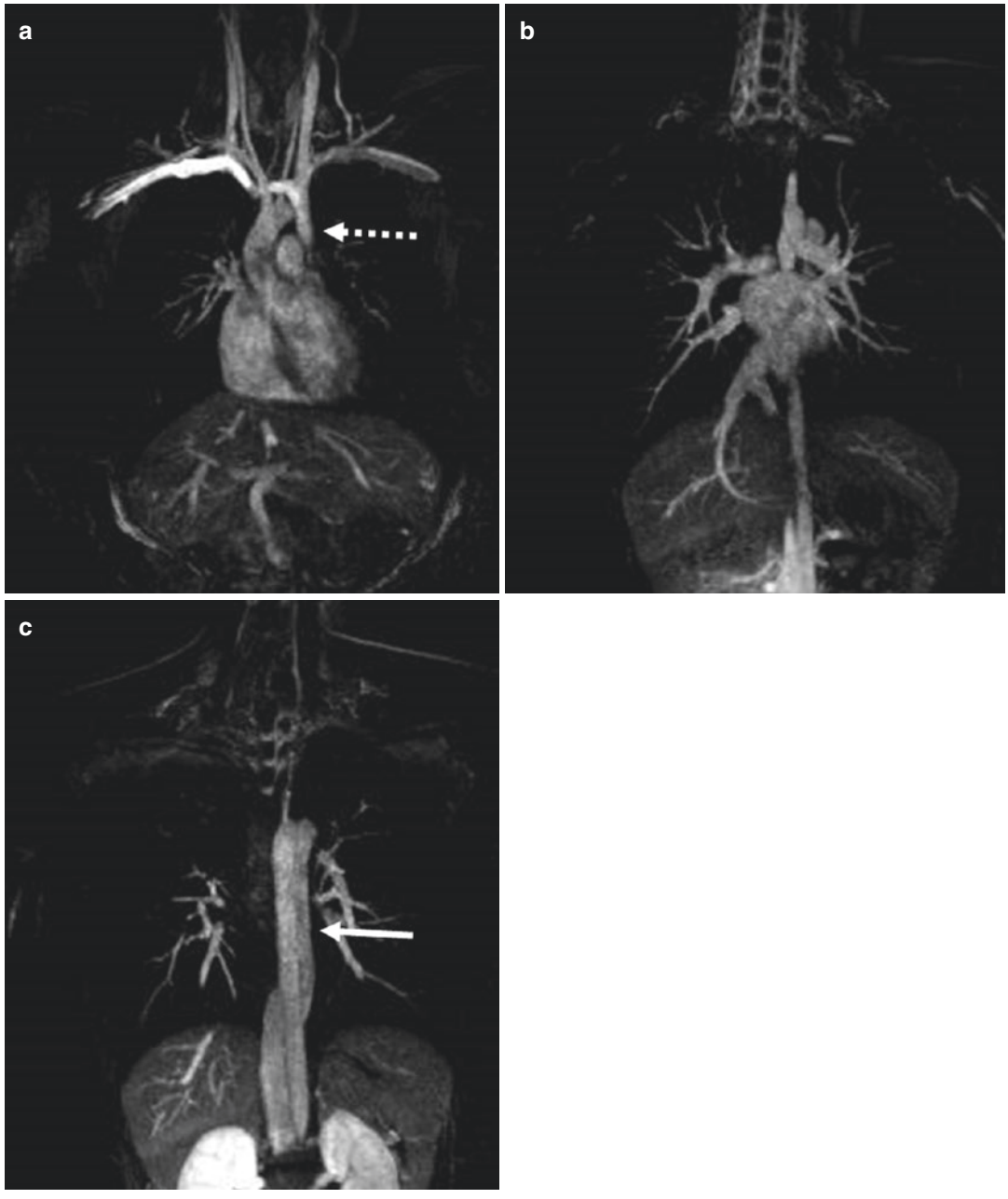

Fig. 6 (**a**)–(**c**) Interruption of inferior vena cava with hemiazygos continuation (*white arrow*) and drainage into a left superior vena cava (*white dotted arrow*) on coronal MR angiography

Obstruction of superior vena cava pathway appears postoperatively in 5–10%. The location of obstruction is distal to the superior vena cava entrance, at the site of excision of the superior remnant of the atrial septum (Fig. 8). Despite severe obstruction, patients can be asymptomatic because of decompression of the RSVC by the azygos/hemiazygos system. Obstruction of IVC is a serious but infrequent complication (1%) (Wernovsky 2008).

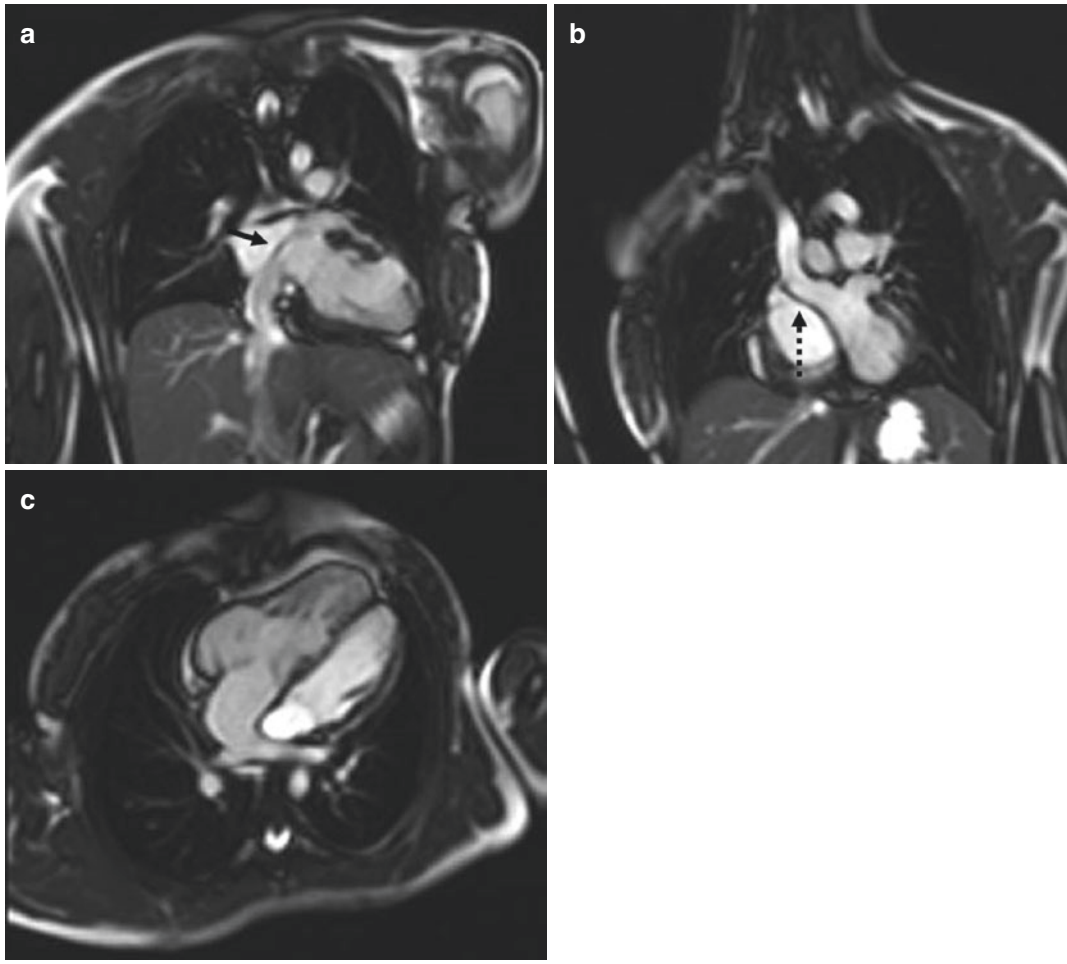

Fig. 7 Atrial switch (Mustard procedure) for D-transposition of great arteries at cardiac MRI. (**a**), (**b**) Coronal oblique cine TruFISP MRI sequence images demonstrate drainage of right superior (*black dotted arrow*) and inferior (*black arrow*) vena cava into the left atrium. (**c**) Four-chamber view cine TruFISP MRI sequence image shows drainage of pulmonary veins into the right atrium and right ventricular hypertrophy

3 Pulmonary Venous Anomalies

3.1 Normal Anatomy

In normal conditions, two superior and two inferior pulmonary veins drain into the left atrium. The right superior pulmonary vein drains the right upper and the middle lobes, the left superior drains the left upper lobe including the lingula, and the inferior pulmonary veins drain their respective lower lobes (Porres et al. 2013).

Almost 25% of the population has a deviation from the normal pulmonary venous drainage: common vein, accessory vein, or early branching vein (Türkvatan et al. 2017). Common pulmonary vein occurs when superior and inferior veins join proximally to the left atrium. By definition, a distance of 0.5 cm or larger between the virtual border of the left atrium and the pulmonary venous bifurcation is necessary for diagnosis. This is more common on the left side (14%) than on the right side (2%). Another variation is accessory vein defined by extra-veins draining

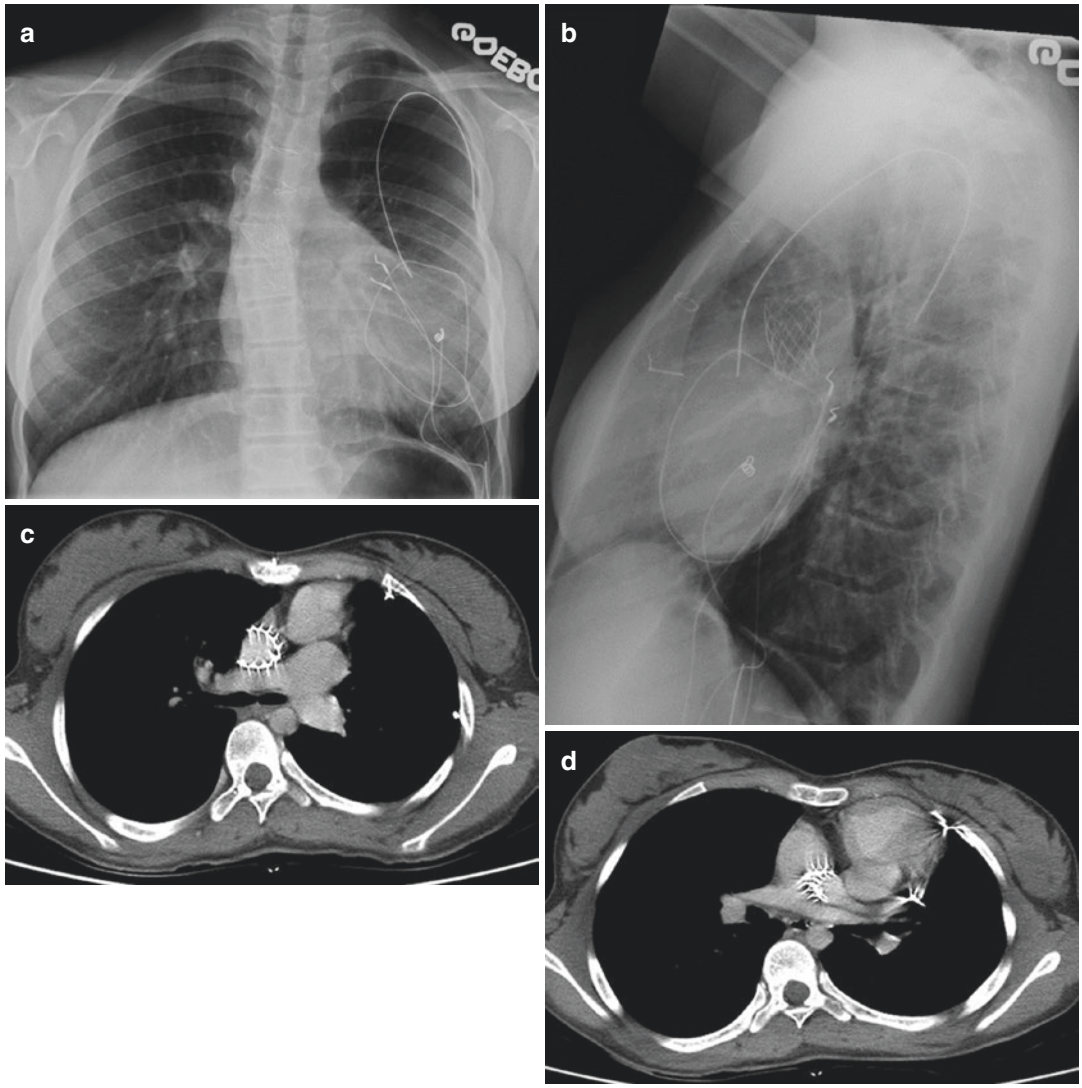

Fig. 8 Atrial switch (Mustard procedure) for D-transposition of great arteries and stent placement for obstruction of superior vena cava pathway on (**a**) frontal and (**b**) lateral chest radiographs; and on (**c**) and (**d**) axial contrast-enhanced CT images. Note the presence of epicardial leads of a pacemaker for arrhythmia

into the left atrium. The most frequent is separate drainage of the right middle lobe or superior segment of the right upper lobe with typically narrower atriopulmonary venous junction (Kaseno et al. 2008). Early branching is defined as bifurcation of the pulmonary vein in two or more separate branches within 1 cm of the origin of the left atrium.

All of these variations are incidental findings without any functional repercussion. However, these variations are important to describe in patient undergoing interventions on the pulmonary veins, such as radiofrequency catheter ablation for atrial fibrillation (Kaseno et al. 2008).

3.2 Congenital Anomalies

3.2.1 Partial Anomalous Pulmonary Venous Return (PAPVR)

The prevalence of PAPVR in general population is 0.4–0.7% (Porres et al. 2013; Herlong

et al. 2000). By definition, at least one, but not all pulmonary veins, drains outside of the left atrium. This anomaly creates a left-to-right shunt similar to atrial septal defect. The majority of patients are asymptomatic during infancy and childhood. The signs and symptoms depend on the magnitude of the shunt, on the hemodynamic change created by the shunt, and on the presence of associated cardiac anomalies (Ruano et al. 2015). A pulmonary-to-systemic flow ratio (QP:QS) of 1.5:1 generally requires surgical repair with low morbidity and mortality. Imaging findings on chest radiography will depend on the configuration of anomalous drainage and the degree of left-to-right shunting.

(a) **Right Upper Lobe PAPVR**
The right PAPVR is twice more frequent than the left. In this condition, the right superior pulmonary vein drains into the RSVC, the azygos vein, the right atrium, or the coronary sinus (Fig. 9). The most common type of PAPVR is right upper lobe drainage into the RSVC below the azygos vein through one large or two or three smaller veins (Geva and Van Praagh 2008b) (Fig. 10). The anomalous pulmonary venous return always involves the right superior pulmonary lobe but the middle pulmonary lobe can also be affected. Usually, the vein from the right lower lobe drains normally into the left atrium. A sinus venosus type of atrial septal defect is highly associated with right upper lobe PAPVR in pediatric population (80–90%) whereas a recent study in adults by Ho et al. showed a moderate association of 47% (Katre et al. 2012; Ho et al. 2009). The cephalic position of sinus venosus atrial septal defect is difficult to diagnose at transthoracic echocardiography. CT angiography and MR imaging are excellent modalities to demonstrate this anatomic region.

(b) **Left Upper Lobe PAPVR**
This anomaly represents the second most frequent type of PAPVR. On adult CT chest examinations, it is the most frequently detected anomalous pulmonary venous connection (Haramati et al. 2003). It is characterized by an aberrant vertical vessel that conducts blood in a cephalic direction from the left superior pulmonary vein to the LBCV which eventually drains into the normal RSVC (Fig. 11). The anomalous pulmonary venous return always involves the left superior pulmonary lobe or the entire left lung.
The anomalous vessel (the vertical vein) can be confused with the appearance of the LSVC. Both entities can be differentiated on

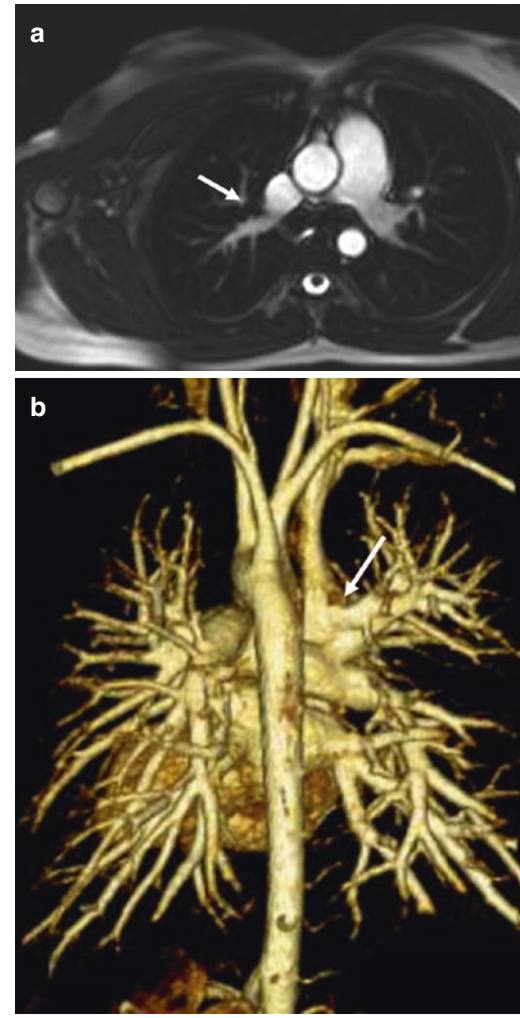

Fig. 9 Right superior anomalous pulmonary venous return at cardiac MRI. (**a**) Axial view image obtained from cine FLASH MRI sequence and (**b**) posterior volume rendering image demonstrate an anomalous drainage of right superior pulmonary vein into the right superior vena cava (*white arrows*)

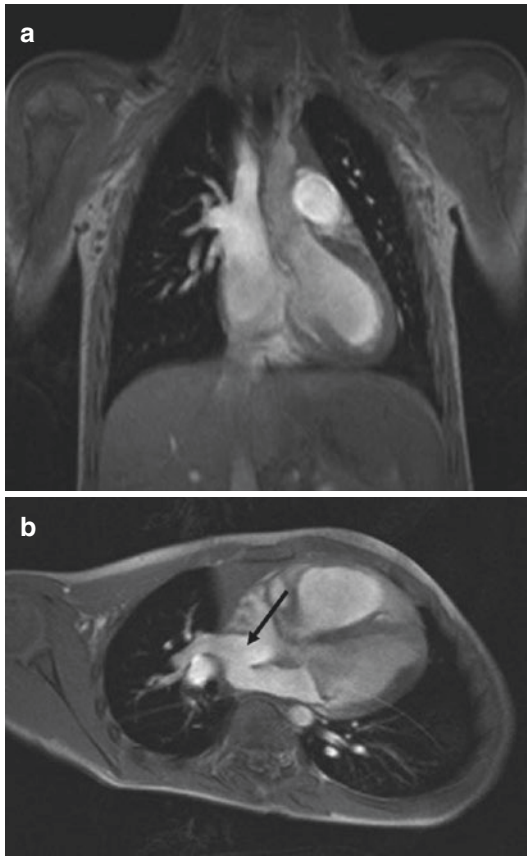

Fig. 10 Right superior anomalous pulmonary venous return at MRI. (**a**) Coronal oblique view and (**b**) axial oblique view images obtained from cine FLASH MRI sequence demonstrate an anomalous drainage of right superior pulmonary vein through two veins into the right superior vena cava (RSVC) and a sinus venosus type of atrial septal defect (*black arrow*). The anomalous drainage involves the right superior and middle pulmonary lobes. Note the drainage into RSVC is below the azygos vein

cross-sectional imaging by the following features: (1) the LSVC can be followed inferiorly to the coronary sinus (which is usually dilated); in PAPVR, the intra-parenchymal upper lobe vessels connect with the anomalous vein; (2) in patients with LSVC, two vessels are seen anterior to the left main bronchus, the normal left superior pulmonary vein, and the LSVC; in patients with PAPVR, no vessel is seen anterior to the bronchus; (3) LSVC conducts blood caudally from the left subclavian and jugular veins into the right atrium; in PAPVR, the abnormal vein conducts blood cranially from the left upper lobe to the LBCV (Ruano et al. 2015; Katre et al. 2012; Maldonado et al. 2010; Dillon and Camputaro 1993).

(c) **Scimitar Syndrome**

Scimitar syndrome or pulmonary venolobar syndrome is a rare and complex form of PAPVR that almost exclusively involves the right lung (Türkvatan et al. 2017). This anomaly is characterized by an anomalous pulmonary vein draining a portion or the entire right pulmonary venous flow to the supradiaphragmatic or infradiaphragmatic IVC. The crescent-shaped abnormal vein descends in a caudal direction toward the diaphragm. The radiologic appearance of this anomalous vein resembles a curved Turkish sword or "scimitar" from which the name of this condition is derived (Gudjonsson and Brown 2006). The anomalous right pulmonary vein usually drains the entire right lung but rarely may drain only the middle and lower lobes (Katre et al. 2012). It is associated most of the time with hypoplasia of the right lung and right pulmonary artery, and cardiac dextroposition (Fig. 12). The right lung may have abnormal lobation with only two lobes (Konen et al. 2003). The atrial septum is usually intact (Geva and Van Praagh 2008b). An anomalous arterial supply to the right lower lung from the aorta or its branches is also frequent and often supplies pulmonary sequestration. This late finding is more commonly seen in infancy.

The presentation of the syndrome can be incomplete or complete. The scimitar syndrome is usually divided into three main forms: infantile form with symptoms and pulmonary hypertension, an "older" adult form, which is typically asymptomatic in infancy, and a form with associated CHD (Vida et al. 2010).

Goodman and colleagues described an entity closely related to scimitar syndrome: meandering pulmonary vein or pseudo-scimitar

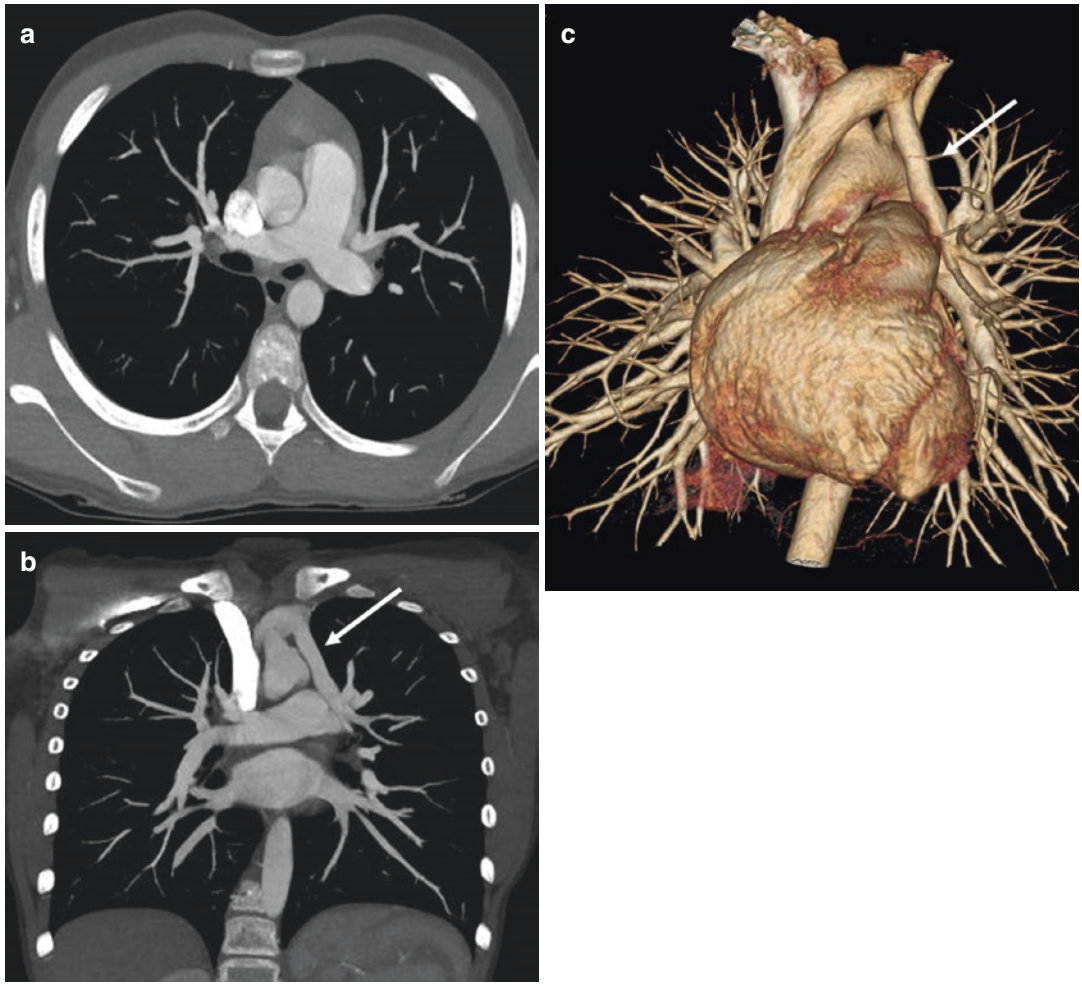

Fig. 11 Left superior anomalous pulmonary venous return at CT angiography. (**a**) Axial, (**b**) coronal thin maximum intensity projection, and (**c**) anterior volume rendering images demonstrate an anomalous drainage of left superior pulmonary vein into the left brachiocephalic vein through an aberrant vertical vessel (*white arrows*)

syndrome (Goodman et al. 1972). It consists of an anomalous right pulmonary vein that courses through the right lung presenting as a scimitar-shaped structure on the chest radiograph, but ultimately drains into the left atrium (Goodman et al. 1972; Lee 2007). Most reported cases of pseudo-scimitar syndrome or scimitar variant connect to the left atrium and IVC simultaneously (Lee 2007; Mohiuddin et al. 1966; Morgan and Forker 1971; Gazzaniga et al. 1969; Pearl 1987; Tumbarello et al. 1991) (Fig. 13). Either surgery or transcatheter endovascular treatments can be performed to close this dual venous drainage anomaly depending on individual anatomy.

(d) **Other**

Anomalous dual pulmonary venous drainage can exist as a PAPVR equivalent described with levoatrial cardinal vein (Türkvatan et al. 2017) (Fig. 14). The levoatrial cardinal vein connects the left atrium or one of the pulmonary veins to a systemic vein, usually the left innominate vein. In this situation, a portion of the lung drains into the left atrium and a systemic vein. The direction of the flow is predominantly

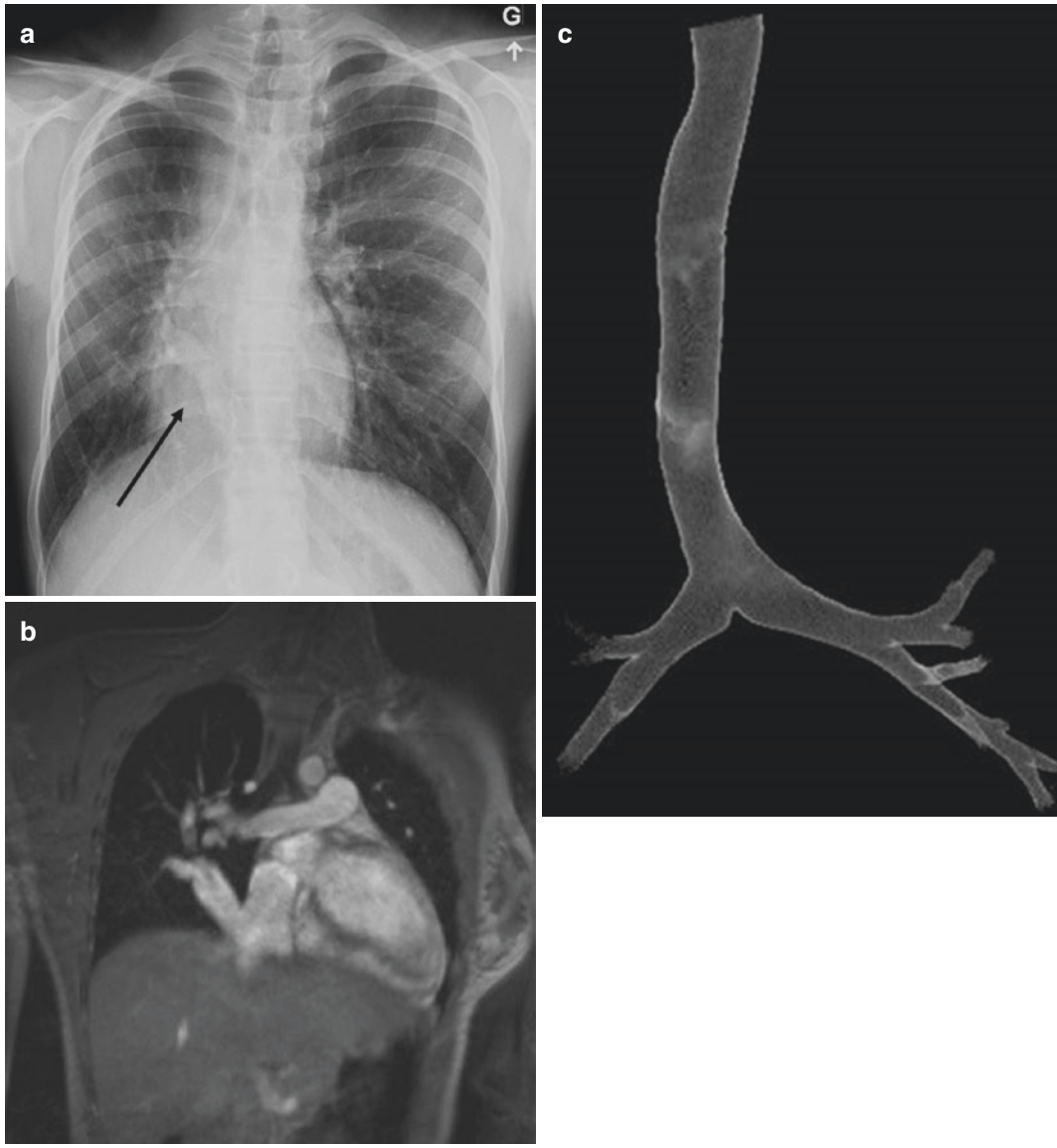

Fig. 12 Scimitar syndrome. (**a**) Frontal chest radiograph shows hypoplasia of right lung, cardiac dextroposition, and a crescent-shaped abnormal vein (*black arrow*). (**b**) Coronal oblique view image obtained from cine FLASH MRI sequence demonstrates a right inferior pulmonary vein draining into the inferior vena cava. (**c**) Coronal volume-rendered CT image helps confirm abnormal bronchial lobation with only two right pulmonary lobes

cephalad away from the left atrium, resulting in a left-to-right shunt. The flow can also be bidirectional, so patients are at risk of right-to-left shunting complications. Transcatheter endovascular treatments have been described (Peynircioglu et al. 2005).

Also, this entity can be associated with obstructive left heart lesions. In this situation, this abnormal draining vein permits the decompression of pulmonary venous blood flow into the systemic venous circulation.

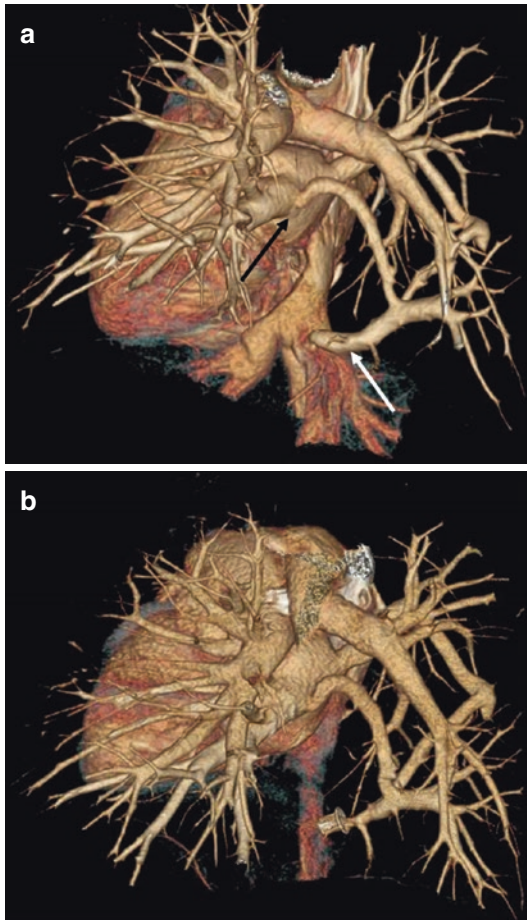

Fig. 13 Pseudo-scimitar syndrome at CT angiography. (**a**) Posterior oblique volume rendering image demonstrates a right inferior pulmonary vein draining abnormally into the inferior vena cava (*white arrow*) and also into the left atrium (*black arrow*). (**b**) Posterior oblique volume rendering image from CT angiography realized after percutaneous intervention shows a device occluding the connection between the right inferior pulmonary vein and inferior vena cava

Fig. 14 Levoatrial cardinal vein at CT angiography. Coronal thin maximum intensity projection image demonstrates a levoatrial cardinal vein (*white arrow*) connecting the left superior pulmonary vein to the left brachiocephalic vein. The left superior pulmonary vein drains also normally into left atrium

3.2.2 Total Anomalous Pulmonary Venous Return (TAPVR)

TAPVR is a rare form of CHD in which all pulmonary veins have no connection to the left atrium. Other cardiac lesions are found in 15% of patients (Seale et al. 2010). TAPVR can occur in patients with heterotaxy syndrome with asplenia. It is classified in four major subtypes based on the level of drainage as follows: type I, anomalous connection at the supracardiac level; type II, anomalous connection at the cardiac level; type III, anomalous connection at the infracardiac level; and type IV, anomalous connection at two or more above levels (Geva and Van Praagh 2008b).

The supracardiac type represents the most frequent subtype, 40–55% of cases (Katre et al. 2012). In this type, connection to the left innominate vein is found frequently (Karamlou et al. 2007), giving the classical snowman appearance on chest X-ray (Fig. 15). Other less common supracardiac venous connections include RSVC and azygos veins. In type II, the second most common type, the pulmonary veins connect to coronary sinus or the right atrium (Fig. 16). In type III, the pulmonary veins connect in 80–90% of cases to the portal vein through a common vertical descending vein which courses anterior to the esophagus and crosses the diaphragm at the esophagus hiatus. Rarely, the vertical vein can connect to the ductus venosus, IVC or hepatic veins (Katre et al. 2012). With this type, the

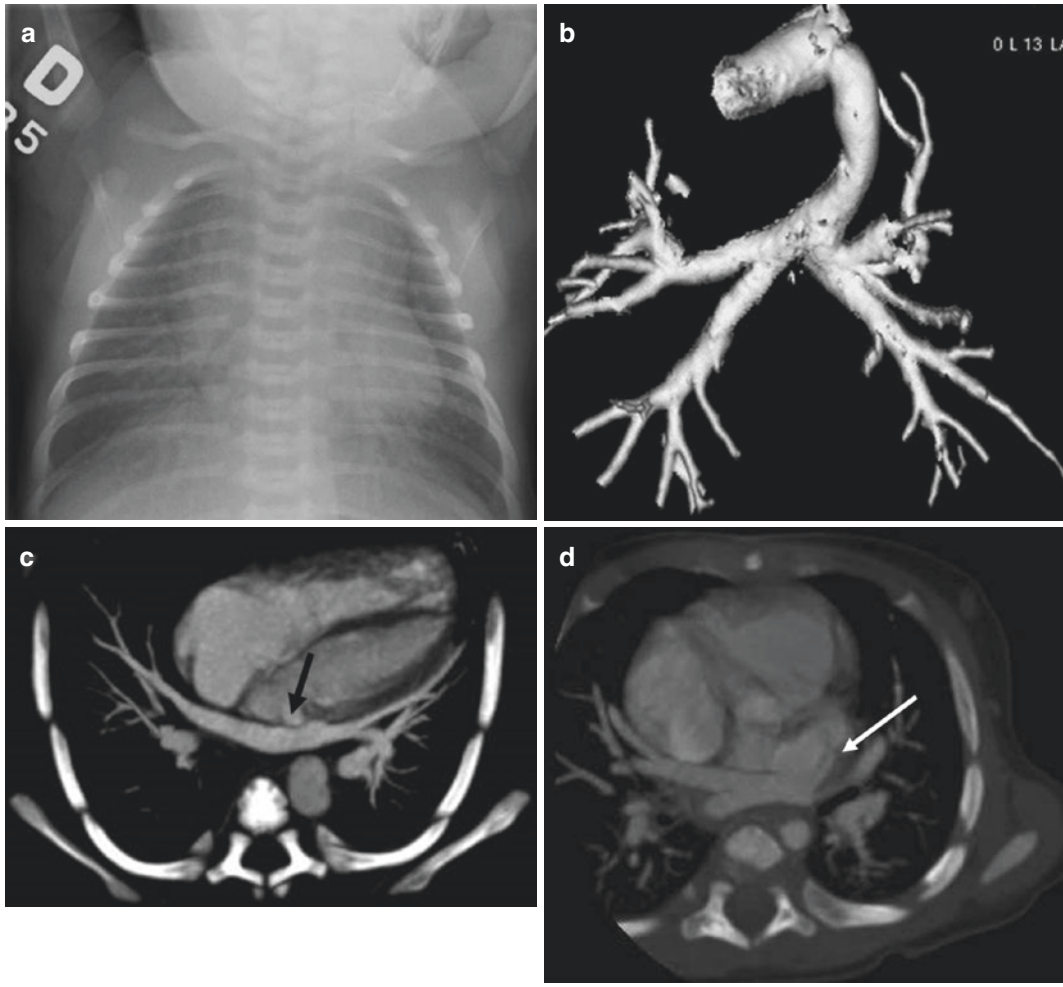

Fig. 15 Supracardiac type of total anomalous pulmonary venous return (type 1). (**a**) Frontal chest radiograph shows an enlargement of superior mediastinum snowman shape and increased pulmonary arterial vascularization. (**b**) Anterior volume rendering image from CT angiography shows all pulmonary veins draining into common pulmonary vein that connects to left brachiocephalic vein through a vertical vein. (**c**) Four-chamber view thin maximum intensity projection image demonstrates a posterior position to the left atrium of pulmonary vein confluence (*black arrow*). (**d**) Axial oblique thin maximum intensity projection image from CT angiography realized 10 days after surgical correction shows a large anastomosis between the left atrium and the pulmonary vein confluence (*white arrow*)

anomalous connection is virtually always accompanied by some degree of venous obstruction.

This entity induces cyanosis and an atrial septal defect or patent foramen ovale is necessary to sustain life. Anatomically, for most types of TAPVR, the pulmonary veins from each lung join to form a confluence posterior to the left atrium and then connect abnormally. The patients with such a condition should be corrected surgically as soon as possible.

The basis of the correction is the creation of a large anastomosis between the left atrium and the pulmonary vein confluence (Geva and Van Praagh 2008b). The long-term prognostic appears to depend mainly on the state of the pulmonary vascular bed at the time of operation and the adequacy of the pulmonary venous-left atrial anastomosis. Despite an initial satisfactory course, pulmonary venous obstruction (PVO) develops in 5–18%, often within 3 to 6

Fig. 16 Total anomalous pulmonary venous return into coronary sinus at CT angiography. Posterior volume rendering image shows all pulmonary veins draining into common pulmonary vein (*black arrow*) that connects to coronary sinus (*white arrow*)

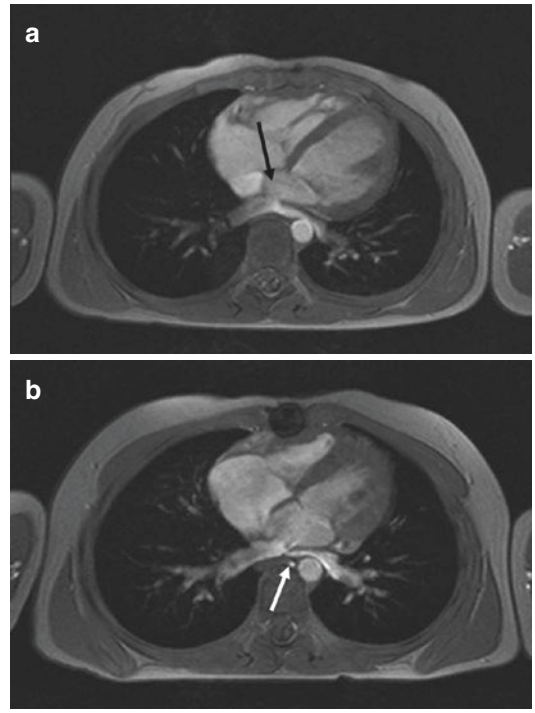

Fig. 17 Postoperative pulmonary venous obstruction after surgical repair of total anomalous pulmonary venous return at MRI. (**a**) MRI realized one month after repair. Four-chamber view image obtained from cine FLASH MRI sequence demonstrates a large anastomosis between the left atrium and the pulmonary vein confluence (*black arrow*) and good size of pulmonary veins. (**b**) MRI realized four months after repair. Four-chamber image obtained from cine FLASH MRI sequence demonstrates a progressive stenosis on the left pulmonary vein near the venoatrial anastomosis (*white arrow*)

months and can be progressive (Seale et al. 2010; Karamlou et al. 2007; Lacour-Gayet et al. 1999; Caldarone et al. 1998) (Fig. 17). Identified risk factors for development of postoperative pulmonary venous obstruction are preoperative hypoplasic/stenotic pulmonary veins and absence of a common confluence (Seale et al. 2010; Caldarone et al. 1998). Estimates of 30-day, 1-year, and 3-year survival for all patients with postoperative PVO were 95.8%, 62.0%, and 58.7%, respectively, which are worse than that of patients without postoperative PVO, in whom 30-day, 1-year, and 3-year survivals were 94.0%, 91.2%, and 91.2%, respectively (Seale et al. 2010, 2013). Risk factors for death included earlier presentation after TAPVC repair, diffusely small pulmonary veins at presentation of postoperative PVO, and an increased number of lung segments affected by obstruction (Seale et al. 2013). According to the study of Seale et al., patients presenting with pulmonary venous obstruction six months after surgical correction had less severe disease (Seale et al. 2013). Postoperative PVO may be a consequence of an inadequate anastomosis between the left atrium and the pulmonary venous confluence, inadequate postoperative growth of the surgical anastomosis, a reaction of tissues to prosthetic material used, or pre/postoperative pulmonary vein hypoplasia/stenosis (Seale et al. 2010; Sano et al. 1989; Whight et al. 1978).

3.2.3 Cor Triatriatum

Cor triatriatum is a rare congenital anomaly defined by the presence of a fibromuscular membrane dividing the left atrium into proximal and distal chambers. The proximal (superior and posterior) accessory chamber receives inflow from all four pulmonary veins and the distal (inferior and anterior) main left atrial chamber (including the left atrial appendage and mitral orifice) delivers blood flow to the mitral valve (Figs. 18 and 19). The proximal chamber has been described as

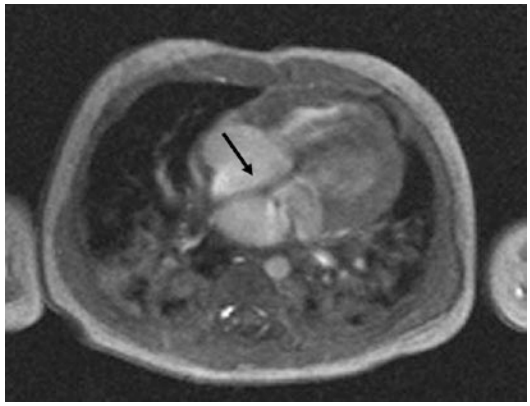

Fig. 18 Obstructive cor triatriatum at MRI. Four-chamber view image obtained from cine FLASH MRI sequence shows an obstructive membrane (*black arrow*) dividing the left atrium into proximal and distal chambers. Pulmonary parenchymal edema was also noted

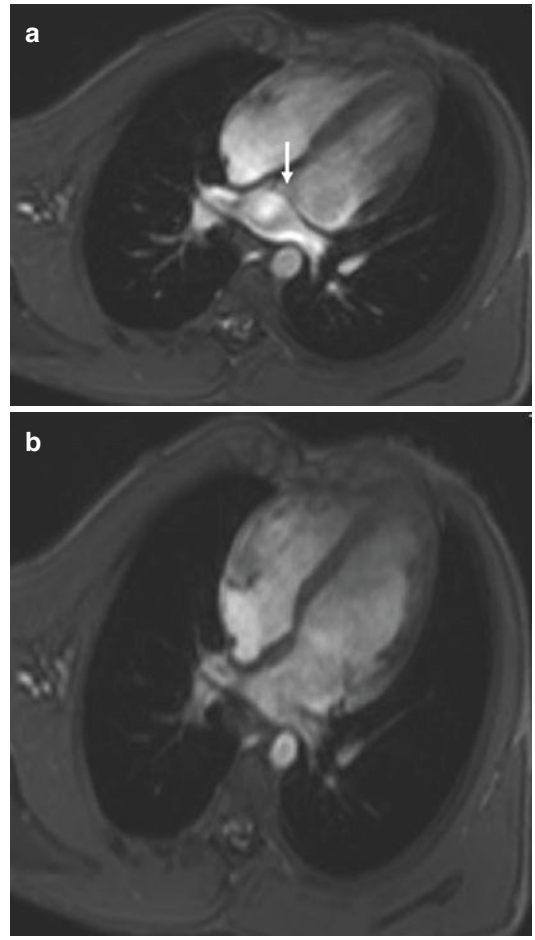

Fig. 19 Non-obstructive cor triatriatum at MRI. (**a**), (**b**) Four-chamber view images obtained from cine TruFISP MRI sequence show a membrane (*white arrow*) dividing the left atrium into proximal and distal chambers. During the cardiac cycle, a large opening was demonstrated through the membrane

common pulmonary vein or third atrium. The reported incidence is 0.1–0.4% (Niwayama 1960).

Many classifications exist and depend on the presence of other anomalies (Capdeville et al. 2014) (Fig. 20). The most common congenital defect is atrial septal defect or patent foramen ovale. A secundum atrial septal defect can communicate with either or both chambers, and the foramen ovale almost always communicates with the true left atrium. The other variation coexisting with this entity is total or partial anomalous pulmonary venous return (Kouchoukos et al. 2003). In right-sided partial anomalous return, the right-sided veins join with each other to drain into the anomalous proximal chamber, while left-sided pulmonary veins drain into the left atrium. In left-sided partial anomalous venous return, left-sided veins join to form a left vertical vein which connects to the left innominate vein and the right-sided pulmonary veins connect to the anomalous proximal chamber (Kouchoukos et al. 2003) (Fig. 21).

The natural history depends on the size of the membrane fenestration and the presence or absence of an atrial septal defect, as well as its location (Capdeville et al. 2014). When fenestration is small and no ASD is present, the presentation is typically in infancy. Conversely, if an atrial septal defect communicates with the pulmonary venous chamber, partial decompression can occur, thereby potentially delaying the presentation. Symptoms usually associated with that pathology can be similar to the symptoms of mitral valve stenosis such as dyspnea, orthopnea, and hemoptysis, but some are asymptomatic (incidental finding) (Eichholz et al. 2013). It is

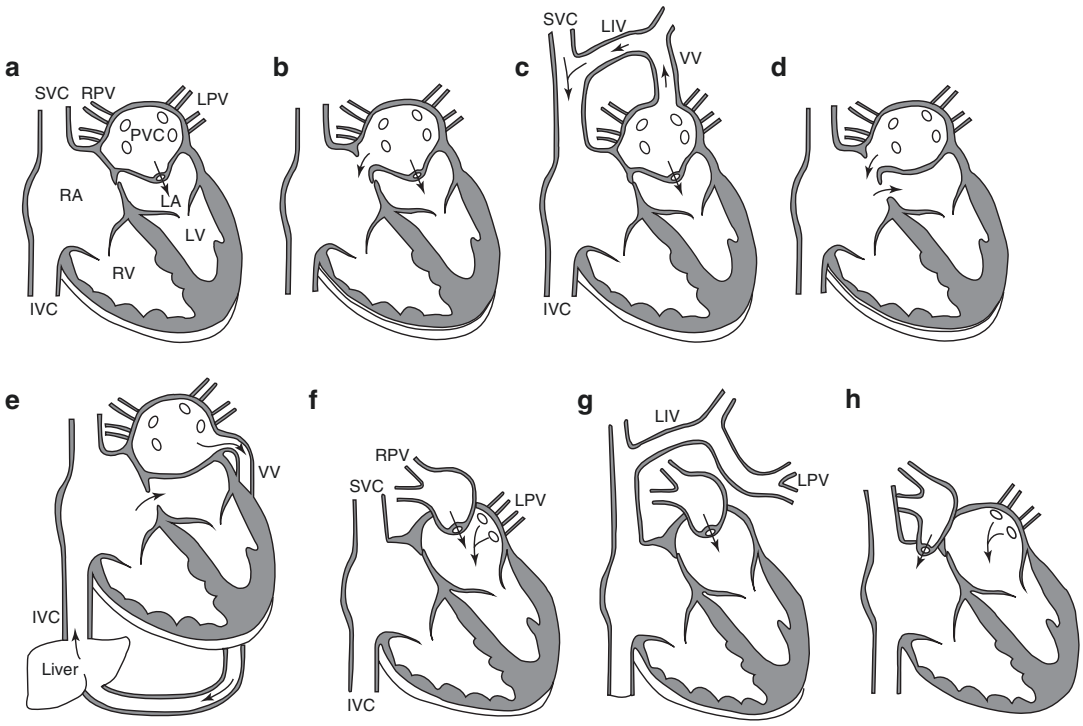

Fig. 20 Schematic representation of various types of cor triatriatum. The difference between the various types is based mainly on the pulmonary venous return and the location of the atrial septum defect. *Reprinted with permission from Allen* et al. (Geva and Van Praagh 2008b)

not clear why patients with large fenestration become symptomatic in adulthood. Potential factors include fibrosis or calcification of the membrane's orifice and the development of mitral regurgitation or atrial fibrillation (Eichholz et al. 2013).

3.2.4 Congenital Pulmonary Vein Stenosis

Congenital pulmonary vein stenosis is a rare and severe form of CHD. The congenital pulmonary vein stenosis may represent a hypoplasia of the entire vein or a focal lesion along the course of pulmonary vein (Türkvatan et al. 2017) (Figs. 22, 23, and 24). This anomaly can be unilateral or bilateral. It is usually found during the newborn period and often leads to progressive pulmonary hypertension and premature death. Few cases have been reported in the adult population (Kim et al. 2011; Kapoor et al. 2011; Omasa et al. 2004). No consensus exists regarding the optimal treatment strategy for this anomaly (Devaney et al. 2006; Gordon and Moore 2010; Seale et al. 2006; Peng et al. 2010). Several interventions have been proposed: balloon angioplasty, surgical dilatation, and surgical marsupialization. No statistically significant difference in mortality or re-intervention rate was present among these different therapeutic modalities according to Charlagorla et al. (Charlagorla et al. 2016). Patients with bilateral disease have increased mortality and decreased 5-year survival. According to this same study (the longest follow-up of this pathology to date), the overall survival rate at 58 months is 78% (Charlagorla et al. 2016).

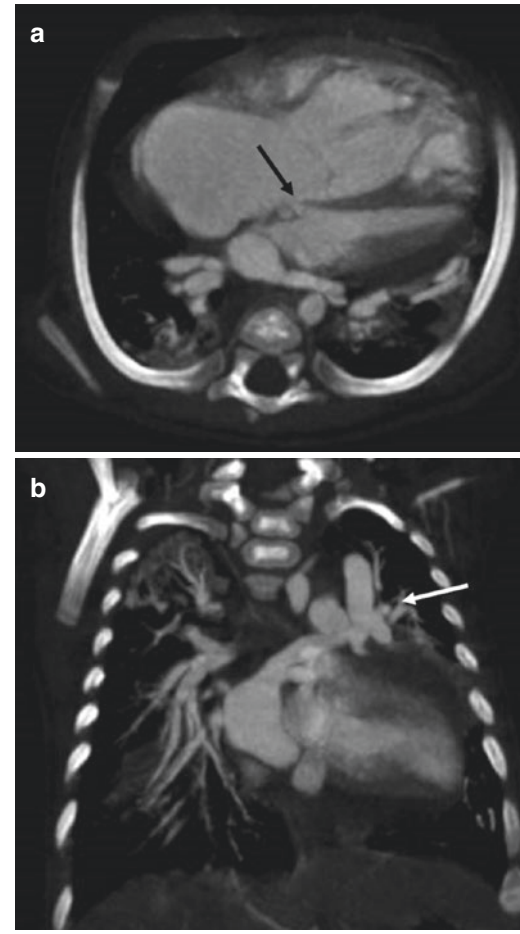

Fig. 21 Obstructive cor triatriatum and left partial anomalous pulmonary venous return at CT angiography. (**a**) Axial oblique and (**b**) coronal oblique thin maximum intensity projection images demonstrate membrane dividing the left atrium and a partial anomalous pulmonary venous return of the left superior pulmonary vein into a vertical vein (*white arrow*). The right pulmonary veins and the left inferior pulmonary veins drain into the anomalous proximal chamber. A small secundum atrial septal defect (*black arrow*) is also present between the right and the left atrium (distal chamber)

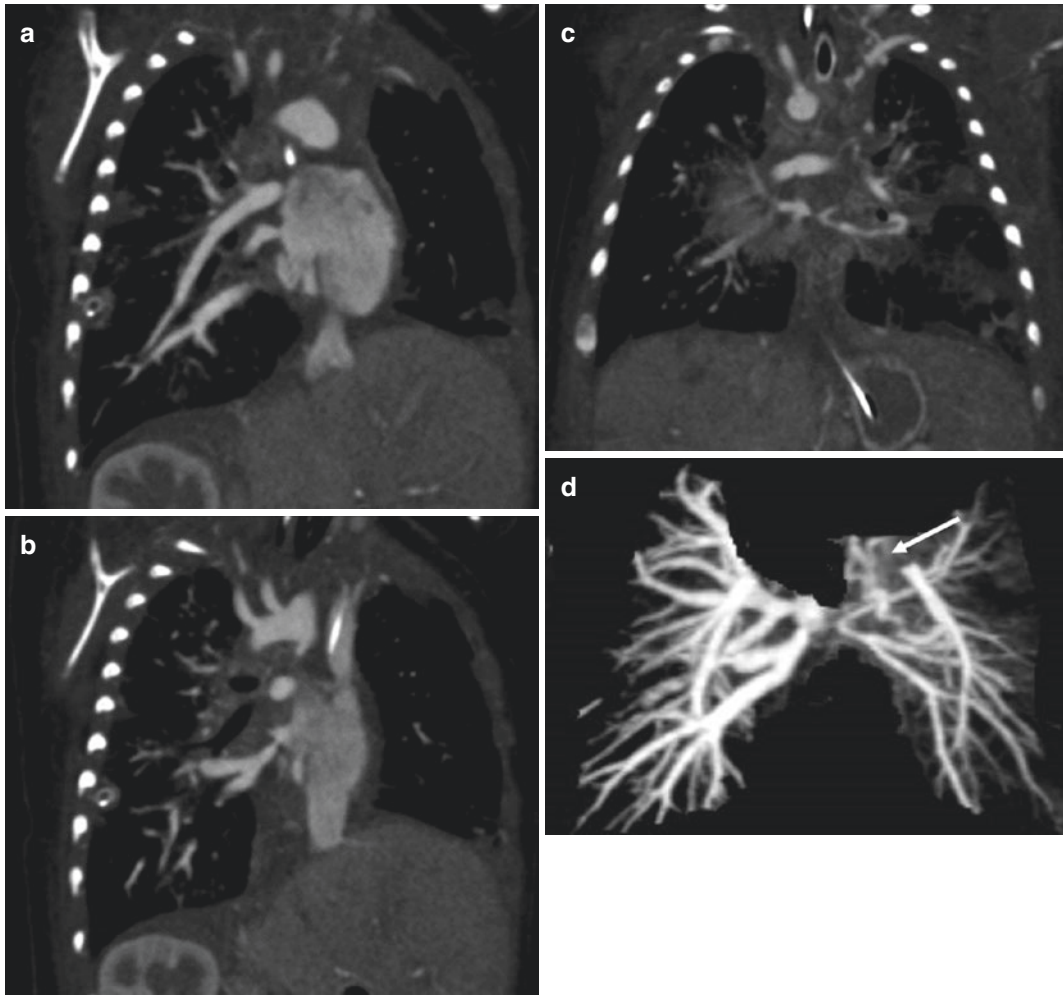

Fig. 22 Pulmonary vein stenosis at CT angiography. (**a**)–(**c**) Coronal oblique thin maximum intensity projection (MIP) images and (**d**) volume rendering demonstrate hypoplasia of the left pulmonary veins and focal stenosis involving all the pulmonary veins at the venoatrial junction. On the left side, venous collaterals are visualized (*white arrow*)

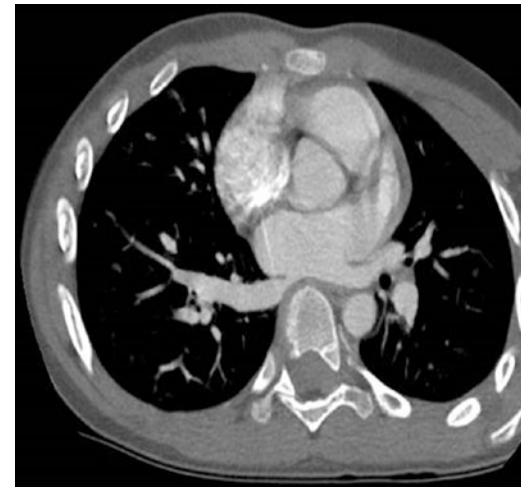

Fig. 23 Right inferior pulmonary vein stenosis at CT angiography. Axial oblique thin maximum intensity projection images demonstrate a focal stenosis of right inferior pulmonary vein near the venoatrial junction

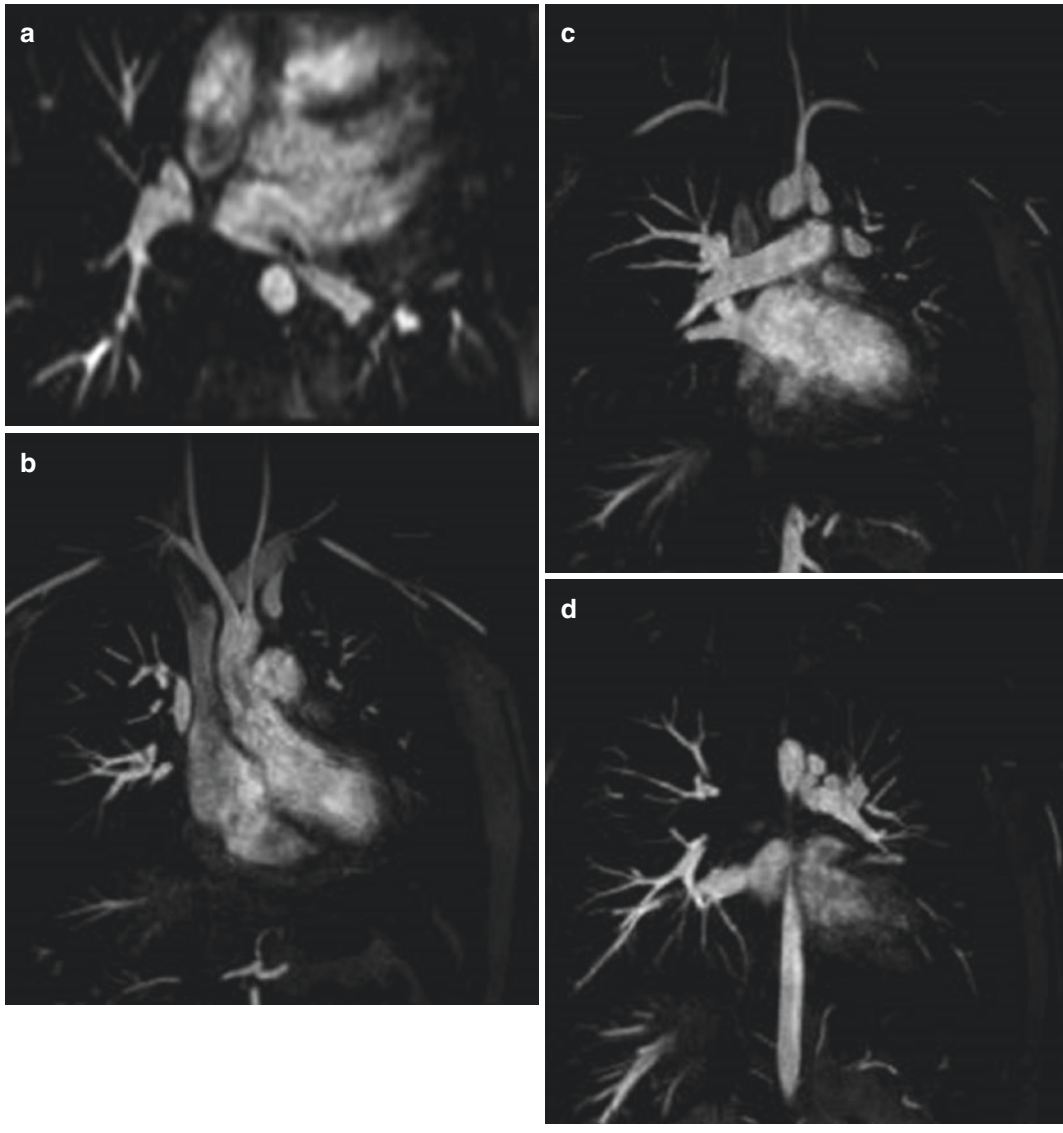

Fig. 24 Left pulmonary vein stenosis at cardiac MRI. (**a**) Axial oblique view image obtained from cine TruFISP MRI sequence shows a severe stenosis involving the left common pulmonary vein. (**b**)–(**g**) Coronal thin maximum intensity projection and (**h**) posterior volume rendering images from MR angiography demonstrate severe focal stenosis of left pulmonary vein (*black arrow*) with presence of venous collaterals draining into the left brachiocephalic through the left superior intercostal vein (*white arrow*)

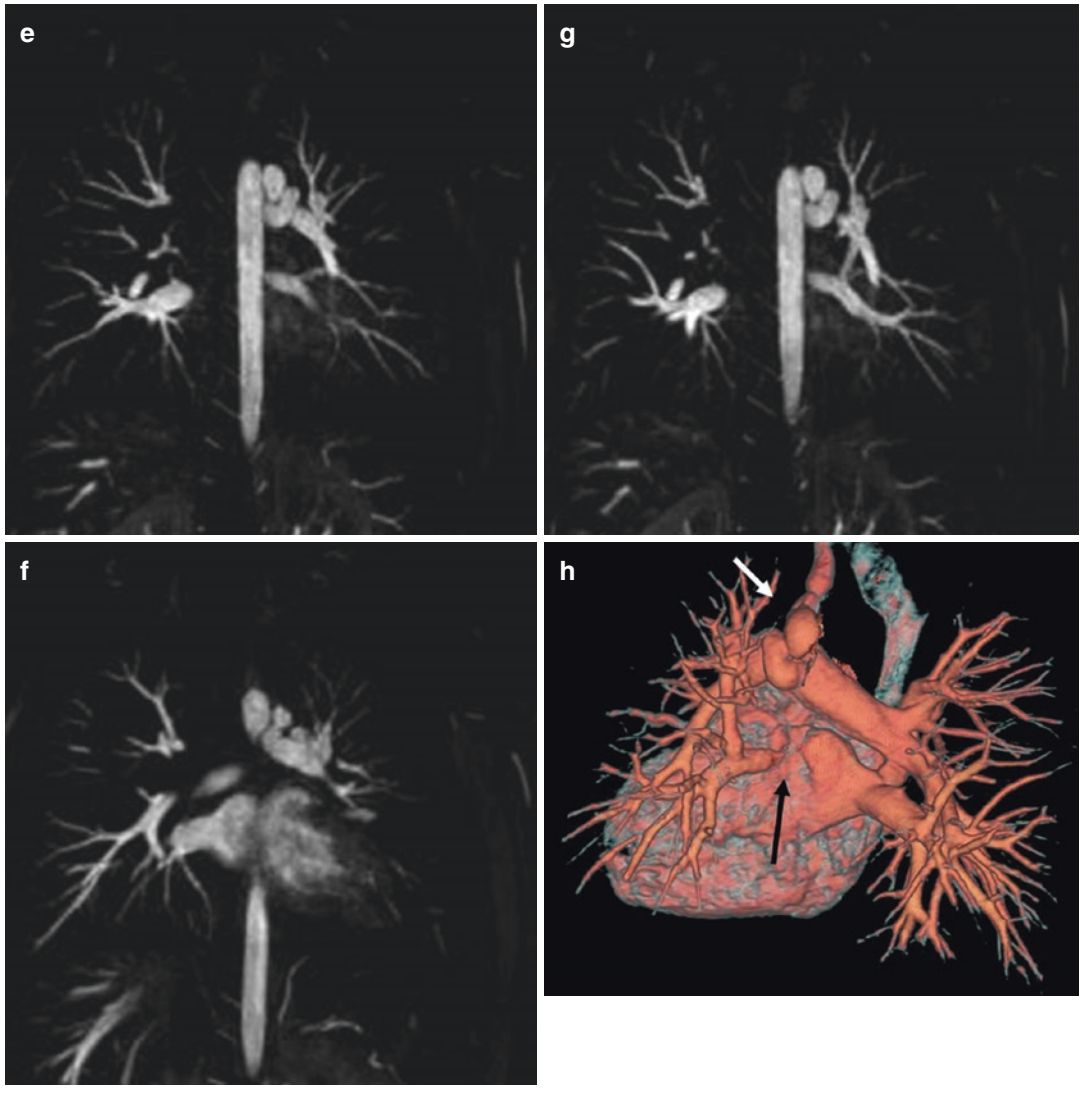

Fig. 24 (continued)

Conclusion

Congenital pulmonary and systemic venous anomalies have a broad spectrum and their clinical presentations vary. CT or MR imaging is usually necessary in order to characterize accurately these entities.

References

Biffi M, Boriani G, Frabetti L et al (2001) Left superior vena cava persistence in patients undergoing pacemaker or cardioverter-defibrillator implantation: a 10-year experience. Chest 120(1):139–144

Caldarone CA, Najm HK, Kadletz M, Smallhorn JF, Freedom RM, Williams WG, Coles JG (1998) Relentless pulmonary vein stenosis after repair of total anomalous pulmonary venous drainage. Ann Thorac Surg 66(5):1514–1520

Capdeville M, Brozzi N, Pettersson G, Gillinov AM, Niezgoda J (2014) Case 3–2014: Cor triatriatum sinister presenting in adulthood. J Cardiothorac Vasc Anesth 28(2):408–416

Cha EM, Khoury GH (1972) Persistent left superior vena cava. Radiologic and clinical significance. Radiology 103(2):37–81

Charlagorla P, Becerra D, Patel PM, Hoyer M, Darragh RK (2016) Congenital pulmonary vein stenosis: encouraging mid-term outcome. Pediatr Cardiol 37:125–130

Cormier MG, Yedlicka JW, Gray RJ et al (1989) Congenital anomalies of the superior vena cava: a CT study. Semin Roentgenol 24:77–83

Devaney EJ, Chang AC, Ohye RG, Bove EL (2006) Management of congenital and acquired pulmonary vein stenosis. Ann Thorac Surg 81(3):992–996

Dillon EH, Camputaro C (1993) Partial anomalous pulmonary venous drainage of the left upper lobe vs duplication of the superior vena cava: distinction based on CT findings. Am J Roentgenol 160(2):375–379

Dudiak CM, Olson MC, Posniak HV (1991) CT evaluation of congenital and acquired abnormalities of the azygos system. Radiographics 11(2):233–246

Eichholz JL, Hodroge SS, Crook JJ 2nd, Mack JW Jr, Wortham DC (2013) Cor triatriatum sinister in a 43-year-old man with syncope. Tex Heart Inst J 40(5):602–605

Freedom RM, Schaffer MS, Rowe RD (1982) Anomalous low insertion of right superior vena cava. Br Heart J 48:601–603

Gazzaniga AB, Matloff JM, Harken DE (1969) Anomalous right pulmonary venous drainage into the inferior vena cava and left atrium. J Thorac Cardiovasc Surg 57(2):251–254

Geva T, Van Praagh S (2008a) Chapter 38: Abnormal systemic venous connections. In: Allen HD, Driscoll DJ, Shaddy RE, Feltes TF (eds) Moss and Adams' heart disease in infants, children, and adolescents including the fetus and young adult (volume 2), 7th edn. Wolters Kluwer, Lippincott, Williams and Wilkins, Philadelphia, pp 792–817

Geva T, Van Praagh S (2008b) Chapter 37: Anomalies of the pulmonary veins. In: Allen HD, Driscoll DJ, Shaddy RE, Feltes TF (eds) Moss and Adams' heart disease in infants, children, and adolescents including the fetus and young adult (volume 2), 7th edn, Wolters Kluwer, Lippincott, Williams and Wilkins, Philadelphia, pp 761–792

Gonzalez-Juanatey C, Testa A, Vidan J et al (2004) Persistent left superior vena cava draining into the coronary sinus: report of 10 cases and literature review. Clin Cardiol 27(9):515–518

Goodman LR, Jamshidi A, Hipona FA (1972) Meandering right pulmonary vein simulating the scimitar syndrome. Chest 62(4):510–512

Gordon BM, Moore JW (2010) Treatment of pulmonary vein stenosis with expanded polytetrafluoroethylene covered stents. Catheter Cardiovasc Interv 75(2):263–267

Gudjonsson U, Brown JW (2006) Scimitar syndrome. Semin Thorac Cardiovasc Surg Pediatr Card Surg Annu 56–62

Haramati LB, Moche IE, Rivera VT et al (2003) Computed tomography of partial anomalous pulmonary venous connection in adults. J Comput Assist Tomogr 27(5):743–749

Hellinger JC, Daubert M, Lee EY, Epelman M (2011) Congenital thoracic vascular anomalies: evaluation with state-of-the-art MR imaging and MDCT. Radiol Clin N Am 49(5):969–996

Herlong JR, Jaggers JJ, Ungerleider RM (2000) Congenital heart surgery nomenclature and database project: pulmonary venous anomalies. Ann Thorac Surg 69(4 Suppl):S56–S69

Ho ML, Bhalla S, Bierhals A, Gutierrez F (2009) MDCT of partial anomalous pulmonary venous return (PAPVR) in adults. J Thorac Imaging 24(2):89–95

James TN, Marshall TK, Edwards JE (1976) De subitaneis morbitus. XX. Cardiac electrical instability in the presence of a left superior vena cava. Circulation 54(4):689–697

Kapoor A, Walia R, Jain SK, Kumar S, Radhakrishnan S (2011) Isolated congenital left-sided pulmonary vein stenosis in an adult patient misdiagnosed as primary pulmonary hypertension. Echocardiography 28(5):E97–100

Karamlou T, Gurofsky R, Al Sukhni E et al (2007) Factors associated with mortality and reoperation in 377 children with total anomalous pulmonary venous connection. Circulation 115(120):1591–1598

Kaseno K, Tada H, Koyama K et al (2008) Prevalence and characterization of pulmonary vein variants in patients with atrial fibrillation determined using 3-dimensional computed tomography. Am J Cardiol 101(11):1638–1642

Katre R, Burns SK, Murillo H et al (2012) Anomalous pulmonary venous connections. Semin Ultrasound CT MR 33(6):485–499

Kim YH, Pak HN, Park SM, Shim WJ (2011) Congenital pulmonary vein stenosis in an adult patient treated with

transcatheter balloon angioplasty. Eur J Echocardiogr 12(3):E13
Konen E, Raviv-Zilka L, Cohen RA et al (2003) Congenital pulmonary venolobar syndrome: spectrum of helical CT findings with emphasis on computerized reformatting. Radiographics 23(5):1175–1184
Kouchoukos NT, Blackstone EH, Doty DB, Hanley FL, Karp RB (eds) (2003) Cardiac surgery. In: Cor triatriatum sinistra, 3rd edn, vol 1. Churchill Livingstone, Philadelphia, pp 781–789
Lacour-Gayet F, Zoghbi J, Serraf AE, Belli E, Piot D, Rey C, Marcon F, Bruniaux J, Planché C (1999) Surgical management of progressive pulmonary venous obstruction after repair of total anomalous pulmonary venous connection. J Thorac Cardiovasc Surg 117(4):679–687
Lee ML (2007) Isolated and complex scimitar vein anomalies and their differentiation from the meandering right pulmonary vein. Yonsei Med J 48(6):973–980
Maldonado JA, Henry T, Gutiérrez FR (2010) Congenital thoracic vascular anomalies. Radiol Clin N Am 48(1):85–115
Modry DL, Hidvegi RS, La Fleche LR (1980) Congenital saccular aneurysm of the superior vena cava. Ann Thorac Surg 29(3):258–262
Mohiuddin SM, Levin HS, Runco V et al (1966) Anomalous pulmonary venous drainage. A common trunk emptying into the left atrium and inferior vena cava. Circulation 34(1):46–51
Morgan JR, Forker AD (1971) Syndrome of hypoplasia of the right lung and dextroposition of the heart: "scimitar sign" with normal pulmonary venous drainage. Circulation 43(1):27–30
Mueller GC, Lu JC, Mahani MG, Dorfman AL, Agarwal PP (2015) MR imaging of thoracic veins. Magn Reson Imaging Clin N Am 23:293–307
Niwayama G (1960) Cor triatriatum. Am Heart J 59:291–317
Omasa M, Hasegawa S, Bando T, Okano Y, Otani H, Nakashima Y et al (2004) A case of congenital pulmonary vein stenosis in an adult. Respiration 71(1):92–94
Park HM, Summerer MH, Preuss K et al (1983) Anomalous drainage of the right superior vena cava into the left atrium. J Am Coll Cardiol 2(2):358–362
Pearl W (1987) Scimitar variant. Pediatr Cardiol 8(2):139–141
Peng LF, Lock JE, Nugent AW, Jenkins KJ, McElhinney DB (2010) Comparison of conventional and cutting balloon angioplasty for congenital and postoperative pulmonary vein stenosis in infants and young children. Catheter Cardiovasc Interv 75(7):1084–1090
Peynircioglu B, Williams DM, Rubenfire M et al (2005) Endograft repair of partially anomalous pulmonary venous connection with dual drainage. J Vasc Surg 42(6):1221–1225
Porres DV, Morenza OP, Pallisa E et al (2013) Learning from the pulmonary veins. Radiographics 33(4):999–1022
Pretorius PM, Gleeson FV (2004) Case 74: right-sided superior vena cava draining into left atrium in a patient with persistent left-sided superior vena cava. Radiology 232(3):730–734
Rahmani N, White CS (2008) MR imaging of thoracic veins. Magn Reson Imaging Clin N Am 16(2):249–262
Ruano CA, Marinho-da-Silva A, Donato P (2015) Congenital thoracic venous anomalies in adults: morphologic MR imaging. Curr Probl Diagn Radiol 44(4):337–345
Sano S, Brawn WJ, Mee RB (1989) Total anomalous pulmonary venous drainage. J Thorac Cardiovasc Surg 97(6):886–892
Seale AN, Daubeney PE, Magee AG, Rigby ML (2006) Pulmonary vein stenosis: initial experience with cutting balloon angioplasty. Heart 92(6):815–820
Seale AN, Uemura H, Webber SA et al (2010) Total anomalous pulmonary venous connection: morphology and outcome from an international population-based study. Circulation 122(25):2718–2726
Seale AN, Uemura H, Webber SA, Partridge J, Roughton M, Ho SY, McCarthy KP, Jones S, Shaughnessy L, Sunnegardh J, Hanseus K, Berggren H, Johansson S, Rigby ML, Keeton BR, Daubeney PE (2013) British congenital cardiac association. Total anomalous pulmonary venous connection: outcome of postoperative pulmonary venous obstruction. J Thorac Cardiovasc Surg 145(5):1255–1262
Tumbarello R, Abbruzzese PA, Meloni G et al (1991) A variant of the scimitar syndrome with stenosed drainage of the inferior vena cava. Am Heart J 121(2 Pt 1):616–618
Türkvatan A, Güzeltaş A, Tola HT, Ergül Y (2017) Multidetector computed tomographic angiography imaging of congenital pulmonary venous anomalies: a pictorial review. Can Assoc Radiol J 68(1):66–76. Oct 6. pii: S0846–5371(16)30040–7
Vida VL, Padalino MA, Boccuzzo G et al (2010) Scimitar syndrome: a European congenital heart surgeons association (ECHSA) multicentric study. Circulation 122(12):1159–1166
Wernovsky G (2008) Chapter 51: Transposition of the great arteries. In: Allen HD, Driscoll DJ, Shaddy RE, Feltes TF (eds) Moss and Adams' heart disease in infants, children, and adolescents including the fetus and young adult (volume 2), 7th edn. Wolters Kluwer, Lippincott, Williams and Wilkins, Philadelphia, pp 1038–1087
Whight CM, Barratt-Boyles BG, Calder AL, Neutze JM, Brandt PW (1978) Total anomalous pulmonary venous connection: long-term results following repair in infancy. J Thorac Cardiovasc Surg 75(1):52–63
White CS (2000) MR imaging of thoracic veins. Magn Reson Imaging Clin N Am 8(1):17–32
White CS, Baffa JM, Haney PJ, Pace ME, Campbell AB (1997) MR imaging of congenital anomalies of the thoracic veins. Radiographics 17(3):595–608

Septal Defects

Stephan Waelti, Julie Déry, and Chantale Lapierre

Contents

Abstract

Cardiac septal defects are the most common form of congenital heart disease if bicuspid aortic valve is excluded. This category includes atrial septal defect (ASD), atrioventricular septal defect, and ventricular septal defect (VSD). The different types of ASD are: primum, secundum, sinus venosus, and unroofed coronary sinus. The most common forms of atrioventricular septal defect are complete and partial whereas the four main groups of VSDs are inlet, muscular, membranous, and outlet. A good knowledge of the anatomy is necessary to classify adequately the ASDs and VSDs. Transthoracic echocardiography is the primary and most important imaging modality and MRI can be useful when echocardiography is not feasible or not diagnostic.

1 Introduction

Septal defects, in general, are the most common form of congenital heart disease. In the adult population, they represent most of the new congenital heart disease cases. The interventricular septum and the interatrial septum separate the pulmonary

S. Waelti, M.D. • J. Déry, M.D. • C. Lapierre, M.D. (✉)
Medical Imaging Department, CHU Sainte-Justine, 3175, Cote-Sainte-Catherine, Montreal, QC, Canada, H3T 1C5
e-mail: chantal_lapierre@ssss.gouv.qc.ca

Med Radiol Diagn Imaging (2017)
DOI 10.1007/174_2017_83, © Springer International Publishing AG
Published Online: 12 July 2017

circulation and the systemic circulation. When either the interventricular or the interatrial septum is deficient, systemic and pulmonary circulation can become in contact and create a shunt lesion. There are several types of septal defects that will be described in this chapter. Usually, septal defects are classified in three types: atrial septal defects (ASD), ventricular septal defects (VSD), and atrioventricular septal defects (AVSD). The primary imaging modality for those kinds of pathologies remains the transthoracic echocardiography, but MRI and to a lesser degree CT can precise the diagnosis and its repercussion on the cardiac chambers. In the first section of this chapter, several types of ASD will be described, the most common being the ostium secundum type. Atrioventricular septal defects will be discussed in the ASD section since an ostium primum type ASD is an inherent part of this pathology. The different types of VSDs will be described and discussed in the second section.

2 Atrial Septal Defects

Atrial septal defects (ASD) are common congenital heart defects. The incidence has been estimated to be approximately 100 per 100.000 live births. They constitute 8–10% of congenital cardiac malformations in children (Hugh et al. 2016; Hoffman and Kaplan 2002; Wang et al. 2003; Botto et al. 2001).

The majority of ASDs occur sporadically with no identifiable cause. This anomaly can be isolated or occur in association with other congenital cardiovascular malformations. In some congenital heart defects, the ASD may even be crucial for survival of the patient, such as D-transposition of the great arteries, total anomalous pulmonary venous return (TAPVR), tricuspid atresia, and hypoplastic left heart syndrome (Hugh et al. 2016; Saremi 2014).

The vast majority of children with isolated ASD, even if a large left-to-right shunt is present, are asymptomatic and the defects are usually an incidental finding on imaging studies. Only 1% becomes symptomatic in the first year (Rajiah and Kanne 2010). In the second decade, patients might still be asymptomatic or present with palpitations or shortness of breath during strenuous activities. By contrast, almost all adult patients with a large defect are symptomatic (Geva et al. 2014; Campbell 1970). Untreated large atrial septal defect is associated with a reduced life expectancy mainly because of the changes induced in the pulmonary vasculature bed and in the myocardium (Campbell 1970). In the first two decades, the annualized mortality rate is low (0.6% and 0.7%, respectively), then increases to 4.5% in the fourth decade to reach 7.5% in the sixth decade (Geva et al. 2014; Campbell 1970).

The evaluation of an interatrial septal defect usually begins with a transthoracic echocardiography (TTE). However, this method is operator dependent and can be limited by acoustic window (Rajiah and Kanne 2010). If the findings on echocardiography are uncertain, computed tomography angiography (CTA) and/or magnetic resonance imaging (MRI) are valuable tools for further evaluation. Both can be used to define the anatomy of an ASD, its impact on the cardiac chambers and associated anomalies (mainly the pulmonary venous return) (Sadler 2015; Hagen et al. 1984). However, cardiac MRI stays the cross-section modality of choice because in addition to provide a comprehensive assessment of the cardiac anatomy, it can accurately quantify shunts, ventricular size, as well as cardiac and valve functions. Computed tomography angiography (CTA) should be reserved for patients with known contraindications to MRI or when the ability to tolerate MRI is limited by claustrophobia. The role of chest radiographs is limited. In children with an isolated ASD, it is almost always normal. Enlargement of the right cardiac chambers and the pulmonary artery may be seen only with a hemodynamically significant ASD. Hemodynamically significant are generally the ASDs with a pulmonic-to-systemic flow ratio (QP/QS) > 1.5:1.

ASD can be found at several sites. Knowledge of the development of interatrial septum helps understanding the different types of ASD. So, the next sections review briefly the embryologic development of the interatrial and the different types of ASD. Then, the indications and options of treatment are presented.

2.1 Embryologic Development of the Interatrial Septum

The interatrial and interventricular septa are formed between the 27th and 37th days of development. At the beginning, a pulsatile tube is transformed into a hollow, single-chambered pump (Rajiah and Kanne 2010). Then, tissue masses, the so-called *endocardial cushions*, appear in the atrioventricular region, separate the heart into right and left upper and lower chambers, and take part in the formation of the interatrial septum, the inlet portion of the interventricular septum, and the atrioventricular valves (Rajiah and Kanne 2010; Sadler 2015).

From the roof of the common atrium arises a septum, the *septum primum*, and grows caudally toward the endocardial cushions (Sadler 2015). The orifice between the septum primum and the endocardial cushions is the *ostium primum*. During further growth of the septum primum, perforations in the upper portion appear, forming the secondary interatrial communication, the *ostium secundum*. Then a second fold begins to grow in the atrium, the *septum secundum*. By further growth, it overlaps the ostium secundum, but an oblique cleft between the two atria is maintained, the *foramen ovale* (Fig. 1).

The foramen ovale represents a normal interatrial communication that is present throughout fetal life. This normal fetal interatrial communication is commonly encountered in the neonatal period. After birth, left atrial pressure normally exceeds right atrial pressure, leading to apposition and fusion of the septum primum and septum secundum (Saremi 2014; Hagen et al. 1984).

In order to complete the development, the endocardial cushions fused with the anterior and posterior walls of the heart chamber dividing the atrioventricular canal into the mitral and tricuspid inlets. The position of the tricuspid annulus is normally more apical than the mitral annulus (Rajiah and Kanne 2010).

2.2 Locations (Types) of ASD

Interatrial communications can be found at several sites (Fig. 2). Although they are often summarized as atrial septal defects (ASDs), they do not necessarily involve the interatrial septum. They are classified according to their location and the anatomical structure that is involved:

- Septum primum and atrioventricular septum → Ostium primum ASD (20%)
- Fossa ovalis → Ostium secundum ASD (70%)
- Sinus venosus (embryologic structure) → Sinus venosus defect (5–10%)
- Coronary sinus → Unroofed coronary sinus (1%)
- Foramen ovale → Patent foramen ovale

A proper classification is crucial for an optimal therapeutic decision-making.

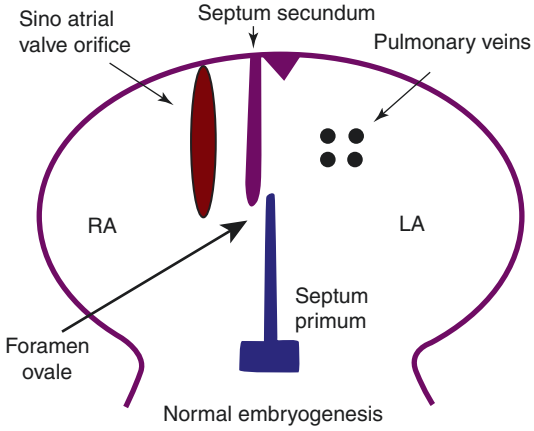

Fig. 1 Coronal view of the atrial septa. *RA* right atrium, *LA* left atrium

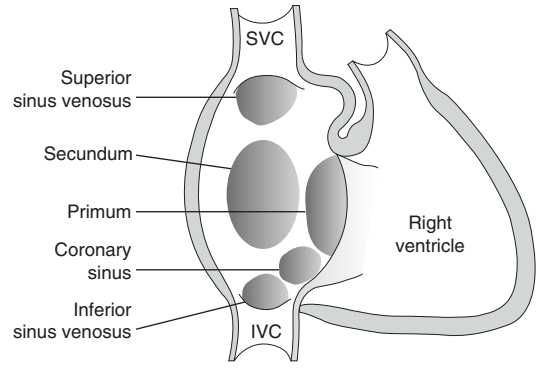

Fig. 2 View from the right atrium showing the different types of ASDs. *IVC* inferior vena cava, *SVC* superior vena cava. *Reprinted with permission from Slovis et al.* (2008)

2.2.1 Ostium Primum Defect and Atrioventricular Septum Defect (AVSD)

The ostium primum ASD is part of the spectrum of the atrioventricular septum defects (AVSD) or endocardial cushion defects. Therefore, we group them in the same section. The defect occurs in the region of endocardial cushions. The fusion of the endocardial cushions not only divides the embryonic atrioventricular canal into a right and a left orifice, but it is also crucial for the closure of the ostium primum and the formation of the interventricular septum. A failure of fusion of the endocardial cushions results in a persistent atrioventricular canal and a defect in the interatrial and interventricular septa. It also results in a common atrioventricular valve with one valve ring and five leaflets (Saremi 2014; Sadler 2015; Anderson et al. 1998).

A partial, a transitional, an intermediate, and a complete form are described (Fig. 3). The complete form includes an ostium primum ASD, a large ventricular septal defect of the inlet type, and a common AV valve with one single orifice consisting of the five leaflets (Fig. 4) (Anderson et al. 1998; Prasad et al. 2004). In the intermediate form, there is also common valve ring, but the free margins of the bridging leaflets are fused, creating two separate valve orifices. The resulting left atrioventricular valve has three leaflets, contrary to a normal mitral valve with only two leaflets. This abnormality of the mitral valve is also called "cleft mitral valve" (Fig. 5) (Van Praagh et al. 1994). The cleft mitral valve is usually regurgitant. With time, the valve becomes thickened and similar to mitral valve prolapse. In partial form, the mitral and tricuspid annuli are separate but always located at the

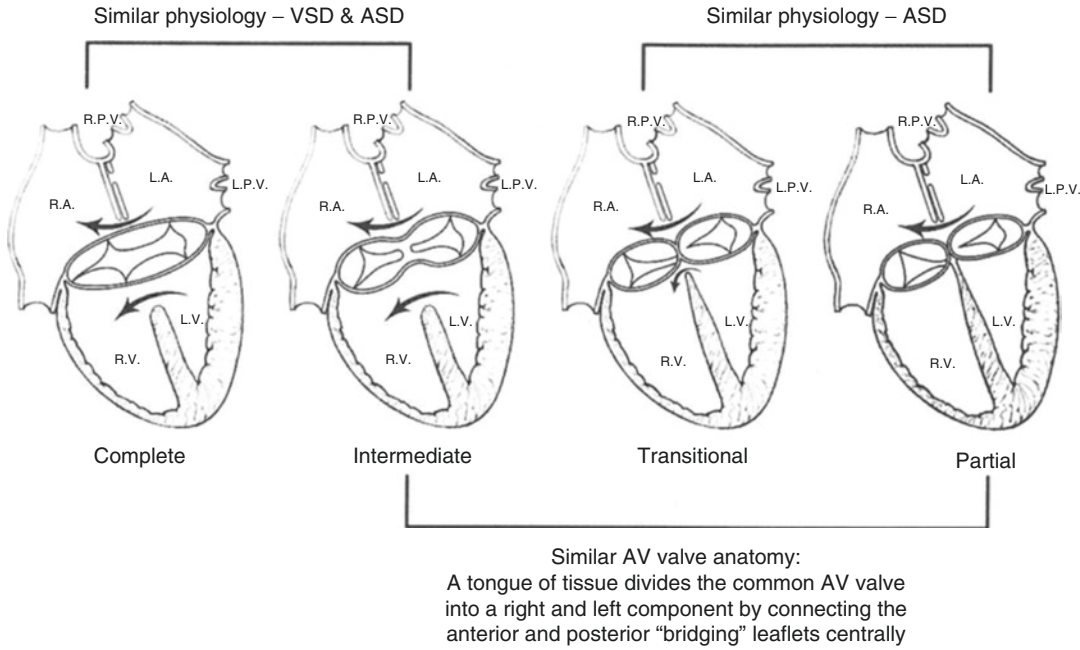

Fig. 3 Summary of AVSD. Physiologic and anatomic similarities between the different forms of atrioventricular septal defects are illustrated. *Reprinted with permission from Allen HD et al.*

- Complete AVSDs have one annulus with large interatrial and interventricular communications. Intermediate defects (one annulus, two orifices) are a subtype of complete AVSD.
- Complete AVSDs have physiology of ventricular septal defects (VSD) and atrial septal defects (ASD).
- Transitional AVSDs are a form of partial AVSD in which a small inlet VSD is also present.
- Partial defects and the intermediate form of complete AVSD share a similar anatomic feature: a tongue of tissue divides the common atrioventricular valve into distinct right and left orifices.
- Partial and transitional AVSDs have physiology of ASDs.
- *LA* left atrium, *LPV* left pulmonary vein, *LV* left ventricle, *RA* right atrium, *RPV* right pulmonary vein, *RV* right ventricle

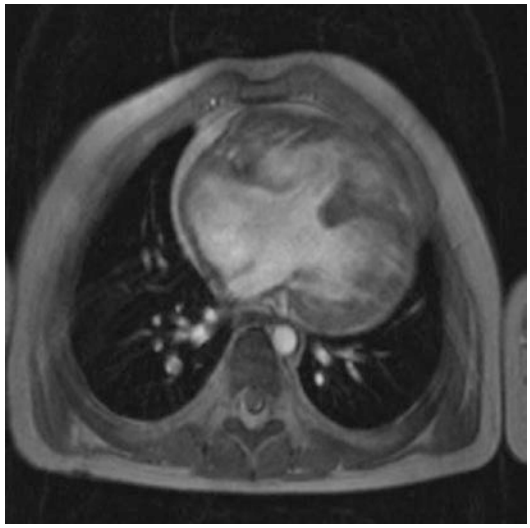

Fig. 4 Complete atrioventricular septal defect. Four-chamber view image obtained from cine FLASH MRI sequence demonstrates a common atrioventricular valve, a large ostium primum ASD, and an inlet VSD

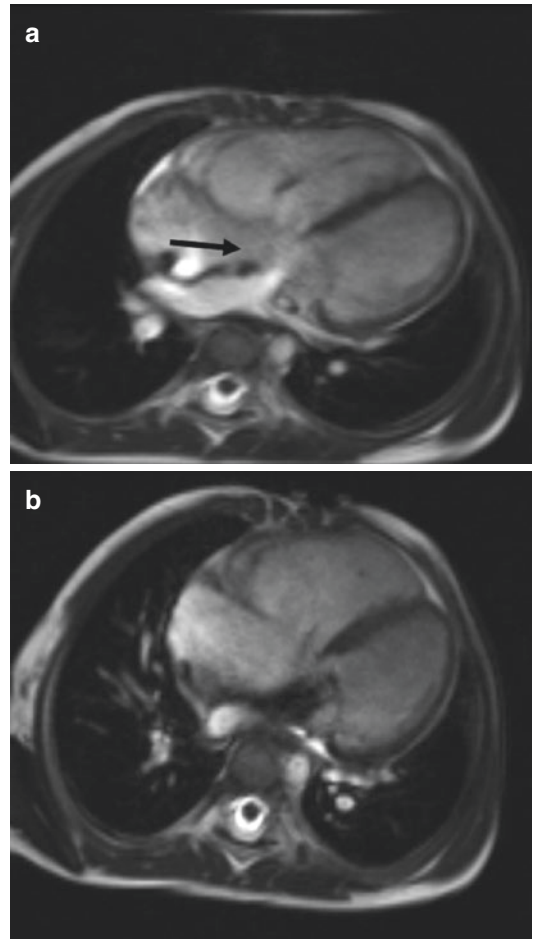

Fig. 5 Partial atrioventricular septal defect. (**a**), (**b**) Four-chamber view images obtained from cine FLASH MRI sequence demonstrate mitral and tricuspid valves at the same level due to the common ring, ostium primum ASD (*black arrow*) and mitral regurgitation

same level. A cleft mitral valve is present and the bridging leaflets fuse to the crest of the interventricular septum, leaving only an ostium primum atrial septal defect (Sadler 2015). Transitional AVSD is a subtype of partial AVSD. This term is used when a partial AVSD also has a small inlet VSD that is partially occluded by dense chordal attachments to the ventricular septum. Whatever the employed imaging modalities, this type of ASD are well demonstrated on the four-chamber view.

Atrioventricular septal defects constitute approximately 20% of ASDs and are particularly common in Down syndrome (Hugh et al. 2016). In fact, it accounts for 40% of cardiac defects in patients with Down syndrome. Other associated syndromes are DiGeorge syndrome and Ellis-Van Creveld syndrome. It may also be associated with a persistent left SVC and a secundum ASD (Webb and Gatzoulis 2006). Ostium primum defects are usually larger than ostium secundum defects and are symptomatic at a younger age (Rajiah and Kanne 2010).

2.2.2 Ostium Secundum Defect

This atrial septal defect occurs in the fossa ovalis, the central part of the atrial septum as a result of either excessive resorption of the septum primum or deficient growth of septum secundum (Figs. 6 and 7) (Prasad et al. 2004). In case of excessive resorption of the septum primum, the defect is central with one or multiple holes. In case of abnormal development of the septum secundum, the defect is superiorly located and larger (Blom et al. 2005). The size of ostium secundum defects varies from several millimeters to 2–3 cm (Geva et al. 2014).

Secundum ASDs are by far the most common ASDs, accounting for almost 70% of all ASDs. Associations with several syndromes have been described, such as Down, Holt-Oram, Klinefelter, Ellis-van Creveld, Noonan, Treacher-Collins, and others.

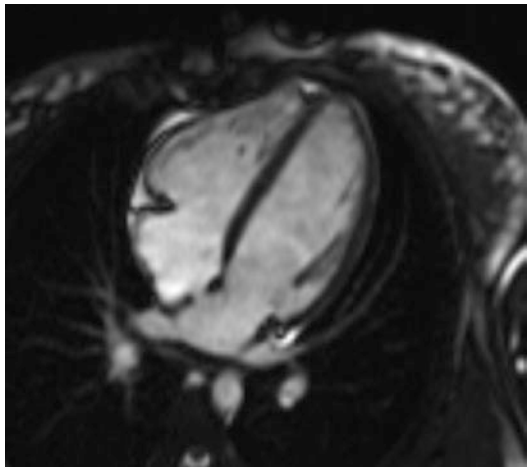

Fig. 6 Isolated secundum ASD. Four-chamber view image obtained from cine TRUFISP MRI sequence demonstrates an ostium secundum defect of less than 10 mm in diameter. The QP/QS ratio was estimated to be 1.2:1

2.2.3 Sinus Venosus Defect

Embryologically, this defect results of an incomplete resorption of the embryonic sinus venosus leading to a communication between the right pulmonary veins and the SVC, IVC, or the right atrium. The anomaly is a deficient separation of the pulmonary venous connection to one of the caval veins located at the junction of the right atrium rather than a true defect in the interatrial septum (Webb and Gatzoulis 2006; Van Praagh et al. 1994). Therefore, blood with high oxygen content from the pulmonary veins is directed into the vena cava/right atrium instead of the left atrium. Most commonly, this type of ASD is related to the superior vena cava where blood from the right superior and middle pulmonary veins flows in the right atrium (Fig. 8). In rare cases, it occurs in relation with the inferior vena cava where blood from the right lower pulmonary vein flows in (Fig. 9) (Van Praagh et al. 1994; Brickner et al. 2000; al Zaghal et al. 1997; Kafka and Mohiaddin 2009).

This produces a larger left-to-right shunt than ostium secundum defects and leads to a threefold higher risk of developing pulmonary artery hypertension (Rajiah and Kanne 2010; Vogel et al. 1999). It is a relatively uncommon type of ASD, constituting approximately 5–10% of all ASDs (Webb and Gatzoulis 2006; Davia et al. 1973).

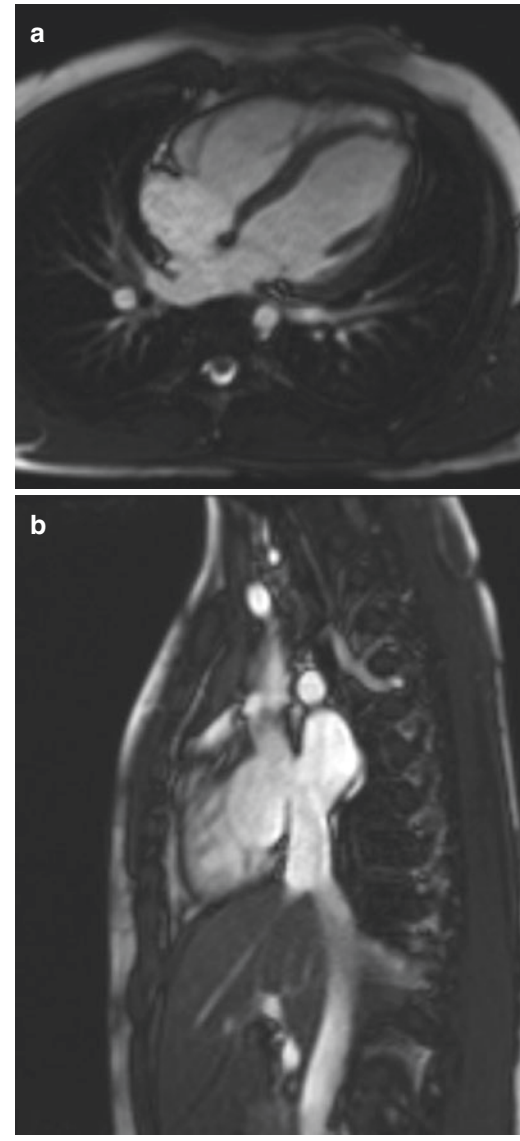

Fig. 7 Secundum ASD. (**a**) Four-chamber view and (**b**) perpendicular view of the interauricular septum images obtained from cine TRUFISP MRI sequence demonstrate an isolated, high-riding ostium secundum defect. The QP/QS ratio was estimated to be 1.4:1

2.2.4 Fenestrated (Unroofed) Coronary Sinus

The term fenestrated or unroofed coronary sinus corresponds to a defect of the wall between the coronary sinus and the left atrium allowing a left-to-right shunt (Van Praagh et al. 1994). It is a spectrum, ranging from partial fenestration to complete absence of the

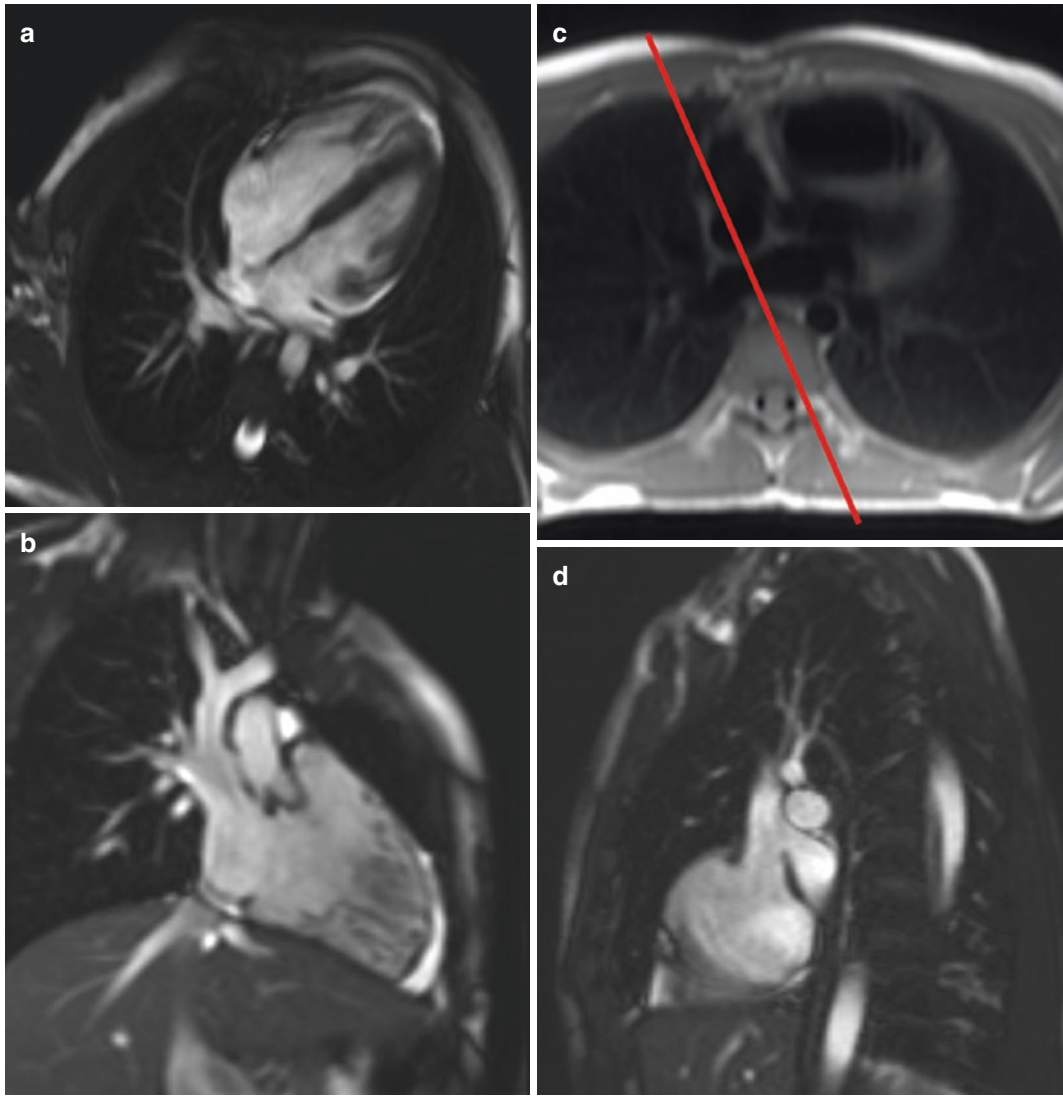

Fig. 8 Superior sinus venosus atrial septal defect. (**a**) Four-chamber view image obtained from cine TRUFISP MRI sequence shows superior type sinus venosus defect located in the posterior and superior aspect of atrial septum at the opening of right superior vena cava. (**b**) Coronal-view image obtained from cine TRUFISP MRI sequence demonstrates a partial anomalous pulmonary venous return. Blood from the right superior and middle pulmonary veins is drained into the right superior vena cava instead of the left atrium. (**c**) Axial HASTE MRI image. The red line indicates the best orientation to depict sinus venosus ASD. (**d**) Sagittal oblique image obtained from cine TRUFISP MRI sequence (the orientation displayed by the red line in Fig. 8c) demonstrates a defect in the posterior and inferior aspects of right SVC like that found in the superior sinus venosus atrial septal defect ASD

wall between the left atrium and the coronary sinus. In the majority of cases, the communication is in the mid-portion of the coronary sinus. It is a rare cardiac anomaly accounting for only 1% of all ASDs (Ootaki et al. 2003a). It may occur as an isolated finding, often of little functional importance, or as part of another congenital heart disease (Saremi 2014). An unroofed coronary sinus is almost always associated with a left SVC (Fig. 10) and sometimes with a secundum ASD (Ootaki et al. 2003a). It is relatively common in left isomerism heterotaxy syndromes (Matsuwaka et al. 1987).

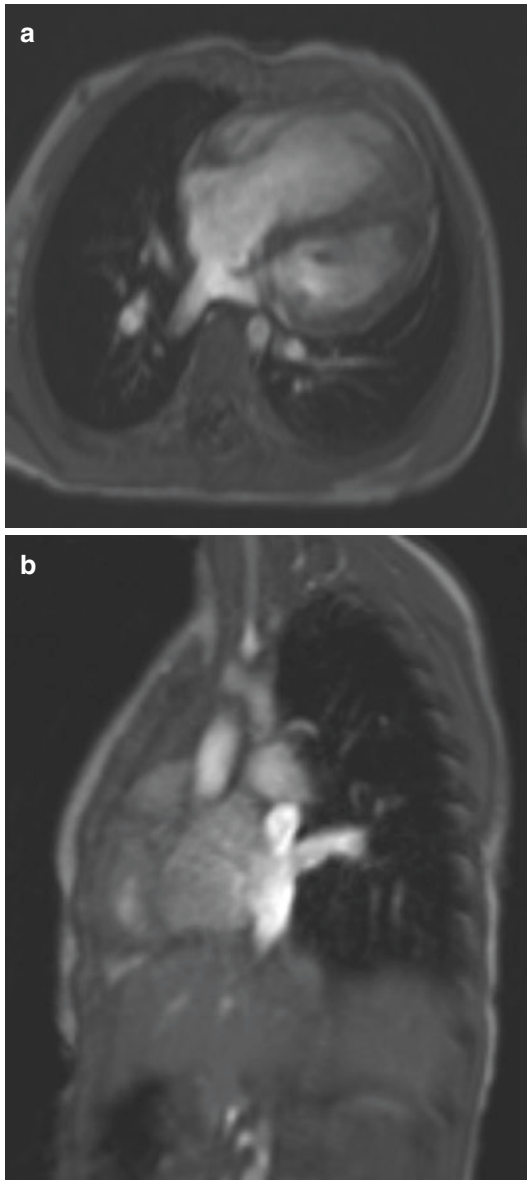

Fig. 9 Inferior sinus venosus atrial septal defect. (**a**) Four-chamber view image obtained from cine FLASH MRI sequence shows a communication between the posterior aspect of inferior vena cava and the left atrium. Blood from the right inferior pulmonary vein is directed into the inferior vena cava/right atrium instead of the left atrium. The QP/QS ratio was 2.8:1. (**b**) Sagittal oblique view image obtained from cine FLASH MRI sequence demonstrates the right inferior pulmonary vein draining into the right atrium near the opening of inferior vena cava

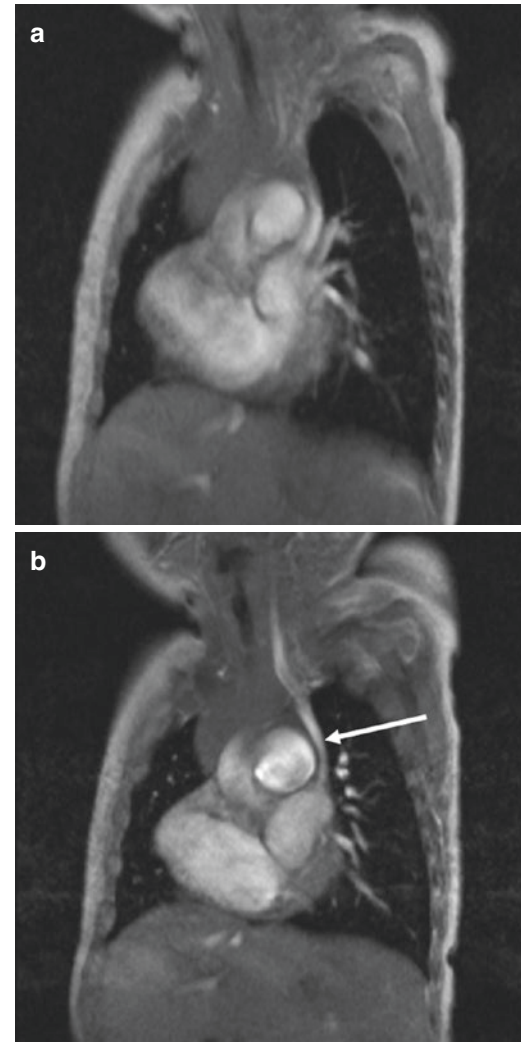

Fig. 10 (**a**), (**b**) Totally unroofed coronary sinus defect. Sagittal oblique images of cine FLASH MRI sequence show a persistent left superior vena cava (*white arrow*) draining directly into the left atrium due to a complete absence of common wall between the left atrium and the coronary sinus and interatrial communication corresponding to the opening of coronary sinus

2.2.5 Patent Foramen Ovale

Complete closure of foramen ovale occurs in almost 75% within the first two years of life. In 25% of people, anatomic closure does not occur. In case of persistent foramen ovale and patent valve of fossa ovalis, it may be of little or no clinical relevance and is therefore a quite common incidental finding on imaging studies and autopsies. In some cases, the valve is incompetent leading to a left-to-right shunt across the foramen. Therefore, these patients are at risk of right-to-left shunting complications. Also, this communication can be used as approach for angiographic cardiac evaluation or intervention by cardiologists.

2.3 Hemodynamic Consequence of ASD

The amount of shunting through the defect is determined by the size of the defect, by the difference of resistance in the systemic and pulmonary circulation, which relates to the compliance of the left and right ventricles, and by associated cardiac anomalies (Rajiah and Kanne 2010; Geva et al. 2014). In most patients, an ASD results in a left-to-right shunt. Defects smaller than 10 mm in diameter are usually associated with a small shunt and little or no enlargement of the right heart structures. Those with a pulmonic-to-systemic flow ratio (QP/QS) > 1.5:1 are usually hemodynamically significant. This is the magnitude of shunt needed for a right-sided volume overload and pulmonary overcirculation triggering a cascade of changes in the myocardium and in the pulmonary vasculature (Geva et al. 2014; Driscoll et al. 2006). A long-standing significant shunt will result in an impaired right atrial pump function, right ventricular dilatation, and myocardial changes (Sugimoto et al. 2011). It also comes to a remodeling of the pulmonary vascular bed, leading to pulmonary hypertension (Steele et al. 1987). In children with ASD, pulmonary hypertension is rare (Sachweh et al. 2006). In adults with a large ASD, pulmonary artery hypertension is a common finding and tends to increase with age (Geva et al. 2014; Humenberger et al. 2011). Eisenmenger syndrome is present in 5–10% of adults with untreated ASDs (Steele et al. 1987; Sachweh et al. 2006).

Ostium primum/endocardial cushion defects and sinus venosus defects are usually associated with a hemodynamically significant shunt and they do not improve over time (Geva et al. 2014). Therefore, they need surgical repair.

The natural history of secundum ASD is more variable. The probability of spontaneous closure depends on the size of the secundum ASD. Spontaneous closure occurs in approximately 56% of patients with an initial defect size of 4–5 mm, in 30% with a defect of 6–7 mm, and in 12% with a defect of 8–10 mm. If the secundum ASD does not close spontaneously, the size of the defect can decrease or even increase with age (Hanslik et al. 2006; Helgason and Jonsdottir 1999; McMahon et al. 2002; Saxena et al. 2005). Patients with a defect >2 cm are usually symptomatic in childhood (Ko et al. 2009).

2.4 Indications for Defect Closure

A hemodynamically significant shunt causing enlargement of the right heart structures should be closed once the diagnosis is made, independently of symptoms (Geva et al. 2014; Baumgartner et al. 2010; Warnes et al. 2008). As mentioned above, a hemodynamically significant shunt is defined by a pulmonary-to-systemic flow ratio (QP/QS) > 1.5:1. Patients with an ASD and unexplained paradoxical embolism should be treated as well (Warnes et al. 2008). Studies have shown that even in patients older than 40 years, closure of ASDs increases long-term survival and limits the deterioration of function due to heart failure (Attie et al. 2001; Konstantinides et al. 1995).

Hemodynamically insignificant defects without other indications can be followed conservatively, keeping in mind the possibility of increased shunting in later life (Geva et al. 2014).

2.5 Treatment Strategies and Outcomes

Despite the fact that surgical and interventional approaches are available with the same efficacy, persistent foramen ovale and ostium secundum defects are usually closed with transcatheter septal occluder (Figs. 11 and 12) (Ko et al. 2009). Complications are rare. The most common major periprocedural complications are device embolization (0.7%) and pericardial tamponade (0.1%) (Abaci et al. 2013). Late complications are device embolization (0.1%), device thrombosis (0.2%), and device erosion through the atrial wall or aortic root (0.1%) (Abaci et al. 2013).

Large atrial septal occluders, especially in small pediatric patients, can become in contact or protrude with adjacent structures, especially the roof of the left atrium and the aortic root. In a study of Lapierre et al. (Lapierre et al. 2012), it has been demonstrated that with the growth of the children, the distance between the septal

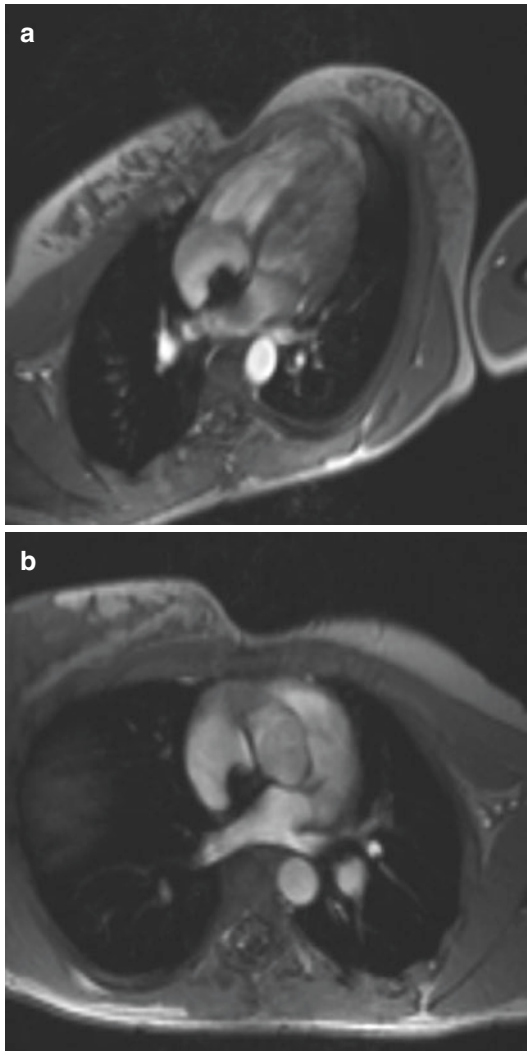

Fig. 11 Secundum ASD treated with septal device occluder. MRI obtained 2 years after procedure. Four-chamber view (**a**) and axial view (**b**) images of cine FLASH MRI sequence demonstrated an adequate position of septal device occluder for closure of ASD without residual shunt. Note the normal size of the right cardiac chambers

occluder device and the adjacent structures increases. In this study, there were no long-term complications with large atrial septal occluder devices. MRI remains the modality of choice to evaluate the effect of the ASD closure on the right cardiac chambers. MRI can also evaluate the atrial septal occluder itself and its relationship with other cardiac structures without significant blooming artifacts (Lapierre et al. 2012; Weber et al. 2008).

Sinus venosus defects as well as unroofed coronary sinus defects need surgical closure (Geva et al. 2014). Treatment of a sinus venosus defect also consists of diversion of the anomalous pulmonary vein into the left atrium (Rajiah and Kanne 2010).

In patients with AVSD (complete or partial), the treatment of choice remains surgical. The overall 10-year survival rate is variable in the literature, ranging from 70% to 100%, depending on the complexity of the anatomy and the era of surgery (Calkoen et al. 2016). Arrhythmias, including complete heart block that necessitates pacemaker placement, range from 0.5% to 7.5%. The most frequent indication for reoperation is left atrioventricular valve regurgitation. Other indications for reoperation are: subaortic stenosis, residual ASD or VSD, left ventricular outflow tract obstruction, left atrioventricular valve stenosis, and right atrioventricular valve regurgitation (Figs. 13 and 14). So, patients with repaired AVSD need echocardiographic follow-up exams on regular basis since these various complications can occur over time. Cross-sectional imaging, such as CT or MRI, can be required depending on the echocardiographic findings.

3 Ventricular Septal Defects

Ventricular septal defect (VSD) is the most common congenital heart disease if the bicuspid aortic valve is excluded. VSD is defined as a communication between the right and left ventricles through an opening or hole in the interventricular septum. Since many ventricular septal defects close with time and many patients are asymptomatic, the prevalence varies between studies and examination techniques. A screening study with highly sensitive color Doppler study reported prevalence in newborns of up to 5%, much higher than in postmortem investigations in adults (Hoffman and Kaplan 2002; Roguin et al. 1995; Hoffman et al. 2004; Penny and Vick 2011).

VSD can occur as an isolated cardiac malformation, but it is frequently found as a part of complex cardiac malformations, including

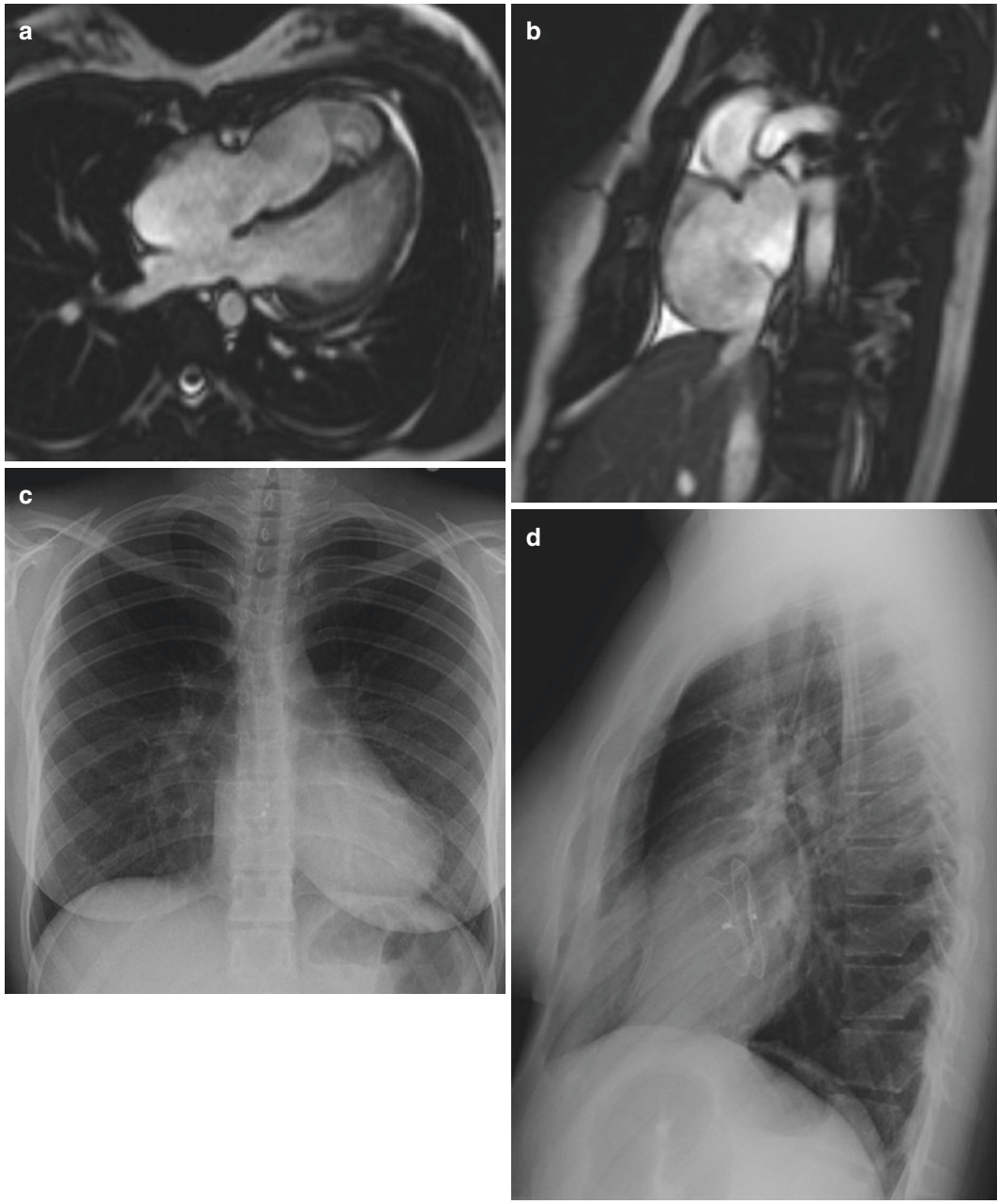

Fig. 12 Secundum ASD treated by septal device occluder. Four-chamber view (**a**) and perpendicular view (**b**) images of cine TRUFISP MRI sequence demonstrate large secundum ASD. Frontal (**c**) and lateral (**d**) radiographs obtained four years after percutaneous treatment show septal device occluder in a good place, normal cardiac size, and normal arterial pulmonary vascularization

double outlet right ventricle, tetralogy of Fallot, univentricular atrioventricular connection, transposition of the great arteries, congenitally corrected transposition, or coarctation of the aorta (Penny and Vick 2011; Wald and Powell 2006). Also, VSD represents the most common cardiac lesion found with chromosomal syndromes as trisomy 13, 18, and 21 (Allen et al. 2008).

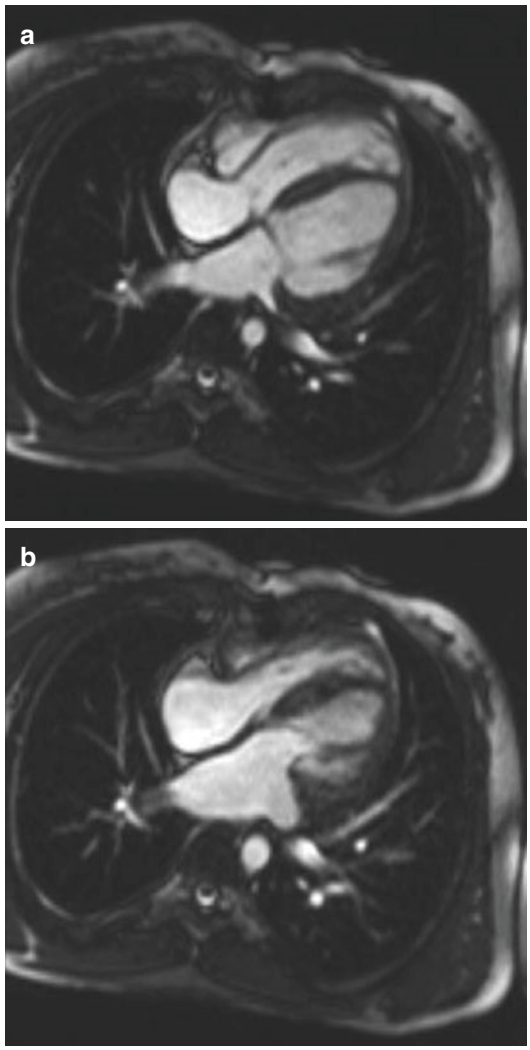

Fig. 13 Postoperative complete atrioventricular septal defect with stenosis of the mitral valve. (**a**), (**b**) Four-chamber view images of cine TRUFISP MRI sequence demonstrate no residual ASD or VSD but a limited opening of mitral valve creating a stenosis with secondary enlargement of the left atrium

In patients in which ventricular septal defects are the main pathology, echocardiography is usually sufficient and another imaging modality is rarely needed. Nowadays, the anomalies can be studied using CT or MRI with well-known advantages and limitations. Both can be used to define the anatomy of VSDs, its influence on the cardiac chambers, and associated anomalies. However, cardiac MRI stays the cross-section modality of choice because, in addition to provide a comprehensive assessment of the cardiac anatomy, it can accurately quantify shunts, ventricular size, as well as cardiac and valve functions. Computed tomography angiography (CTA) should be reserved for patients for whom MRI is almost impossible or difficult to perform. However, VSDs can be difficult to analyze at cardiac MRI for radiologist or cardiologist unfamiliar with this subject.

In this section, a review of the classification of ventricular septal defects and the associated abnormalities is presented. Also, a MRI approach for the evaluation of VSD is proposed and the data that should be obtained by cardiac MRI prior to surgery or intervention are outlined.

3.1 Classification of Ventricular Septal Defect

Ventricular septal defects can occur in any portion of the ventricular septum (Allen et al. 2008). Several nomenclature schemes of ventricular septal defects are in use. Jacobs et al. (Jacobs et al. 2000) summarized the different nomenclatures in a paper published in the year 2000. The choice of the classification system to use for ventricular septal defects is not especially important. What is important is that all of the cardiologists, radiologists, and heart surgeons in a clinic use the same nomenclature as much as possible, as a way to avoid misunderstandings.

For a more precise description and classification, knowledge of the anatomy of the ventricular septum is necessary. The ventricular septum is made of four basic components (Fig. 15): the *inlet* septum, which is contiguous with the atrioventricular valves; the *muscular* component, which represents the main portion of the ventricular septum; the *outlet* septum between the aortic and the pulmonary valve, also referred to as the infundibular, conal, supracristal, or subarterial septum; and the *membranous* component, which is found at the base of the heart where the three other components converge and below the right and non-coronary cusps of the aortic valve (Hugh et al. 2016; Gersony 2001; Minette and Sahn 2006). Ventricular septal defects can also be divided into these four main categories, according to their location: inlet, muscular, outlet, and

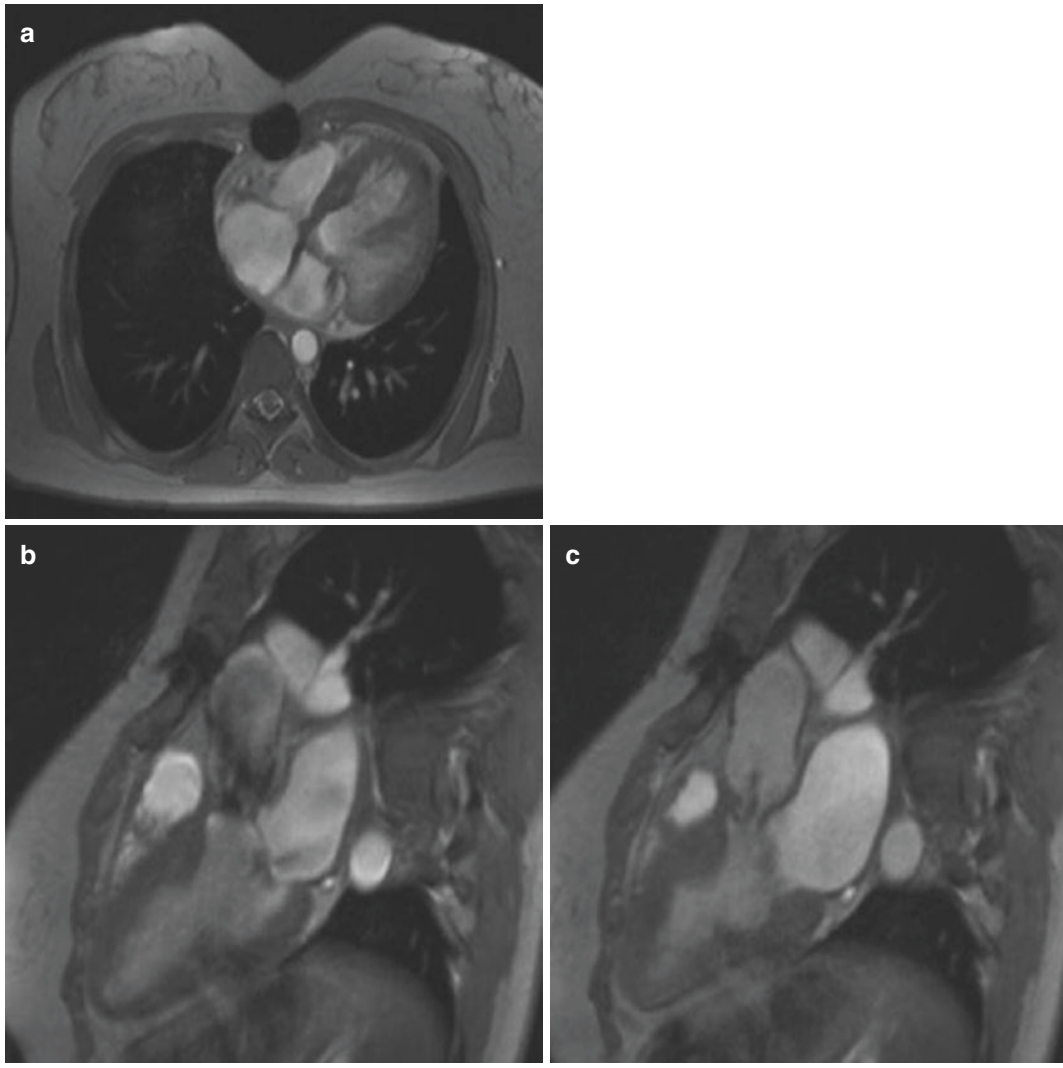

Fig. 14 Postoperative complete atrioventricular septal defect with aortic and mitral regurgitation and subaortic stenosis. (**a**) Four-chamber view image of cine FLASH MRI sequence shows correction of complete atrioventricular septal defect without any residual shunt but with left atrioventricular valve regurgitation. (**b**), (**c**) Three-chamber view images of cine FLASH MRI sequence demonstrate a reduction in caliber of the left ventricular outflow tract associated with a membrane in the subaortic region creating a subaortic stenosis. Aortic regurgitation is also visualized

membranous (Soto et al. 1980). Defects can be limited to one component of the ventricular septum or can include several components. Thus, accordingly, more subtypes of the four main types may be mentioned.

3.1.1 Inlet Septum Defects

Isolated inlet septum defects are uncommon. This type accounts for 5–8% of all VSDs. Inlet defects are located posterior and inferior to the membranous defect, beneath the septal leaflet of the tricuspid valve (Fig. 16). They are often small, but rarely close spontaneously (Gersony 2001).

Inlet septum defects can also be found in association with atrial septal defects and abnormalities of the atrioventricular valves, forming a so-called atrioventricular canal defect, more precisely described in the section about atrial septal defects (Gersony 2001). This anomaly is frequently seen in patients with trisomy 21.

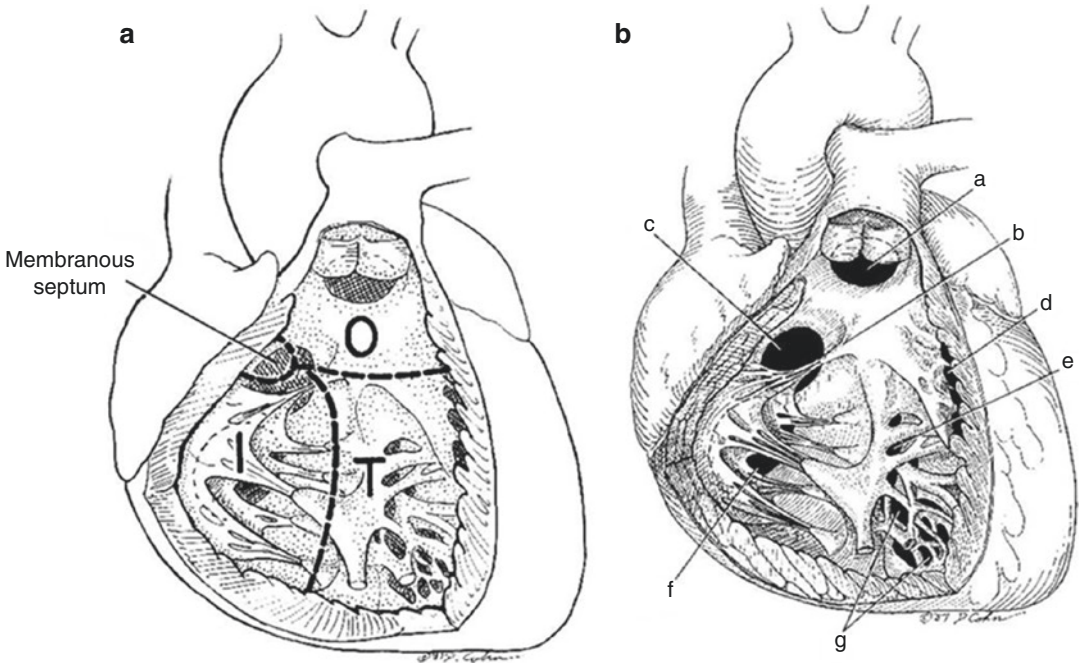

Fig. 15 (**a**) Components of the ventricular septum as viewed from the right ventricle. I: inlet septum; T: trabecular septum; O: outlet septum. (**b**) Anatomic position of defects: a, outlet defect; b, papillary muscle of the conus; c, perimembranous defect; d, marginal muscular defects; e, central muscular defects; f, inlet defect; g, apical muscular defects. *Reprinted with permission from Allen et al.* (2008)

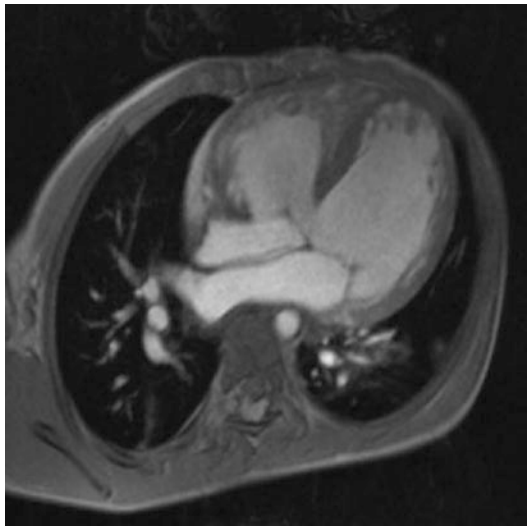

Fig. 16 Four-chamber view cine FLASH MRI sequence image showing an inlet ventricular septal defect. Note that both atrioventricular valves are located at the same level

3.1.2 Muscular Ventricular Septal Defects

Muscular VSD accounts for 5–20% of all VSDs. They are located entirely within the muscular septum. The location of VSD can be central, apical, or marginal (Wang et al. 2003; Allen et al. 2008). Central muscular VSD is located posterior to the septal band and in the mid-portion of the septum (Fig. 17). Apical defects, the most common, are found in the apical portion of the ventricles (Fig. 18). Small muscular defects near the septal-free margins have been called marginal defects. Muscular VSDs are frequently multiple and may give a "Swiss cheese" appearance (Allen et al. 2008).

Frequently, this type of VSD is difficult to analyze from the right ventricle because they are usually multiple bordering and overlying trabeculae, giving the appearance of multiple channels whereas on the left ventricular side, fewer overlying trabeculae are present and the multiple channels seen from the right ventricular side, coalesce to a single defect.

Small, isolated muscular defects often close spontaneously due to muscular growth at the margins of the defect. Muscular ventricular septal defects seen in fetal echocardiography may not be visible anymore at birth (Gersony 2001).

3.1.3 Membranous Ventricular Septal Defects

Membranous ventricular septal defects are the most common VSDs, accounting for 80% of all

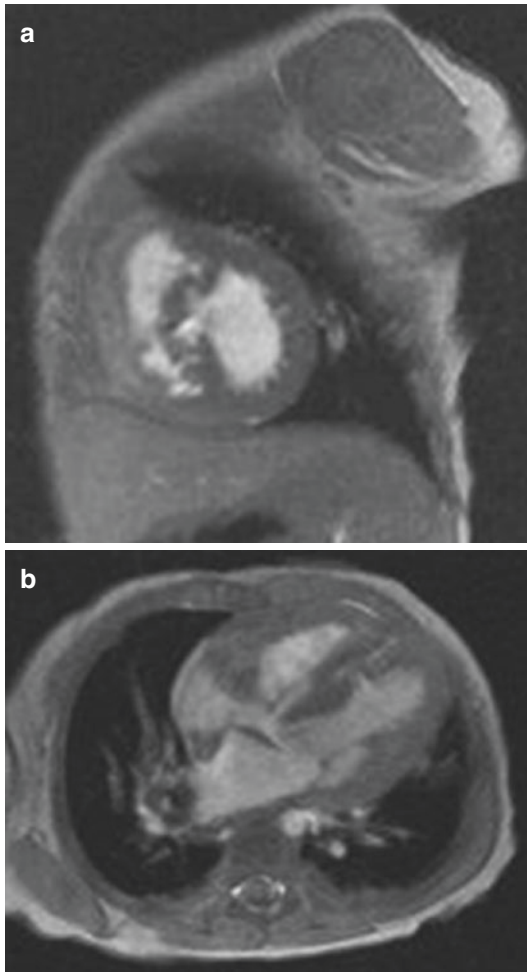

Fig. 17 Central muscular VSD. (**a**) Short-axis view and (**b**) four-chamber view cine FLASH MRI sequence images showing a central muscular ventricular septal defect. Note that on the right ventricular side, multiple channels are apparent and coalesce to a single defect on the left side

VSDs (Allen et al. 2008). They lie in the membranous part of the septum at the base of the heart, in the outflow tract of the left ventricle beneath the aortic valve (Fig. 19). Through this defect, there is a fibrous continuity between leaflets of the tricuspid and aortic valves (Penny and Vick 2011).

Pure membranous septal defects surrounded by fibrous tissue are rare. Most of the time, defects involve the membranous septum and an adjacent component. So the term "perimembranous" is more appropriate and can be subclassified as perimembranous inlet, perimembranous muscular, and perimembranous outlet, depending

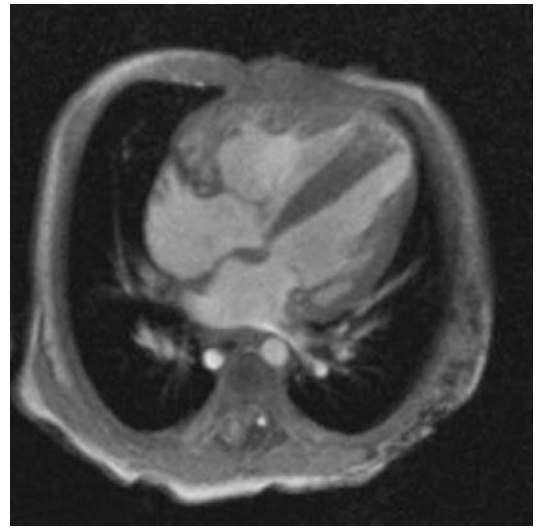

Fig. 18 Apical muscular VSD. Four-chamber view cine FLASH MRI sequence image showing a small apical muscular ventricular septal defect

on the extension of the defect (Allen et al. 2008; Minette and Sahn 2006). When the defect opens all part of the ventricle, it is called confluent defect (Penny and Vick 2011).

Small membranous defects may become smaller or close spontaneously as will be described in more detail in the section entitled Aneurysm of the membranous septum (Gersony 2001).

3.1.4 Outlet Ventricular Septal Defects

Outlet ventricular septal defects account for 5–7% of all VSDs, except for some Asiatic countries as Japan, where the incidence is approximately 30% (Allen et al. 2008). They are found in the muscular infundibulum, an area that, in the normal heart, constitutes a free-standing tube of muscular tissue which supports the pulmonary valve and separates the right and left ventricular outflow tract (Penny and Vick 2011; Minette and Sahn 2006). Defects of the outlet ventricular septum are also called subarterial, subpulmonary, conal, supracristal (superior to the crista interventricularis), or infundibular.

Anatomically, the defects in this region can be in the inferior or middle muscular part of the infundibulum (called also subaortic VSD) with a muscular rim always present under the pulmonary valve or in the subpulmonary region

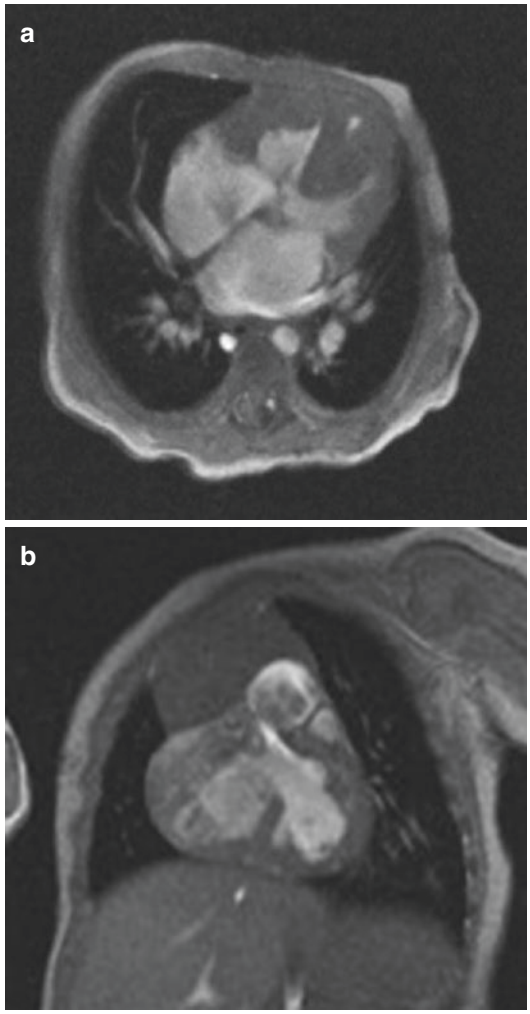

Fig. 19 Perimembranous VSD. (**a**) Four-chamber view and (**b**) short-axis view cine FLASH MRI sequence images showing a perimembranous ventricular septal defect with inlet extension

(directly under the pulmonary valve). Defects in this region therefore result in continuity between aortic and pulmonary valves (Penny and Vick 2011). These defects do not close spontaneously, but may become smaller over time. As outlet ventricular septal defects can involve the aortic sinuses, they may even close on the basis of prolapse of aortic valve leaflet tissue and/or sinus into the ventricular septal defect. This will be described in more detail in the section entitled Prolapse of the aortic valve and aortic regurgitation (Gersony 2001).

3.2 Associated Findings

3.2.1 Prolapse of the Aortic Valve and Aortic Regurgitation

In perimembranous and outlet septum ventricular septal defects, the defects are located near the annulus of the aortic valve, and therefore the anatomical support of the aortic valve can be insufficient (Tatsuno et al. 1973). As a result, prolapse of the unsupported aortic valve leaflet and sinus of Valsalva through the ventricular septal defect can occur (Wald and Powell 2006). Hemodynamic factors may promote and augment prolapse, as described by Tatsuno et al. (Tatsuno et al. 1973) (Fig. 20). The blood shunting through the ventricular septal defect in early systole forces the aortic valve to prolapse through the defect. Thereby the opening of the ventricular septal defect becomes narrower and the velocity of the blood shunting through the defect increases. This in turn pulls the aortic cusps into the right ventricular cavity. During diastole, the intra-aortic pressure forces the cusps of the aortic valve to close. The unsupported cusp is shifted toward the right ventricle and is separated from the other two cusps, resulting in incompetency of the aortic valve with subsequent regurgitation (Tatsuno et al. 1973). That means that although the leaflet prolapse reduces the orifice size of the ventricular septal defect, it may lead to an important impairment of the blood flow by causing aortic insufficiency. Usually, the right coronary cusp of the aortic valve is involved in patient with outlet VSD. In contrast, patients with perimembranous VSD can have herniation of the right coronary cusp or much less common the non-coronary cusps (Wald and Powell 2006). The prevalence of this complication is higher in patients with outlet VSD and the associated aortic regurgitation increases with age.

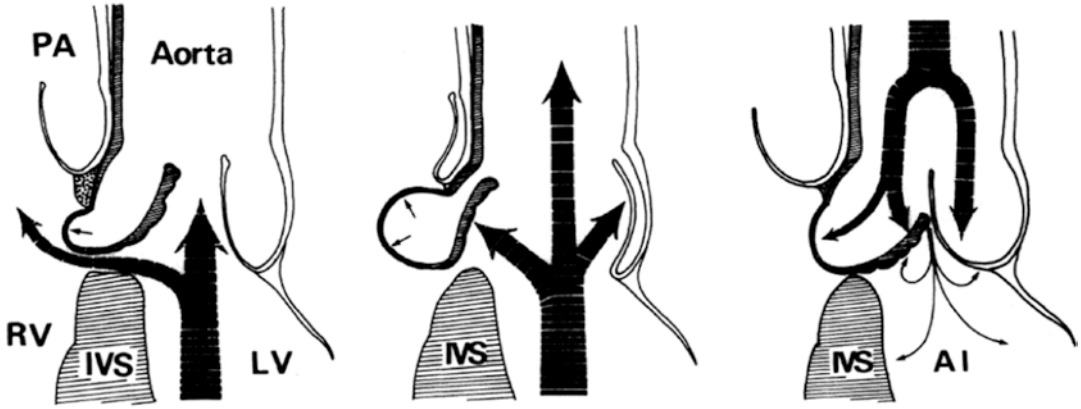

Fig. 20 Prolapse of the aortic valve and sinus of Valsalva and subsequent regurgitation: (*Left*) The flow of the shunting blood during early systole pulls the anatomically unsupported aortic valve and sinus through the VSD into the right ventricular lumen. (*Center*) In mid systole, the blood ejected from the left ventricle pushes unsupported sinus outward, producing a large bulge. (*Right*) In diastolic phase, the intra-aortic pressure separates the unsupported cusp from the other two cusps, resulting in sufficiency of the aortic valve with subsequent regurgitation. *LV* left ventricle, *RV* right ventricle, *IVS* interventricular septum, *PA* pulmonary artery, *AI* aortic incompetency. *Reprinted with permission from Tatsuno et al*. (1973)

3.2.2 Aneurysm of the Membranous Septum

The septal leaflet of the tricuspid valve arises from the membranous septum. The membranous septum has two portions, the atrioventricular portion and the interventricular portion (Fig. 21). The atrioventricular portion lies superior to the attachment of the septal leaflet of the tricuspid valve and separates the left ventricle from the right atrium. The interventricular portion lies inferior to the attachment of the septal leaflet of the tricuspid valve and separates the two ventricles (Tandon and Edwards 1973).

As mentioned above, small membranous ventricular septal defects may become smaller over time or even close spontaneously. There are two contributing factors for the closure of the defect: growth of fibrous tissue at the margins of the defect and adhesion of the septal tricuspid leaflet to the edges of the ventricular septal defect. Due to the higher pressure in the left ventricle, a pouch protruding toward the right ventricle may form, referred to as aneurysm of the membranous septum (AMS) (Gersony 2001; Tandon and Edwards 1973). AMS is a rare disease, mostly

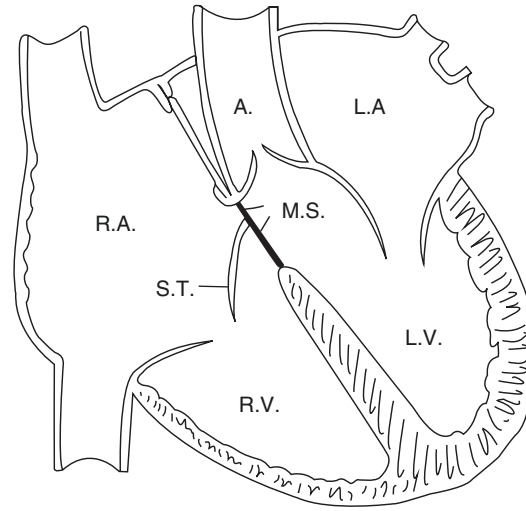

Fig. 21 Anatomy of the membranous septum. The membranous portion of the ventricular septum (M.S.) lies beneath the origin of the aorta (A). The septal leaflet of the tricuspid valve (S.T.) originates from the membranous septum. The atrioventricular portion lies superiorly to the attachment of the septal leaflet of the tricuspid valve and separates the left ventricle (L.V.) from the right atrium (R.A.). The interventricular portion lies inferiorly and separates the two ventricles. Right ventricle (R.V.). L.A. = left atrium. *Reprinted with permission from Tandon et al*. (Tandon and Edwards 1973)

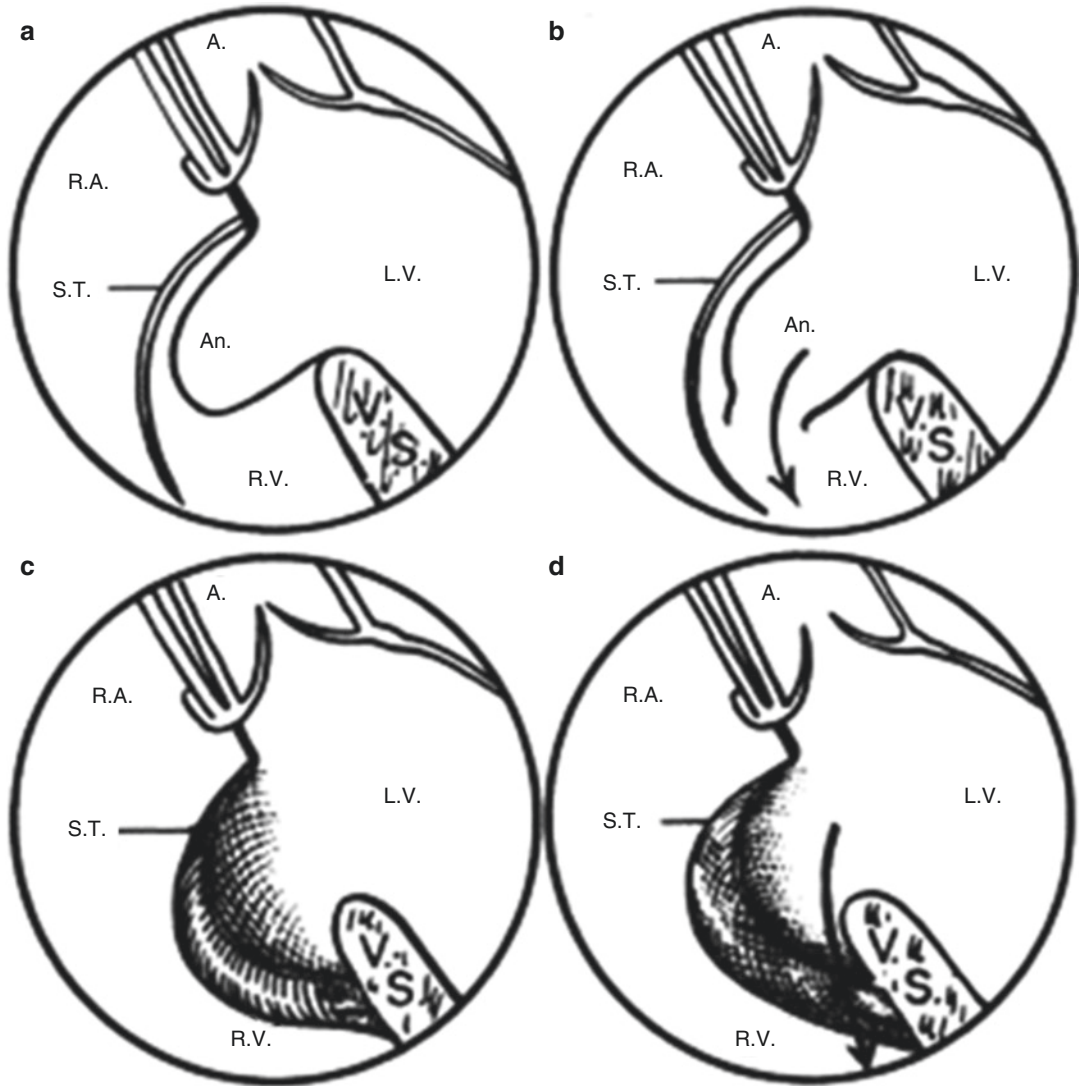

Fig. 22 Different aspects of the aneurysm of the membranous septum: (**a**) Congenital aneurysm of membranous septum. It is possible to distinguish the aneurysm from the septal leaflet of the tricuspid valve. (**b**) Ruptured congenital aneurysm of the septum. (**c**) Spontaneous closure of membranous ventricular septal defect by adhesion of septal tricuspid leaflet to the ventricular septal defect. (**d**) Incomplete closure of the membranous ventricular septal defect by the septal leaflet of the tricuspid valve. *Reprinted with permission from Tandon et al*. (Tandon and Edwards 1973)

associated with other anomalies but occurring in up to 19–22.4% with VSD and in 20% with perimembranous VSD (Langer et al. 2007; Yavuz et al. 2010; Loukas et al. 2006). Basically, AMS may be congenital or acquired. Most congenital aneurysms are intact so that there is no interventricular communication (Fig. 22). Rarely, a congenital aneurysm of the membranous septum may rupture leading to an interventricular communication. Congenital aneurysms are characterized by the identification of a septal leaflet of the tricuspid valve distinct from the wall of the aneurysm. In contrast, in aneurysms after spontaneous closure of ventricular septal defects, the septal leaflet forms an integral part of the aneurysm (Fig. 23). The closure may be complete or incomplete allowing some communication between the ventricles. Anomalies of the tricuspid

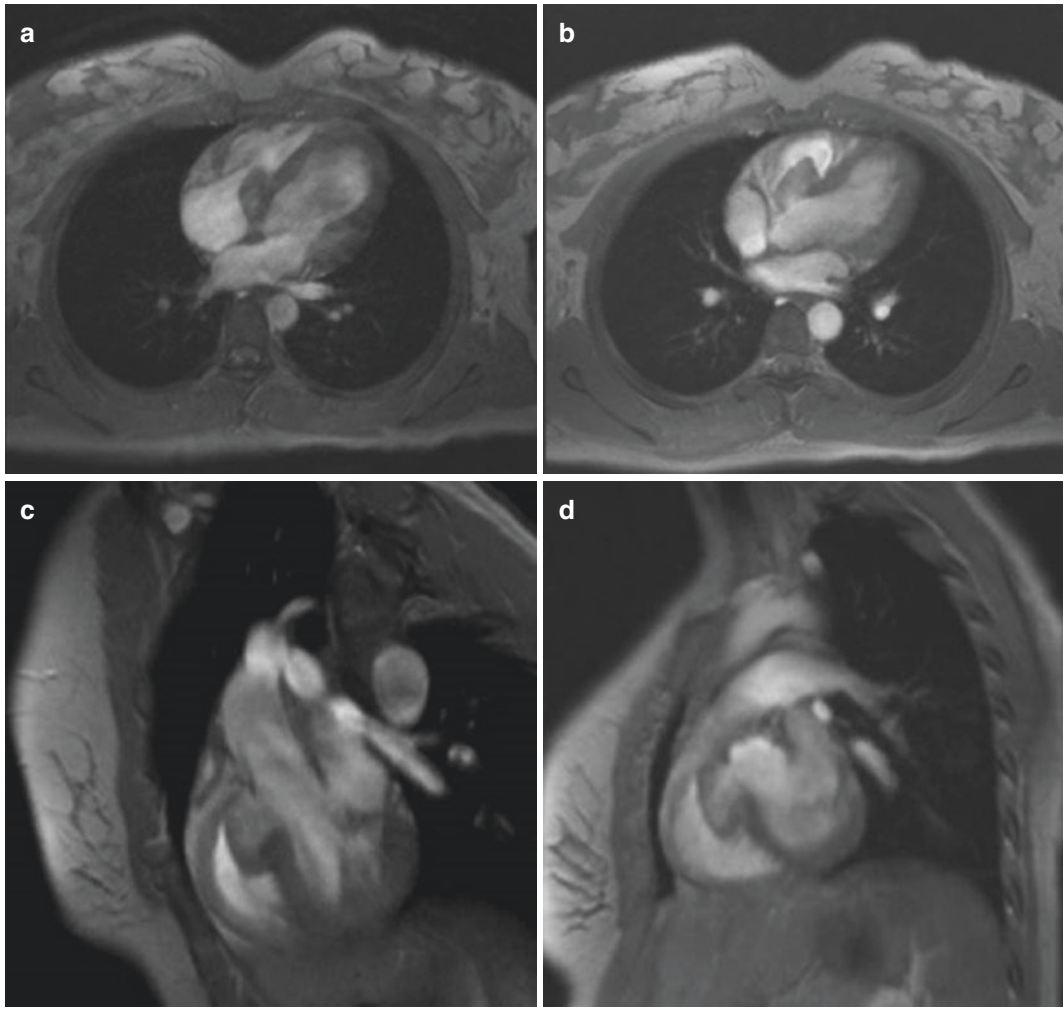

Fig. 23 Aneurysm of the membranous interventricular septum at cine FLASH MRI sequence. (**a**), (**b**) Four-chamber view, (**c**) three-chamber view, and (**d**) short-axis view images show a large aneurysm of the membranous interventricular septum protruding into the right ventricle and limiting the opening of the tricuspid valve. The septal leaflet of the tricuspid valve forms the wall of the aneurysm. The aneurysm closes almost completely the perimembranous VSD with only a small remaining defect

valve, which may be acquired for the left-to-right shunting, are frequently associated and result in tricuspid regurgitation.

Most AMS appear in the interventricular portion of the membranous septum (Tandon and Edwards 1973). Rarely, a defect can occur in the atrioventricular portion of the membranous septum (Gerbode's defect) producing an isolated left ventricular-to-right atrial shunt.

At imaging, AMS should be distinguished from sinus of Valsalva aneurysm. AMS arises from the right ventricular aspect of the membranous septum, beneath the septal leaflet of the tricuspid valve, and bulging forward into the right ventricle (Yilmaz et al. 1997). The criteria for the diagnosis of Valsalva sinus aneurysm include an origin above the aortic annulus, a saccular shape and normal dimensions of the adjacent aortic root and ascending aorta (Bricker et al. 2010).

3.2.3 Obstruction of the Ventricular Outflow Tract

VSDs can be associated with obstruction of the right or left ventricular outflow tract. The outflow

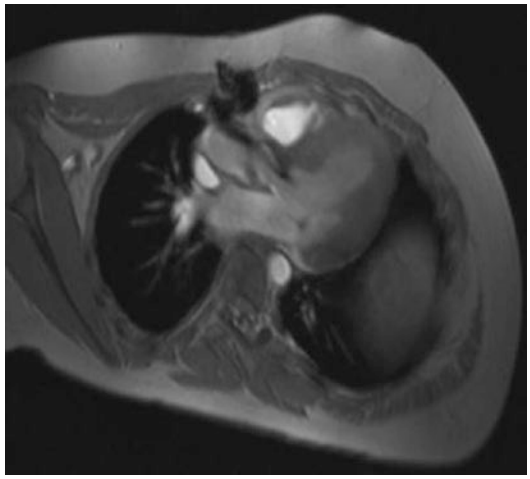

Fig. 24 Posterior deviation of the outlet septum. Three-chamber view of cine FLASH MRI sequence image demonstrates a posterior deviation of the outlet septum creating subaortic stenosis. Note that the associated VSD is not well shown. The anomaly is associated with a left ventricular hypertrophy

tract obstruction can arise from the VSD itself due to a certain malalignment of the outlet septum and the remainder of the ventricular septum. In consequence of anterior and posterior deviation of the outlet septum, either the right or left outflow tract can be obstructed (Fig. 24) (Saremi 2014). An anomalous or hypertrophic muscle bundle crossing the right ventricle from the interventricular septum to the right ventricular free wall, also known as double-chambered right ventricle, can be associated with VSD and cause obstruction of the right ventricular outflow tract/subpulmonary stenosis (Fig. 25) (Pongiglione et al. 1982; Kucher et al. 2001). Myotomy may remove this subpulmonary stenosis (van Son et al. 1993; Newfeld et al. 1976). Likewise, a crescent-shaped ridge of fibro-elastic tissue protruding from the left septal surface into the subaortic region can cause left ventricular outflow tract obstruction in patients with VSD (Newfeld et al. 1976).

3.2.4 Hemodynamic Consequences of VSD

The size of the ventricular septal defect and the pulmonary vascular resistance determine largely the shunt volume. If there is no obstruction of the right ventricular outflow tract and no pulmonary hypertension, the direction of shunt is left-to-right. Left heart volume overload can occur with large left-to-right shunts but not right ventricular dilatation (Saremi 2014; Wald and Powell 2006). The shunt volume may decrease in the setting of right ventricular outflow tract obstruction or pulmonary vascular hypertension. In extreme cases, the shunt direction may invert, causing a right-to-left shunt (Eisenmenger syndrome).

3.3 Diagnostic Evaluation

In patient in whom ventricular septal defects are the main pathology, echocardiography is usually sufficient and another imaging modality is rarely needed. Nowadays, the anomalies can be studied using CT or MRI with well-known advantages and limitations. Both can be used but cardiac MRI remains the cross-section modality of choice with a reported sensitivity of more than 90% for detection of VSDs (Wang et al. 2003; Didier and Higgins 1986; Didier et al. 1986).

MRI evaluation is mainly indicated in the diagnosis of defects in the outlet septum as echocardiography is often unable to adequately image this region of the ventricular septum (Wang et al. 2003; Wald and Powell 2006; Bremerich et al. 1999). A cardiac MRI is considered to be superior to an ultrasound where there are multiple muscular ventricular septal defects. Furthermore, the ventricular septum is visible on MRI until the apex, which is not always possible when using echocardiography. In addition, MRI can depict complications of outlet septal defects, including secondary right ventricular hypertrophy (Bremerich et al. 1999).

Cardiac MRI can give many important information such as: (a) the location, the number, and the size of the ventricular component of the defect, (b) the relationship between the defects and the position of great vessels, (c) the presence or not of complications (aortic valve prolapse and aortic regurgitation), and (d) the quantification of the hemodynamic burden of the defect by providing reliable quantitative data on the shunt and by quantifying cardiac chamber volumes and function (the most accurate technique). All of these

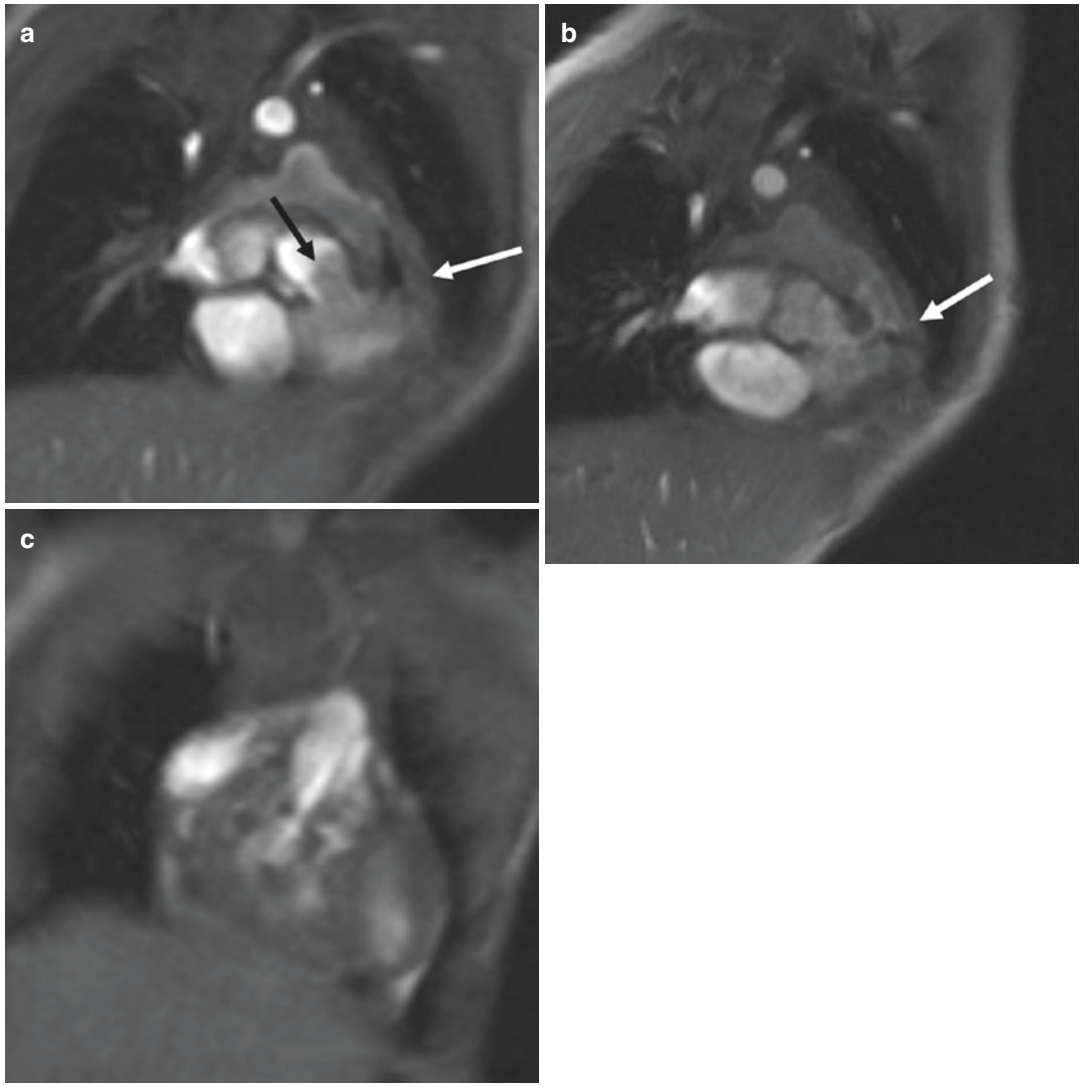

Fig. 25 Double-chambered right ventricle. Cine 2D–Flash sequence. (**a**), (**b**) Coronal oblique images show multiple infundibular muscular bands (*white arrows*) creating a stenosis and a large perimembranous VSD (*black arrow*). (**c**) Note that the distal portion is of normal size. This feature helps to distinguish a double-chambered right ventricle from a Tetralogy of Fallot. In Tetralogy of Fallot, the outlet septum has a leftward and anterior deviation

abovementioned criteria can be evaluated using a systematic MRI protocol and may influence the timing and the approach of correction (Table 1) (Parsons et al. 1990; Studer et al. 1982; Pennell et al. 2004; Wald et al. 2015).

However, VSD can be difficult to analyze at cardiac MRI for radiologist or cardiologist unfamiliar with this subject. An approach similar to the echocardiography is helpful.

The inlet, membranous, and muscular VSD can be evaluated by the coverage of entire interventricular septum in the four-chamber and short-axis views. In using these two different standard plans, it is possible to analyze the anatomy of the interventricular septum and the repercussion on the tricuspid valve and cardiac chambers.

Another acquisition that can be used to clarify membranous and outlet ventricular septal defects

Table 1 Institutional cardiovascular MRI protocol for ventricular septal defects

1. Localizers through the thorax images
2. Morphologic examination with half Fournier shot turbo spin echo (HASTE) or balanced steady-state free precession (SSFP) according to heart rate in axial plane of the thorax
3. Four-chamber SSFP cine stack views to cover all the interventricular septum
4. Short-axis SSFP cine stack views to cover all the interventricular septum
5. Three-chamber SSFP view of the left ventricular outflow tract
6. Sagittal SSFP cine view of the right ventricular outflow tract
7. Axial true plane of the aortic root in SSFP cine view
8. Perpendicular SSFP cine view or gradient echo cine view on the VSD and on the aortic root (planes depend on the site of the VSD)
9. Qp/Qs evaluation by flow mapping on:
(a) Left pulmonary artery
(b) Right pulmonary artery
(c) Main pulmonary artery
(d) Ascending aorta

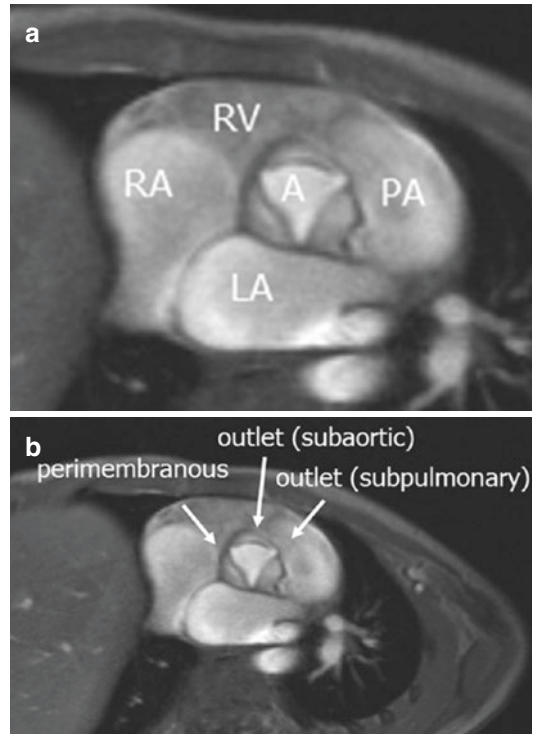

Fig. 26 (**a**), (**b**) Location of the VSD based on the aortic valve acquisition

is an image in the plane of the aortic valve (Fig. 26). This acquisition can be obtained from a coronal image. On the plane of the aortic valve, the membranous VSD appears at the 10 o'clock to 11 o'clock positions (Fig. 27). It is in relationship with the left part of the non-coronary sinus and the right part of right coronary sinus of Valsalva. The infundibular muscular (subaortic) outlet VSD appears at the 11 o'clock to 12 o'clock positions whereas the subpulmonary VSD appears at the 12 o'clock to 1 o'clock positions. Both are in relationship with the right coronary sinus of Valsalva. Most of the time, VSD are identified on the aortic valve plan by a flow void due to a small size of the defect creating blood flow acceleration. When a flow void is found in the plane of aortic valve, a complementary image should be taken. In order to visualize the relationship between the VSD and the aortic valve, an acquisition perpendicular to the aortic valve, parallel to the jet, and crossing the center of the aortic valve should be obtained (Fig. 28). The resulting image is almost a three-chamber view and this projection permits to look for a prolapse of aortic valve and aortic regurgitation (Fig. 29). To evaluate adequately the ventricular outflow tract, a three-chamber view imaging for left side should be obtained and a sagittal plan for the right side.

3.4 Indications for Defect Closure and Treatment Options

A Qp:Qs value of >1.5 to 2.0 is considered by many cardiologists and cardiac surgeons as a therapeutic indication. Ventricular enlargement, pulmonary hypertension, or aortic regurgitation are also accepted indications for defect closure, either surgically or by transcatheter closure using occluder devices (Figs. 30 and 31) (Mongeon et al. 2010; Lun et al. 2001; YC et al. 2006). Small, isolated muscular defects often close spontaneously (Gersony 2001). However, multiple muscular defects with "Swiss cheese" appearance do not close spontaneously and require surgery (Saremi 2014). The surgical treatment of multiple muscular VSDs is technically difficult due to

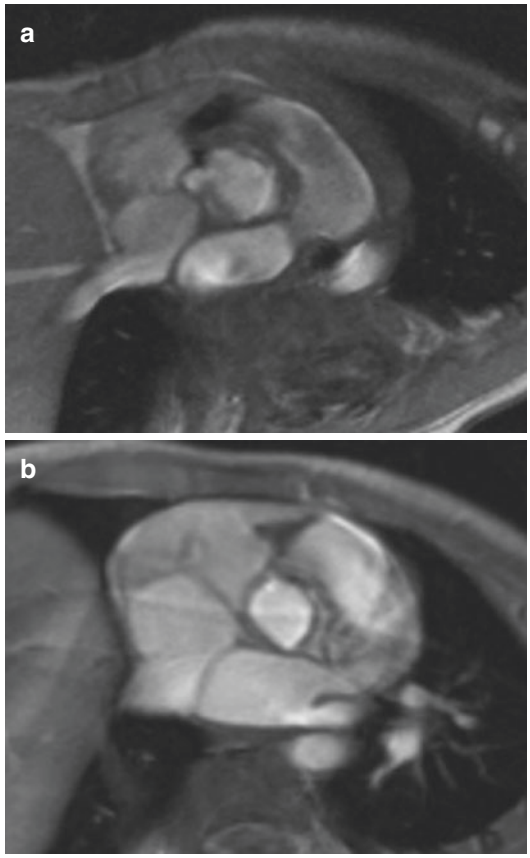

Fig. 27 Classification of VSD based on the aortic valve acquisition. Cine FLASH MRI sequence images show in (**a**) a jet 10 o'clock position indicating a perimembranous VSD and in (**b**) at 12 o'clock position, a small subaortic outlet VSD

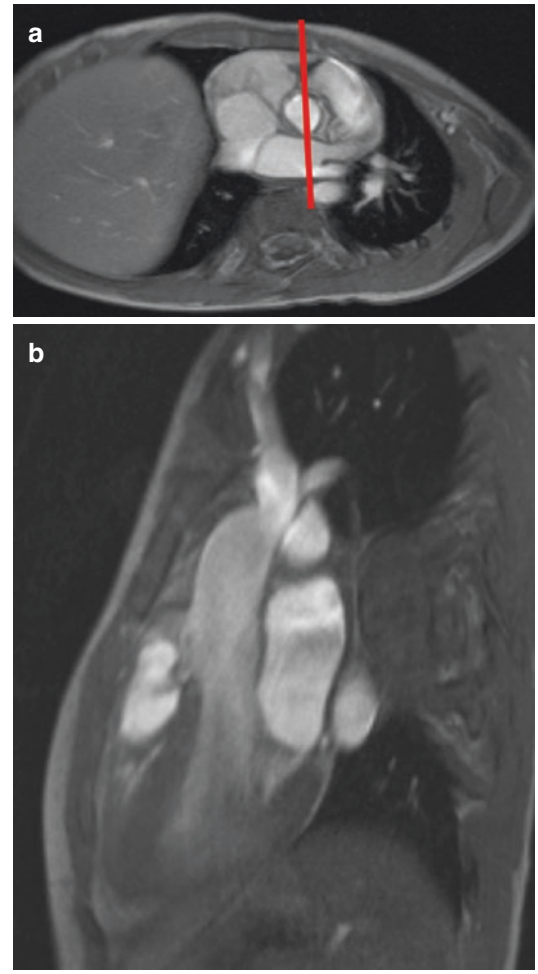

Fig. 28 Acquisition sequence to depict prolapse of the aortic valve. (**a**) In order to visualize the relationship between the VSD and the aortic valve, an acquisition perpendicular to the aortic valve, parallel to the jet, and crossing the center of the aortic valve, should be obtained. The red line delineates the optimal orientation. (**b**) The resulting image, almost a three-chamber view, shows the prolapse of the aortic valve reducing the size of the VSD

often inadequate exposure of the defects and due to significant operative mortality and complications (Corno et al. 2013; Alsoufi et al. 2006; Stellin et al. 2000). Several techniques have been described, including single-stage repair with a transatrial or a transventricular approach (Wollenek et al. 1996; Kirklin et al. 1980; Kitagawa et al. 1998), initial pulmonary artery banding and closure of the residual VSDs in a second step (Alsoufi et al. 2006; Serraf et al. 1992; Seddio et al. 1999), interventional catheter device closure (Holzer et al. 2004), or a hybrid approach with operative patch and interventional device closure techniques (Bacha et al. 2005; Ootaki et al. 2003b; Brizard et al. 2004). Preoperative pulmonary artery banding is reserved for pediatric patients with other associated cardiac anomalies like double outlet right ventricle or with congestive heart failure uncontrolled by medical management before definitive correction.

A small VSD is defined as <1 cm in diameter with a left-to-right shunt of <50%, without pulmonary stenosis and pulmonary artery hypertension. Isolated, small VSDs only need prophylactic treatment for endocarditis (Saremi 2014; Neumayer et al. 1998).

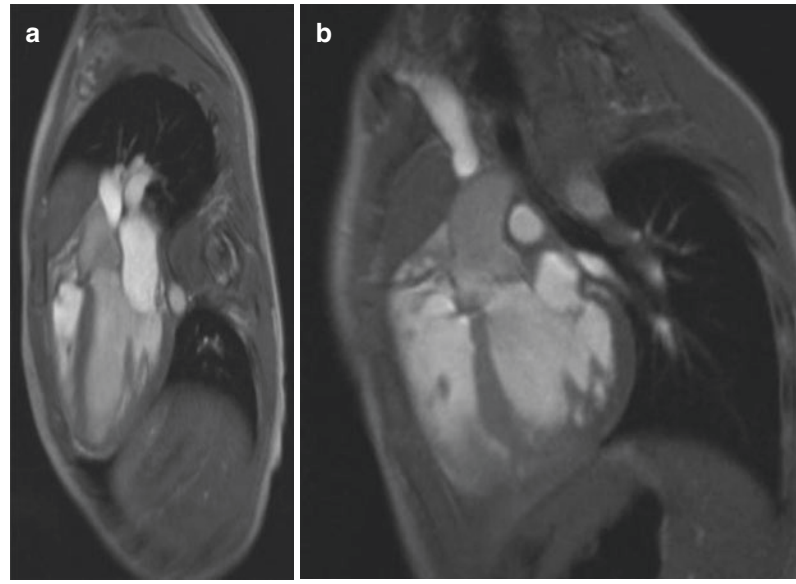

Fig. 29 Two examples of VSD associated with prolapse of the right coronary cusp at cine FLASH MRI sequence images. (**a**) A saccular and (**b**) a more diffuse deformation are visualized as shown in Fig. 20 on the left and right respectively

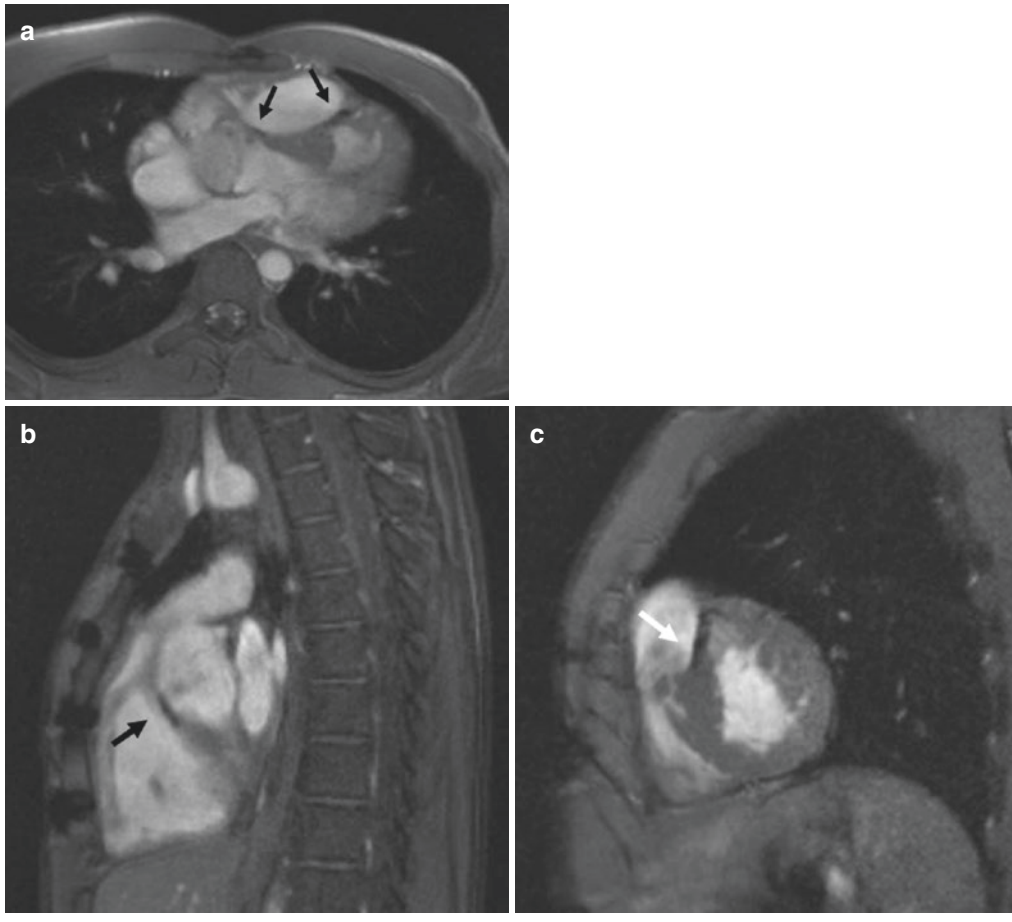

Fig. 30 Surgical closure of a perimembranous and muscular VSD at cine FLASH MRI sequence. (**a**) Axial, (**b**) sagittal oblique, and (**c**) short-axis view images show the hypointense surgical patch at two locations: perimembranous (*black arrow*) and muscular interventricular septum (*white arrow*)

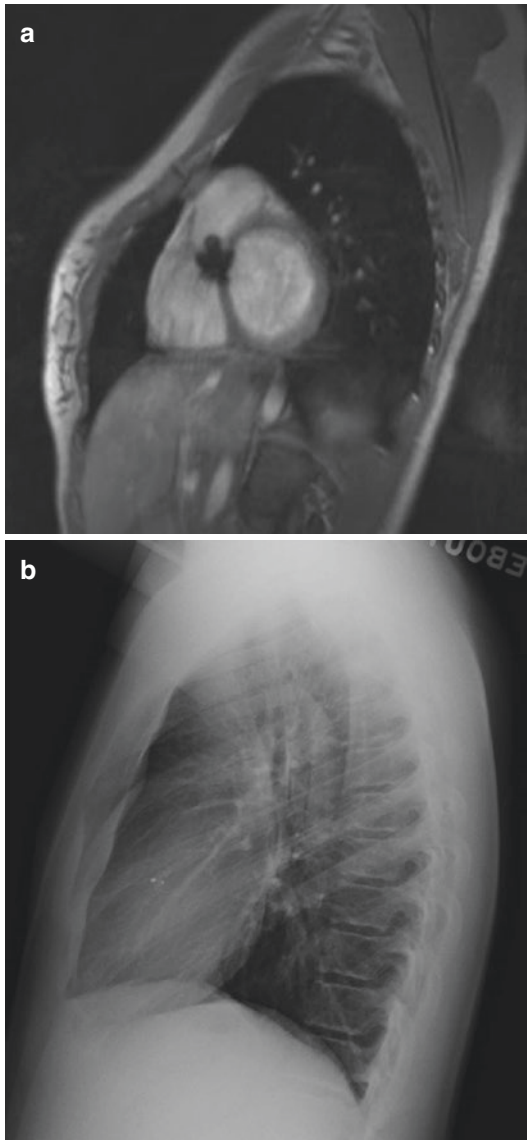

Fig. 31 (**a**) Short-axis view (*left*) and (**b**) lateral chest X-ray (*right*) in a patient with a perimembranous VSD treated with a septal occluder device

3.5 Outcomes

In general, children with VSDs have good outcomes and excellent long-term survival. Therefore, these patients are frequently seen in adult cardiology dealing with GUCH patients (Grow-Ups with Congenital Heart defects).

Conclusion

Atrial septal defects and ventricular septal defects are among the most common congenital cardiac anomalies. They can occur as isolated defects or in association with other congenital heart lesions. They are classified according to their location or embryologic origin. Important features include location, number, and size. Small defects are often hemodynamically insignificant, whereas larger defect can cause heart failure and alteration of the pulmonary vasculature. Echocardiography is often sufficient for diagnosis and treatment decision. Cross-section imaging (either MRI or CT) can be necessary for surgical or interventional planning, for functional analysis, and for the detection of posttreatment complications. In general, patients with ASDs and VSDs have good outcomes and long-term survival.

References

Abaci A, Unlu S, Alsancak Y, Kaya U, Sezenoz B (2013) Short and long term complications of device closure of atrial septal defect and patent foramen ovale: meta-analysis of 28, 142 patients from 203 studies. Catheter Cardiovasc Interv 82:1123–1138

al Zaghal AM, Li J, Anderson RH, Lincoln C, Shore D, Rigby ML (1997) Anatomical criteria for the diagnosis of sinus venosus defects. Heart 78:298–304

Allen HD, Driscoll DJ, Shaddy RE, Feltes TF (2008) Moss and Adams heart disease in infants, children, and adolescents, 7th edn. Lippincott Williams & Wilkins, Philadelphia

Alsoufi B, Karamlou T, Osaki M et al (2006) Surgical repair of multiple muscular ventricular septal defects: the role of re-endocardialization strategy. J Thorac Cardiovasc Surg 132:1072–1080

Anderson RH, Ho SY, Falcao S, Daliento L, Rigby ML (1998) The diagnostic features of atrioventricular septal defect with common atrioventricular junction. Cardiol Young 8:33–49

Attie F, Rosas M, Granados N, Zabal C, Buendia A, Calderon J (2001) Surgical treatment for secundum atrial septal defects in patients >40 years old. A randomized clinical trial. J Am Coll Cardiol 38:2035–2042

Bacha EA, Cao QL, Galantowicz ME et al (2005) Multicenter experience with perventricular device closure of muscular ventricular septal defects. Pediatr Cardiol 26:169–175

Baumgartner H, Bonhoeffer P, De Groot NM et al (2010) ESC guidelines for the management of grown-up congenital heart disease (new version 2010). Eur Heart J 31:2915–2957

Blom NA, Ottenkamp J, Jongeneel TH, DeRuiter MC, Gittenberger-de Groot AC (2005) Morphogenetic differences of secundum atrial septal defects. Pediatr Cardiol 26:338–343

Botto LD, Correa A, Erickson JD (2001) Racial and temporal variations in the prevalence of heart defects. Pediatrics 107:E32

Bremerich J, Reddy GP, Higgins CB (1999) MRI of supracristal ventricular septal defects. J Comput Assist Tomogr 23:13–15

Bricker AO, Avutu B, Mohammed TL et al (2010) Valsalva sinus aneurysms: findings at CT and MR imaging. Radiographics 30:99–110

Brickner ME, Hillis LD, Lange RA (2000) Congenital heart disease in adults. Second of two parts. N Engl J Med 342:334–342

Brizard CP, Olsson C, Wilkinson JL (2004) New approach to multiple ventricular septal defect closure with intraoperative echocardiography and double patches sandwiching the septum. J Thorac Cardiovasc Surg 128:684–692

Calkoen EE, Hazekamp MG, Blom NA et al (2016) Atrioventricular septal defect: from embryonic development to long-term follow-up. Int J Cardiol 202:784–795

Campbell M (1970) Natural history of atrial septal defect. Br Heart J 32(6):820

Corno AF, Kandakure PR, Dhannapuneni RR, Gladman G, Venugopal P, Alphonso N (2013) Multiple ventricular septal defects: a new strategy. Front Pediatr 1:16

Davia JE, Cheitlin MD, Bedynek JL (1973) Sinus venosus atrial septal defect: analysis of fifty cases. Am Heart J 85:177–185

Didier D, Higgins CB (1986) Identification and localization of ventricular septal defect by gated magnetic resonance imaging. Am J Cardiol 57:1363–1368

Didier D, Higgins CB, Fisher MR, Osaki L, Silverman NH, Cheitlin MD (1986) Congenital heart disease: gated MR imaging in 72 patients. Radiology 158:227–235

Driscoll A, Worrall-Carter L, Stewart S (2006) Rationale and design of the National Benchmarking and evidence-based National Clinical Guidelines for chronic heart failure management programs study. J Cardiovasc Nurs 21:276–282

Gersony WM (2001) Natural history and decision-making in patients with ventricular septal defect. Prog Pediatr Cardiol 14:125–132

Geva T, Martins JD, Wald RM (2014) Atrial septal defects. Lancet 383:1921–1932

Hagen PT, Scholz DG, Edwards WD (1984) Incidence and size of patent foramen ovale during the first 10 decades of life: an autopsy study of 965 normal hearts. Mayo Clin Proc 59:17–20

Hanslik A, Pospisil U, Salzer-Muhar U, Greber-Platzer S, Male C (2006) Predictors of spontaneous closure of isolated secundum atrial septal defect in children: a longitudinal study. Pediatrics 118:1560–1565

Helgason H, Jonsdottir G (1999) Spontaneous closure of atrial septal defects. Pediatr Cardiol 20:195–199

Hoffman JI, Kaplan S (2002) The incidence of congenital heart disease. J Am Coll Cardiol 39:1890–1900

Hoffman JI, Kaplan S, Liberthson RR (2004) Prevalence of congenital heart disease. Am Heart J 147:425–439

Holzer R, Balzer D, Cao QL, Lock K, Hijazi ZM (2004) Amplatzer muscular ventricular Septal defect I. Device closure of muscular ventricular septal defects using the Amplatzer muscular ventricular septal defect occluder: immediate and mid-term results of a U.S. registry. J Am Coll Cardiol 43:1257–1263

Hugh D, Allen RES, Daniel J (2016) Penny, Timothy F. Feltes, Frank Cetta. Moss and Adams' Heart Disease in infants, children and adolescents. 9th edn

Humenberger M, Rosenhek R, Gabriel H et al (2011) Benefit of atrial septal defect closure in adults: impact of age. Eur Heart J 32:553–560

Jacobs JP, Burke RP, Quintessenza JA, Mavroudis C (2000) Congenital heart surgery nomenclature and database project: ventricular septal defect. Ann Thorac Surg 69:S25–S35

Kafka H, Mohiaddin RH (2009) Cardiac MRI and pulmonary MR angiography of sinus venosus defect and partial anomalous pulmonary venous connection in cause of right undiagnosed ventricular enlargement. AJR Am J Roentgenol 192:259–266

Kirklin JK, Castaneda AR, Keane JF, Fellows KE, Norwood WI (1980) Surgical management of multiple ventricular septal defects. J Thorac Cardiovasc Surg 80:485–493

Kitagawa T, Durham LA III, Mosca RS, Bove EL (1998) Techniques and results in the management of multiple ventricular septal defects. J Thorac Cardiovasc Surg 115:848–856

Ko SF, Liang CD, Yip HK et al (2009) Amplatzer septal occluder closure of atrial septal defect: evaluation of transthoracic echocardiography, cardiac CT, and transesophageal echocardiography. AJR Am J Roentgenol 193:1522–1529

Konstantinides S, Geibel A, Olschewski M et al (1995) A comparison of surgical and medical therapy for atrial septal defect in adults. N Engl J Med 333:469–473

Kucher N, Seiler C, Allemann Y, Eberli FR (2001) Double-chambered right ventricle. Circulation 103:E105–E106

Langer C, Horstkotte D, Piper C (2007) Aneurysm of the membranous septum causes pre-syncopes and transient bilateral blindness. Eur Heart J 28:784

Lapierre C, Hugues N, Dahdah N, Dery J, Raboisson MJ, Miro J (2012) Long-term follow-up of large atrial septal occluder (Amplatzer device) with cardiac MRI in a pediatric population. AJR Am J Roentgenol 199:1136–1141

Loukas M, Tubbs RS, Louis RG Jr, Curry B (2006) Pseudoaneurysm of the membranous septum, case report and review of the literature. Surg Radiol Anat 28:564–568

Lun K, Li H, Leung MP et al (2001) Analysis of indications for surgical closure of subarterial ventricular septal defect without associated aortic cusp prolapse and aortic regurgitation. Am J Cardiol 87:1266–1270

Matsuwaka R, Tomokuni T, Ishikawa S, Watanabe F, Matsushita T, Matsuda H (1987) Partially unroofed coronary sinus associated with tricuspid atresia. An important associated lesion in the Fontan operation. Eur J Cardiothorac Surg 1:180–182

McMahon CJ, Feltes TF, Fraley JK et al (2002) Natural history of growth of secundum atrial septal defects and implications for transcatheter closure. Heart 87:256–259

Minette MS, Sahn DJ (2006) Ventricular septal defects. Circulation 114:2190–2197

Mongeon FP, Burkhart HM, Ammash NM et al (2010) Indications and outcomes of surgical closure of ventricular septal defect in adults. JACC Cardiovasc Interv 3:290–297

Neumayer U, Stone S, Somerville J (1998) Small ventricular septal defects in adults. Eur Heart J 19:1573–1582

Newfeld EA, Muster AJ, Paul MH, Idriss FS, Riker WL (1976) Discrete subvalvular aortic stenosis in childhood. Study of 51 patients. Am J Cardiol 38:53–61

Ootaki Y, Yamaguchi M, Yoshimura N, Oka S, Yoshida M, Hasegawa T (2003a) Unroofed coronary sinus syndrome: diagnosis, classification, and surgical treatment. J Thorac Cardiovasc Surg 126:1655–1656

Ootaki Y, Yamaguchi M, Yoshimura N, Oka S, Yoshida M, Hasegawa T (2003b) Surgical management of trabecular ventricular septal defects: the sandwich technique. J Thorac Cardiovasc Surg 125:508–512

Parsons JM, Baker EJ, Anderson RH et al (1990) Morphological evaluation of atrioventricular septal defects by magnetic resonance imaging. Br Heart J 64:138–145

Pennell DJ, Sechtem UP, Higgins CB et al (2004) Clinical indications for cardiovascular magnetic resonance (CMR): consensus panel report. Eur Heart J 25:1940–1965

Penny DJ, Vick GW III (2011) Ventricular septal defect. Lancet 377:1103–1112

Pongiglione G, Freedom RM, Cook D, Rowe RD (1982) Mechanism of acquired right ventricular outflow tract obstruction in patients with ventricular septal defect: an angiocardiographic study. Am J Cardiol 50:776–780

Prasad SK, Soukias N, Hornung T et al (2004) Role of magnetic resonance angiography in the diagnosis of major aortopulmonary collateral arteries and partial anomalous pulmonary venous drainage. Circulation 109:207–214

Rajiah P, Kanne JP (2010) Computed tomography of septal defects. J Cardiovasc Comput Tomogr 4:231–245

Roguin N, ZD D, Barak M, Nasser N, Hershkowitz S, Milgram E (1995) High prevalence of muscular ventricular septal defect in neonates. J Am Coll Cardiol 26:1545–1548

Sachweh JS, Daebritz SH, Hermanns B et al (2006) Hypertensive pulmonary vascular disease in adults with secundum or sinus venosus atrial septal defect. Ann Thorac Surg 81:207–213

Sadler TW (2015) Langman's medical embryology. 13th edn

Saremi F (2014) Cardiac CT and MR for adult congenital heart disease. Springer, New York

Saxena A, Divekar A, Soni NR (2005) Natural history of secundum atrial septal defect revisited in the era of transcatheter closure. Indian Heart J 57:35–38

Seddio F, Reddy VM, McElhinney DB, Tworetzky W, Silverman NH, Hanley FL (1999) Multiple ventricular septal defects: how and when should they be repaired? J Thorac Cardiovasc Surg 117:134–139. discussion 39-40

Serraf A, Lacour-Gayet F, Bruniaux J et al (1992) Surgical management of isolated multiple ventricular septal defects. Logical approach in 130 cases. J Thorac Cardiovasc Surg 103:437–42; discussion 43

Slovis TL (2008). Caffey's pediatric diagnostic imaging. 11th edition.

Soto B, Becker AE, Moulaert AJ, Lie JT, Anderson RH (1980) Classification of ventricular septal defects. Br Heart J 43:332–343

Steele PM, Fuster V, Cohen M, Ritter DG, McGoon DC (1987) Isolated atrial septal defect with pulmonary vascular obstructive disease--long-term follow-up and prediction of outcome after surgical correction. Circulation 76:1037–1042

Stellin G, Padalino M, Milanesi O et al (2000) Surgical closure of apical ventricular septal defects through a right ventricular apical infundibulotomy. Ann Thorac Surg 69:597–601

Studer M, Blackstone EH, Kirklin JW et al (1982) Determinants of early and late results of repair of atrioventricular septal (canal) defects. J Thorac Cardiovasc Surg 84:523–542

Sugimoto M, Ota K, Kajihama A, Nakau K, Manabe H, Kajino H (2011) Volume overload and pressure overload due to left-to-right shunt-induced myocardial injury. Evaluation using a highly sensitive cardiac troponin-I assay in children with congenital heart disease. Circ J 75:2213–2219

Tandon R, Edwards JE (1973) Aneurysmlike formations in relation to membranous ventricular septum. Circulation 47:1089–1097

Tatsuno K, Konno S, Ando M, Sakakibara S (1973) Pathogenetic mechanisms of prolapsing aortic valve and aortic regurgitation associated with ventricular septal defect. Anatomical, angiographic, and surgical considerations. Circulation 48:1028–1037

Van Praagh S, Carrera ME, Sanders SP, Mayer JE, Van Praagh R (1994) Sinus venosus defects: unroofing of the right pulmonary veins—anatomic and echocardiographic findings and surgical treatment. Am Heart J 128:365–379

van Son JA, Schaff HV, Danielson GK, Hagler DJ, Puga FJ (1993) Surgical treatment of discrete and tunnel subaortic stenosis. Late survival and risk of reoperation. Circulation 88:II159–II169

Vogel M, Berger F, Kramer A, Alexi-Meshkishvili V, Lange PE (1999) Incidence of secondary pulmonary

hypertension in adults with atrial septal or sinus venosus defects. Heart 82:30–33
Wald RM, Powell AJ (2006) Simple congenital heart lesions. J Cardiovasc Magn Reson 8:619–631
Wald RM, Silversides CK, Kingdom J et al (2015) Maternal cardiac output and fetal Doppler predict adverse neonatal outcomes in pregnant women with heart disease. J Am Heart Assoc 4:ii
Wang ZJ, Reddy GP, Gotway MB, Yeh BM, Higgins CB (2003) Cardiovascular shunts: MR imaging evaluation. Radiographics 23(Spec issue):S181–S194
Warnes CA, Williams RG, Bashore TM et al (2008) ACC/AHA 2008 guidelines for the management of adults with congenital heart disease: a report of the American College of Cardiology/American Heart Association task force on practice guidelines (writing committee to develop guidelines on the Management of Adults with Congenital Heart Disease). Developed in collaboration with the American Society of Echocardiography, Heart Rhythm Society, International Society for Adult Congenital Heart Disease, Society for Cardiovascular Angiography and Interventions, and Society of Thoracic Surgeons. J Am Coll Cardiol 52:e143–e263
Webb G, Gatzoulis MA (2006) Atrial septal defects in the adult: recent progress and overview. Circulation 114:1645–1653
Weber C, Weber M, Ekinci O et al (2008) Atrial septal defects type II: noninvasive evaluation of patients before implantation of an Amplatzer Septal Occluder and on follow-up by magnetic resonance imaging compared with TEE and invasive measurement. Eur Radiol 18:2406–2413
Wollenek G, Wyse R, Sullivan I, Elliott M, de Leval M, Stark J (1996) Closure of muscular ventricular septal defects through a left ventriculotomy. Eur J Cardiothorac Surg 10(8):595
Yavuz S, Eris C, Goncu T, Sezen M, Ata Y, Turk T (2010) An incidental aneurysm of the interventricular membranous septum. Arch Iran Med 13(4):363
YC F, Bass J, Amin Z et al (2006) Transcatheter closure of perimembranous ventricular septal defects using the new Amplatzer membranous VSD occluder: results of the U.S. phase I trial. J Am Coll Cardiol 47:319–325
Yilmaz AT, Ozal E, Arslan M, Tatar H, Ozturk OY (1997) Aneurysm of the membranous septum in adult patients with perimembranous ventricular septal defect. Eur J Cardiothorac Surg 11:307–311

Tricuspid Valve Abnormalities

Daniel Tobler, Laura Jimenez-Juan,
Andrew M. Crean, and Rachel M. Wald

Contents

Abstract

Tricuspid valve abnormalities are relatively rare lesions in the spectrum of congenital heart disease which can affect the leaflets, chordal apparatus, and/or papillary muscles of the tricuspid valve. Ebstein anomaly is the most common form of congenital tricuspid valve disease. Although outcomes remain poor in neonates with important tricuspid valve disease, Ebstein anomaly can be managed successfully in children, adolescents, and young adults with recent surgical advances and current interventional techniques. Comprehensive cardiac imaging is essential to allow for accurate diagnosis and appropriate decision-making, and should always be performed by an advanced cardiac imaging specialist with expertise in congenital heart disease. In this chapter, anatomical features pertaining to the range of congenital heart defects which affect the tricuspid valve are reviewed, current imaging techniques are detailed, and contemporary approaches to management are discussed.

D. Tobler, M.D., F.E.S.C.
Department of Cardiology, University Hospital Basel, University of Basel, Petersgraben 4, CH-4031 Basel, Switzerland

L. Jimenez-Juan, M.D.
Department of Medical Imaging, University of Toronto, Toronto, ON, Canada

Department of Medical Imaging, Sunnybrook Health Sciences Centre, Toronto, ON, Canada

A.M. Crean, M.R.C.P., F.R.C.R.
Sanghvi Endowed Chair in Cardiovascular Imaging, University of Cincinnati Medical Center and Cincinnati Children's Hospital Medical Center, Cincinnati, OH, USA

R.M. Wald, M.D., F.R.C.P.C. (✉)
Division of Cardiology, Peter Munk Cardiac Centre, University Health Network, Toronto, ON, Canada

Departments of Pediatrics, Medicine, Medical Imaging and Obstetrics & Gynecology, University of Toronto, Toronto, ON, Canada
e-mail: Rachel.Wald@uhn.ca

Med Radiol Diagn Imaging (2017)
DOI 10.1007/174_2017_108, © Springer International Publishing AG
Published Online: 15 July 2017

1 Morphology of the Normal Tricuspid Valve

In the structurally normal heart, the tricuspid valve guards the inlet portion of the right ventricle. The three leaflets of the tricuspid valve are located in septal, anterior, and posterior (also called inferior or mural) positions. The papillary muscles (medial, anterior, inferior) provide support for the tricuspid valve leaflets. Unlike the mitral valve, however, chordal attachments from the septal leaflet of the tricuspid valve to the ventricular septum are present. The tricuspid valve septal attachments are more apically positioned compared to the anterior mitral leaflet (creating an "offset" between the right and left atrioventricular valve positions); a distance of up to 8 mm/m^2 between the attachment of the septal tricuspid leaflet and the anterior mitral leaflet is considered normal (Edwards 1993; Seward 1993).

2 Congenital Defects of the Tricuspid Valve

Isolated congenital malformations of the tricuspid valve are relatively rare lesions. Tricuspid valve disease can affect the leaflets, chordal apparatus, and/or papillary muscles. For the purposes of this discussion, tricuspid valve disease will be reviewed according to morphologic abnormalities pertaining to:

(a) Displacement of the valve leaflets from the atrioventricular junction towards the apex of the right ventricle (Ebstein anomaly)
(b) Hypoplasia of the valve annulus or thickening of the valve leaflets (tricuspid valve stenosis)
(c) Abnormal/incomplete leaflet development (tricuspid valve dysplasia) or
(d) Tricuspid valve disease present in the context of other forms of complex congenital heart disease

2.1 Ebstein Anomaly

Although a rare disease (occurring in approximately 3–5 per 100,000 live births and accounting for less than 1% of all forms of congenital heart disease) (Samanek and Voriskova 1999; Correa-Villasenor et al. 1994), Ebstein anomaly is one of the most striking abnormalities of the tricuspid valve. The malformation is often complex and typically involves the tricuspid valve leaflets, the chordal apparatus, and the myocardium of the right ventricle. Additionally, Ebstein anomaly is frequently associated with additional lesions affecting the right or left heart and can encompass an unusually wide clinical spectrum. Diagnostic criteria for Ebstein anomaly typically include (1) apical (downward) displacement of the tricuspid valve functional annulus (hinge point of the valve from the atrioventricular ring >8 mm/m^2), (2) adherence of the tricuspid valve leaflets to underlying myocardium (failure of delamination), (3) redundancy, fenestrations, and/or tethering of the anterior leaflet, (4) dilation of the true tricuspid valve annulus (right atrioventricular junction), and (5) dilation of the atrialized portion of the right ventricle (Attenhofer Jost et al. 2012a).

While Ebstein anomaly diagnosed in fetal or neonatal life continues to be associated with dismal outcomes (perinatal mortality estimated at 45%) even in contemporary series (Yetman et al. 1998; Wald et al. 2005; Bove et al. 2009; Freud et al. 2015), in some instances underlying Ebstein anomaly may remain undetected throughout adult life to be discovered only at the time of autopsy (Celermajer et al. 1994). The clinical presentation of symptomatic Ebstein anomaly in the adult may include fatigue, palpitations, decreased exercise tolerance, edema, and/or cyanosis. Tachyarrhythmias (atrial or ventricular), heart failure, paradoxical embolism, transient ischemic attacks or stroke, endocarditis, and sudden death are recognized sequelae of Ebstein anomaly (Celermajer et al. 1994). Contemporary guidelines suggest that symptomatic patients should be considered for operative repair or replacement of the tricuspid valve (Attenhofer Jost et al. 2012b; Warnes et al. 2008; Baumgartner et al. 2010). Younger age at diagnosis, male gender, cardiothoracic ratio ≥0.65, and the severity of tricuspid valve leaflet displacement on echocardiography have been identified as independent predictors of cardiac

mortality in patients with Ebstein anomaly (Attie et al. 2000). The functional integrity of the tricuspid valve in Ebstein anomaly generally depends on several factors which include the degree of displacement of the right atrioventricular junction, extent of dysplasia of septal and posterior leaflets, presence and size of fenestrations, size and restriction of the anterior leaflet, and dilatation of the "functional" tricuspid valve annulus.

Comprehensive cardiac imaging is crucial for accurate diagnosis and decision-making, and should always be performed by an advanced cardiac imaging specialist with expertise in congenital heart disease. Multi-modality imaging should be employed to characterize morphology of the tricuspid valve leaflets and underlying mechanism of their dysfunction (transthoracic ± transesophageal echocardiography); to quantify dimensions of the right atrium, atrialized right ventricle, and functional right ventricle (cardiac magnetic resonance imaging [CMR] or cardiac CT); and to delineate associated congenital heart disease lesions as well as structure of the left myocardium (echocardiography ± cardiac magnetic resonance imaging or cardiac CT).

2.1.1 Displacement of the Atrioventricular Junction

Ebstein anomaly arises from an arrest in fetal development which results in incomplete delamination of the tricuspid valve leaflets (persistent adherence of the septal ± posterior leaflets to the underlying myocardium) resulting in an apically displaced attachment of the leaflet(s) into the right ventricle in a spiral fashion such that the valve is displaced anteriorly and rightward. A distance of >8 mm/m^2 between the hinge points of the anterior mitral valve leaflet and tricuspid valve septal leaflet is considered diagnostic for Ebstein anomaly (Seward 1993). The apical displacement of the right atrioventricular junction results in two components of the right ventricle. The portion between the true tricuspid annulus and the functional annulus is termed the "atrialized" right ventricle and the remainder of the right ventricle is designated as the "functional" right ventricle (Fig. 1). The degree of adherence of the posterior and septal leaflets determines the spectrum of disease severity, ranging from mild forms with minimal displacement of the septal leaflet to complete failure of delamination of the leaflets resulting in an imperforate membrane (tricuspid sac).

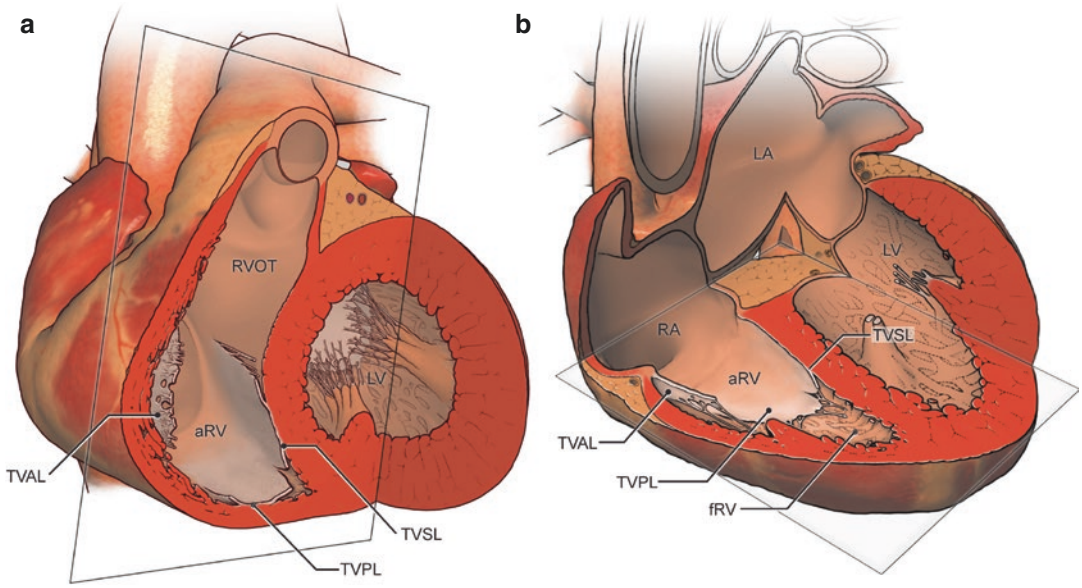

Fig. 1 Schematic demonstrating Ebstein anomaly in the short axis view (**a**) and axial view (**b**). *aRV* atrialized right ventricle, *fRV* functional right ventricle, *LA* left atrium, *LV* left ventricle, *RA* right atrium, *RVOT* right ventricular outflow tract, *TVAL* tricuspid valve anterior leaflet, *TVPL* tricuspid valve posterior leaflet, *TVSL* tricuspid valve septal leaflet

2.1.2 Development of the Septal and Posterior Leaflets

In Ebstein anomaly, the displaced septal and posterior leaflets of the tricuspid valve can often appear thickened or dysplastic (Freedom 1997). The septal leaflet can assume a wide spectrum of anatomic malformations or may be altogether absent. Chordae may be few or even absent and are typically shortened and dysplastic with anomalous insertions into the right ventricular wall (Freedom 1997). Tricuspid regurgitation is commonly seen in Ebstein anomaly, often a result of leaflet malcoaptation, although fenestrations can provide an additional mechanism for valve insufficiency; tricuspid valve stenosis has been described although is infrequently observed (Fig. 2).

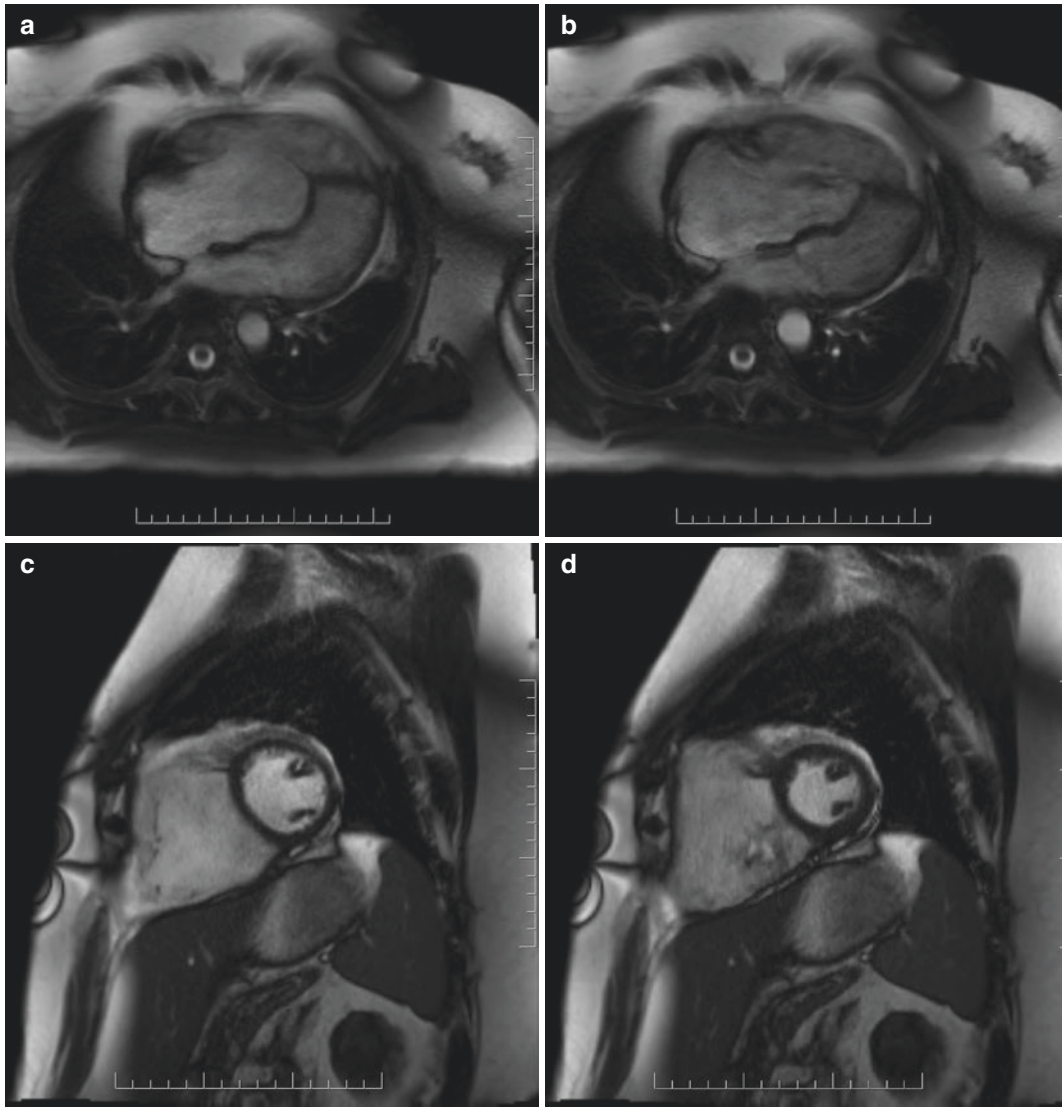

Fig. 2 Cardiac magnetic resonance imaging of severe tricuspid regurgitation in Ebstein anomaly; (**a**) four chamber view in diastole, (**b**) four chamber view in systole, (**c**) short axis view in diastole, (**d**) short axis view in systole

2.1.3 Morphology of the Anterior Leaflet

In contrast to the septal leaflet, the anterior leaflet of the tricuspid valve is rarely displaced. The anterior leaflet is characteristically elongated and, if sufficiently redundant, may contribute to obstruction of the right ventricular outflow tract. Fenestrations within the leaflet are commonly seen. Tethering of the anterior leaflet frequently arises from chordal attachments to the ventricular free wall and/or displaced papillary muscles. Size and mobility of the anterior leaflet are important determinants for tricuspid valve anatomic repair (Cone reconstruction) (Brown 2011), and therefore detailed description of leaflet morphology is critical when surgery referral is being considered. In rare situations, the anterior leaflet forms an atretic membrane (Ho et al. 2005).

2.1.4 Development of the Right Ventricle

The atrialized portion of the right ventricle is typically dilated and thinned in the patient with Ebstein anomaly. Size of the atrialized right ventricle has been associated with poor prognosis in both children (Celermajer et al. 1992) and adults (Celermajer et al. 1994; Attie et al. 2000). Morphologic features of the functional right ventricle apex often include increased trabeculations although the myocardium itself may be thinned or even aneurysmal. In the extreme form, replacement of the myocardium with fibrous tissue has been observed. Hypoplasia of the functional right ventricle in neonates and children is typically a result of marked apical displacement of the atrioventricular junction. In contrast, the functional portion of the right ventricle is often described as normal in size or even dilated in the adult (Yalonetsky et al. 2011; Lee et al. 2012; Fratz et al. 2012) and has been attributed to chronicity and severity of tricuspid valve regurgitation (Tobler et al. 2011).

2.1.5 Associated Cardiac Abnormalities

Numerous additional congenital heart lesions have been described in conjunction with Ebstein anomaly. An interatrial communication, such as a secundum atrial septal defect or a patent foramen ovale, is the most frequently reported association (80% of cases) (Danielson et al. 1992) (Fig. 3). Right-to-left shunting at atrial level may give rise to cyanosis or may allow for paradoxical emboli which may result in transient ischemic attacks or stroke. Ventricular septal defects are occasionally associated with Ebstein anomaly. Associated right heart lesions include pulmonary stenosis, pulmonary atresia, or tetralogy of Fallot; associated left heart lesions include bicuspid aortic valve, aortic stenosis, aortic atresia, coarctation of the aorta, and mitral valve defects. Noncompaction of the left ventricular myocardium is a well-described association (Attenhofer Jost et al. 2005) (Fig. 4). The apical displacement of the septal tricuspid valve may result in discontinuity of the central fibrous body and septal atrioventricular ring, thereby allowing for accessory pathway formation, as seen in Wolff–Parkinson–White syndrome (Khositseth et al. 2004), which provides a substrate for supraventricular tachycardia. Atrial enlargement may give rise to atrial fibrillation or atrial flutter. Ventricular arrhythmias, in the setting myocardial fibrosis or left ventricular noncompaction, have been described although are far less common than atrial arrhythmias.

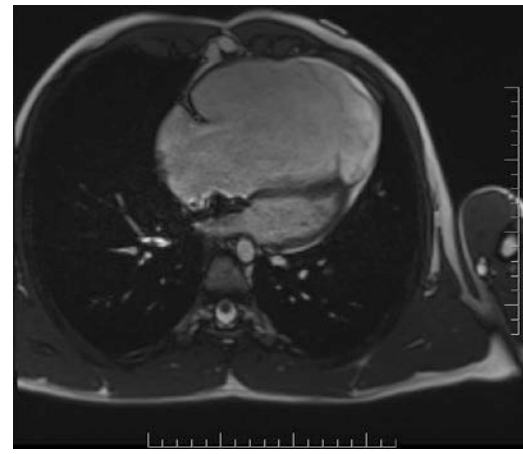

Fig. 3 Cardiac magnetic resonance imaging of an Amplatzer device closure of an atrial septal defect in a patient with Ebstein anomaly

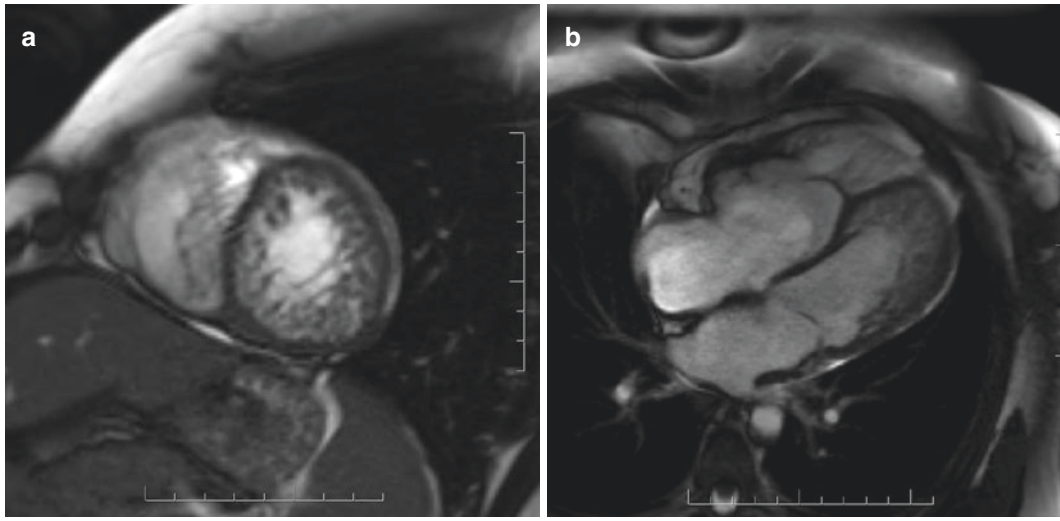

Fig. 4 Cardiac magnetic resonance imaging of left ventricular noncompaction in a patient with Ebstein anomaly in short axis (**a**) and four chamber views (**b**)

2.2 Tricuspid Stenosis

Isolated stenosis of the tricuspid valve stenosis is a rare lesion and is typically congenital. Stenosis is usually seen at valvular level due to hypoplasia or underdevelopment of the tricuspid annulus or thickening of the valve leaflets with reduced valve orifice. Occasionally, stenosis is supravalvular, and occurs as a result of a supravalvular ring or membrane at the level of the tricuspid annulus or at the midportion of the leaflets. In isolated valvular tricuspid stenosis the reduced valve orifice may result from thickened or hypoplastic tricuspid leaflets, underdeveloped or fused commissures, abnormal chordal attachments (i.e., parachute deformity) (Freedom 1997), and/or annular hypoplasia. Significant tricuspid stenosis can result in dilation and hypertrophy of the right atrium, and in some cases, hepatomegaly.

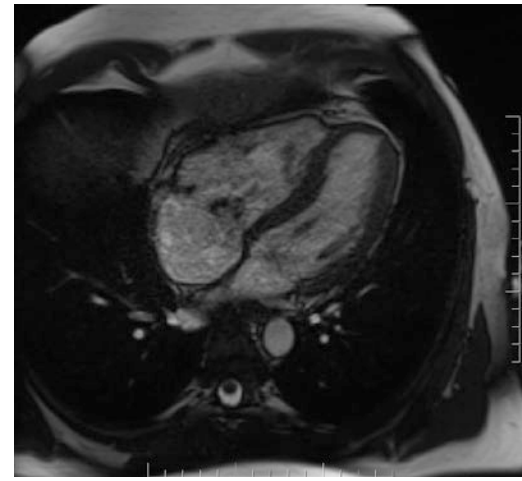

Fig. 5 Cardiac magnetic resonance imaging of a tricuspid valve dysplasia and severe TR

2.3 Tricuspid Valve Dysplasia

Tricuspid regurgitation is commonly a secondary finding in the presence of right ventricular disease (i.e., pressure/volume overload, systolic/diastolic dysfunction). Rarely, tricuspid regurgitation is a primary manifestation of tricuspid valve dysplasia. Tricuspid valve dysplasia is not a single entity but encompasses various congenital malformations such as malformation of the valve leaflets, hypoplasia of the papillary muscles, and/or abnormalities of tendinous chordae apparatus. Tricuspid valve leaflet hypoplasia and tethering, most commonly involving the septal leaflet, resulting in tricuspid regurgitation, is the most frequent expression of tricuspid valve dysplasia (Edwards 1993) (Fig. 5).

2.4 Tricuspid Valve Disease Associated with Other Congenital Lesions

The tricuspid valve may be involved in more complex forms of congenital heart disease. Congenital corrected transposition of the great arteries (cc-TGA) is often associated with an Ebstein-like malformation of the tricuspid valve (Fig. 6). In this condition, the tricuspid valve serves as a systemic atrioventricular valve and, therefore, is exposed to higher pressure than in typical Ebstein anomaly where the tricuspid valve is a subpulmonary atrioventricular valve. The tricuspid valve leaflets in this condition are often dysplastic and, as in usual Ebstein anomaly, apical displacement of the atrioventricular junction may be present. Unless bona fide Ebstein disease, the anterior leaflet is usually not elongated and the incomplete delamination of the septal and posterior leaflets are limited such that the atrialized portion of the right ventricle is not particularly enlarged (hence the designation Ebstein-like anomaly) (Allwork et al. 1976; Silverman et al. 1995; Anderson et al. 1978; Horvath et al. 1994). Annular hypoplasia and tricuspid stenosis have been described in various forms of complex congenital heart disease such as tetralogy of Fallot, pulmonary atresia with intact ventricular septum, transposition of the great arteries, and double-outlet right ventricle. A rare form of tricuspid valve disease is the so-called "double-orifice tricuspid valve" which has been seen in association with Ebstein anomaly, tricuspid valve dysplasia, tetralogy of Fallot, and atrioventricular septal defect (AVSD). Extreme forms of Ebstein anomaly or severe tricuspid stenosis/atresia will result in profound underdevelopment (hypoplasia) of the right ventricle resulting in "single ventricle physiology" of the left ventricular type.

3 Management

Much of the literature pertaining to management of the adult with tricuspid valve disease focuses on those with Ebstein anomaly given the rarity of the other tricuspid valve lesions (described above). With advancing age, survival in the adult with unrepaired Ebstein anomaly substantially decreases over time. In a cohort of 72 unoperated patients over the age of 25 years, Attie and colleagues demonstrated that survival was 76% at 10 years of follow-up with a marked decrease to 41% at 20 years (Attie et al. 2000). The American Heart Association states that surgery in the adult with Ebstein anomaly should only be performed by

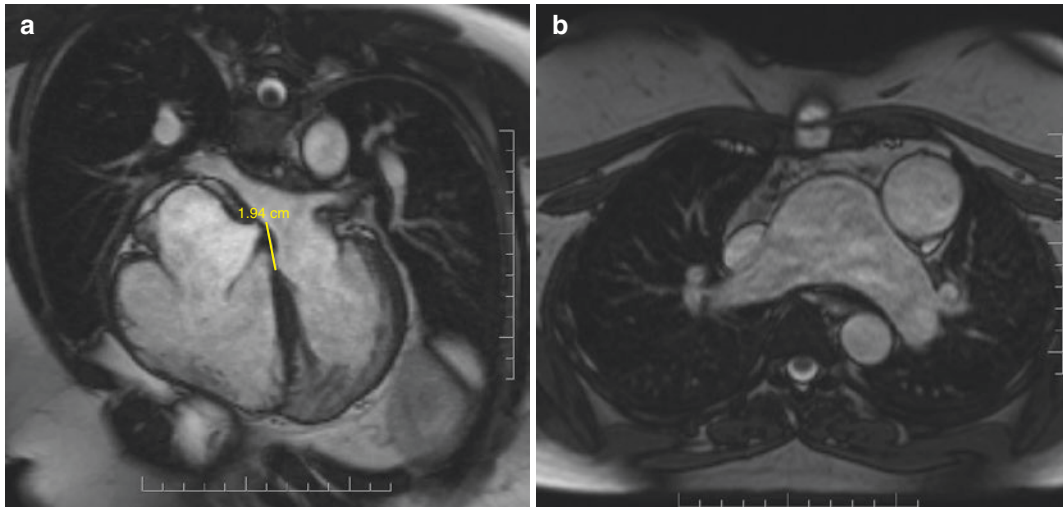

Fig. 6 Cardiac magnetic resonance imaging of congenitally corrected transposition of the great arteries with Ebstein-like anomaly of the tricuspid valve (systemic atrioventricular valve) (**a**) and demonstration of anterior and leftward position of the aorta relative to the pulmonary artery (**b**)

surgeons with training and expertise in adult congenital heart disease and outlines the following as class 1 indications for operative intervention: development of symptoms/decline in exercise testing, development of cyanosis, presence of paradoxical emboli, progressive enlargement of cardiothoracic silhouette on chest X-ray, and progressive enlargement or dysfunction of the right ventricle (grade of evidence B for all listed criteria) (Warnes et al. 2008). The European Society of Cardiology lists virtually identical criteria for surgical intervention (class 1 or IIa for factors listed above, grade of evidence C) (Baumgartner et al. 2010).

The goals of surgery typically include improvement in tricuspid valve function, closure of residual intracardiac shunts (atrial/ventricular septal defects), down-sizing of the right atrium through plications and/or arrhythmia surgery (typically the Maze procedure). Specific surgical strategies may include tricuspid valve repair (traditionally monocusp repair and more recently Cone repair), or tricuspid valve replacement, and in the event of extreme right ventricular hypoplasia insertion of a direct superior vena cava to pulmonary artery connection (i.e., a "Glenn" shunt to offload the right ventricle, or a one and a half ventricle repair) (Fig. 7). In rare occasions, severe Ebstein anomaly with a markedly attenuated right ventricle is best treated with a Fontan palliation (single ventricle strategy) (Fig. 8). Given the variability in right heart function and the challenges in assessment of systolic function in the presence of significant tricuspid valve regurgitation, surgery for Ebstein anomaly

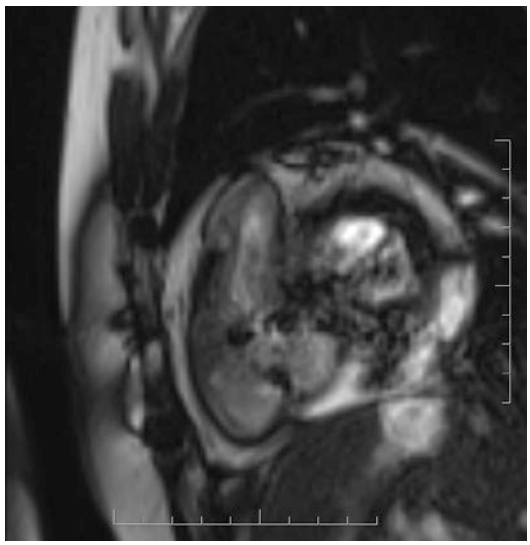

Fig. 7 Cardiac magnetic resonance imaging demonstrating prosthetic tricuspid valve replacement in a patient with Ebstein anomaly

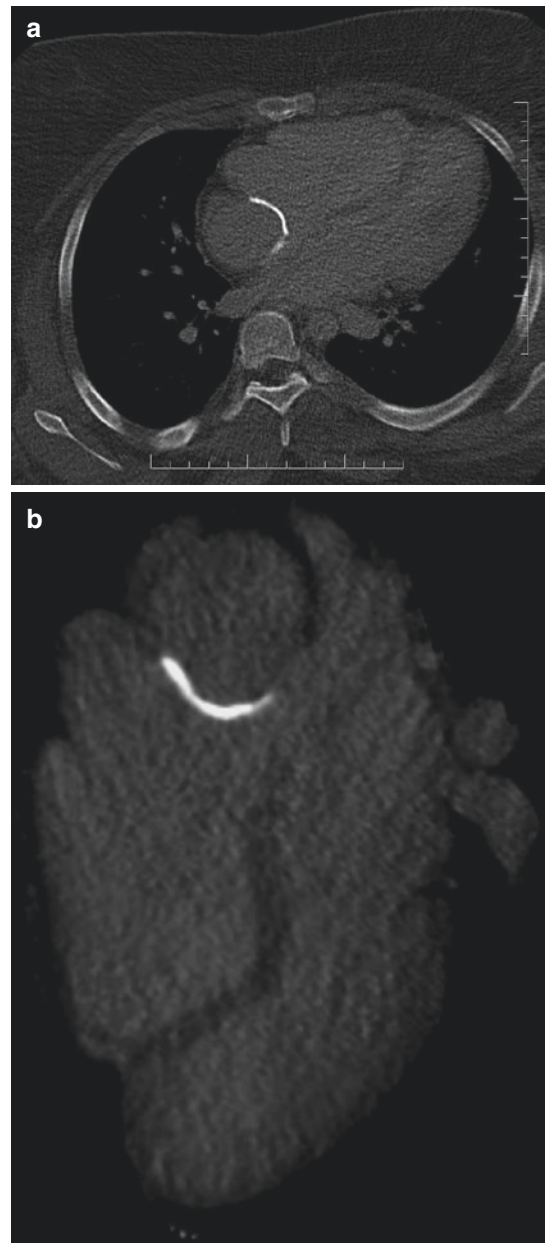

Fig. 8 Cardiac CT of a patient with underlying Ebstein anomaly palliated with a lateral tunnel Fontan, now calcified. Axial view (**a**) and reconstructed four chamber view (**b**)

can incur a perioperative mortality not typically seen in other forms of congenital heart disease. Therefore, the decision to proceed with surgery in a given individual should involve detailed discussion amongst a specialized team of adult congenital heart disease specialists, congenital heart disease surgeons, cardiac anesthesiologists, and in some cases, electrophysiologists. The cone surgical repair, first described by da Silva (da Silva et al. 2007), involving the delamination and rotation of the anterior septal leaflet with use of remnant septal and posterior leaflets to create a cone with bicuspid coaptation of valve leaflets, is now the considered the surgical repair of choice and is directed by the adequacy of the anterior leaflet size and morphology. Recent CMR studies have demonstrated that following Cone repair, right ventricular end-diastolic volumes decrease, right ventricular ejection fraction remains the same or decreases (Lange et al. 2015; Li et al. 2016), and pulmonary forward flow and left ventricular filling increases corresponding to an improvement in aerobic capacity on exercise testing (Ibrahim et al. 2015).

4 Imaging Techniques

4.1 Chest X-Ray

The (erect) chest X-ray can be normal or nearly normal in mild cases of Ebstein anomaly. The characteristic findings of a "globular" cardiac silhouette, described in patients with severe Ebstein anomaly, relates to marked enlargement of the right atrium. Cardiomegaly on X-ray is independently associated with adverse outcomes in patients with Ebstein anomaly (Attie et al. 2000). Contemporary management guidelines for adults with congenital heart disease suggest that enlarged or enlarging cardiothoracic ratio, as measured on chest X-ray, can be considered an indication for operative repair (Warnes et al. 2008; Baumgartner et al. 2010).

4.2 Echocardiography

Transthoracic echocardiography is considered the imaging modality of choice for the initial diagnosis of tricuspid valve disease. Characterization of valve morphology and function (i.e., stenosis or regurgitation) can be reliably achieved using transthoracic echocardiography primarily, and transesophageal echocardiography occasionally. Estimation of right ventricular pressure, cardiac chamber dimensions (right atrial, atrialized right ventricular, and ventricle sizes), and ventricular systolic function can be achieved; evaluation of associated congenital heart disease lesions (such as atrial or ventricular septal defects) can be accomplished. Following initial diagnosis, transthoracic echocardiography remains the imaging modality of choice for first-line surveillance of disease progression in the adult given its widespread availability. Detailed anatomic and functional review of the right heart, with specific focus on tricuspid valve morphology, as detailed above, is essential for patients referred for surgical repair. Severity of Ebstein anomaly, as determined by linear extent of apical displacement of the septal leaflet indexed to body surface area (Seward 1993) or a ratio of the areas of the right atrium and atrialized right ventricle as compared with the remainder of the heart can be readily accomplished by echocardiography (Celermajer et al. 1992).

4.3 Cardiovascular Magnetic Resonance Imaging (CMR)

Virtually all aspects of Ebstein anomaly are reliably characterized using CMR, with the exception of detailed characterization of some aspects of valve morphology. As such, CMR is an important, although emerging imaging modality in the preoperative and postoperative assessment of patients with tricuspid valve disease, such as Ebstein anomaly. CMR can provide morphologic and physiologic information not reliably obtained using echocardiography alone. Steady-state free-precession (SSFP) cine imaging can allow for characterization of tricuspid valve morphology in patients with poor acoustic windows, can provide quantification of right heart volumes (atrialized right ventricle and functional right ventricle) and ventricular systolic function (Yalonetsky et al. 2011). Several authors have reported lower interobserver variability in the axial plane as compared with the short axis view

(Yalonetsky et al. 2011; Fratz et al. 2012). Phase contrast flow analysis can allow for estimation of magnitude of an intracardiac shunt (using comparison of flow volumes through the main pulmonary artery and aorta) and measurement of tricuspid regurgitation (by comparison of main pulmonary artery flow and right ventricular stroke volume). Magnetic resonance angiography (MRA) should be used for assessment of associated vascular abnormalities, such as abnormalities in pulmonary arterial development, coarctation of the aorta, or patent ductus arteriosus.

The role of CMR for risk stratification and preoperative assessment of the patient with Ebstein anomaly is emerging, although as of yet is incompletely defined. Given the complexities of right ventricular anatomy in the patient with Ebstein anomaly it is not surprising that echocardiographic indices of right ventricular systolic function correlate poorly with CMR-derived assessment of right ventricular function (Kuhn et al. 2016). A recent prospective study of 16 patients with Ebstein anomaly at the Mayo clinic comparing information provided by echocardiography and CMR as compared with interoperative findings revealed that CMR is superior to echocardiography for assessment of some aspects of tricuspid valve anatomy (specifically posterior leaflet morphology and presence of valve fenestrations) and that quantification of right heart size and function was only possible with CMR; these authors concluded that it is their opinion that CMR be a "compulsory" component of preoperative screening for the patient with Ebstein anomaly (Attenhofer Jost et al. 2012a). That the functional right ventricle is not diminutive, as suggested by echocardiography, but is normal in size or, more commonly, is enlarged when indexed for body surface area (some reports suggest a median increase in right ventricular end-diastolic volume more than twice normal) is a relatively new observation afforded by CMR and is likely explained by the presence of chronic tricuspid regurgitation (Fratz et al. 2012; Tobler et al. 2011). A severity score for Ebstein anomaly was first described by Celermajer derived from chamber areas apparent in the four chamber view on echocardiography ([right atrium + atrialized right ventricle]/[functional right ventricle + left atrium + left ventricle]) and was related to adverse outcomes (Celermajer et al. 1992). The first CMR-derived index of severity of Ebstein anomaly was described by Tobler and colleagues, specifically the ratio of functional right ventricular end-diastolic volume/left ventricular end-diastolic volume ratio was inversely related to peak aerobic capacity on cardiopulmonary exercise testing; however volume of the atrialized right ventricle, another novel measure, was the only CMR variable found to be independently predictive of exercise capacity (Tobler et al. 2011). More recently, Hosch et al. proposed a simplified severity index relating CMR-derived volumes of all right heart to all left heart structures ([right atrium + atrialized right ventricle + functional right ventricle/left atrium + left ventricle]) which was found to be correlated to a range of clinical parameters of heart failure and functional capacity (Hosch et al. 2014).

Although CMR is widely cited as the imaging modality of choice to evaluate anatomy, physiology, and ventricular function in the patient with Ebstein anomaly, in certain situations CMR may not be performed successfully. Given relatively limited availability and cost, CMR is still considered a restricted imaging modality. In the presence of ongoing irregularities in heart rhythm (such as frequent ectopy or ongoing atrial arrhythmias) image quality may be significantly impaired due to suboptimal cardiac gating resulting in a non-diagnostic examination. CMR is generally contraindicated in pregnancy (particularly with regard to administration of gadolinium and if scanning occurs in the first trimester), in patients with in-dwelling devices (pacemakers and/or defibrillators) and in those who are claustrophobic. Anesthesia is generally required to complete a CMR study in younger children.

4.4 Cardiac Computerized Tomography

Cardiac CT is generally regarded as a partial alternative to CMR. Strengths include rapidity of data acquisition, ability to acquire isotropic data at high spatial resolution (allowing for subsequent off-line analysis), and ability to demonstrate intracardiac shunting following opacification of one side of the

heart (atrium and ventricle) with dense contrast. For the patient with Ebstein anomaly in particular, CT will allow for precise visualization of the tricuspid valve position, morphology of the chordae tendinae and papillary muscles, presence of an intracardiac shunt, and extent of myocardial trabeculation. Limitations in temporal resolution and acute administration of beta-blockade for heart rate modulation to optimize image acquisition may affect accuracy of assessment of ventricular function by cardiac CT. With contemporary dose reduction strategies, cardiac CT is achievable at relatively low radiation exposure (generally in the order of 1–2 mSv) (da Silva et al. 2007; Lange et al. 2015; Li et al. 2016; Ibrahim et al. 2015).

References

Allwork SP, Bentall HH, Becker AE, Cameron H, Gerlis LM, Wilkinson JL, Anderson RH (1976) Congenitally corrected transposition of the great arteries: morphologic study of 32 cases. Am J Cardiol 38:910–923

Anderson KR, Danielson GK, McGoon DC, Lie JT (1978) Ebstein's anomaly of the left-sided tricuspid valve: pathological anatomy of the valvular malformation. Circulation 58:187–191

Attenhofer Jost CH, Connolly HM, O'Leary PW, Warnes CA, Tajik AJ, Seward JB (2005) Left heart lesions in patients with Ebstein anomaly. Mayo Clin Proc 80:361–368

Attenhofer Jost CH, Edmister WD, Julsrud PR, Dearani JA, Savas Tepe M, Warnes CA, Scott CG, Anavekar NS, Ammash NM, Connolly HM (2012a) Prospective comparison of echocardiography versus cardiac magnetic resonance imaging in patients with Ebstein's anomaly. Int J Cardiovasc Imaging 28:1147–1159

Attenhofer Jost CH, Connolly HM, Scott CG, Burkhart HM, Warnes CA, Dearani JA (2012b) Outcome of cardiac surgery in patients 50 years of age or older with Ebstein anomaly: survival and functional improvement. J Am Coll Cardiol 59:2101–2106

Attie F, Rosas M, Rijlaarsdam M, Buendia A, Zabal C, Kuri J, Granados N (2000) The adult patient with Ebstein anomaly. Outcome in 72 unoperated patients. Medicine 79:27–36

Baumgartner H, Bonhoeffer P, De Groot NM, de Haan F, Deanfield JE, Galie N, Gatzoulis MA, Gohlke-Baerwolf C, Kaemmerer H, Kilner P, Meijboom F, Mulder BJ, Oechslin E, Oliver JM, Serraf A, Szatmari A, Thaulow E, Vouhe PR, Walma E, Task Force on the Management of Grown-Up Congenital Heart Disease of the European Society of C, Association for European Paediatric C and Guidelines ESCCfP (2010) ESC guidelines for the management of grown-up congenital heart disease (new version 2010). Eur Heart J 31:2915–2957

Bove EL, Hirsch JC, Ohye RG, Devaney EJ (2009) How I manage neonatal Ebstein's anomaly. Semin Thorac Cardiovasc Surg Pediatr Card Surg Annu:63–65

Brown ML, Dearani JA, PEF D (2011) Ebstein anomaly. In: Gatzoulis MA, Webb G, PEF D (eds) Diagnosis and management of adult congenital heart disease. Elsevier, Philadelphia, pp 288–294

Celermajer DS, Cullen S, Sullivan ID, Spiegelhalter DJ, Wyse RK, Deanfield JE (1992) Outcome in neonates with Ebstein's anomaly. J Am Coll Cardiol 19:1041–1046

Celermajer DS, Bull C, Till JA, Cullen S, Vassillikos VP, Sullivan ID, Allan L, Nihoyannopoulos P, Somerville J, Deanfield JE (1994) Ebstein's anomaly: presentation and outcome from fetus to adult. J Am Coll Cardiol 23:170–176

Correa-Villasenor A, Ferencz C, Neill CA, Wilson PD, Boughman JA (1994) Ebstein's malformation of the tricuspid valve: genetic and environmental factors. The Baltimore-Washington Infant Study Group. Teratology 50:137–147

Danielson GK, Driscoll DJ, Mair DD, Warnes CA, Oliver WC Jr (1992) Operative treatment of Ebstein's anomaly. J Thorac Cardiovasc Surg 104:1195–1202

Edwards WD (1993) Embryology and pathologic features of Ebstein's anomaly. Prog Pediatr Cardiol 2:5–15

Fratz S, Janello C, Muller D, Seligmann M, Meierhofer C, Schuster T, Schreiber C, Martinoff S, Hess J, Kuhn A, Vogt M, Stern H (2012) The functional right ventricle and tricuspid regurgitation in Ebstein's anomaly. Int J Cardiol 167:258–261

Freedom RM, Mawson JB, Yoo SJ, Benson LN (1997) Ebstein's malformation of the tricuspid valve. Armonk, NY, Futura Publishing Co

Freud LR, Escobar-Diaz MC, Kalish BT, Komarlu R, Puchalski MD, Jaeggi ET, Szwast AL, Freire G, Levasseur SM, Kavanaugh-McHugh A, Michelfelder EC, Moon-Grady AJ, Donofrio MT, Howley LW, Tierney ES, Cuneo BF, Morris SA, Pruetz JD, van der Velde ME, Kovalchin JP, Ikemba CM, Vernon MM, Samai C, Satou GM, Gotteiner NL, Phoon CK, Silverman NH, DB ME, Tworetzky W (2015) Outcomes and predictors of perinatal mortality in fetuses with Ebstein anomaly or tricuspid valve dysplasia in the current era: a multicenter study. Circulation 132:481–489

Ho SY, Rigby ML, Anderson RH (2005) Ebstein malformation. In: Ho SY, Rigby ML, Anderson RH (eds) Echocardiography in congenital heart disease made simple. Imperial College Press, London, pp 214–218

Horvath P, Szufladowicz M, de Leval MR, Elliott MJ, Stark J (1994) Tricuspid valve abnormalities in patients with atrioventricular discordance: surgical implications. Ann Thorac Surg 57:941–945

Hosch O, Sohns JM, Nguyen TT, Lauerer P, Rosenberg C, Kowallick JT, Kutty S, Unterberg C, Schuster A, Fasshauer M, Staab W, Paul T, Lotz J, Steinmetz M (2014) The total right/left-volume index: a new and simplified cardiac magnetic resonance measure to evaluate the severity of Ebstein anomaly of the tricuspid valve:

a comparison with heart failure markers from various modalities. Circ Cardiovasc Imaging 7:601–609

Ibrahim M, Tsang VT, Caruana M, Hughes ML, Jenkyns S, Perdreau E, Giardini A, Marek J (2015) Cone reconstruction for Ebstein's anomaly: patient outcomes, biventricular function, and cardiopulmonary exercise capacity. J Thorac Cardiovasc Surg 149:1144–1150

Khositseth A, Danielson GK, Dearani JA, Munger TM, Porter CJ (2004) Supraventricular tachyarrhythmias in Ebstein anomaly: management and outcome. J Thorac Cardiovasc Surg 128:826–833

Kuhn A, Meierhofer C, Rutz T, Rondak IC, Rohlig C, Schreiber C, Fratz S, Ewert P, Vogt M (2016) Non-volumetric echocardiographic indices and qualitative assessment of right ventricular systolic function in Ebstein's anomaly: comparison with CMR-derived ejection fraction in 49 patients. Eur Heart J Cardiovasc Imaging 17:930–935

Lange R, Burri M, Eschenbach LK, Badiu CC, da Silva JP, Nagdyman N, Fratz S, Horer J, Kuhn A, Schreiber C, Vogt MO (2015) Da Silva's cone repair for Ebstein's anomaly: effect on right ventricular size and function. Eur J Cardiothorac Surg 48:316–320. discussion 320–1

Lee CM, Sheehan FH, Bouzas B, Chen SS, Gatzoulis MA, Kilner PJ (2012) The shape and function of the right ventricle in Ebstein's anomaly. Int J Cardiol 167:704–710

Li X, Wang SM, Schreiber C, Cheng W, Lin K, Sun JY, Yang D, Luo SH, An Q, Chen YC (2016) More than valve repair: effect of cone reconstruction on right ventricular geometry and function in patients with Ebstein anomaly. Int J Cardiol 206:131–137

Samanek M, Voriskova M (1999) Congenital heart disease among 815,569 children born between 1980 and 1990 and their 15-year survival: a prospective Bohemia survival study. Pediatr Cardiol 20:411–417

Seward JB (1993) Ebstein's anomaly: ultrasound imaging and hemodynamic evaluation. Echocardiography 10:641–664

da Silva JP, Baumgratz JF, da Fonseca L, Franchi SM, Lopes LM, Tavares GM, Soares AM, Moreira LF, Barbero-Marcial M (2007) The cone reconstruction of the tricuspid valve in Ebstein's anomaly. The operation: early and midterm results. J Thorac Cardiovasc Surg 133:215–223

Silverman NH, Gerlis LM, Horowitz ES, Ho SY, Neches WH, Anderson RH (1995) Pathologic elucidation of the echocardiographic features of Ebstein's malformation of the morphologically tricuspid valve in discordant atrioventricular connections. Am J Cardiol 76:1277–1283

Tobler D, Yalonetsky S, Crean AM, Granton JT, Burchill L, Silversides CK, Wald RM (2011) Right heart characteristics and exercise parameters in adults with Ebstein anomaly: new perspectives from cardiac magnetic resonance imaging studies. Int J Cardiol 165:146–150

Wald RM, Adatia I, Van Arsdell GS, Hornberger LK (2005) Relation of limiting ductal patency to survival in neonatal Ebstein's anomaly. Am J Cardiol 96(6):851

Warnes CA, Williams RG, Bashore TM, Child JS, Connolly HM, Dearani JA, del Nido P, Fasules JW, Graham TP Jr, Hijazi ZM, Hunt SA, King ME, Landzberg MJ, Miner PD, Radford MJ, Walsh EP, Webb GDACC (2008) AHA 2008 guidelines for the management of adults with congenital heart disease: a report of the American College of Cardiology/American Heart Association Task Force on Practice Guidelines (writing committee to develop guidelines on the management of adults with congenital heart disease). Circulation 118:e714–e833

Yalonetsky S, Tobler D, Greutmann M, Crean AM, Wintersperger BJ, Nguyen ET, Oechslin EN, Silversides CK, Wald RM (2011) Cardiac magnetic resonance imaging and the assessment of ebstein anomaly in adults. Am J Cardiol 107:767–773

Yetman AT, Freedom RM, McCrindle BW (1998) Outcome in cyanotic neonates with Ebstein's anomaly. Am J Cardiol 81:749–754

Tetralogy of Fallot

R. W. Sprengers, A. A. W. Roest, and L. J. M. Kroft

Contents

1 Introduction

Tetralogy of Fallot (TOF) is the most common of cyanotic congenital heart diseases. In this chapter essential background information regarding etiology, clinical presentation, and treatment options in TOF are presented. The main focus is on imaging adult TOF, discussing the full spectrum of image modalities with special attention for CT and MRI. Findings in TOF, late outcome aspects, follow-up of complications, and the role of imaging in guiding therapy are discussed.

1.1 Etiology

Tetralogy of Fallot (TOF) is named after Étienne-Louis Arthur Fallot, who refined earlier descriptions of the condition in his work "L'anatomie pathologique de la maladie bleu." TOF classically consists of a tetrad of (1) right ventricular outflow tract obstruction, (2) ventricular septal defect (VSD), (3) misalignment (dextroposition, also referred to as "overriding") of the aorta, and (4) right ventricular hypertrophy (Fig. 1).

The key pathological components in TOF are anterocephalad deviation of the insertion of the outflow septum and hypertrophy of the septoparietal trabeculations of the right ventricular outflow tract, resulting in pulmonary stenosis. The anterocephalad deviation of the outflow septum results in an interventricular communication (VSD) in continuity with the aortic valve (Pacheco Duro et al. 2010).

R. W. Sprengers • L. J. M. Kroft (✉)
Department of Radiology, Leiden University Medical Center, Postbus 9600, 2300 RC, Leiden, The Netherlands
e-mail: L.J.M.Kroft@lumc.nl

A. A. W. Roest
Department of Pediatric Cardiology, Leiden University Medical Center, Leiden, The Netherlands

Med Radiol Diagn Imaging (2017)
DOI 10.1007/174_2017_107, © Springer International Publishing AG
Published Online: 13 July 2017

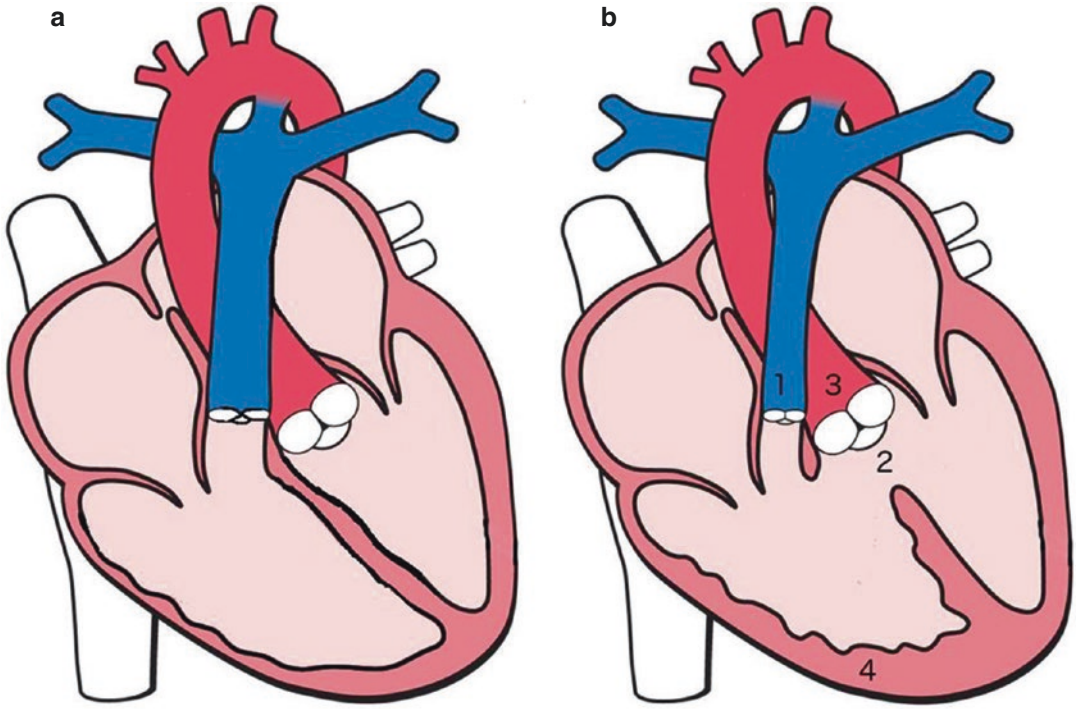

Fig. 1 (**a**) Schematic drawing of a normal heart. (**b**) Schematic drawing of the tetralogy of Fallot. Tetralogy of Fallot consists of (*1*) right ventricular outflow tract obstruction, (*2*) a ventricular septum defect, (*3*) overriding of the aorta over the interventricular septum, and (*4*) right ventricular hypertrophy. Drawing adapted from www.obgenkey.com

The aortic valve thus has a biventricular connection and the degree to which the aortic valve is positioned above the right ventricle is referred to as the degree of "overriding." Misalignment between the outflow septum and the septoparietal trabeculations leads to hypertrophy of the latter and subsequently results in pulmonary valve stenosis or infundibular stenosis. TOF with pulmonary atresia is a severe variant with complete obstruction of the right ventricular outflow tract and agenesis of the pulmonary trunk. The forth feature of the tetrad, right ventricular hypertrophy, is a hemodynamic consequence of the anatomical anomalies.

In addition to the tetrad described above, TOF is associated with a variety of other anomalies, including a bicuspid pulmonary valve, stenosis of the left pulmonary artery, dextroposition of the aortic arch, a patent oval foramen or atrial septal defect (ASD) (also referred to as the pentalogy of Fallot), an atrioventricular septum defect (AVSD) and anomalous pulmonary venous return.

1.2 Clinical Presentation

Fetal circulation is not affected by TOF. After birth however, the lungs replace placental blood oxygenation; adequate blood flow to the lungs is essential. TOF results in lower levels of oxygenated blood due to the right-to-left shunt of deoxygenated blood from the right ventricle through the VSD. The VSD is usually large, and in combination with the right ventricular outflow obstruction, results in equal pressure in both ventricles. Because of the right ventricular outflow tract obstruction preferential blood flow from both ventricles is through the aortic valve, resulting in a right-to-left shunt and cyanosis (Sommer et al. 2008). However, in case of mild outflow tract obstruction this shunt may be small, and sufficient blood flow to the lungs results in normal levels of oxygenation (non-cyanotic or "pink" Fallot).

TOF is frequently diagnosed during fetal life, but most patients present in the first months after

birth (Apitz et al. 2009). The primary symptom is low blood oxygenation resulting in failure to thrive, dyspnea, and cyanosis. The severity of symptoms is determined by the amount of pulmonary blood flow, which is influenced by the functional behavior of the right ventricular outflow tract obstruction, and physiological aspects such as ventricular and systemic arterial pressures and the origin of pulmonary blood flow (i.e., coming from the right ventricle, or through the ductus arteriosus or collateral arteries from the aorta or bronchopulmonary arteries). Most patients have adequate pulmonary blood flow at birth and become cyanotic weeks to months after birth, due to progressive outflow tract stenosis and right-to-left shunting. However, if blood oxygenation is severely hampered after birth, patients present with cyanosis immediately.

A particular presentation of TOF are recurrent hypercyanotic spells, presumably caused by transient increased pulmonary blood flow resistance or contraction of the right ventricular infundibulum, resulting in increased preferential flow of deoxygenated blood to the systemic circulation. This results in sudden onset of (increased) cyanosis and may lead to syncope, hypoxic injury, and death.

1.3 Current Treatment Options

Before surgical intervention was introduced about 35% of the patients with TOF died within the first year of life, 50% reached the age of 3 years, and survival after the age of 30 years was exceptional (Bertranou et al. 1978). Nowadays, almost all patients that receive surgical correction can expect to reach adult life. Corrective surgery aims to completely close the VSD and create an unobstructed ventricular outflow tract, with preservation of the right ventricular function and pulmonary valve function. In the early years of corrective surgery, repair was performed by means of right ventriculotomy. From the mid sixties transatrial-transpulmonary approaches with or without patch repair of the outflow tract improved early to middle-term outcome (Karl et al. 1992). Currently, correction of TOF has evolved from complete relief of outflow obstruction with extensive resection of infundibular muscles, often at the expense of pulmonary valve regurgitation, towards accepting residual obstruction in order to preserve pulmonary valve function, with the aim to minimize late adverse effects (Van Arsdell et al. 2005).

The best age for elective surgical repair is now considered to be within the first year of life (Van Arsdell et al. 2000; Al Habib et al. 2010). Surgical repair in patients younger than 3 months has been associated with extended intensive care stay and hospitalization (Van Arsdell et al. 2000). Many centers reserve such early repair for patients presenting with severe cyanosis or hypercyanotic spells. Potential disadvantages of surgical correction later in life include complications of long-lasting right ventricle pressure overload and cardiomyopathy due to long-term hypoxemia, which has been related to ventricular dysfunction and arrhythmias (Chowdhury et al. 2006).

In patients who are not fit for primary corrective surgery (contraindications include aberrant coronary arteries, small caliber pulmonary arteries, and coexisting cardiac malformations) palliative surgery is performed. The goal of palliative surgery is to increase the pulmonary blood flow and/or to create a time-window as to allow pulmonary arteries to grow in preparation for corrective repair at second stage. Various types of palliative procedures have been developed over time, but have also been abandoned because of complications or imposing difficulties on secondary corrective procedures. The current palliative surgery procedure of choice is the modified Blalock-Taussig shunt, where a Gore-Tex graft is placed between one of the arch vessels and the pulmonary artery. This shunt increases pulmonary blood flow and helps the pulmonary arteries to develop (Jahangiri et al. 1999). The risk of complications related to the arch vessel is small.

1.4 Complications and Treatment Options

Most corrective surgery procedures have an uncomplicated course. A minority of infants develops a low cardiac output syndrome or junctional

ectopic tachycardia (Cullen et al. 1995; Tharakan et al. 2014). These conditions are presumably caused by mechanical trauma to the myocardium or the conductive tissue and are of a transient nature, but require prolonged and intensive care.

Some TOF patients may have major aortopulmonary collateral arteries (MACPAs). MAPCAs are intersegmental arteries arising at various points from the descending aorta that connect to the pulmonary hilum to supply the lungs with blood. With normal development of the pulmonary arteries these connections regress during embryogenesis, but MAPCAs may persist in case of pulmonary atresia (Boshoff et al. 2006). Because of their similar anatomy MAPCAs are likely dilated bronchial arteries (Nørgaard et al. 2006). MAPCAs increase in size with physical growth and large MAPCAs may lead to pulmonary hypertension, often necessitating intervention early in life (Prieto 2005). MAPCAs may further lead to compression of the esophagus and airways. Importantly, MAPCAs may cause major and fatal bleeding (Miyazaki et al. 2001; Lanjewar et al. 2012; Sharma et al. 2016).

The majority of late complications is related to pulmonary valve regurgitation and are major cause of reoperation. Other complications include aortic root dilatation, regurgitation of the tricuspid and aortic valve, and shunt-related complication after palliative surgery.

Previously, surgery focused on complete relief of right ventricular outflow tract obstruction, accepting freely regurgitant pulmonary flow and dilatation of the outflow tract. However, the degree of pulmonary valve regurgitation has now been related to adverse late outcomes, including biventricular heart failure, ventricular arrhythmia, and sudden death. Imaging plays an essential role in the evaluation and follow-up of TOF patients.

2 Imaging Goals

The natural course of pulmonary valve regurgitation is slow and late adverse effects usually present only after decades. Although complications can occur at young age, they are few during the first 30 years of life. Older patients with important pulmonary valve regurgitation may rapidly develop progressive and fatal right ventricular failure (Shimazaki et al. 1984). Studies have demonstrated a direct relation between the severity of pulmonary valve regurgitation and right ventricular dilatation (Carvalho et al. 1992; Rebergen et al. 1993). Pulmonary valve regurgitation also relates to right ventricular afterload that is increased in patients with coexisting pulmonary artery stenosis (Chaturvedi et al. 1997). Moreover, a multicenter study in almost 800 patients has demonstrated that pulmonary valve regurgitation is an important determinant of symptomatic ventricular arrhythmia (Berul et al. 1997). Imaging plays an important part in the follow-up of patients with TOF and mainly focuses on the assessment of pulmonary valve regurgitation and right ventricular dilatation. With quantifying changes in pulmonary valve regurgitation and right ventricular dilatation over time, imaging assists in decision-making and timing pulmonary valve replacement. Optimal timing of pulmonary valve replacement is a topic of ongoing research.

Furthermore, imaging is used for the assessment of coexisting abnormalities and other late-term complications, such as aortic root dilatation. Progressive aortic valve regurgitation and a root diameter over 55 mm are commonly accepted as indication for aortic root surgery, especially when an indication for pulmonary valve replacement already exists (Apitz et al. 2009). In addition, with increasing survival, late adult life conditions such as atherosclerotic coronary artery disease are new aspects in the management of (older) TOF patients (Coutu et al. 2004). Imaging assists in early detection and therapy guidance (e.g., preoperative surgical revascularization assessment).

Various imaging modalities are involved in the assessment of TOF patients, each with specific aims and/or possibilities. The role of echocardiography, conventional X-ray, CT and MR techniques and nuclear imaging will be discussed below.

3 Imaging Techniques

3.1 Echocardiography

Echocardiography provides real-time assessment of ventricular size and function, myocardial wall thickness and motion, valvular anatomy and

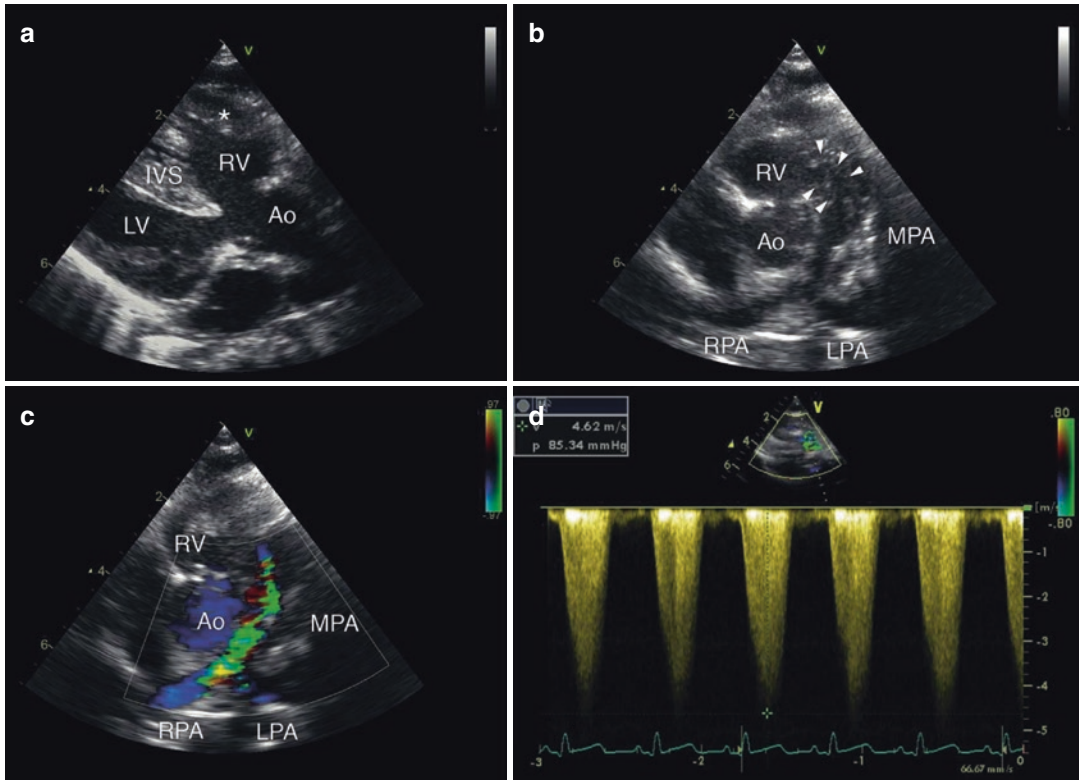

Fig. 2 Two-month-old female patient with uncorrected tetralogy of Fallot. Using echocardiography with 2D grey-scale imaging the tetrad of abnormalities can be evaluated (**a**, **b**): overriding of the aorta (Ao) over the interventricular septum (IVS), with subsequent ventricular septal defect, hypertrophy of the right ventricle (RV, *asterisk*) and narrowing of the right ventricular outflow tract (*arrowheads*). Using 2D color Doppler echocardiography (**c**) turbulence starting in the right ventricular outflow tract and continuing in the main pulmonary artery (MPA) can be seen. Continuous wave Doppler measurements (**d**) allow the evaluation of the pressure gradient over the right ventricular outflow tract and the MPA, with the use of the modified Bernouilli equation. Maximum velocity was 4.6 m/s, corresponding to a pressure gradient of 85 mmHg (*LV* left ventricle, *RPA* right pulmonary artery, *LPA* left pulmonary artery)

function, and hemodynamic information. It is readily available, non-invasive, fast, and inexpensive. Echocardiography plays a crucial role during fetal life and in small children with TOF (Fig. 2), as well as during early follow-up after corrective surgery. Over time, increasing emphasis is put towards recognizing pulmonary valve regurgitation and right ventricular dysfunction. Objective, reliable, and repeatable measurements for right ventricular size and function and pulmonary valve regurgitation are needed to guide future follow-up and therapy. Children can be evaluated well with echocardiography; however, imaging in adults may become limited by restricted acoustic window (Valente et al. 2014).

Quantitative functional analysis of the right ventricle encompasses both geometrical measurement of the volume, and nongeometrical parameters including TAPSE (tricuspid annular plane systolic excursion) and Doppler studies. The right ventricular volume and function can be derived from 2D echocardiographic measurements, using methods like the RVOT fractional shortening and the fractional area change. These parameters can be readily acquired. However, calculation of the right ventricular ejection fraction from the fractional area change is suboptimal because the calculation assumes a conical ventricular shape. Although applicable for the left ventricle, it is not for the right ventricle, in particular not in TOF patients with surgically corrected RVOT and right ventricular dilatation, especially at the apical level (Van der Hulst et al. 2011; Carminati et al. 2015). Three-dimensional (3D)

echocardiography may improve right ventricular evaluation but is still hampered by limited spatial and temporal resolution. 3D echocardiography underestimates the right ventricular volume and function, especially in larger right ventricles (with an end-diastolic volume over 200 mL), which is often the case in TOF patients (Iriart et al. 2009; Khoo et al. 2009; Shimada et al. 2010).

TAPSE measures the systolic displacement of the annular plane towards the ventricular apex and is widely used as an indicator for right ventricular function in the general population. However, the longitudinal shortening of the right ventricle is measured only while contractions may be dominant in other directions, especially in ventricular hypertrophy. A study in TOF patients has shown weak correlation between TAPSE and right ventricular function (i.e., ejection fraction) (Koestenberger et al. 2011).

Doppler echocardiography delivers hemodynamic information, such as measurement of the pulmonary gradient, which can help in decision-making for pulmonary valve replacement (Carminati et al. 2015).

Thus, although echocardiography is readily available and widely used as the primary imaging modality for follow-up TOF patients after corrective surgery, the reliability and repeatability specifically for right ventricular measures is limited (Carminati et al. 2015). Follow-up of adult TOF patients is therefore often complimented with other imaging modalities, especially when echocardiographic findings indicate deteriorating right ventricular function. The current guidelines for the management of adults with congenital heart disease recommend annual 2D echocardiography, complimented with cardiac MRI every 2–3 years (Warnes et al. 2008).

3.2 Radiography

Chest radiographs in patients with TOF may classically demonstrate a boot-shaped appearance of the heart (Fig. 3). Right ventricular hypertrophy may elevate the left ventricular apex, resulting in the upturned appearance of the heart. A small main pulmonary artery may further result in a narrow mediastinum, the "upper part of the boot." The upturning of the heart apex increases with the severity of RVOT obstruction. Although it is said to be classic, only infants with severe TOF demonstrate the sign (Haider 2008). Historically, the sign could be seen in older patients too, demonstrated by an old study in patients aged 14 weeks to 32 years, showing the boot-shaped heart sign in up to 70% of cases (Johnson 1965). Because the diagnosis of congenital heart disease is currently usually made early in (prenatal) life by echocardiography and followed by treatment within the first year of life, the sign is now only seen in infants with severe pulmonary atresia or older patients who have not been treated. Noteworthy, a frontal chest radiograph of a normal heart with a lordotic projection may result in a "false-positive" boot-shaped heart sign as well.

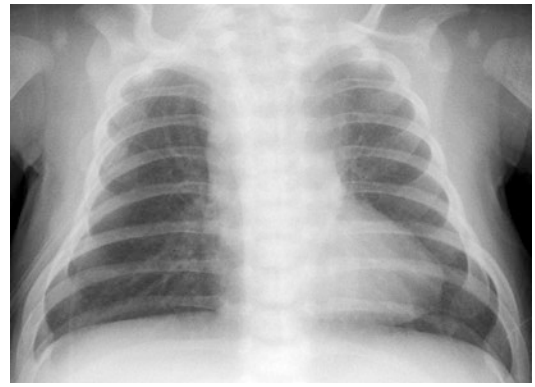

Fig. 3 Six-week-old female patient with uncorrected TOF. Frontal chest X-ray taken preoperatively, showing a boot-shaped appearance of the heart with elevated left ventricular apex

The role of chest radiographs in the follow-up of adults with TOF is limited. The anteriorly located right ventricle occupies little of the cardiac silhouette; chest radiographs have therefore low sensitivity in the evaluation of right ventricular failure (Boxt 1999). Also, indirect signs of deteriorating right ventricular function (e.g., changes in pulmonary circulation) cannot be depicted well enough, and chest radiographs are insufficient to guide follow-up or therapy. However, chest radiographs may be useful for the detection of stent fractures in patients with valve-containing pulmonary artery stent grafts (McElhinney 2011) (Fig. 4).

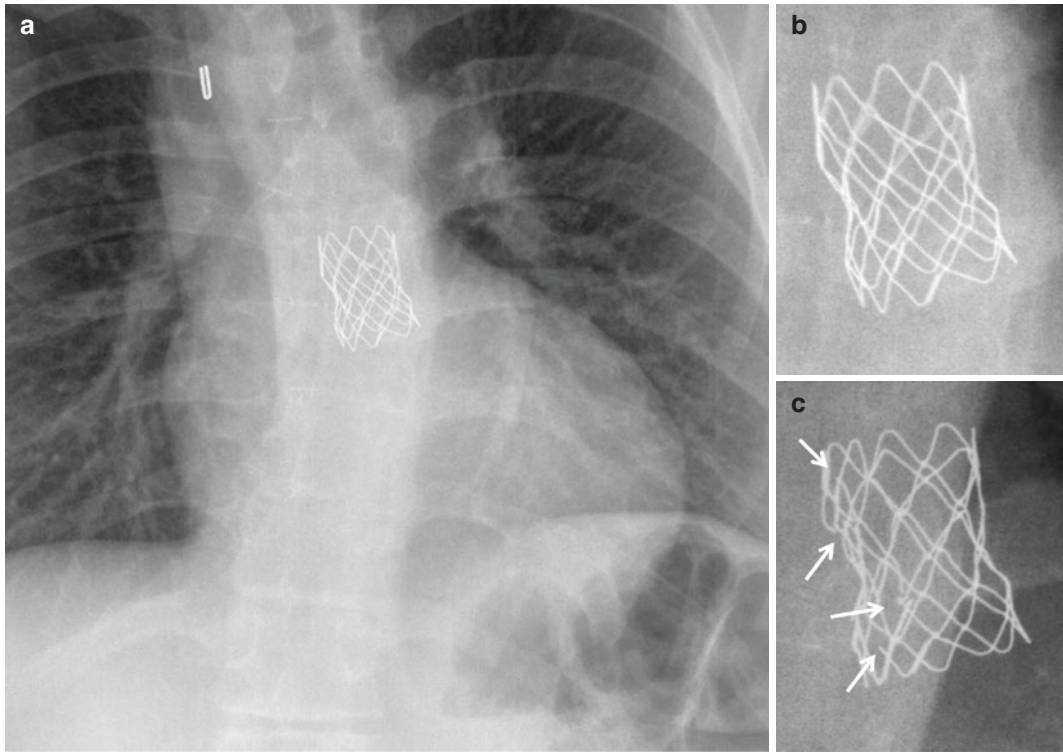

Fig. 4 Twelve-year-old female patient with corrected TOF after pulmonary valve replacement with a valve-containing stent graft. Frontal chest X-ray (**a**) and detailed views (**b**, **c**). Suboptimal deployment of the stent graft with slight residual stenosis at the level of the pulmonary valve (**a**, **b**). Approximately 6 months later (**c**): multiple stent-strut fractures (*arrows*) with signs of progressive stenosis

3.3 CT

Advances in multidetector row computed tomography (CT) technology have resulted in increased spatial and temporal resolution. New reconstruction algorithms allow improved image quality with a substantial reduction in ionizing radiation dose. The improvements in temporal resolution have also greatly boosted the application of CT for cardiac imaging, nowadays allowing for imaging of the whole heart in a single breath-hold, or even in a fraction of a second.

Because CT images are reconstructed from multiple projections, CT is sensitive to motion that result in blurring artifacts. To reduce motion artifacts, data acquisition is performed during breath-hold (minimizing respiration related motion artifacts) and prospective ECG triggering. ECG triggering is used to time data acquisition during the rest phase of the cardiac cycle, when motion of the heart itself is at minimum. In patients with slow heart rates (e.g., <65 bpm), this is at mid-diastole. In patients with higher heart rates (e.g., >75 bpm), the mid-diastolic rest phase becomes too short and the best phase shifts to the end-systolic phase of the RR-interval. A slow heart rate improves image quality. For certain indications (e.g., coronary artery CT angiography) pharmacological heart rate control is usually indicated and beta-blockers are generally used. For selective indications imaging may be performed using retrospective ECG gating, where data is acquired during the full cardiac cycle (RR-interval) at the expense of higher radiation dose. Specific phases can then be retrospectively selected throughout the RR-interval. Also, the dataset can be reconstructed as a "movie-loop," for ventricular function analysis.

3.3.1 Ventricular Volume and Function

Right and left ventricular volumes and function can be determined with CT by using retrospective ECG reconstruction when acquired throughout

the cardiac cycle. Acquisition must include the end-systolic and end-diastolic phases. Multiple phases of the RR-interval are reconstructed with a 5 or 10% interval that can be displayed as movie-loop. A 10% interval is sufficient for global function analysis with reduced post-processing time and data transfer (Joemai et al. 2008). Global and regional function such as motion and wall thickening can be visually evaluated. End-diastolic volume, end-systolic volume, stroke volume, and ejection fraction can be (automatically) calculated after (automatically) drawing endocardial contours on the end-diastolic and end-systolic phases (Fig. 5 shows an example of left ventricular volume analysis). By drawing epicardial contours, ventricular mass can be calculated as well. CT

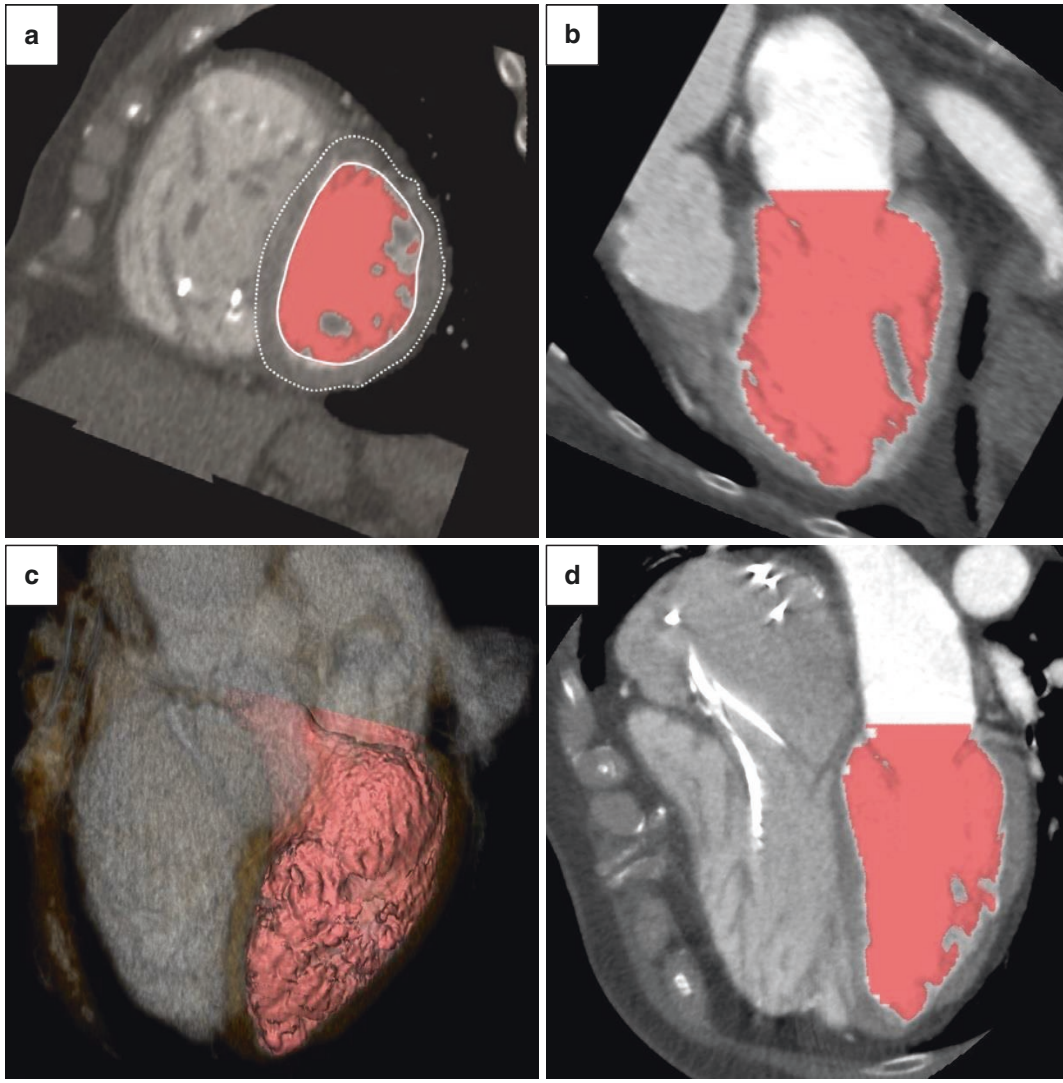

Fig. 5 Fifty-nine-year-old female patient with corrected TOF. CT views of the left ventricle in short axis (**a**), vertical long axis (**b**, **d**), and volume rendering (**c**). Automated detection of endocardial (continuous *line*) and epicardial (*dotted line*) contours of the left ventricle (**a**).The ventricular volume is automatically segmented (shaded areas in **a**, **b**, **c,** and **d**), with exclusion of the papillary muscles. This is automatically performed for all available phases throughout the cardiac cycle, including end-diastolic (**b**) and end-systolic phase (**d**). The end-diastolic volume, end-systolic volume, stroke volume, and ejection fraction are automatically calculated. The myocardial mass can be calculated from the difference between the endocardial volume from the epicardial volume. A volume rendering of the segmented volume (**c**) aids visual assessment of the ventricular function during playback of the "movie-loop." Note the pacemaker leads visible in the right atrium and ventricle in the end-systolic phase (**d**)

measurements of ventricular volume and function correlate well with cardiac MRI (Lembcke et al. 2005; Raman et al. 2006). Because of inherit radiation exposure, ventricular function assessment with cardiac CT should be reserved for patients with contraindications for cardiac MRI (see paragraph on MRI limitations).

3.3.2 Pulmonary Arteries

Because of its excellent spatial resolution, CT is an excellent tool for imaging the pulmonary arteries. Congenital abnormalities such as pulmonary artery stenosis and morphologic abnormalities after palliative surgical correction are often seen. With multiplanar reconstruction tools, CT provides an easy way to evaluate the pulmonary artery diameter or to visualize abnormal pulmonary artery course (Fig. 6).

CT allows for detailed imaging of the extent and course of MAPCAs (Fig. 7), often necessary before treatment.

Treatment of pulmonary artery stenosis is increasingly performed by means of balloon angioplasty and stenting (Fig. 8). The effects of treatment and complications such as intimal hyperplasia or stent fracture may be evaluated with CT.

3.3.3 Aortic Root

TOF may be complicated by aortic root dilatation. Both cardiac MRI and CT can be used to assess aortic dimensions. CT acquisition must be performed with ECG gating to prevent motion artifacts. Measurements should be performed in double oblique fashion (perpendicular to the axis of blood flow) and include the vessel wall for reproducibility and comparison reasons (Hiratzka et al. 2010). The topic aortic root dilatation is further discussed in the MRI section of this chapter.

3.3.4 Coronary Arteries

The role of CT in the assessment of atherosclerotic coronary artery disease and related risk stratification is well established. Increasing number of TOF patients reach age where atherosclerotic coronary artery disease may become relevant. Assessment of coronary artery disease in TOF patients is similar to any other patient. Preoperative

Fig. 7 Four-month-old male patient with pulmonary atresia. CT parasagittal view shows a major aortopulmonary collateral artery (MAPCA), arising from the descending aorta and connecting to the right hilum

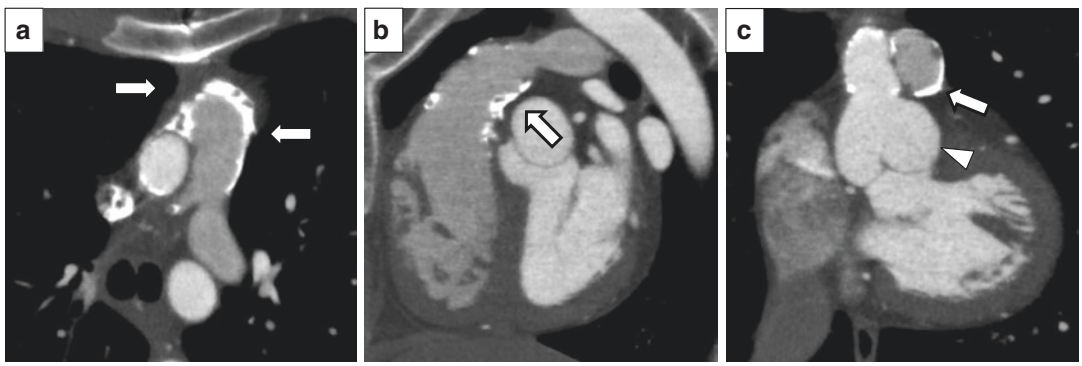

Fig. 6 Twenty-one-year-old male patient with a homograft conduit between the right ventricle and pulmonary arteries. CT multiplanar reconstruction (MPR) centered on the conduit with axial oblique (**a**), parasagittal (**b**), and double oblique semi-coronal view (**c**). MPR provides an easy way to evaluate the pulmonary artery diameter. Note the extensive calcifications in the RVOT and homograft (*arrows*), as well as a dilated aortic root (*arrowhead*)

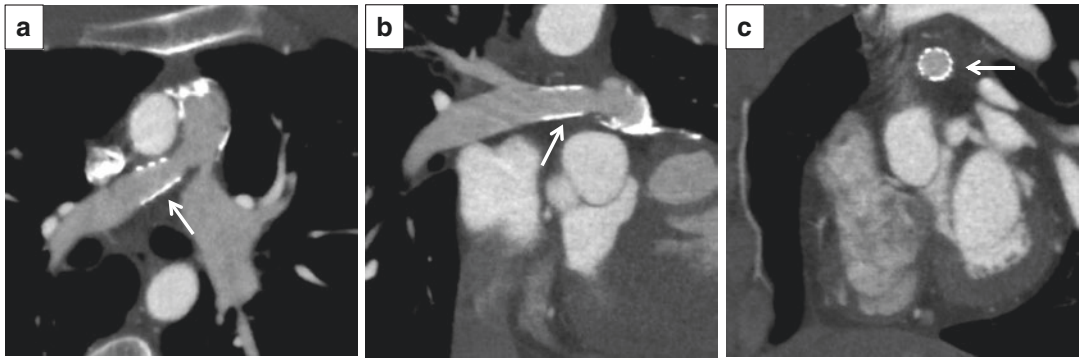

Fig. 8 Twenty-one-year-old male patient with corrected pulmonary atresia and right pulmonary artery stenosis. CT multiplanar reconstruction centered on the right pulmonary artery with axial oblique (**a**), coronal oblique (**b**), and double oblique view (**c**), showing a stent placed in the right pulmonary artery to treat the stenosis (*arrows*). The stent is well deployed without signs of restenosis or in-stent stenosis. The effects of treatment and the presence of complications can be easily evaluated with CT

Fig. 9 Same patient as in Fig. 8. CT angiography with maximum intensity projection (MIP) of the coronary arteries, demonstrating an aberrant course of the right coronary artery (*arrows*) arising from the left coronary sinus with retro-aortic course to the right atrioventricular groove. A retro-aortic course is benign

assessment of the coronary artery anatomy in TOF patients, e.g., before (percutaneous) pulmonary valve implantation, may be performed by cardiac CT or MRI. Despite advances in cardiac MRI that improved the visualization of the coronary arteries, CT has much higher diagnostic accuracy (Hamdan et al. 2011). If evaluation of the origin or proximal course of the coronaries is uncertain on cardiac MRI, additional assessment with cardiac CT may be needed for planning surgical or percutaneous interventions (Fig. 9).

3.3.5 CT Limitations

The use of ionizing radiation is a drawback of CT. Since the risk for cancer increases with dose and repeated exposure, this is particularly true for follow-up (Brenner et al. 2003). Risks related to the administration of iodinated contrast agent are contrast-induced nephropathy and risk for allergic reaction (Weisbord et al. 2008; Andreucci et al. 2014).

3.4 MRI

Cardiac MRI is the imaging modality of first choice in adult TOF patients for follow-up and for assessing complications. Cardiovascular anatomy, biventricular size and function, myocardial viability, and blood flow and function can be evaluated. MRI is considered the reference standard for quantification of right ventricular size and function and pulmonary regurgitation (Kilner et al. 2010). Using an imaging protocol that combines multiple MRI techniques, morphologic and hemodynamic changes can be monitored over time (Fratz et al. 2013). Because of the variety in MR imaging sequences that can be used, imaging protocols may vary from simple and short to complex and extensive. We use sequences depending on the clinical question that has to be answered. A minimal standard follow-up protocol includes at least axial cine-series for assessing right and left

ventricular function and morphology (when the morphology is rather normal, the pulmonary morphology can often be evaluated on these images as well). Also, phase-contrast flow series of the pulmonary artery are made for assessing regurgitation and stenosis, series of the aortic valve for calculating shunt fraction by comparing flow with that of the pulmonary artery, and series of the tricuspid valve for assessing right ventricular diastolic function. Table 1 shows an overview of commonly used imaging sequences and their indications.

Table 1 Overview of MRI sequences and their purpose

Acquisition	Orientation	Purpose	Sequence
Localizer	–Axial –Sagittal –Coronal –Oblique	–Planning other sequences –Anatomical survey –Extracardial findings	
Black blood	–Axial –Sagittal –Coronal	–Cardiac anatomy	Double IR FSE
Single slice cine	–2-Chamber LV –2-Chamber RV –3-Chamber LV (LVOT) –4-Chamber (long axis) –RVOT	–Cardiac anatomy –Ventricular wall motion –Outflow obstruction	SSFP GE
Multi-slice cine	–Axial (preferred) –Ventricular short axis	–Cardiac anatomy –Ventricular wall motion –Outflow obstruction –Ventricular volume –Ventricular wall mass –Ventricular function	SSFP GE
Flow	Perpendicular to: –Proximal MPA –Proximal aorta –Mitral valve –Tricuspid valve	Quantifying: –Pulmonary flow –Systemic flow –Valve regurgitation –Peak flow velocity Assessment of ventricular diastolic dysfunction	PC GE
Flow	Perpendicular to: –Proximal LPA –Proximal RPA	Quantifying differential pulmonary artery flow	PC GE
Flow	4D dataset	Quantifying: –Pulmonary flow –Systemic flow –Valve regurgitation –Shunt fraction (direct shunt measurement) –Eccentric jets	PC GE echo planar
Late enhancement	–Ventricular short axis –2-Chamber LV –3-Chamber LV (LVOT) –4-Chamber	Myocardial scarring	Phase sensitive IR
Late enhancement	3D dataset	Myocardial scarring	Phase sensitive IR
MRA	Sagittal oblique	Vascular anatomy	3D spoiled GE

LV left ventricle, *RV* right ventricle, *LVOT* left ventricular outflow tract, *RVOT* right ventricular outflow tract, *MPA* main pulmonary artery, *LPA* left pulmonary artery, *RPA* right pulmonary artery, *ECG* electrocardiography-triggered, *IR* inversion recovery, *FSE* fast spin echo, *SSFP* steady-state free precession, *PC* phase-contrast, *GE* gradient echo

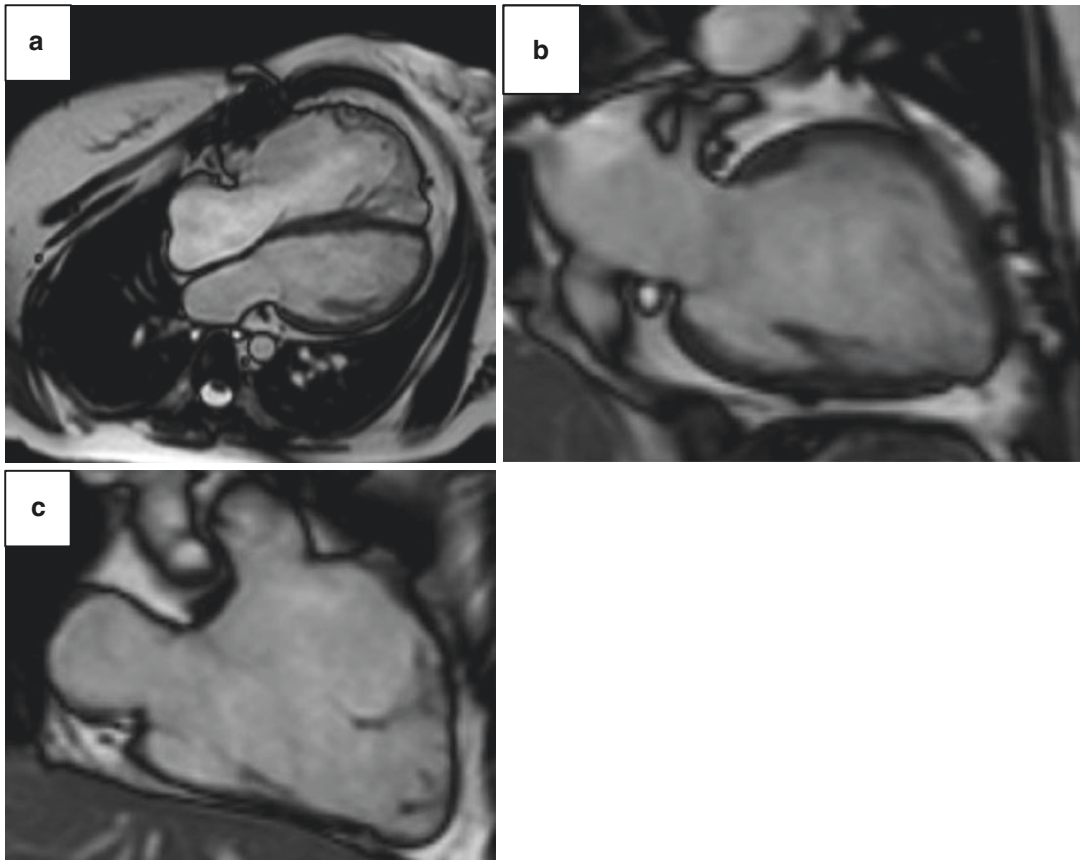

Fig. 10 Forty-nine-year-old female with corrected TOF. MRI bright blood (SSFP) images in axial (**a**), 2-chamber left (**b**), and 2-chamber right (**c**) view. Note the asymmetric chest wall, with ventral displacement at the level of the dilated right ventricle. SSFP images acquired throughout the cardiac cycle allow for visual assessment of ventricular size, function, and wall motion

In general, SSFP (steady-state free precession gradient-echo technique) imaging is typically used for imaging and measuring ventricular function and mass, as well as for visualizing valve leaflets and to assess the cardiac and surrounding anatomy. Images are acquired at standard cardiac planes (e.g., 2-chamber, 3-chamber, and 4-chamber views) throughout the cardiac cycle and allow for the visual assessment of ventricular function, wall motion, and valve function (Fig. 10). Continuous stacks of cine images are acquired in axial plane and include the entire ventricles to allow for reliable quantification of the ventricular end-diastolic and end-systolic volumes, as to calculate stroke volume and ejection fraction. Because the right ventricular morphology, global and regional function are best evaluated on axial ("transverse") series, and the left ventricle can be adequately evaluated regarding volumes and ejection fraction on these series as well, axial series are preferred over "left ventricular short-axis views" in TOF patients. Double inversion recovery (IR) fast spin-echo (FSE) sequences, also known as "black blood imaging" (Fig. 11), or ECG-triggered, respiratory-navigated SSFP "white blood" sequences can be used to produce high-resolution, high-contrast static images (Valente et al. 2014).

Furthermore, non-contrast and contrasted-enhanced MR angiography sequences allow for

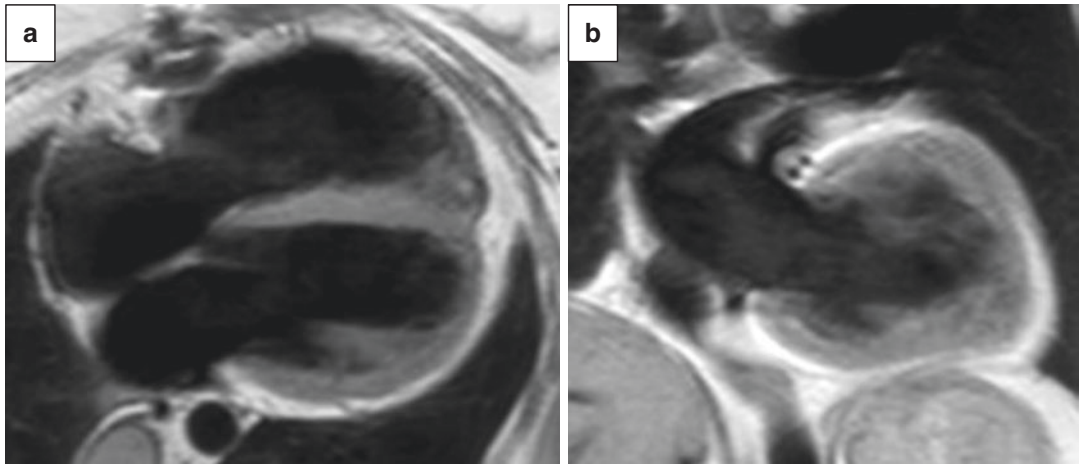

Fig. 11 Same patient as in Fig. 10. MRI black blood (double IR FSE) images in axial view (**a**) and coronal view (**b**). Black blood sequences produce high-resolution, high-contrast static images

the acquisition of 3D datasets for the assessment of systemic and pulmonary vessels and ECG-triggered phase-contrast sequences may be used to measure blood flow and quantify valve regurgitation fractions. Late enhancement sequences allows for the assessment of myocardial scaring and fibrosis after surgical correction.

3.4.1 Ventricular Volume and Function

Cardiac MRI is the reference standard for quantification of the ventricular volume and mass. To determine the volume of a ventricle, the blood pool area on all slices on which the ventricle is visible (n) is pooled and multiplied with the slice thickness according to the equation:

$$\text{Volume}\left(mL\right) = \sum_{i=1}^{n} \text{blood pool area}_i \left(mm^2\right) \times \text{slice thickness}\left(mm\right).$$

For calculating the blood pool volume, the area is drawn on each slice at the endocardium-blood boundary. Papillary muscles and trabeculations may be included or excluded from the blood pool volume; this should be done so consistently for end-systolic and end-diastolic phases to avoid over- or underestimation of volumes and function. Also, this should be done consistently during follow-up to allow for reliable comparison of volumes over time. Volumes are traced in end-diastolic and end-systolic phases (Fig. 12) and the difference between these two volumes represents the stroke volume:

Stroke volume (mL) = end diastolic volume (mL) – end systolic volume (mL).

From this, the ejection fraction and cardiac output can be calculated:

$$\text{Ejection fraction}\left(\%\right) = \frac{\text{stroke volume}\left(mL\right)}{\text{end diastolic volume}\left(mL\right)}$$

and

$$\text{Cardiac output}\left(\frac{mL}{min}\right) = \text{stroke volume}\left(mL\right) \times \text{heart rate}\left(bpm\right).$$

In patients with surgically corrected TOF, particular attention should be paid to selecting the correct end-diastolic and end-systolic phases for each ventricle individually, as these may differ due to conduction delay in the right ventricle (Geva 2011).

The ventricular mass can be calculated the same way by additionally tracing the epicardial border of the ventricle, thus creating an epicardial volume. The difference between the epicardial

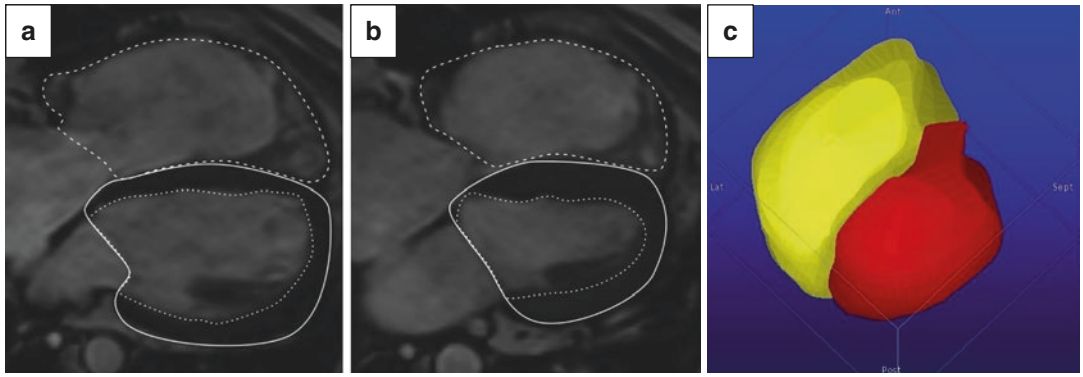

Fig. 12 Same patient as in Fig. 10. Volume tracing on MRI cine images. The blood pool area of the left ventricle (*fine dotted line*) and right ventricle (*dotted line*) are traced in end-diastolic (**a**) and end-systolic (**b**) phase. From this the ventricular volume and function can be calculated (volume rendering of both ventricles shown in **c**). End-diastolic volumes for left and right ventricles are 156 mL and 358 mL, respectively. End-systolic volumes for left and right ventricles are 74 mL and 264 mL, respectively. Stroke volume of the left ventricle is 82 mL, of the right ventricle is 94 mL. Ejection fractions: 52% and 26%, respectively. By tracing the epicardial contours the mass can be calculated, for the left ventricle (*continuous line*). This is 191 g. Similarly, this can be done for the right ventricle, but is less reliable

volume and blood pool volume results in the ventricular wall muscle volume that can be converted to mass by multiplying it with the specific gravity of myocardial muscle (1.05):

$$\text{Ventricular wall mass (g)} = (\text{epicardial volume (mL)} - \text{blood pool volume (mL)}) \times 1.05.$$

Increased right ventricular mass in patients with surgically corrected TOF has been associated with increased risk of adverse outcomes. However, because of the complex right ventricular morphology, the right ventricular contours for mass calculation are rather difficult to analyze, with large variation in accuracy and reproducibility (Valente et al. 2014).

Table 2 shows normal values for end-systolic and end-diastolic volumes of the left and right ventricle, differentiated for gender and age decile, obtained from 120 healthy subjects (Maceira et al. 2006). In the follow-up of TOF patients it is important to determine the volume and function for both ventricles. The ejection fractions of the right and left ventricle are closely correlated and right ventricular dilatation and dysfunction may lead to left ventricular dysfunction (Geva et al. 2004). Systolic dysfunction of the left ventricle is present in 20% of patients with surgically corrected TOF, and is strongly associated with arrhythmia (Broberg et al. 2011; Khairy et al. 2010). In a multivariate analysis on patients with repaired TOF, a left ventricular ejection fraction below 55% showed to be an independent predictor for major adverse clinical outcome including death, sustained VT, and progression to NYHA class III or IV (Knauth et al. 2008).

Surgically corrected TOF patients may have impaired diastolic function of the right ventricle (Van den Berg et al. 2007). Diastolic ventricular filling happens by active relaxation of the myocardium at early diastole (the E-wave) and passive relaxation at late diastole (the A-wave, during atrial contraction). The two major determinants of ventricular filling are ventricular relaxation and chamber compliance, reflected by the inflow pattern of blood from the atrium. The inflow patterns of the right and left ventricles can be evaluated by means of the flow curves across the tricuspid valve and mitral valve, respectively. Measured variables include peak velocities of the E-wave and A-wave and the deceleration time of the E-wave. The E/A-ratio represents the difference between the peak velocities of the E-wave and A-wave. The E-wave is influenced by atrial pressure at atrioventricular valve opening and the rate of ventricular relaxation. The A-wave occurs at atrial contraction after ventricular relaxation, and depends on ventricular compliance.

Table 2 Normal absolute end-diastolic (EDV) and end-systolic (ESV) volumes in mL, papillary muscles excluded from volume

	Normal left ventricular volumes					
Males	20–29	30–39	40–49	50–59	60–69	70–79
EDV	126–208	121–204	117–200	113–196	109–191	105–187
ESV	35–80	33–78	31–76	29–74	27–72	25–70
EDV/BSA	68–103	66–101	64–99	62–97	60–95	58–93
ESV/BSA	19–41	18–39	17–38	15–37	14–36	13–35
Females	20–29	30–39	40–49	50–59	60–69	70–79
EDV	112–193	108–189	104–185	100–181	96–177	91–172
ESV	32–73	30–71	28–69	26–67	24–65	21–62
EDV/BSA	67–101	64–98	62–96	59–93	57–91	54–88
ESV/BSA	19–39	18–38	16–36	15–35	14–34	12–32
	Normal right ventricular volumes					
Males	20–29	30–39	40–49	50–59	60–69	70–79
EDV	127–227	121–221	116–216	111–210	105–205	100–200
ESV	38–98	34–94	29–89	25–85	20–80	16–76
EDV/BSA	68–114	65–111	62–108	59–105	56–101	52–98
ESV/BSA	21–50	18–47	16–45	13–42	11–40	8–37
Females	20–29	30–39	40–49	50–59	60–69	70–79
EDV	100–184	94–178	87–172	81–166	75–160	69–153
ESV	29–82	25–77	20–72	15–68	11–63	6–58
EDV/BSA	65–102	61–98	57–94	53–90	49–86	45–82
ESV/BSA	20–45	17–43	14–40	11–37	8–34	6–32

Data adapted from Maceira et al. 2006a and b. 95% confidence interval of normal ventricular volumes per age decile for adult males and females (10 subjects per subdivision, 120 subjects in total). Values indexed to body surface area (BSA) in mL/m^2 (mean BSA in males was 1.96, mean BSA in females was 1.71)

Normal diastolic function has an E/A-ratio > 1. Impaired relaxation is the earliest manifestation of diastolic dysfunction. Impaired relaxation leads to a lower early filling velocity (lower E-wave peak, with prolonged E-wave deceleration time). A compensatory increased flow at atrial contraction leads to an increased A-wave peak. The E/A-ratio may become reversed (<1) (Fig. 13). This flow pattern also occurs naturally with physical aging and is usually seen in patients over 70 years (Strait et al. 2012). With progressive decrease of ventricular compliance, diastolic dysfunction increases. High atrial pressure at atrioventricular valve opening leads to fast early filling of the ventricle (high E-wave peak). A more rapid increase in ventricular pressure shortens the E-wave deceleration time. The increased ventricular pressure also hampers forward flow during atrial contraction, leading to a lower A-wave peak. The flow pattern of decreased ventricular compliance (also referred to as restriction to ventricular filling) thus resembles the flow pattern of normal diastolic function with E/A-ratio > 1. This phenomenon is referred to as pseudo-normalization of the E/A-ratio. Determining the flow direction in the inferior vena cava or hepatic veins may aid in distinguishing normal right ventricular diastolic function from pseudo-normalization. Normal flow in the veins has a forward direction during systole and diastole and a retrograde direction during atrial contraction. With decreased compliance of the ventricle, forward flow decreases and retrograde flow during atrial contraction increases. The ratio between ventricular forward flow and retrograde venous flow is an indicator of ventricular compliance. With further progression of restrictive filling the E-wave increases and E-wave deceleration time decreases, leading to a steep, short E-wave. In severe diastolic dysfunction, the E/A-ratio

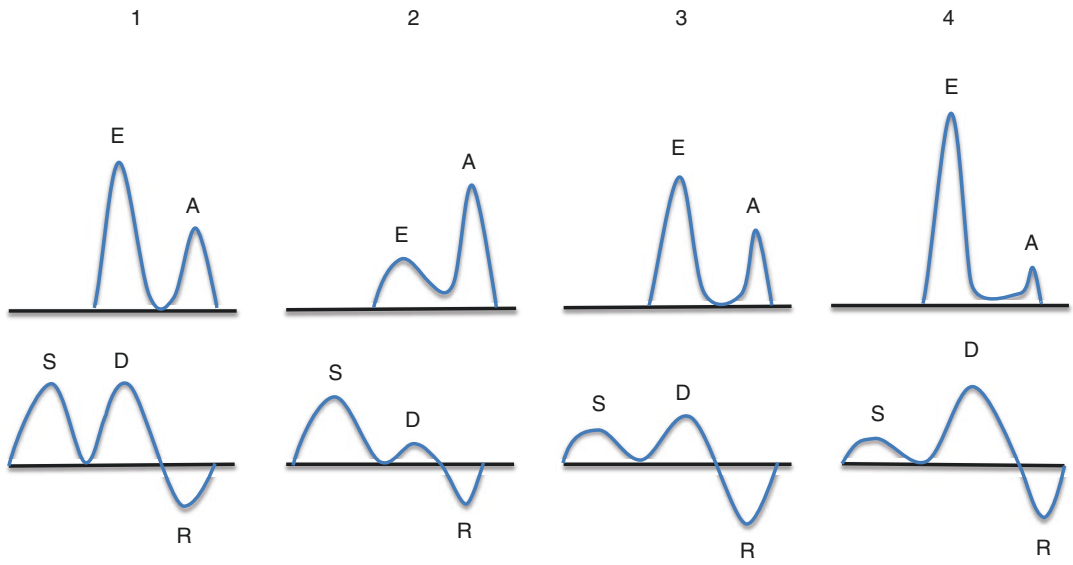

Fig. 13 Atrioventricular valve flow patterns (*upper row*) with early ventricular filling (E-wave) and ventricular filling during atrial contraction (A-wave) in normal diastolic function (*1*), impaired relaxation (*2*), reduced ventricular compliance or "pseudo-normalization" (*3*), and severe restriction to ventricular filling (*4*). In the lower row associated flow patterns in pre-atrial veins (*S* systolic flow, *D* diastolic flow, *R* retrograde flow during atrial contraction)

usually becomes >2 (Nishimura et al. 1997). Noteworthy, age-dependent variation, respiration, and inter-individual variation may hamper interpretation of inflow patterns. Furthermore, care should be taken to correct for pulmonary regurgitation, especially while interpreting the patterns in TOF patients.

The fundamental abnormality of impaired relaxation/restriction to right ventricle filling in TOF patients is ventricular hypertrophy due to an increased afterload of the right ventricle (Lam et al. 2007). The decreased compliance of the right ventricle leads to filling resistance. When this filling resistance exceeds the pulmonary vascular resistance, the right ventricle acts as conduit between the right atrium and pulmonary artery. As a result end-diastolic antegrade flow in the pulmonary artery may be observed. End-diastolic antegrade flow is present in a significant portion of TOF patients (Gatzoulis et al. 1995a; Van den Berg et al. 2007). Reports on the presence of restrictive physiology in adult TOF patients during long-term follow-up have been equivocal. Interestingly, some authors have found a protective effect on exercise performance (Gatzoulis et al. 1995b), while others found an association with severe pulmonary regurgitation and decreased exercise capacity (Van den Berg et al. 2007). These different results have been explained by different methods used to assess diastolic dysfunction. 3D velocity-encoded MR imaging may provide more accurate diastolic flow measurements than 2D techniques in assessing diastolic function (Van der Hulst et al. 2010). 3D velocity-encoded MR confirmed impaired right ventricular relaxation and restrictive right ventricular filling in TOF patients with end-diastolic antegrade flow in the pulmonary artery. This may help in assessing right ventricular diastolic dysfunction (Van der Hulst et al. 2010).

3.4.2 Right Ventricular Outflow Tract

Reconstruction of the right ventricular outflow tract is part of the corrective surgery procedure in TOF. Long-term pulmonary regurgitation affects the reconstructed outflow tract. Dilatation and wall motion abnormalities (akinesia and dyskinesia) are commonly observed in the right ventricular outflow tract. Wall

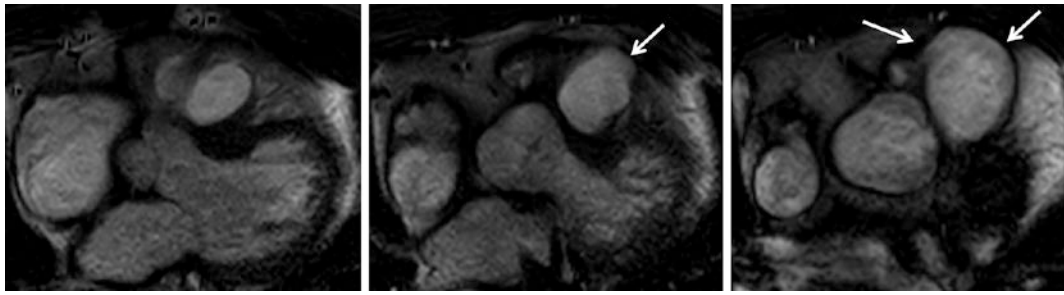

Fig. 14 Fifty-six-year-old male with corrected TOF. MRI bright blood (SSFP) images in three adjacent axial views of the RVOT, showing an aneurysm (*arrows*). SSFP cine images provide dynamic anatomical information about outflow tract dilatation or obstruction

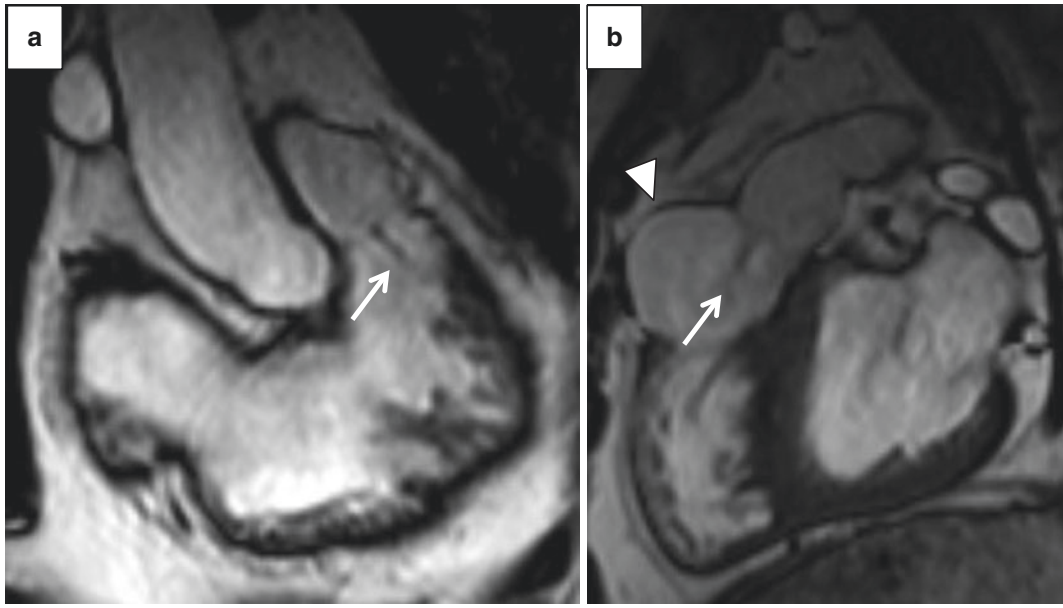

Fig. 15 Same patients as in Fig. 14. MRI bright blood (SSFP) images in 2-chamber view of the right ventricle (**a**) and RVOT view (**b**), demonstrating a flow-related jet caused by pulmonary regurgitation (*arrows*). Note the aneurysm of the RVOT in (**b**) (*arrowhead*)

motion abnormalities can be assessed using SSFP cine images. Evaluation can be done in the standard axial plane, as well as in outflow tract oriented 2-chamber and sagittal oblique views (Fig. 14). SSFP images provide dynamic anatomical information on outflow tract dilatation or obstruction, and flow-related signal loss or flow jets may be observed depending on the technique used (Fig. 15). Signal voids on SSFP images are related to acceleration rather than velocity, while SSFP images allow for visual assessment of turbulent flow, they may underestimate the degree of flow disturbance (Myerson 2012). In case of dilatation and aneurysm formation, SSFP images may depict thrombus at locations of slow flow. Furthermore, assessment of the right ventricular outflow tract morphology is necessary before considering percutaneous pulmonary valve replacement. A pyramidal shape of the right ventricular outflow tract, as can be seen in patients with previous transannular patch repair, is unsuited for percutaneous valve replacement (Saremi et al. 2013).

3.4.3 Pulmonary Valve and Pulmonary Arteries

Flow through the pulmonary arteries can be assessed using phase-contrast sequences and flow velocity measurements can aid in determining the severity of pulmonary branch stenosis. ECG-triggered phase-contrast sequences are used for flow measurements and quantification of pulmonary regurgitation (Fig. 16). The imaging plane is perpendicular to flow in the main pulmonary artery. Regurgitation percentage is calculated by dividing backward flow by forward flow and pulmonary valve regurgitation can be graded as mild (<20%), moderate (20–40%), or severe (>40%) (Mercer-Rosa et al. 2012).

Phase-contrast imaging can also be used to determine peak flow velocity that allows calculating the hemodynamic significance of a stenosis by applying the modified (simplified) Bernoulli equation (Wallerson et al. 1987): $\Delta P\left(\text{mmHg}\right) = 4 \times \upsilon^2 \left(\frac{\text{m}}{\text{sec}}\right)$, where the pressure

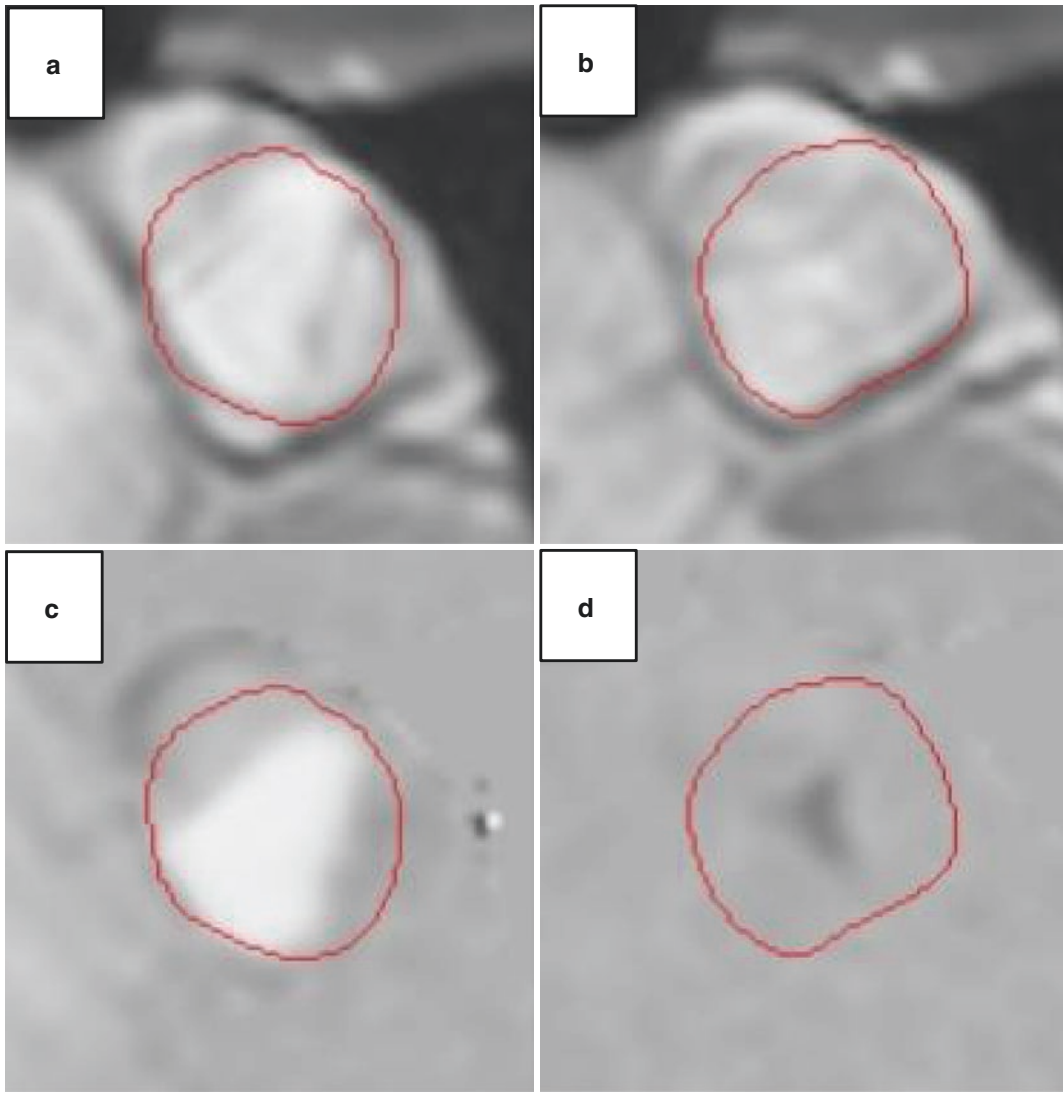

Fig. 16 Fifty-two-year-old male with corrected TOF. MRI anatomical modulus images (**a**, **b**) and phase-contrast (PC) images (**c**, **d**) showing pulmonary valve regurgitation. Systolic forward flow (*bright signal*) in the pulmonary artery at the level of the pulmonary valve (**a**, **c**). Backward flow (note that the signal is *black*, due to opposed flow direction) during diastole, indicating regurgitation (**b**, **d**). The flow over the valve can be quantified by drawing contours on the phase-contrast images (see graph): forward flow: 85 mL (above baseline), backward flow: 11 mL (below baseline). The net forward flow is 74 mL. Regurgitation fraction: 13% (backward flow divided by forward flow)

Fig. 16 (continued)

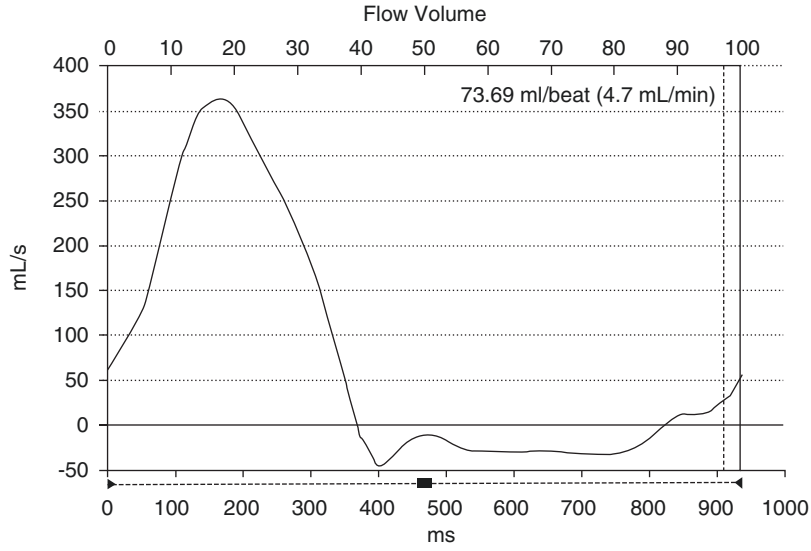

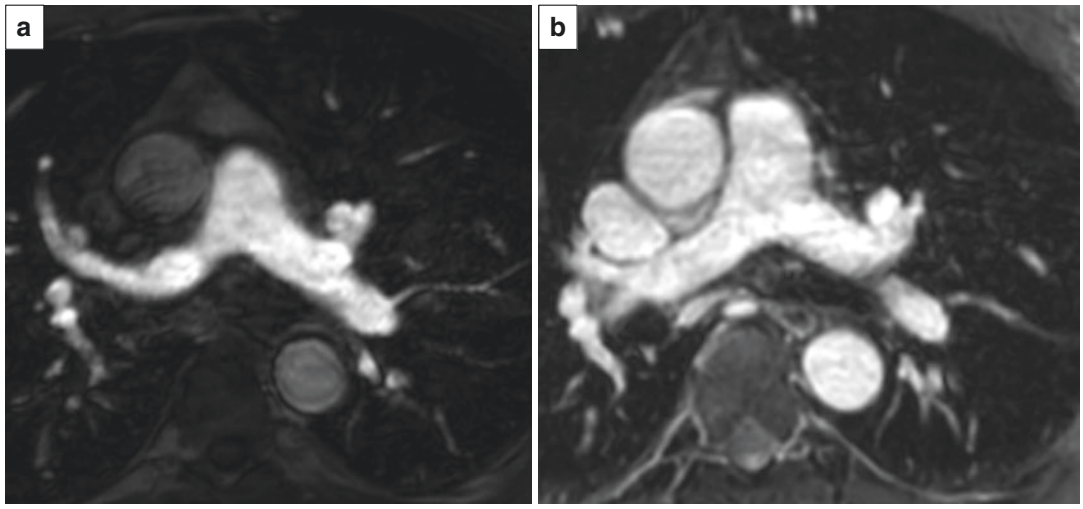

Fig. 17 Fifty-two-year-old male with corrected TOF. Contrast-enhanced MRA (**a**) of the pulmonary artery. MRA can be used to evaluate pulmonary artery (branch) stenosis. Alternative MRI sequences can produces comparable images without contrast (**b**, courtesy prof. H.J. Lamb)

(*P*) gradient equals four time the squared flow velocity distal from the stenosis (v^2). For example, the calculated pressure gradient over a stenosis with a measured peak flow velocity of 3.5 m/s is 49 mmHg. No absolute pressure gradient has been reported that indicates therapeutic intervention in TOF patients, however, a high systolic pressure in the right ventricle equal or larger than 70% of the systolic pressure in the systemic circulation could be considered an indication for pulmonary valve replacement (see also below).

Pulmonary artery or pulmonary artery branch stenosis may lead to pressure overload and right ventricular hypertrophy. Stenosis can be depicted anatomically by a variety of sequences, including static black blood (Double IR FSE) or white blood (SSFP) sequences or dynamic cine white blood techniques (SSFP). Contrast-enhanced MRA techniques can be used as well. MRA sequences provide a three-dimensional datasets which aids the visualization of the pulmonary arteries in relation to their anatomic surroundings and can be used for the evaluation of branch stenosis (Fig. 17). Excellent agreement between MRA and conventional angiography has been demonstrated (Greil et al. 2002). Regarding (pulmonary artery)

stent evaluation, FSE sequences have a high spatial resolution and are less susceptible to metal artifacts as compared to (contrast-enhanced) MRA, and may therefore provide additional information. The best sequence for determining in-stent stenosis with MRI is subject of ongoing research and improves over time with new developments in MRI techniques. By comparing flow measurements between the right and left pulmonary artery, flow differences between the lungs can be calculated (Weber et al. 2006).

3.4.4 Myocardial Scarring/Fibrosis

Late enhancement (or late gadolinium enhancement, LGE, also known as "delayed enhancement") refers to the presence of bright signal in the myocardium 15–20 min after administration of gadolinium contrast. After injection, gadolinium contrast reaches the myocardial interstitial space via the coronary circulation and washes out from the normal interstitium within approximately 10 min. Gadolinium contrast is retained in areas with increased extracellular space, such as in acute or chronic myocardial infarction. Late enhancement may also be seen in myocarditis, various cardiomyopathies, and myocardial storage diseases (Vogel-Claussen et al. 2006).

In TOF patients, late enhancement is common at locations of surgical corrections, such as the right ventricular outflow tract and in and around patched septal defects, due to retention of gadolinium contrast in scarred or fibrotic tissue. In patients who underwent surgery with the use of a transapical vent in the left ventricle, focal transmural late enhancement may be observed at the insertion point at the left ventricular apex (Babu-Narayan et al. 2006).

In TOF, late enhancement may also be typically observed in the right ventricular anterior wall and at the junction points of the right ventricle and the ventricular septum. The reason for late enhancement at these sites is unclear, but most likely reflects previous myocardial damage that occurred early in life, perioperative, or progressively due to myocardial strain. One hypothesis for enhancement at these particular locations is progressive right ventricular fibrosis from stretching, dilatation, and hypertrophy, due to pulmonary regurgitation or stenosis (Babu-Narayan et al. 2006). Late enhancement at these locations has been associated with ventricular dysfunction, arrhythmias, and exercise intolerance (Oosterhof et al. 2005; Babu-Narayan et al. 2006; Wald et al. 2009).

Identification of areas of myocardium scarring may guide treatment of patients with arrhythmias by radio frequency or cyro-catheter ablation therapy. Catheter ablation is generally performed under fluoroscopy guidance, where using the late enhancement MRI containing scar focus information in the electro-anatomical mapping system can facilitate the mapping procedure and aid in planning ablation therapy (Kolandaivelu et al. 2009).

3.4.5 Aortic Root

Aortic root dilatation is a known complication in TOF that may lead to aortic valve regurgitation that needs surgery. The reported incidence ranges from 15 to 88% (Grotenhuis et al. 2009). Dilatation may result from increased aortic flow from right-to-left shunting prior to corrective surgery (Niwa et al. 2002). However, dilatation has also been shown to progress after surgery. It has been hypothesized that hemodynamic stress leads to damage of the aortic wall media (Dobbs et al. 1997). MRI studies have shown that aortic dilatation could attribute to wall pathology indeed, as is reflected by abnormal aortic wall distensibility (Grotenhuis et al. 2009). Furthermore, reduced aortic elasticity may have a negative effect on aortic valve function (Grotenhuis et al. 2009).

Aortic root dilatation can be assessed with MRI using cine SSFP sequences parallel and perpendicular to the aortic root, as well as with ECG-triggered 3D SSFP sequences (Fig. 18). Similar to CT, measurements of the aortic diameter should be performed in double oblique fashion (perpendicular to the axis of blood flow) and include the vessel wall for reproducibility and comparison reasons.

Contrast-enhanced MRA may also be used for assessing aortic root dilatation, but it should be noted that images with non-ECG-triggered sequences can be blurred by motion artifacts (Kaiser et al. 2008). Aortic valve regurgitation can be quantified with phase-contrast imaging perpendicular to the aortic root.

3.4.6 Shunts

Shunts in TOF, such as a residual VSD or ASD after patch closure, are usually recognized with echocardiography, but can also be visualized with MRI using SSFP or TSE sequences

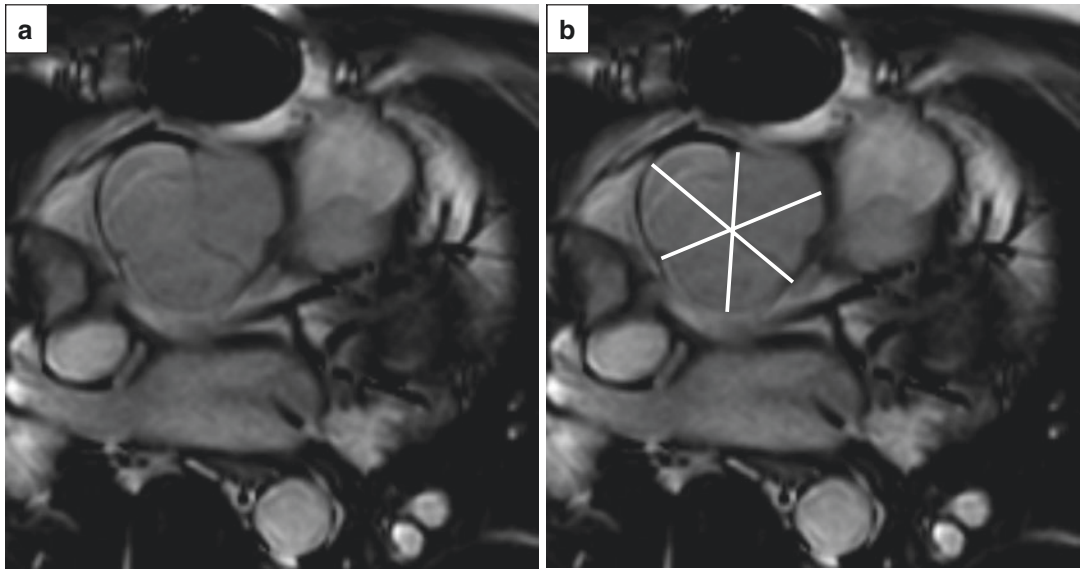

Fig. 18 Forty-four-year-old male with corrected TOF. MRI bright blood (SSFP) images of the aortic root, demonstrating aortic root dilatation (**a**). The mean cusp-commissure diameter can be measured at this level (**b**, *lines*). The mean diameter was 46 mm

perpendicular and in plane parallel to the atrioventricular septum. Flow over the septum defect can be quantified with phase-contrast imaging, which should be planned perpendicular to the direction of the jet. In case of an eccentric jet, the perpendicular plane may be difficult to establish at the time of acquisition. Non-perpendicular acquired phase-contrast images may underestimate the magnitude of the shunt flow. Four-dimensional, three-directional flow sequences may be used for optimal shunt calculation (Roes et al. 2009). Alternatively, to quantify a left-to-right shunt, the shunt ratio can be calculated by the formula Qp:Qs, where Qp represents the flow volume in the main pulmonary artery and Qs the flow volume in the ascending aorta (s, systemic). A shunt ratio > 1.5 is generally used as an indication for surgical closure (Baumgartner et al. 2010).

3.4.7 Timing Pulmonary Valve Replacement

The negative effect of pulmonary valve regurgitation and the resulting right ventricular volume overload is well known and has been extensively described in literature. Largely dilated right ventricles (e.g., EDV 172 mL/m^2 in female and 185 mL/m^2 in male) are associated with adverse outcomes (Knauth et al. 2008). Adult patients with too largely dilated right ventricles have also been shown to no longer benefit from pulmonary valve replacement (Thierrien et al. 2000). Preoperative thresholds for diastolic and systolic volumes have therefore been suggested; normalization of the right ventricular volume can be achieved when the EDV is <160 mL/m^2 before pulmonary valve replacement (Fig. 19) (Oosterhof et al. 2007). Nevertheless, consensus on optimal timing of pulmonary valve replacement is still lacking and may be especially difficult for asymptomatic patients (Apitz et al. 2009, Geva 2013). For timing surgery, the risk of the procedure has to outweigh the risk for further decline. According to the ESC guidelines, pulmonary valve replacement should be performed in symptomatic patients with severe pulmonary regurgitation and/or stenosis. Pulmonary valve replacement should also be considered in asymptomatic patients with severe pulmonary regurgitation and/or stenosis and objective decrease in exercise capacity, progressive right ventricular dilatation or systolic dysfunction, progressive tricuspid regurgitation, right ventricular outflow tract obstruction with right ventricular systolic pressure > 80 mmHg, or sustained atrial or ventricular arrhythmias (Baumgartner et al. 2010). Based on interpretation of available literature, Geva individually proposed similar

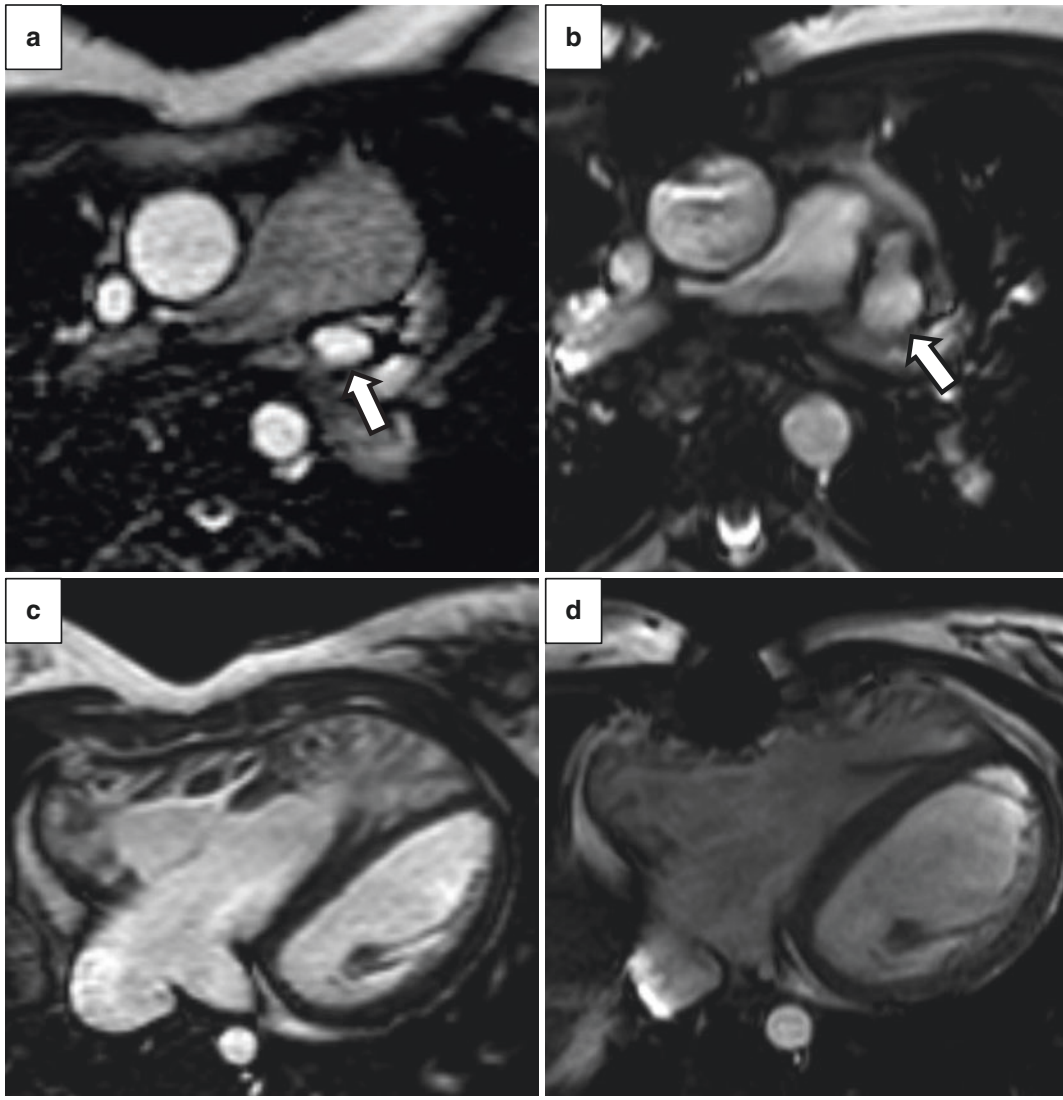

Fig. 19 Forty-four-year-old female with corrected TOF. MRI bright blood (SSFP) images of the pulmonary artery and right ventricle before (**a**, **c**) and after pulmonary valve replacement (**b**, **d**). Dilated pulmonary artery (**a**) and right ventricular dilatation and hypertrophy (**c**) before pulmonary valve replacement. After surgery pulmonary artery size has been normalized (**b**) and the right ventricular size decreased (**d**). Note the coexisting persist left superior vena cava (*arrows*) displaced backwards by the dilated pulmonary artery in (**a**)

indications for pulmonary valve replacement in repaired TOF patients, as well as some additional indications (Geva 2013). Table 3 summarizes the indications proposed in both publications.

Currently, the role of N-terminal B-type natriuretic peptide (NT-proBNP) is subject of investigation in the follow-up of TOF patients. NT-proBNP is a biomarker that reflects general cardiac function. In patients with chronic heart failure, NT-proBNP guided therapy has shown to reduce all-cause mortality (Troughton et al. 2014). Interestingly, in TOF patients increased NT-proBNP has been shown to correlate with deteriorated left ventricular MRI parameters (ejection fraction, mass, end-systolic and end-diastolic volume index), but not with any volumetric or functional parameters of the right ventricle. Moreover, NT-proBNP was shown superior to MRI regarding risk assessment. This suggests that while right ventricular parameters

Table 3 Proposed indications for pulmonary valve replacement

Indication for pulmonary valve replacement	
ESC recommended indications:	
Symptomatic patients	Additional 1 or more criteria for asymptomatic patients
Severe pulmonary regurgitation	Decrease in objective exercise capacity
Severe pulmonary stenosis (right ventricular systolic pressure > 60 mmHg)	Progressive right ventricular dilatation
	Progressive right ventricular systolic dysfunction
	Progressive tricuspid valve regurgitation (at least moderate)
	RVOT obstruction with right ventricular systolic pressure > 80 mmHg
	Sustained arrhythmias
Proposed indications by Geva based on available literature:	
Symptomatic patients with one or more of the following criteria or asymptomatic patients with two or more of the following criteria:	
Ventricular dilatation	Hemodynamic abnormalities
Right ventricular EDV index >150 mL/m^2	RVOT obstruction with right ventricular systolic pressure ≥ 0.7 systemic systolic pressure
Right ventricular ESV index >80 mL/m^2	Severe branch pulmonary artery stenosis (<30% flow to affected lung) not amenable to transcatheter therapy
Ventricular function	Pulmonary valve regurgitation greater than or equal to moderate tricuspid regurgitation
Right ventricular ejection fraction <47%	Left-to-right shunt from residual septal defects with pulmonary-to-systemic flow ratio ≥ 1.5
Left ventricular ejection fraction <55%	Severe aortic regurgitation
Conduction abnormalities	Morphologic abnormalities
QRS duration >160 ms	Large RVOT aneurysm
Sustained tachyarrhythmia related to right-sided heart volume load	

Adapted from Baumgartner et al. 2010 and Geva 2013.
RVOT right ventricular outflow tract

reflect severity of pulmonary regurgitation, left ventricular parameters are important for long-term clinical outcome (Westhoff-Bleck et al. 2016). Even in mildly symptomatic patients with pulmonary regurgitation after TOF repair, NT-proBNP was shown a strong predictor of adverse outcome (supraventricular tachycardia or heart failure).

Thus, while MRI plays a crucial role in the follow-up of morphological and functional changes that direct therapy, biomarkers such as NT-proBNP may be of additional prognostic value. Further research should include biomarkers to determine their value for timing pulmonary valve replacement (Westhoff-Bleck et al. 2016).

3.4.8 MRI Limitations

Cardiac MRI quality can be severely hampered by susceptibility artifacts caused by implants or other ferromagnetic objects (e.g., containing iron, nickel, or cobalt). These materials have positive magnetic susceptibility that affects the homogeneity of the magnetic field and results in signal loss and spatial distortion, observed as dark spots or areas that can hamper diagnosis. Furthermore, presence of a strong magnetic field and/or field changes during acquisition impose an absolute contraindication for patients with certain implanted electronic devices (e.g., neurostimulating devices). Until recently, having a pacemaker was considered an absolute contraindication for cardiac MRI. Nowadays many new implantable devices contain little or no ferromagnetic material and an increasing number of MRI-safe devices become available (Shinbane et al. 2011; Hwang et al. 2016). Patients with implanted pacemakers or defibrillators may be scanned, provided that (1) no alternative imaging modality for diagnosis (e.g., CT or echocardiography) is available, (2) the MRI examination is strongly indicated, (3) planning and performance of the MRI investigation follows strict guidelines and communication with involved clinicians/technicians, and (4) that the patient is not pacemaker-rhythm dependent (Horwood et al. 2016). In our department MRI procedures in these patients are performed under direct supervision of the radiologist at the MRI scanner and with clinical guidance by the cardiologist and/or pacemaker

technician. Relative contraindications exist for patients with residual epicardial pacemaker leads due to the possible risk of heat or electric current generation in the lead wires.

The MRI bore is generally small; the patient is positioned in the tight tunnel, while the examination time is usually long (between 30 and 60 min). This can be a contraindication for patients with severe claustrophobia. In milder cases sedation may help in performing the MRI examination.

Regarding risk, nephrogenic systemic fibrosis (NSF) is a rare but severe complication of gadolinium-bases contrast agents. NSF is characterized by skin thickening and tethering that causes flexion contractures of joints (Bernstein 2012). Patients with end-stage kidney disease (glomerular filtration rate (GFR) < 15 mL/min or on hemodialysis) are predominantly affected, but NSF has been reported in patients with less severe chronic kidney disease (Bernstein 2012). After recognition of the relation between gadolinium-based contrast agent administration and NSF, the U.S. Food and Drug Administration has recommended against using gadolinium-based contrast agents in patients with GFR <30 mL/min. Changes in guidelines and regulations have led to NSF occurrence decline to near zero since 2009 (Forghani 2016).

3.5 Nuclear Imaging

Historically, nuclear imaging has been used to evaluate cardiac function, myocardial perfusion, and to quantify blood flow in cardiac patients. Currently, cardiac MRI has replaced nuclear imaging as the first imaging modality of choice for many indications. MRI provides superior anatomic detail without radiation exposure (Valente et al. 2014). Nuclear imaging in TOF is reserved for quantification of (asymmetrical) lung perfusion in patients with contraindications for cardiac MRI. Asymmetrical lung perfusion may be observed in TOF patients with pulmonary artery stenosis that can be predictive for prognosis. The gold standard for quantifying pulmonary perfusion is quantitative perfusion scintigraphy with intravenous injection of radioactive Technetium-99m (99Tc) macroaggregated albumin (MAA). Count images of both lungs are acquired using a gamma camera (Fathala 2010). In TOF patients with normal pulmonary arteries, lung perfusion is comparable to the normal population, with slightly larger perfusion to the right lung than to the left lung reflecting the differences in lung volumes (Fathala 2010). In patients with pulmonary artery stenosis, scintigraphy may demonstrate segmental or unilateral hypoperfusion (Fig. 20).

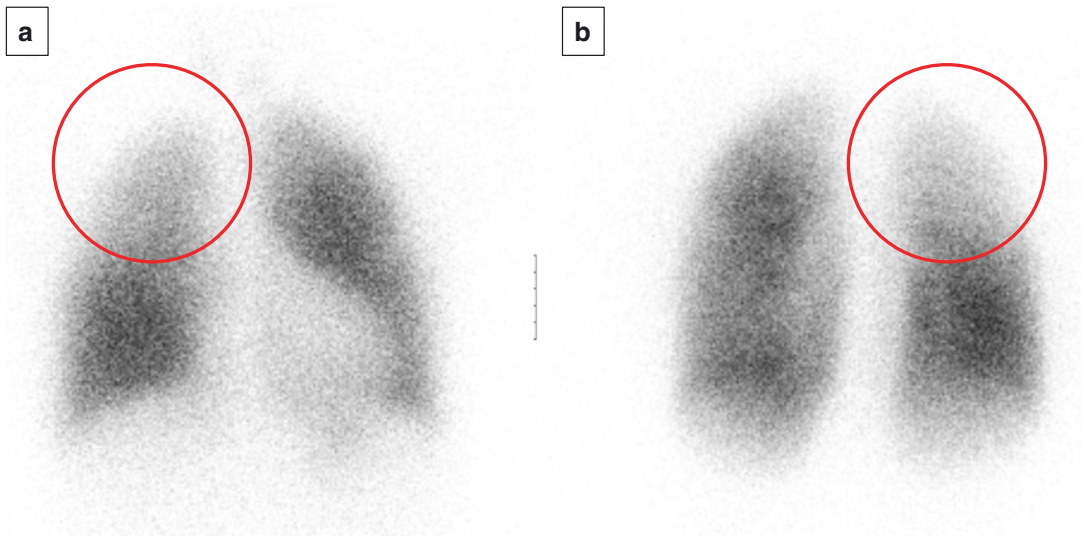

Fig. 20 Same patient as in Fig. 8. 99Tc-MAA perfusion scintigraphy in anterior (**a**) and posterior (**b**) view. Besides the stenosis of the right pulmonary artery, treated with a stent, right pulmonary branch stenosis was also suspected. Anterior and posterior views confirm a segmental hypoperfusion of the right upper lobe (*encircled*). Note that due to the shape and location of the heart less perfusion is seen in the left lower field in anterior view, but not in posterior view

Perfusion scintigraphy may guide decision-making for treating pulmonary artery or branch stenosis and can be used to evaluate the treatment effect.

Conclusion

Imaging plays an important role in the follow-up of patients with TOF and mainly focuses on the assessment of late complications after surgical corrections, in particular pulmonary valve regurgitation and right ventricular dilatation. Several imaging modalities are available for follow-up, including echocardiography, cardiac MRI, and cardiac CT.

Cardiac MRI is the imaging modality of first choice for the assessment of repaired TOF, because it allows for complete assessment of the cardiovascular morphology and physiology. Cardiac MRI provides reproducible and accurate measurements of the right ventricular volume and function, pulmonary flow volumes, regurgitation and stenosis, and has the ability to detect myocardial scarring. MRI is attractive as longitudinal follow-up imaging modality because of lack of harmful ionizing radiation.

Cardiac CT is a good alternative imaging modality for follow-up of patients with contraindication for cardiac MRI. CT can be safely performed in patients with implanted cardiac devices (e.g., pacemaker). CT provides excellent spatial resolution that allows for detailed visualization of complex cardiovascular anatomy and may be used as a complementary imaging modality in cases where MRI is inconclusive (e.g., evaluation of stent related complications).

Over the years, surgical correction of TOF has changed from complete relief of outflow obstruction at the expense of pulmonary valve regurgitation, towards accepting a residual obstruction but preserving pulmonary valve function, in order to prevent the late complications of right ventricular dilatation. A largely dilated right ventricle, but also left ventricular dysfunction determine outcome in TOF patients. Optimal timing of pulmonary valve replacement is difficult where the risk of surgery is weighted against the expected health benefits. MRI in particular plays a crucial role in detecting the morphological and functional changes that guide therapy.

References

Andreucci M et al (2014) Side effects of radiographic contrast media: pathogenesis, risk factors, and prevention. Biomed Res Int 2014:741018

Apitz C et al (2009) Tetralogy of Fallot. Lancet 374:1462–1471

Van Arsdell GS et al (2000) What is the optimal age for repair of tetralogy of Fallot? Circulation 102(Suppl 3):III123–III129

Van Arsdell G et al (2005) An apology for primary repair of tetralogy of Fallot. Semin Thorac Cardiovasc Surg Pediatr Card Surg Annu:128–131

Babu-Narayan SV et al (2006) Ventricular fibrosis suggested by cardiovascular magnetic resonance in adults with repaired tetralogy of Fallot and its relationship to adverse markers of clinical outcome. Circulation 113(3):405–413

Baumgartner B et al (2010) ESC guidelines for the management of grown-up congenital heart disease (new version 2010). Eur Heart J 31:2915–2957

Van den Berg J et al (2007) Diastolic function in repaired tetralogy of Fallot at rest and during stress: assessment with MR imaging. Radiology 243(1):212–219

Bernstein EJ et al (2012) Nephrogenic systemic fibrosis: a systemic fibrosing disease resulting from gadolinium exposure. Best Pract Res Clin Rheumatol 26(4):489–503

Bertranou EG et al (1978) Life expectancy without surgery in tetralogy of Fallot. Am J Cardiol 42:458–466

Berul CI et al (1997) Electrocardiographic markers of late sudden death risk in postoperative tetralogy of Fallot children. J Cardiovasc Electrophysiol 8:1349–1356

Boshoff D et al (2006) A review of the options for treatment of major aortopulmonary collateral arteries in the setting of tetralogy of Fallot with pulmonary atresia. Cardiol Young 16(3):212–220

Boxt LM (1999) Radiology of the right ventricle. Radiol Clin N Am 37(2):379–400

Brenner DJ et al (2003) Cancer risks attributable to low doses of ionizing radiation: assessing what we really know. Proc Natl Acad Sci U S A 100(24):13761–13766

Broberg CS et al (2011) Prevalence of left ventricular systolic dysfunction in adults with repaired tetralogy of Fallot. Am J Cardiol 107:1215–1220

Carminati M et al (2015) Echocardiographic assessment after surgical repair of tetralogy of Fallot. Front Pediatr 3:3

Carvalho JS et al (1992) Exercise capacity after complete repair of tetralogy of Fallot: deleterious effects of residual pulmonary regurgitation. Br Heart J 67:470–473

Chaturvedi RR et al (1997) Increased airway pressure and simulated branch pulmonary artery stenosis increase pulmonary regurgitation after repair of tetralogy of Fallot. Circulation 95:643–649

Chowdhury UK et al (2006) Histopathology of the right ventricular outflow tract and its relationship to clinical outcomes and arrhythmias in patients with tetralogy of Fallot. J Thorac Cardiovasc Surg 132:270–277

Coutu M et al (2004) Late myocardial revascularization in patients with tetralogy of Fallot. Ann Thorac Surg 77:1454–1455

Cullen S et al (1995) Characterization of right ventricular diastolic performance after complete repair of tetralogy of Fallot. Restrictive physiology predicts slow postoperative recovery. Circulation 91:1782–1789

Dobbs GA et al (1997) Aortic valve replacement after repair of pulmonary atresia and ventricular septal defect or tetralogy of Fallot. J Thorac Cardiovasc Surg 113(4):736–741

Fathala A (2010) Quantitative lung perfusion scintigraphy in patients with congenital heart disease. Heart Views 11(3):109–114

Forghani R (2016) Adverse effects of gadolinium-based contrast agents: changes in practice patterns. Top Magn Reson Imaging 25(4):163–169

Fratz S et al (2013) Guidelines and protocols for cardiovascular magnetic resonance in children and adults with congenital heart disease: SCMR expert consensus group on congenital heart disease. J Cardiovasc Magn Reson 15:51

Gatzoulis MA et al (1995a) Right ventricular diastolic function 15 to 35 years after repair of tetralogy of Fallot. Restrictive physiology predicts superior exercise performance. Circulation 91:1775–1781

Gatzoulis MA et al (1995b) Mechanoelectrical interaction in tetralogy of Fallot. QRS prolongation relates to right ventricular size and predicts malignant ventricular arrhythmias and sudden death. Circulation 92(2):231–237

Geva T et al (2004) Factors associated with impaired clinical status in long-term survivors of tetralogy of Fallot repair evaluated by magnetic resonance imaging. J Am Coll Cardiol 43:1068–1074

Geva T (2011) Repaired tetralogy of Fallot: the roles of cardiovascular magnetic resonance in evaluating pathophysiology and for pulmonary valve replacement decision support. J Cardiovasc Magn Reson 13:9

Geva T (2013) Indications for pulmonary valve replacement in repaired tetralogy of Fallot: the quest continues. Circulation 128(17):1855–1857

Greil GF et al (2002) Coronary magnetic resonance angiography in adolescents and young adults with kawasaki disease. Circulation 105(8):908–911

Grotenhuis et al. (2009) Aortic elasticity and size are associated with aortic regurgitation and left ventricular dysfunction in tetralogy of Fallot after pulmonary valve replacement. Heart 95:1931–1936

Haider EA (2008) The boot-shaped heart sign. Radiology 246(1):328–329

Al Habib HF et al (2010) Contemporary patterns of management of tetralogy of Fallot: data from the Society of Thoracic Surgeons database. Ann Thorac Surg 90:813–819

Hamdan A et al (2011) A prospective study for comparison of MR and CT imaging for detection of coronary artery stenosis. JACC Cardiovasc Imaging 4(1):50–61

Hiratzka LF et al (2010) ACCF/AHA/AATS/ACR/ASA/SCA/SCAI/SIR/STS/SVM guidelines for the diagnosis and management of patients with thoracic aortic disease: a report of the American College of Cardiology Foundation/American Heart Association Task Force on Practice Guidelines, American Association for Thoracic Surgery, American College of Radiology, American Stroke Association, Society of Cardiovascular Anesthesiologists, Society for Cardiovascular Angiography and Interventions, Society of Interventional Radiology, Society of Thoracic Surgeons, and Society for Vascular Medicine. Circulation 121(13):e266–e369

Horwood L et al (2016) Magnetic resonance imaging in patients with cardiac implanted electronic devices: focus on contraindications to magnetic resonance imaging protocols. Europace. pii: euw122

Van der Hulst AE et al (2010) Tetralogy of Fallot: 3D velocity-encoded MR imaging for evaluation of right ventricular valve flow and diastolic function in patients after correction. Radiology 256(3):724–734

Van der Hulst AE et al (2011) Real-time three-dimensional echocardiography: segmental analysis of the right ventricle in patients with repaired tetralogy of fallot. J Am Soc Echocardiogr 24(11):1183–1190

Hwang YM et al (2016) Cardiac implantable electronic device safety during magnetic resonance imaging. Korean Circ J 46(6):804–810

Iriart X et al (2009) Right ventricle three-dimensional echography in corrected tetralogy of Fallot: accuracy and variability. Eur J Echocardiogr 10(6):784–792

Jahangiri M et al (1999) Does the modified Blalock-Taussig shunt cause growth of the contralateral pulmonary artery? Ann Thorac Surg 67(5):1397–1399

Joemai RM et al (2008) Clinical evaluation of 64-slice CT assessment of global left ventricular function using automated cardiac phase selection. Circ J 72(4):641–646

Johnson C (1965) Fallot's tetralogy: a review of the radiological appearances in thirty-three cases. Clin Radiol 16:199–210

Kaiser T et al (2008) Normal values for aortic diameters in children and adolescents—assessment in vivo by contrast-enhanced CMR-angiography. J Cardiovasc Magn Reson 10:56

Karl TR et al (1992) Tetralogy of Fallot: favorable outcome of nonneonatal transatrial, transpulmonary repair. Ann Thorac Surg 54:903–907

Khairy P et al (2010) Arrhythmia burden in adults with surgically repaired tetralogy of Fallot: a multi- institutional study. Circulation 122:868–875

Khoo NS et al (2009) Assessments of right ventricular volume and function using three-dimensional echocardiography in older children and adults with congenital heart disease: comparison with cardiac

magnetic resonance imaging. J Am Soc Echocardiogr 22:1279–1288
Kilner PJ et al (2010) Recommendations for cardiovascular magnetic resonance in adults with congenital heart disease from the perspective workings groups of the European Society of Cardiology. Eur Heart J 31:794–805
Knauth AL et al (2008) Ventricular size and function assessed by cardiac MRI predict major adverse clinical outcomes late after tetralogy of Fallot repair. Heart 94(2):211–216
Koestenberger M et al (2011) Tricuspid annular plane systolic excursion and right ventricular ejection fraction in pediatric and adolescent patients with tetralogy of Fallot, patients with atrial septal defect, and age-matched normal subjects. Clin Res Cardiol 100(1):67–75
Kolandaivelu A et al (2009) Cardiovascular magnetic resonance guided electrophysiology studies. J Cardiovasc Magn Reson 11(1):21
Lam YY et al (2007) Restrictive right ventricular physiology: its presence and symptomatic contribution in patients with pulmonary valvular stenosis. J Am Coll Cardiol 50(15):1491–1497
Lanjewar C et al (2012) Aneurysmally dilated major aorto-pulmonary collateral in tetralogy of Fallot. Indian Heart J 64(2):196–197
Lembcke A et al (2005) Multislice computed tomography for preoperative evaluation of right ventricular volumes and function: comparison with magnetic resonance imaging. Ann Thorac Surg 79(4):1344–1351
Maceira AM et al (2006a) Reference right ventricular systolic and diastolic function normalized to age, gender and body surface area from steady-state free precession cardiovascular magnetic resonance. Eur Heart J 27(23):2879–2888
Maceira AM et al (2006b) Normalized left ventricular systolic and diastolic function by steady state free precession cardiovascular magnetic resonance. J Cardiovasc Magn Reson 8(3):417–426
McElhinney DB (2011) Stent fracture, valve dysfunction, and right ventricular outflow tract reintervention after transcatheter pulmonary valve implantation: patient-related and procedural risk factors in the US Melody Valve Trial. Circ Cardiovasc Interv 4(6):602–614
Mercer-Rosa L et al (2012) Quantifying pulmonary regurgitation and right ventricular function in surgically repaired tetralogy of Fallot: a comparative analysis of echocardiography and magnetic resonance imaging. Circ Cardiovasc Imaging 5(5):637–643
Miyazaki O et al (2001) Sudden death due to rupture of major aortopulmonary collateral arteries in a patient with tetralogy of Fallot and pulmonary atresia. Emerg Radiol 8:293–296
Myerson SG (2012) Heart valve disease: investigation by cardiovascular magnetic resonance. J Cardiovasc Magn Reson 14(1):7
Nishimura RA et al (1997) Evaluation of diastolic filling of left ventricle in health and disease: Doppler echocardiography is the clinician's Rosetta Stone. J Am Coll Cardiol 30(1):8–18
Niwa K et al (2002) Progressive aortic root dilatation in adults late after repair of tetralogy of Fallot. Circulation 106:1374–1378
Nørgaard MA et al (2006) Major aorto-pulmonary collateral arteries of patients with pulmonary atresia and ventricular septal defect are dilated bronchial arteries. Eur J Cardiothorac Surg 29(5):653–658
Oosterhof T et al (2005) Corrected tetralogy of Fallot: delayed enhancement in right ventricular outflow tract. Radiology 237(3):868–871
Oosterhof T et al (2007) Preoperative thresholds for pulmonary valve replacement in patients with corrected tetralogy of Fallot using cardiovascular magnetic resonance. Circulation 116:545–551
Pacheco Duro R et al (2010) Anatomophysiologic basis of tetralogy of Fallot and its clinical implications. Rev Port Cardiol 29(04):591–630
Prieto LR (2005) Management of tetralogy of Fallot with pulmonary atresia. Images Paediatr Cardiol 7(3):24–42
Raman SV et al (2006) Multi-detector row cardiac computed tomography accurately quantifies right and left ventricular size and function compared with cardiac magnetic resonance. Am Heart J 151(3):736–744
Rebergen SA et al (1993) Pulmonary regurgitation in the late postoperative follow-up of tetralogy of Fallot. Volumetric quantitation by nuclear magnetic resonance velocity mapping. Circulation 88:2257–2266
Roes SD et al (2009) Flow assessment through four heart valves simultaneously using 3-dimensional 3-directional velocity-encoded magnetic resonance imaging with retrospective valve tracking in healthy volunteers and patients with valvular regurgitation. Investig Radiol 44(10):669–675
Saremi F et al (2013) Right ventricular outflow tract imaging with CT and MRI: part 1, morphology. Am J Roentgenol 200:W39–W50
Sharma A et al (2016) Ruptured aneurysm of major aortopulmonary collateral artery: management using amplatzer vascular plug. Cardiovasc Diagn Ther 6(3):274–277
Shimada YJ et al (2010) Accuracy of right ventricular volumes and function determined by three-dimensional echocardiography in comparison with magnetic resonance imaging: a meta-analysis study. J Am Soc Echocardiogr 23(9):943–953
Shimazaki Y et al (1984) The natural history of isolated congenital pulmonary valve incompetence: surgical implications. Thorac Cardiovasc Surg 32:257–259
Shinbane JS et al (2011) Magnetic resonance imaging in patients with cardiac pacemakers: era of "MR Conditional" designs. J Cardiovasc Magn Reson 13:63
Sommer RJ et al (2008) Pathophysiology of congenital heart disease in the adult. Part III: complex congenital heart disease. Circulation 117:1340–1350

Strait JB et al (2012) Aging-associated cardiovascular changes and their relationship to heart failure. Heart Fail Clin 8(1):143–164

Tharakan JA et al (2014) Post cardiac surgery junctional ectopic tachycardia: a 'Hit and Run' tachyarrhythmia as yet unchecked. Ann Pediatr Cardiol 7(1):25–28

Thierrien J et al (2000) Pulmonary valve replacement in adults late after repair of tetralogy of Fallot: are we operating too late? J Am Coll Cardiol 36(5):1670

Troughton RW et al (2014) Effect of B-type natriuretic peptide-guided treatment of chronic heart failure on total mortality and hospitalization: an individual patient meta-analysis. Eur Heart J 35(23):1559–1567

Valente AM et al (2014) Multimodality imaging guidelines for patients with repaired tetralogy of Fallot: A report from the American Society of Echocardiography. Developed in collaboration with the Society for Cardiovascular Magnetic Resonance and the Society for Pediatric Radiology. J Am Soc Echocardiogr 27:111–141

Vogel-Claussen J et al (2006) Delayed enhancement MR imaging: utility in myocardial assessment. Radiographics 26(3):795–810

Wald RM et al (2009) Effects of regional dysfunction and late gadolinium enhancement on global right ventricular function and exercise capacity in patients with repaired tetralogy of Fallot. Circulation 119(10):1370–1377

Wallerson DC et al (1987) Assessment of cardiac hemodynamics and valvular function by Doppler echocardiography. Bull N Y Acad Med 63(8):762–796

Warnes CA et al (2008) ACC/AHA 2008 guidelines for the management of adult with congenital heart disease: a report of the American College of Cardiology/American Heart Association Task Force on Practice Guidelines (Writing Committee to Develop Guidelines on the Management of Adults with Congenital Heart Disease). Circulation 118:e714–e833

Weber OM et al (2006) MR evaluation of cardiovascular physiology in congenital heart disease: flow and function. J Cardiovasc Magn Reson 8(4):607–617

Weisbord SD et al (2008) Incidence and outcomes of contrast-induced AKI following computed tomography. Clin J Am Soc Nephrol 3(5):1274–1281

Westhoff-Bleck M et al (2016) NT-proBNP indicates left ventricular impairment and adverse clinical outcome in patients with tetralogy of Fallot and pulmonary regurgitation. Can J Cardiol 32(10):1247.e29–1247.e36

Single Ventricle and Fontan Procedures

Lucia Flors, Patrick T. Norton, and Klaus D. Hagspiel

Contents

Abstract

Univentricular congenital heart diseases include a range of pathologies that result in a functionally single ventricular chamber. The most common pathologies in this group are tricuspid atresia, pulmonary atresia with an intact ventricular septum, hypoplastic left heart syndrome, and a double-inlet ventricle. Although the only curative therapy for these patients is cardiac transplantation, there are several palliative surgical techniques that divert part or all the systemic venous circulation into the pulmonary arteries bypassing the single ventricular chamber. The modern Fontan procedure consists in anastomosing both SVC and IVC to the right pulmonary artery; it is nowadays the last step of single ventricle palliation.

The importance of imaging in these pathologies lies not only in the understanding of the new circuit established after surgical correction, but also in the early detection of the wide spectrum of cardiac and extracardiac complications that can happen due to the new physiological condition. Due to the increased survival of these patients, long-term complications are becoming more common. Imaging patients with single ventricle physiology and particularly following single ventricle palliative procedures is challenging due to the altered anatomy and hemodynamics. While MRI and MRA should be considered the modality of choice due to the inherent lack of

Electronic Supplementary Material The online version of this chapter (doi:10.1007/174_2017_109) contains supplementary material, which is available to authorized users.

L. Flors, M.D., Ph.D. (✉)
Department of Radiology and Medical Imaging, University of Virginia Health System, 1215 Lee St., Charlottesville, VA 22908, USA

Department of Radiology, University of Missouri Health System, MO, USA

P.T. Norton, M.D. • K.D. Hagspiel, M.D.
Department of Radiology and Medical Imaging, University of Virginia Health System, 1215 Lee St., Charlottesville, VA 22908, USA
e-mail: lff8p@virginia.edu

Med Radiol Diagn Imaging (2017)
DOI 10.1007/174_2017_109, © Springer International Publishing AG
Published Online: 01 September 2017

ionizing radiation in this patient population, CT angiography is an important alternative noninvasive imaging technique. In this chapter, we review the different palliative surgical techniques in patients with univentricular heart diseases, and we describe the optimal imaging protocol and the expected surgical anatomy as well as the long-term complications.

Keywords

Fontan procedure • Hypoplastic left heart syndrome • Tricuspid atresia • Pulmonary atresia • Magnetic resonance imaging • Computed tomography

1 Introduction

Some congenital heart diseases show impairment of the normal biventricular physiology. In normal circumstances, pulmonary and systemic circulations are separated and driven by their respective ventricular "pump," but there are several congenital heart diseases, such as hypoplastic left heart syndrome (HLHS), tricuspid atresia, or pulmonary atresia, characterized by having a functional single ventricular chamber (Fredenburg et al. 2011; Khanna et al. 2012; Lu et al. 2012). Physiologically, the single ventricle receives the flow from both pulmonary and systemic circulations with subsequent volume overload and long-term dysfunction.

Although the definitive treatment of these patients is cardiac transplantation, there are several palliative surgical techniques that prevent ventricular volume overload diverting part or all the systemic venous circulation into the pulmonary arteries, and therefore bypassing the single ventricular chamber (Fredenburg et al. 2011; Khanna et al. 2012). The result obtained is a single ventricle that functions both as suction and expelling pump.

The dramatic advances in congenital heart surgery and intensive care medicine have substantially increased the life expectancy of these patients and late complications of the failing Fontan physiology are therefore observed more commonly (Khanna et al. 2012).

Imaging follow-up is essential for anatomical and functional assessment before and after surgery, and early detection of cardiac and extracardiac complications (Lu et al. 2012).

The objective of this chapter is to review the different surgical options in patients with functionally univentricular heart, to describe the optimal imaging protocol, to illustrate the expected normal postsurgical anatomy, and to describe the potential (long-term) complications of these procedures and the spectrum of their imaging findings.

2 Surgical Techniques and Normal Postsurgical Anatomy

The goal of palliative therapy in the setting of heart disease with a functioning single ventricle is to unload the ventricular burden imposed by the pulmonary and systemic circuits flowing in parallel to a system in which they operate in series. This is achieved by removing the subpulmonic pump in lieu of passive systemic venous flow directly into the lungs, thus freeing the single ventricle for pumping oxygenated blood systemically. In the 1940s, it was shown that the right ventricle could be excluded from the pulmonary circuit while maintaining adequate pulmonary blood flow (Rodbard and Wagner 1949). Fontan capitalized on this in 1968 when he performed his landmark surgery for tricuspid atresia, by anastomosing the right atrial appendage directly and the pulmonary artery (Fontan and Baudet 1971). Subsequently, this procedure was modified and adapted to other variants of univentricular hearts.

Fontan circulation can be achieved by either anastomosing the vena cava to the pulmonary artery, with the use of baffles or conduits, or connecting the right atrium to the pulmonary artery after excluding tricuspid flow and repairing any atrial septal defect (classic atriopulmonary connection, classic Fontan) (Fig. 1). However, many patients will require a staged approach rather than primary creation of the Fontan circuit due to unfavorable anatomy and physiology. A staged

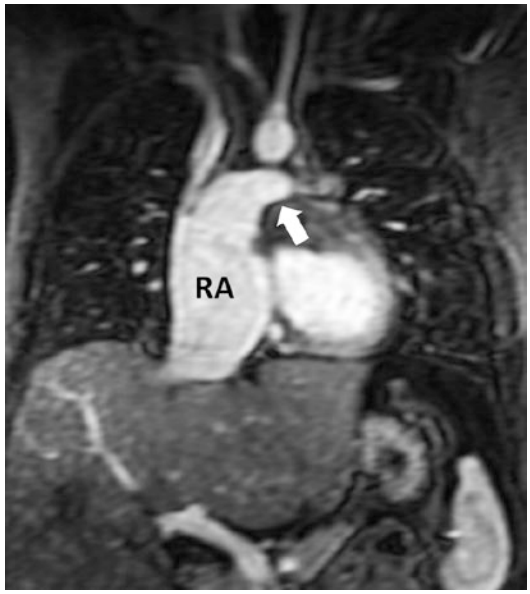

Fig. 1 Classic Fontan procedure for tricuspid atresia correction. Contrast-enhanced MRA image shows the connection between the *right atrium* (RA) and the *right pulmonary artery* (*arrow*). Note the mild dilatation of the RA

Fig. 2 Norwood-Sano procedure for correction of hypoplastic *left heart syndrome* in the neonatal period. Sano conduit seen from the *right ventricle* to the pulmonary artery (*arrow*). Neoaorta created from the amalgamation of the transected MPA with the ascending aorta after the Norwood procedure is also seen (*arrowheads*)

approach allows for appropriate growth of the pulmonary arteries and minimizes acute changes in end-diastolic filling, resulting in a decrease in mortality as compared to a primary Fontan creation (Norwood and Jacobs 1993).

The first stage of palliation of the single ventricle is performed in the neonatal period and consists of controlling pulmonary blood flow, by means of a direct systemic-to-pulmonary artery shunt or pulmonary artery banding; relieving any systemic outflow obstruction; and addressing issues with pulmonary venous return. In cases of HLHS, a Norwood procedure is performed whereby the main pulmonary artery (MPA) is transected and a "neoaorta" is created from the amalgamation of the MPA with the ascending aorta. In combination with aortic arch augmentation, unobstructed systemic flow for aortic growth and coronary perfusion is provided. Pulmonary blood flow (PBF) is regulated via a size-specific conduit from the subclavian or brachiocephalic artery to the pulmonary artery (modified Blalock Taussig shunt) or via a conduit from the right ventricle to the pulmonary artery (Sano shunt) (Fig. 2).

The location of the Blalock Taussig shunt downstream of the neoaortic valve results in continuous PBF in both systole and diastole, creating a situation where retrograde flow could occur in the coronary arteries during diastole. The Sano shunt eliminates the potential for coronary steal, but may lead to decreased ventricular function and increased arrhythmias secondary to the ventriculotomy. However, there is no clear evidence to support superiority of one technique over the other (Ohye et al. 2016).

The second stage of palliation is the creation of a superior cavopulmonary connection, typically occurring at 4–9 months of age, after the pulmonary vasculature has matured. The superior vena cava venous return is directed into the pulmonary arteries, sources of systemic-to-pulmonary arterial blood flow are disconnected or interrupted (e.g., Blalock Taussig shunt, Sano shunt, flow through a stenotic pulmonary valve), and any pulmonary bands are removed. Cardiac output is directed solely to the systemic circulation, reducing the volume work of the heart. The procedure chosen at this stage determines the final technique employed for Fontan completion.

The bidirectional Glenn procedure (BDG) is created by dividing the superior vena cava (SVC) at the SVC-atrial junction, oversewing the atrial

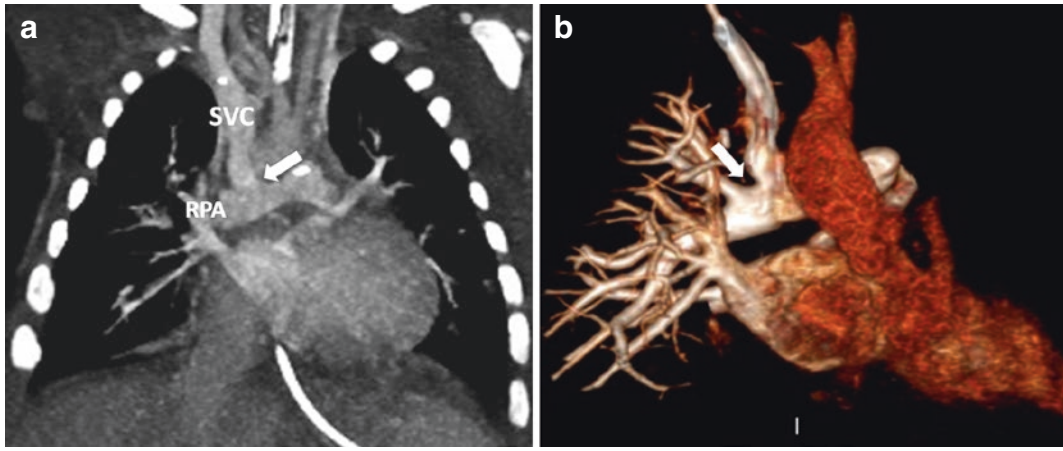

Fig. 3 6-month-old boy with the history of tricuspid atresia status post-bidirectional Glenn. Coronal CT angiography, maximum intensity projection (**a**), and volume rendering 3D (**b**) images show connection (*arrow*) of the superior vena cava (SVC) to the *right pulmonary artery* (RPA)

end, and anastomosing the SVC to the ipsilateral pulmonary artery in an end-to-side fashion (Fig. 3). Continuity of the left and right pulmonary arteries permits blood flow to both lungs. In cases of bilateral SVCs, this anastomosis is performed bilaterally to direct all venous return from the head and upper extremities to the pulmonary arteries. The BDG typically results in a pulmonary-to-systemic blood flow ratio (Qp/Qs) of 0.6:1. BDG is relatively simple as compared to hemi-Fontan procedure (HF), requiring shorter cardiopulmonary bypass time without aortic cross clamping or circulatory arrest. BDG does not address problems with pulmonary artery distortion or stenosis and due to the need for extensive dissection to free the SVC there is an increased risk for phrenic nerve injury (Talwar et al. 2014). In the setting of a BDG, Fontan completion is performed with an extracardiac conduit.

An alternative cavopulmonary connection is the hemi-Fontan procedure (HF), which addresses problems of pulmonary artery anatomy and simplifies lateral tunnel completion of the Fontan. In this procedure, the SVC and pulmonary arteries maintain their anterior-posterior relationship. The SVC is opened along the medial aspect at the atrial junction and amalgamated with the anterior aspect of the pulmonary arteries, using a homograft patch. The pulmonary arteries are augmented with a patch extending from just medial of the right upper lobe branch to the left lobar branch. A homograft patch is also used to create a dam between the right atrium and SVC, directing the superior caval flow into the pulmonary arteries, which can be easily removed at the time of lateral tunnel creation (Spray 2013). Percutaneous completion of the Fontan can be performed by perforation of the dam and stenting from the IVC to the pulmonary artery (Talwar et al. 2014). Additionally, the anteroposterior offset between the caval and pulmonary arterial flow may have some hemodynamic benefit (Bove et al. 2003).

The Fontan completion operation is typically performed at 18–48 months of age. This final stage of single ventricular palliation directs systemic venous return from the inferior vena cava (IVC) into the pulmonary arteries, thereby completing the total cavopulmonary connection. In patients that have undergone HF, a lateral tunnel (LT) is the procedure of choice for completion. The homograft dam is excised and a baffle made of synthetic material is used to isolate flow from the IVC into the pulmonary artery along the lateral aspect of the atrium. The baffle is created so as not to obstruct the atrial septal defect. A fenestration, or hole, is often made in the baffle to maintain cardiac output in high-risk patients. This fenestration maintains

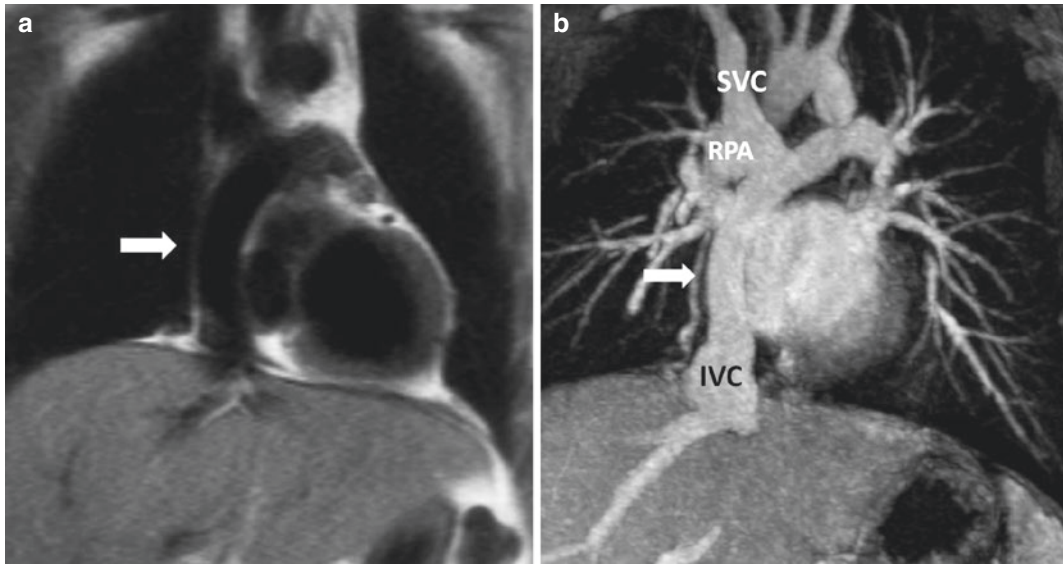

Fig. 4 Fontan procedure for repair of tricuspid atresia. Coronal dark blood spin-echo image (**a**) and contrast-enhanced MRA (**b**) show the total cavopulmonary connection with anastomosis of both the SVC and IVC to the RPA, the latter by means of an extracardiac conduit in this case (*arrow*). An intracardiac lateral tunnel can also be performed

blood flow to the systemic ventricle in the setting of high pulmonary vascular resistance and has the added benefit of reducing the length of postoperative pleural effusions (Bridges et al. 1992).

An extracardiac conduit (ECC) completes the Fontan circuit in the setting of a prior BDG by connecting the IVC above the hepatic veins to the right pulmonary artery by means of an extracardiac synthetic tube graft coursing along the free wall of the right atrium (Fig. 4). Akin to the LT, a fenestration is created by sewing a right atriotomy to a hole in the tube graft. Alternatively, a small ringed tube graft can be connected between the ECC and the right atrium (Bradley 2006). Advantages of ECC as compared to LT include application in a variety of anatomic configurations including heterotaxy syndromes, anomalies of systemic and pulmonary venous drainage, and apico-caval juxtaposition. Furthermore the risk for the right atrium to cause arrhythmias is theoretically lower with an ECC by avoiding exposure to pulmonary artery pressures and a significantly reduced suture burden.

3 Imaging Protocol

Imaging patients with single ventricle physiology and particularly following single ventricle palliative procedures is challenging due to the altered anatomy and hemodynamics. Typically, patients are seen biannually by their cardiologists and echocardiography is performed annually. A routine MRI is often performed 10 years after Fontan operation or when clinical findings and echocardiographic results require further investigation (Rychik 2016). MRI is usually preferred over CTA due to the inherent lack of ionizing radiation in this patient population. Nevertheless, CT angiography is an important alternative noninvasive imaging technique. CTA is particularly useful in emergent situations, in unstable patients, in patients where metal coils obscure structures of interest, and in patients in whom MRI is contraindicated. One of the major advances of CT is the speed of acquisition, and, particularly with the use of modern dual-source scanners, the ability to scan pediatric patients without the use of sedation.

Imaging objectives vary and techniques need to be adopted depending on if the study is performed before or after surgical therapy. In postsurgical patients, the stage of surgical palliation has to be taken into account.

3.1 MRI/MRA Protocol

Evaluation of the patient with single ventricle for surgical planning or postsurgical follow-up should provide information about the size, morphology, and function of the cardiac chambers; the pulmonary arteries and veins; as well as the systemic arteries and veins. It should allow assessment of the baffles and conduits as well as complications of the surgical procedures, which are discussed later in this chapter. MRI is uniquely suited for this purpose due to its lack of ionizing radiation. In our institution, a typical exam lasts approximately 45–60 min (Table 1) and begins with anatomical sequences covering the whole chest using steady-state free precession (SSFP) sequences in axial, sagittal, and coronal planes, as well as black blood axial images using a fast spin-echo (FSE) technique. These are followed by cine SSFP breath-hold images with thin slices and without interslice gap, using stacked axial images in addition to the standard horizontal and vertical long-axis and ventricular short-axis images. These sequences allow functional and morphological assessment of the cardiac chambers, their connections, and the presence of septal defects. Multiphase MR angiography (MRA), preferably using a high-resolution (1 mm isotropic) time-resolved sequence, allows identification and sizing of the pulmonary and systemic arterial and venous

Table 1 CMR imaging protocol at the University of Virginia (1.5 T system preferred over 3 T)

Sequence	Planes	Trade name
1. **Localizers**		
2. **Bright blood imaging** (breath-hold, nongated multislice balanced SSFP images of the entire chest)	Axial Coronal Sagittal	GE: FIESTA, Philips: bFFE, Siemens: TrueFISP
3. **Black blood imaging** of the entire chest with single-shot technique	Axial	GE: SSFSE, Philips: single-shot TSE, Siemens: HASTE
4. **Cine MRI**	Stacked axial without gap standard short and long axes Valve plane Outflow tract	GE: FIESTA, Philips: bFFE, Siemens: TrueFISP
5. **3D contrast-enhanced MRA** in arterial and venous phases (preferably a time-resolved technique) with 1 mm isotropic resolution	Coronal or sagittal oblique	GE: TRICKS, Philips: 4D-TRAK, Siemens: TWIST
6. **Velocity-encoded** cine 2D phase-contrast imaging	Depending on clinical question: pulmonary arteries, aorta, baffle, conduit, systemic veins, pulmonary veins	
7. **Late gadolinium enhancement imaging** 10–15 min after contrast is given 2D segmented inversion recovery GRE or SSFP, PSIR for patients with regular heart rhythm and able to hold breath, otherwise single-shot imaging	2-chamber 3-chamber 4-chamber Short axis	

SSFP steady-state free precession; *FIESTA* fast imaging employing steady-state acquisition; *bFFE* balanced fast field echo; *True FISP* fast imaging with steady-state free precession; *SSFSE* single-shot fast spin echo; *TSE* turbo spin echo; *HASTE* half-Fourier acquisition single-shot turbo spin-echo; *MRA* magnetic resonance angiograph; *TRICKS* time-resolved imaging of contrast kinetics; *TRAK* time-resolved angiography using keyhole; *TWIST* time-resolved angiography with stochastic trajectories; *GRE* gradient-recalled echo; *PSIR* phase-sensitive inversion recovery

system as well as their connections with the heart as well as the baffles and conduits. Due to the lack of radiation and the ability to repeat the image acquisition at multiple time points following the contrast injection, contrast-enhanced MRA is an excellent technique to diagnose thromboembolic complications in the pulmonary vasculature, baffles, and conduits, and assess the systemic veins as well as the arterial system. In general, the spatial resolution of MRA is inferior to CTA and the diagnosis of smaller emboli, pulmonary arteriovenous malformations (PAVMs), and systemic–pulmonary veno-venous shunts frequently requires CTA (Lewis et al. 2015). These complications are discussed later in this chapter. Time-resolved MRA can be performed using dilute contrast and has been shown to provide excellent assessment of the flow dynamics and morphology of the pulmonary circulation as well as the pulmonary perfusion status in Fontan patients (Goo et al. 2007). We typically use 0.1 mmol/kg of gadolinium-based contrast and obtain multiple datasets with a temporal resolution of 3 s with 1 mm isotropic resolution for 90 s with a 10 s scan delay (Video 1). In general, standard extracellular MR contrast agents have been shown to give excellent image quality, and we have not been using blood pool agents in this patient population, which have been used anecdotally (Hashemi et al. 2014).

Velocity-encoded (VENC) cine-phase contrast sequences allow measurement of blood flow in the pulmonary arteries, aorta, baffles and conduits, systemic and pulmonary veins, systemic-to-pulmonary collateral flow, as well as assessment of atrioventricular valves (Latus et al. 2016). The aortopulmonary collateral flow can be quantitated using 2D flow measurements of the ascending aorta, the pulmonary veins, the pulmonary arteries, and the inferior and superior vena cava flow using one of these two equations:

1. Sum of flow in all pulmonary veins—(right + left pulmonary artery flow)
2. Ascending aorta flow—(inferior + superior vena cava flow) (Kutty Heart 2016)

The presence and degree of obstruction in baffles and conduits can also be measured using these techniques. Several newer, albeit not widely available MRI techniques provide even more detailed assessment of the hemodynamics of Fontan patients. Hybrid CMR and X-ray-guided angiography (CMR/XMR) allows to more accurately measure pulmonary vascular resistance than standard catheter techniques (Pushparajah et al. 2015). More recently, the use of particle traces derived from time-resolved 3D MR velocity mapping (4D flow MRI) has been shown to allow in vivo quantification of the caval flow distribution to the PAs in patients with Fontan circulation. It could be demonstrated that 83% of the superior vena cava blood flows to the right pulmonary artery whereas 55% of the inferior vena caval blood flows to the left PA (Bachler et al. 2013).

Late gadolinium enhancement (LGE) of the myocardium using a phase-sensitive ECG-triggered breath-hold inversion recovery sequence allows assessment for myocardial fibrosis and infarction. The presence of LGE is common in late heart Fontan survivors and its presence has been shown to be associated with adverse ventricular mechanics and a higher frequency of nonsustained ventricular tachycardia (Rathod et al. 2010). In one retrospective study involving 215 patients who underwent MRI at a median age of 18.3 years and who underwent the Fontan operation at a median age of 3.6 years, LGE was present in 33% (Rathod et al. 2014).

3.2 CTA Protocol

In cases where MRI is not feasible, CTA is an excellent alternative. We consider high-pitch spiral scanning on dual-source CT scanners without gating or triggering optimal for most patients unless coronary artery evaluation is required in which case we resort to prospective or retrospective techniques. Due to the extreme acquisition speed (up to 74 cm/s table motion) the scan times are

extremely short and we routinely scan children of all ages without sedation or anesthesia. Low kV technique results in effective doses of 1 mSv or less for these scans. If dual-source scanners are not available, at least a 64-channel system should be used—with ECG gating. Proper contrast timing is critical and will depend according to what stage of surgical palliation the study is performed in.

After stage 1 palliation, performed in the neonatal period, patients with systemic-to-pulmonary arterial shunts are typically not at risk to develop pulmonary embolism, due to the absent connection of the pulmonary arteries with systemic veins. They do however have a 1–17% risk of shunt thrombosis, which occasionally leads to the need for imaging beyond echocardiography (Ghadimi Mahani et al. 2016). Conduit stenosis also occurs in a small percentage and can necessitate cross-sectional imaging. In these cases, CT pulmonary angiography (CTPA) is best performed during the pulmonary arterial phase. A venous injection into the lower extremities eliminates streak artifacts that would otherwise affect a scan with an upper extremity venous injection, particularly in children where low kV settings are used (Ghadimi Mahani et al. 2016).

For stage 2, blood from the superior vena cava is redirected to the pulmonary arteries, either via a bidirectional Glenn or a hemi-Fontan procedure. In this stage thrombosis and thromboembolic events are infrequent and often caused by catheters in the upper venous system. CTA in this phase is best performed with lower extremity venous access with the scan started after optimal enhancement of the SVC or bilateral jugular veins with contrast monitoring in the neck or mediastinum. The contrast flows at this stage from the IVC to the ventricle to the systemic arteries, and returns from the brain via the jugular veins. Using this technique, homogeneous enhancement of the pulmonary arteries without inflow of nonopacified blood simulating filling defects is usually achieved. In addition, as the scan is acquired during the arterial phase, the diagnosis of systemic-to-pulmonary arterial collaterals is possible.

The prevalence of thrombosis and thromboembolic events is higher after completion of the total cavopulmonary connection (stage 3). CTPA is suitable to diagnose or exclude thromboembolic in these patients with high accuracy, if performed properly. Standard CTPA techniques using single upper extremity venous access suffer from mixing of opacified blood from the SVC and unopacified blood from the IVC resulting in a large number of nondiagnostic or false-positive studies (Sandler et al. 2014). One way to obviate this problem with single upper extremity venous access is to increase the contrast volume and image with a scan delay of 70–80 s. This results in homogeneous enhancement of the pulmonary arteries and allows the diagnosis of PE. Recommended contrast doses are up to 2 mL/kg in smaller children (we usually hand-inject smaller children and aim for duration of injection of 10–15 s; in older children we use power injectors with flow rates between 0.6 and 2 mL/s) and a total dose of 150 mL in adults with a flow rate of 2 mL/s. If simultaneous aortic enhancement is also desired, the flow rate can be increased to 3–5 mL/s toward the end of the study. A timing bolus or bolus tracking technique is used to determine the time from injection to aortic peak (Ghadimi Mahani et al. 2016). It has to be noted that all intravenous injections in these patients need to be absolutely free of air due to the frequent presence of fenestrations which represent right to left shunts and put the patient at risk of stroke from air emboli.

The optimal technique requires dual venous access, typically one in an antecubital vein and the other in a dorsal foot vein. Alternatively, femoral access can be chosen in adults. Contrast is injected with two power injectors if available with 60% of contrast injected into the lower extremity. Recommended contrast dose is up to 2 mL/kg of 370 mg iodine/mL or up to 3 mL/kg of 300 mg iodine/mL contrast agent. Recommended flow rates are 2–2.5 mL/s in the upper extremity and 3–4 mL/s in the lower extremity. Contrast injection should be followed by a saline flush. A monitoring scan is performed at the level of the carina. The scan is

initiated when the contrast arrives in the left pulmonary artery, which typically occurs after the right PA (Ghadimi Mahani et al. 2016). The dual venous access is also recommended in the ACR–NASCI–SIR–SPR Practice Parameters for the performance of CTA (2016). A 60–90 s delayed scan can be performed in addition depending on the clinical question.

4 Complications

Late complications arising from the new hemodynamic and physiological conditions are observed with increasing frequency due to prolonged survival of these patients. Currently, survival rates are around 85% at 20 years (Khanna et al. 2012).

High pulmonary vascular resistance, anatomical alterations in the pulmonary arteries, increased systemic venous pressure, and ventricular dysfunction are some risk factors that predict a worse outcome and more frequent occurrence of complications (Fredenburg et al. 2011); these can be categorized as cardiac or extracardiac.

4.1 Cardiac Complications

The most common cardiac complication after the classic Fontan technique is atrial enlargement (Fig. 5), which predisposes to arrhythmias and thromboembolic events (Fredenburg et al. 2011; Khanna et al. 2012; de Leval 1998; Soler et al. 2007). Pulmonary embolism secondary to atrial thrombus is the most common cause of out-of-hospital death in patients who have undergone a Fontan procedure (Gewillig 2005). Arrhythmias can also be seen after lateral tunnel total cavopulmonary connection and be the result of atrial suture load and injury to the sinoatrial node during atriotomy (Lewis et al. 2015). When ablation is required, imaging planning is usually helpful.

Ventricular dysfunction is common in longstanding Fontan circuits, usually as a result of chronically elevated afterload and reduced preload. Ventricular dilatation, hypertrophy, and dysfunction can be assessed by imaging.

Atrioventricular valve regurgitation, leak, stenosis (Fig. 6), or thrombosis (Fig. 7) of the conduit are additional potential complications of modern Fontan procedure (Fredenburg et al. 2011;

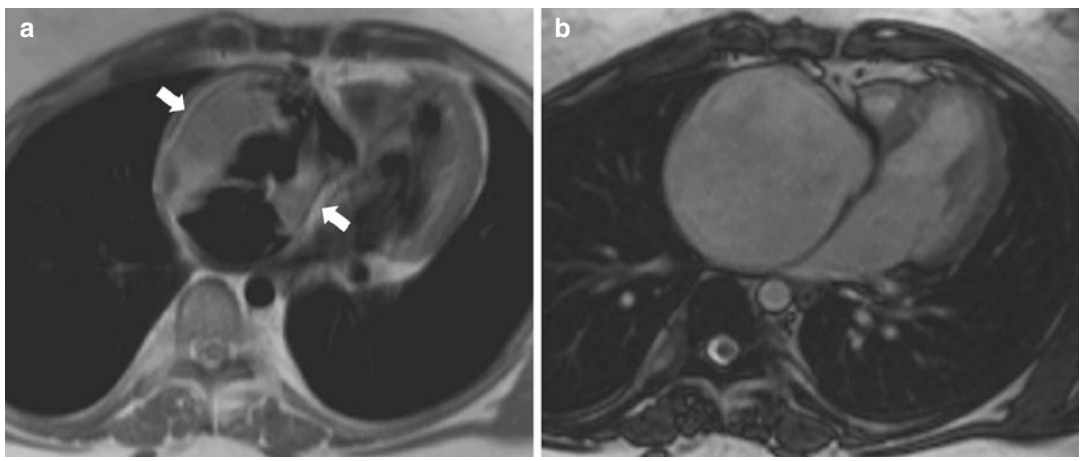

Fig. 5 29-year-old female status post-classic Fontan for tricuspid atresia repair. Dark blood spin-echo (**a**) and bright blood gradient-echo SSFP (**b**) images show severe *right atrial enlargement*. Artifact secondary to slow flow within the dilated atrium (*arrows*) may mimic thrombosis on dark blood imaging (**a**). Patent *right atrium* without evidence of thrombosis was seen on SSFP (**b**) and contrast-enhanced MRA (not shown)

Khanna et al. 2012; de Leval 1998; Soler et al. 2007). Differentiating thrombus from slow-flow artifact may be sometimes challenging (Fig. 5). As described before, optimal contrast timing is paramount to assess conduit thrombosis especially when CTA is performed.

Fig. 6 Fontan procedure for repair of tricuspid atresia. Coronal contrast-enhanced MRA shows mild focal stenosis of the extracardiac Fontan conduit (*arrow*)

4.2 Extracardiac Complications

There is a wide range of extracardiac complications occurring in these patients and imaging plays an important role in the early diagnosis. These can be broadly categorized into complications involving the pulmonary arteries, conditions entailing right-to-left or left-to-right shunting, and hepatic and lymphatic complications.

4.2.1 Pulmonary Arteries

The low pressures achieved after the Fontan repair paradoxically condition an increase in the pulmonary vascular resistance (Fredenburg et al. 2011). This complication is attributed to the absence of pulsatility of the pulmonary arteries, the inability to achieve complete filling of the pulmonary vasculature, and the increase of pulmonary lymphatic pressure (Fredenburg et al. 2011; de Leval 1998). Pulmonary vascular resistance is a determinant factor in the cardiac output of this new hemodynamic condition.

Pulmonary vascular resistance may also be affected by morphological alterations in the pulmonary arteries, mainly stenosis, which frequently occur at the site of anastomosis (Fredenburg et al. 2011). Stenosis of the left pulmonary artery by extrinsic compression of an enlarged aortic root can also be seen; this is

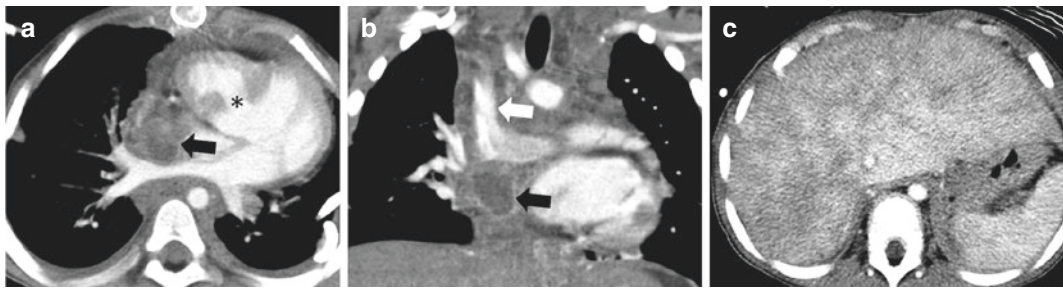

Fig. 7 3-year-old male with recent Fontan procedure for double-outlet *right ventricular repair* and acute thrombosis of the Fontan conduit. Axial (**a**) and coronal (**b**) CTA images show a heterogeneous peripherally enhancing filling defect within the extracardiac inferior vena cava to pulmonary artery shunt (*black arrow*). The superior vena cava has been routed into the *right pulmonary artery* (*white arrow*). A large VSD (*asterisk*) and small *right ventricular chamber* can also be seen on **a**. Hepatic venous congestion is seen on the *upper abdomen* (**c**)

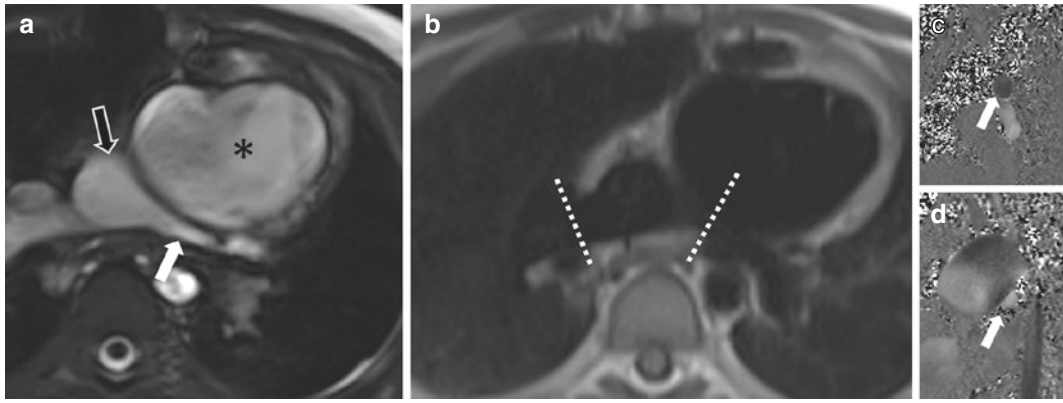

Fig. 8 10-year-old male with the history of hypoplastic *left heart syndrome* status post-staged extracardiac fenestrated Fontan and prior Norwood procedure. Bright blood axial SSFP image (**a**) shows the Fontan conduit (*black arrow*) connecting to the pulmonary arteries. The *left pulmonary artery* is small in size (*white arrow*) with evidence of compression from a severely dilated neo-ascending aorta (*asterisk*). The *right pulmonary artery* is of normal size. Differential pulmonary blood flow calculated using velocity-encoded phase-contrast (VENC) imaging obtained perpendicular to the pulmonary arteries following the plane marked by the dashed lines on the dark blood axial image (**b**), through the *right* (**c**) and *left* (**d**) pulmonary arteries (*arrows*), revealed asymmetric pulmonary flow, 80% of a total flow to the *right* and 20% of total flow to the *left*

particularly common in cases of hypoplastic left ventricle that underwent Fontan palliation and prior Norwood connection (aorta and pulmonary artery connection) due to compression by a dilated neoaorta (Fig. 8) (Lewis et al. 2015). Early detection and treatment of pulmonary artery stenosis can improve system functionality. Stents are often placed in the pulmonary arteries to maintain patency. Due to metallic artifact, these are usually better assessed with CTA.

After completion of the total cavopulmonary connection the prevalence of thrombosis and thromboembolic events has been found to range from 1 to 33%, with the highest risk immediately postsurgery and then again late (10 + years) following the surgery (McCrindle et al. 2013).

4.2.2 Shunting

Right-to-left shunts may occur due to the development of pulmonary arteriovenous fistulae (PAVFs) and the formation of systemic-pulmonary venovenous shunts (VVS) (Fredenburg et al. 2011; Khanna et al. 2012; de Leval 1998) which usually cause desaturation and cyanosis (Khanna et al. 2012).

The lack of pulsatility in the pulmonary arteries and the absence or asymmetrical distribution of the hepatoenteric inflow in the lungs are considered potential etiological factors (Khanna et al. 2012; Ashrafian and Swan 2002; Srivastava et al. 1995) but the exact etiology of PAVF is not clearly known. Some authors attribute the PAVF formation to an unknown "hepatic factor." They hypothesized that the liver may be responsible for the degradation of a vasodilating substance (Duncan and Desai 2003; Kim et al. 2009), and may also be the source of vasoactive substances that function as inhibitors of pulmonary vascular dilatation or recruitment (Duncan and Desai 2003). In fact, an increased risk of occurrence of these malformations in lungs with absent hepatoenteric flow during "the Glenn stage" and reversibility of this condition after the Fontan completion has been seen (Lu et al. 2012).

Venovenous collateral development with connection between the systemic and pulmonary circulation, systemic-pulmonary VVS, is a consequence of the existence of an elevated central venous pressure (Khanna et al. 2012; Ashrafian and Swan 2002; Srivastava et al. 1995). These anomalous vessels are seen in the mediastinum connecting the subclavian veins, the inferior or inferior vena cava, and the hepatic veins with the pulmonary veins.

Maximal intensity projection (MIP) reconstructions can help identifying PAVF and VVs on CTA images (2) (Fig. 9). When clusters of small innumerable PAVFs occur, multifocal ground-glass opacities can be seen on CT (Fig. 10); additional regional early venous drainage is also frequently seen (Figs. 9 and 10). MRI has become an excellent and accurate noninvasive method for quantifying functional parameters, such as pulmonary and systemic flow, and right-to-left shunting resulting from collateral flow and fistulae (Whitehead et al. 2009; Grosse-Wortmann et al. 2009). Excellent hemodynamic assessment of the PAVFs can also be obtained with time-resolved MRA (Fig. 10).

Left-to-right shunting can also occur via major aortopulmonary collaterals, which can arise from the thoracic aorta, and brachiocephalic and internal mammary arteries. Other potential causes of shunting include surgical fenestrations and residual atrial septal defects.

4.2.3 Hepatic Complications

Elevated systemic venous pressure after a Fontan procedure causes chronic passive venous congestion that has negative effects on the liver parenchyma. The increased retrograde pressure in the hepatic sinusoids may ultimately lead to centrilobular, necrosis, sinusoidal fibrosis, cirrhosis, and portal hypertension (Fredenburg et al. 2011; Khanna et al. 2012; Ghaferi and Hutchins 2005). In addition to hepatic vein-centered liver fibrosis, portal-based fibrosis has been demonstrated recently in the majority of patients who died soon after the Fontan procedure, which suggests a multifactorial origin of the disease (Schwartz et al. 2012).

As occurs in all other causes of cirrhosis, patients with cardiac cirrhosis may develop dysplastic nodules and hepatocellular carcinomas

Fig. 9 20-year-old female with multiple PAVF and VVS presented with cyanosis and oxygen saturation of 82%. Contrast-enhanced CT images (MIP reconstructions) show strong and early contrast opacification of the *right upper pulmonary artery* (PA) and *right upper pulmonary vein* (PV) due to the presence of innumerable PAVFs in the *right upper lobe*. Collateral circulation is also seen within the mediastinum (*arrow*) representing several systemic-pulmonary VVS that connect the *left subclavian vein* and the SVC with the pulmonary veins (*black arrow*). *PAVF* pulmonary arteriovenous fistulae; *VVS* venovenous shunts

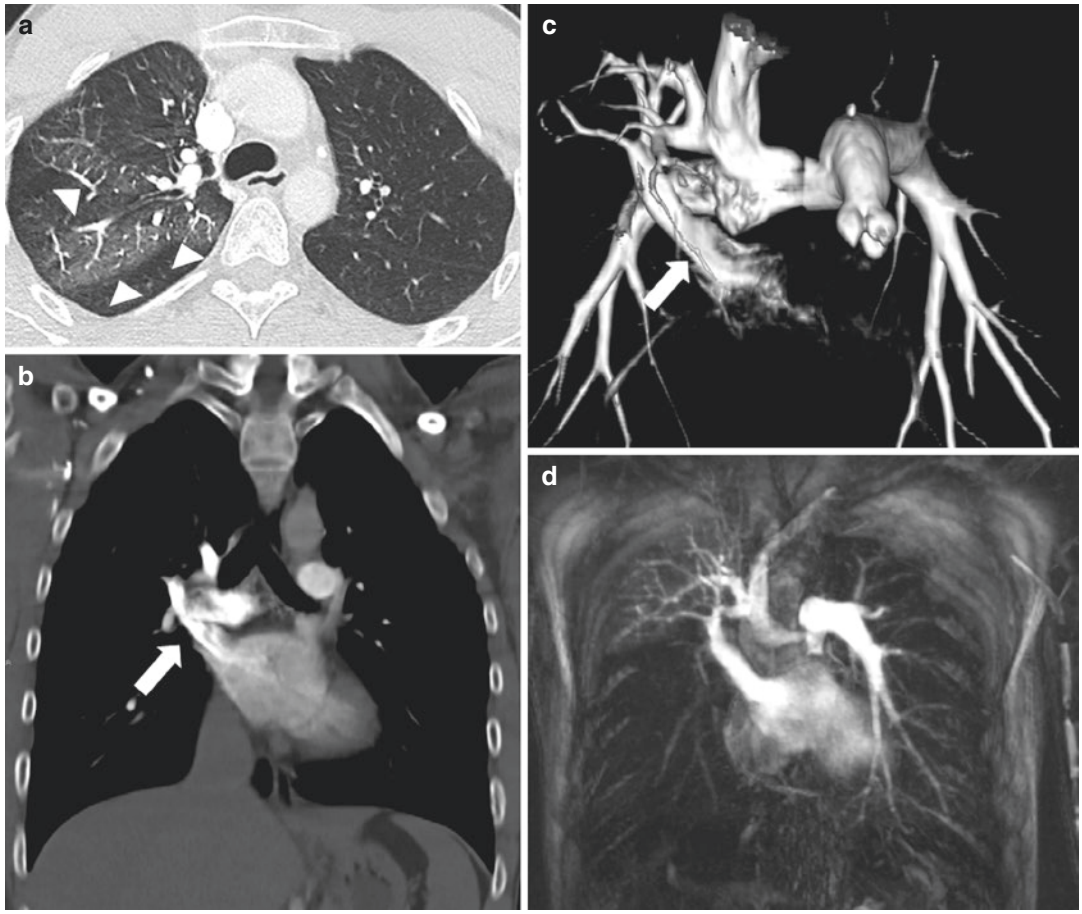

Fig. 10 13-year-old girl with Fontan procedure for pulmonary atresia correction presented with shortness of breath. Contrast-enhanced thoracic CT image shows countless small PAVFs in the RUL presenting as ground-glass opacities (*arrowheads*) (**a**). Strong and early contrast opacification of the *right upper pulmonary vein* (*white arrow*) is seen in the MIP (**b**) and volume-rendering (**c**) reconstructions due to the presence of the PAVFs. Time-resolved contrast-enhanced MRA (**d**) allows excellent assessment of the hemodynamics of the PAVFs

(HCC) (Ghaferi and Hutchins 2005; Asrani et al. 2013). In addition to the alpha-fetoprotein level, imaging surveillance is, therefore, recommended (Ghaferi and Hutchins 2005). Some authors advocate the use of CT and ultrasound, considering MRI and target biopsy for large and enlarging nodules (Kiesewetter et al. 2007).

In the first stage of passive hepatic congestion a typical reticular enhancement pattern in the portal phase, more pronounced in the periphery, is seen (Khanna et al. 2012) (Figs. 7 and 11). Chronic increase of the venous pressure results in the development of regenerative nodules and the formation of intra- and extrahepatic VVS (Khanna et al. 2012; Ghaferi and Hutchins 2005; Kiesewetter et al. 2007; Bryant et al. 2011). Regenerative nodules have a similar appearance to focal nodular hyperplasia (FNH) on dynamic contrast-enhanced imaging—both are brightly hyperenhancing lesions on arterial phase and slightly hyperintense or isointense to the background liver on the venous phase—and must be differentiated from HCC which shows the typical contrast washout on delayed images (2) among other distinctive features. Benign hypervascular hepatic nodules, frequently located in the periphery, are common in the failing Fontan circulation. A recent study showed that postmortem histology

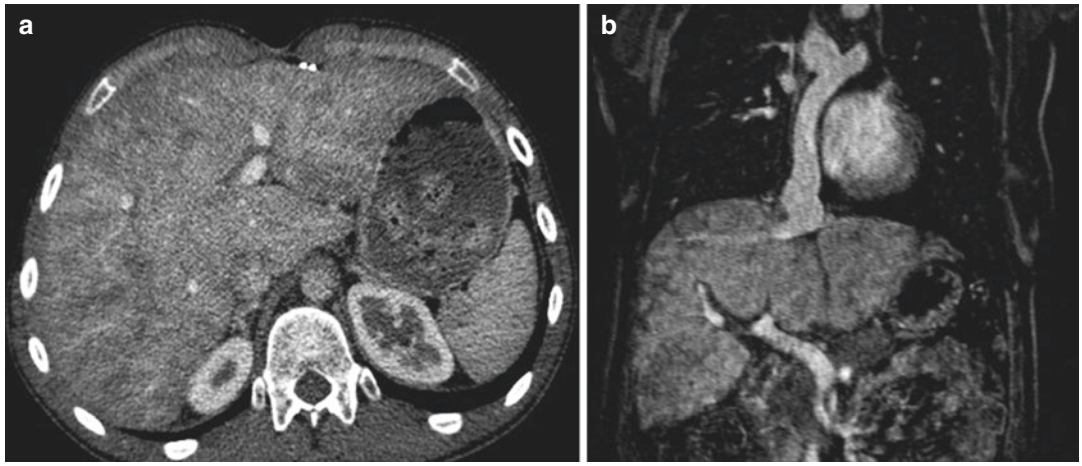

Fig. 11 Hepatic venous congestion after Fontan procedure in two different patients. CT image (**a**) and portal-phase contrast-enhanced MRI (**b**) images show heterogeneity and peripheral perfusion alteration. Extracardiac Fontan conduit is also seen (*arrow*)

suggests that FNH is the underlying pathology and their presence very likely indicates arterialization of hepatic blood flow and reciprocal portal venous deprivation (Bryant et al. 2011).

4.2.4 Lymphatic Complications

In the lungs, the elevated systemic venous pressure and secondary increased lymphatic pressure can cause interstitial pulmonary edema, and pleural and pericardial effusion (de Leval 1998). Plastic bronchitis is another rare potential complication of lymphatic dysfunction (Fredenburg et al. 2011; Goo et al. 2008). Patients usually present with cough and expectoration. Impaired lymphatic drainage and low cardiac output cause hypersecretion of mucin and formation of large and dense secretions that impact into the airway (Khanna et al. 2012). CT findings usually include bronchial wall thickening, mucous plugging, and atelectasis.

Protein-losing enteropathy and ascites are the most relevant abdominal complications derived from the increased lymphatic pressure. Protein-losing enteropathy is a late, serious complication with a poor prognosis (Fredenburg et al. 2011; Khanna et al. 2012; de Leval 1998; Feldt et al. 1996), thought to be associated with the venous and lymphatic congestion that occurs in the splanchnic circuit causing protein loss into the intestinal lumen

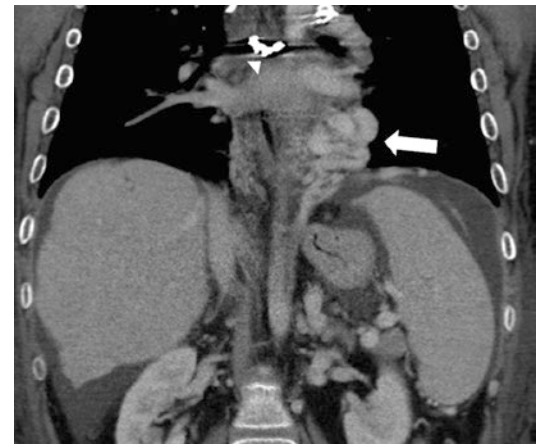

Fig. 12 16-year-old male patient with cardiac cirrhosis, portal hypertension, and protein-losing enteropathy after Fontan procedure. Coronal abdominal CT images show morphologic changes of cirrhosis and portal hypertension with ascites and splenomegaly. Large systemic-pulmonary venovenous shunts (VVS) from the *left suprahepatic vein* to the *left inferior pulmonary vein* are also seen (*arrow*). Coils from prior embolization of VVS also noted in the mediastinum (*arrowhead*)

with the subsequent hypoalbuminemia and immunodeficiency (Fredenburg et al. 2011; Khanna et al. 2012). The hypoproteinemia may also be the cause of pleural effusion and ascites. MRI and CT are rarely helpful in the diagnoses of this condition. Ascites (Fig. 12) and bowel wall thickening are the nonspecific findings usually seen.

Conclusion

The Fontan procedure is a palliative surgical therapy indicated for patients with a variety of congenital cardiac diseases which results in univentricular physiology. Although many modifications to the original description have been employed, the main objective of this technique is based on connecting the systemic venous flow to the pulmonary circulation in order to avoid overloading the single ventricular chamber. Because of its comprehensive assessment, CMR has become the best imaging technique in the postoperative evaluation of these patients. In cases where MRI is not feasible CTA is an excellent alternative. Familiarity with the surgical procedure, the new postsurgical anatomy and physiology, and the spectrum of long-term cardiac and extracardiac complications are becoming more important as the survival of these patients increases.

References

Ashrafian H, Swan L (2002) The mechanism of formation of pulmonary arteriovenous malformations associated with the classic Glenn shunt (superior cavopulmonary anastomosis). Heart 88:639

Asrani SK, Warnes CA, Kamath PS (2013) Hepatocellular carcinoma after the Fontan procedure. N Engl J Med 368:1756–1757

Bachler P, Valverde I, Pinochet N et al (2013) Caval blood flow distribution in patients with Fontan circulation: quantification by using particle traces from 4D flow MR imaging. Radiology 267:67–75

Bove EL, de Leval MR, Migliavacca F, Guadagni G, Dubini G (2003) Computational fluid dynamics in the evaluation of hemodynamic performance of cavopulmonary connections after the Norwood procedure for hypoplastic left heart syndrome. J Thorac Cardiovasc Surg 126:1040–1047

Bradley SM (2006) Extracardiac conduit Fontan procedure. Oper Tech Thorac Cardiovasc Surg 11:123–140

Bridges ND, Mayer JE Jr, Lock JE et al (1992) Effect of baffle fenestration on outcome of the modified Fontan operation. Circulation 86:1762–1769

Bryant T, Ahmad Z, Millward-Sadler H et al (2011) Arterialised hepatic nodules in the Fontan circulation: hepatico-cardiac interactions. Int J Cardiol 151:268–272

ACR NASCI SIR SPR practice parameters for the performance and interpretation of body computed tomography angiography (CTA) (2016). Available: https://www.acr.org/~/media/168A72F0C6004CA9A649DBD6EA9368DE.pdf. Accessed 2 Jan 2017

Duncan BW, Desai S (2003) Pulmonary arteriovenous malformations after cavopulmonary anastomosis. Ann Thorac Surg 76:1759–1766

Feldt RH, Driscoll DJ, Offord KP et al (1996) Protein-losing enteropathy after the Fontan operation. J Thorac Cardiovasc Surg 112:672–680

Fontan F, Baudet E (1971) Surgical repair of tricuspid atresia. Thorax 26:240–248

Fredenburg TB, Johnson TR, Cohen MD (2011) The Fontan procedure: anatomy, complications, and manifestations of failure. Radiographics 31:453–463

Gewillig M (2005) The Fontan circulation. Heart 91:839–846

Ghadimi Mahani M, Agarwal PP, Rigsby CK et al (2016) CT for assessment of thrombosis and pulmonary embolism in multiple stages of single-ventricle palliation: challenges and suggested protocols. Radiographics 36:1273–1284

Ghaferi AA, Hutchins GM (2005) Progression of liver pathology in patients undergoing the Fontan procedure: chronic passive congestion, cardiac cirrhosis, hepatic adenoma, and hepatocellular carcinoma. J Thorac Cardiovasc Surg 129:1348–1352

Goo HW, Yang DH, Park IS et al (2007) Time-resolved three-dimensional contrast-enhanced magnetic resonance angiography in patients who have undergone a Fontan operation or bidirectional cavopulmonary connection: initial experience. J Magn Reson Imaging 25:727–736

Goo HW, Jhang WK, Kim YH et al (2008) CT findings of plastic bronchitis in children after a Fontan operation. Pediatr Radiol 38:989–993

Grosse-Wortmann L, Al-Otay A, Yoo SJ (2009) Aortopulmonary collaterals after bidirectional cavopulmonary connection or Fontan completion: quantification with MRI. Circ Cardiovasc Imaging 2:219–225

Hashemi S, Parks WJ, Slesnick TC (2014) 3D inversion recovery gradient echo respiratory navigator imaging using Gadofosveset Trisodium in a Fontan Y-graft patient. Int J Cardiovasc Imaging 30:993–994

Khanna G, Bhalla S, Krishnamurthy R, Canter C (2012) Extracardiac complications of the Fontan circuit. Pediatr Radiol 42:233–241

Kiesewetter CH, Sheron N, Vettukattill JJ et al (2007) Hepatic changes in the failing Fontan circulation. Heart 93:579–584

Kim SJ, Bae EJ, Lee JY, Lim HG, Lee C, Lee CH (2009) Inclusion of hepatic venous drainage in patients with pulmonary arteriovenous fistulas. Ann Thorac Surg 87:548–553

Latus H, Gerstner B, Kerst G et al (2016) Effect of inhaled nitric oxide on blood flow dynamics in patients after the Fontan procedure using cardiovascular magnetic resonance flow measurements. Pediatr Cardiol 37:504–511

de Leval MR (1998) The Fontan circulation: what have we learned? What to expect? Pediatr Cardiol 19:316–320

Lewis G, Thorne S, Clift P, Holloway B (2015) Cross-sectional imaging of the Fontan circuit in adult congenital heart disease. Clin Radiol 70:667–675

Lu JC, Dorfman AL, Attili AK, Ghadimi Mahani M, Dillman JR, Agarwal PP (2012) Evaluation with cardiovascular MR imaging of baffles and conduits used in palliation or repair of congenital heart disease. Radiographics 32:E107–E127

McCrindle BW, Manlhiot C, Cochrane A et al (2013) Factors associated with thrombotic complications after the Fontan procedure: a secondary analysis of a multicenter, randomized trial of primary thromboprophylaxis for 2 years after the Fontan procedure. J Am Coll Cardiol 61:346–353

Norwood WI, Jacobs ML (1993) Fontan's procedure in two stages. Am J Surg 166:548–551

Ohye RG, Schranz D, D'Udekem Y (2016) Current therapy for hypoplastic left heart syndrome and related single ventricle lesions. Circulation 134:1265–1279

Pushparajah K, Tzifa A, Bell A et al (2015) Cardiovascular magnetic resonance catheterization derived pulmonary vascular resistance and medium-term outcomes in congenital heart disease. J Cardiovasc Magn Reson 17:28

Rathod RH, Prakash A, Powell AJ, Geva T (2010) Myocardial fibrosis identified by cardiac magnetic resonance late gadolinium enhancement is associated with adverse ventricular mechanics and ventricular tachycardia late after Fontan operation. J Am Coll Cardiol 55:1721–1728

Rathod RH, Prakash A, Kim YY et al (2014) Cardiac magnetic resonance parameters predict transplantation-free survival in patients with fontan circulation. Circ Cardiovasc Imaging 7:502–509

Rodbard S, Wagner D (1949) By-passing the right ventricle. Proc Soc Exp Biol Med 71:69

Rychik J (2016) The relentless effects of the Fontan paradox. Semin Thorac Cardiovasc Surg Pediatr Card Surg Annu 19:37–43

Sandler KL, Markham LW, Mah ML, Byrum EP, Williams JR (2014) Optimizing CT angiography in patients with Fontan physiology: single-center experience of dual-site power injection. Clin Radiol 69:e562–e567

Schwartz MC, Sullivan L, Cohen MS et al (2012) Hepatic pathology may develop before the Fontan operation in children with functional single ventricle: an autopsy study. J Thorac Cardiovasc Surg 143:904–909

Soler R, Rodriguez E, Alvarez M, Raposo I (2007) Postoperative imaging in cyanotic congenital heart diseases: part 2 complications. AJR Am J Roentgenol 189:1361–1369

Spray TL (2013) Hemi-Fontan procedure. Oper Tech Thorac Cardiovasc Surg 18:124–137

Srivastava D, Preminger T, Lock JE et al (1995) Hepatic venous blood and the development of pulmonary arteriovenous malformations in congenital heart disease. Circulation 92:1217–1222

Talwar S, Nair VV, Choudhary SK, Airan B (2014) The Hemi-Fontan operation: a critical overview. Ann Pediatr Cardiol 7:120–125

Whitehead KK, Gillespie MJ, Harris MA, Fogel MA, Rome JJ (2009) Noninvasive quantification of systemic-to-pulmonary collateral flow: a major source of inefficiency in patients with superior cavopulmonary connections. Circ Cardiovasc Imaging 2:405–411

Transposition of the Great Arteries

Congenital Heart Diseases in Adults: Imaging and Diagnosis

Matthias Grothoff and Matthias Gutberlet

Contents

M. Grothoff · M. Gutberlet (✉)
Department of Diagnostic and Interventional Radiology, Leipzig Heart Center, Leipzig, Germany
e-mail: Matthias.Gutberlet@helios-gesundheit.de

1 Introduction

Transposition of the great arteries (TGA) is the second most common cyanotic congenital heart disease with a prevalence of 3.5/10,000 live births in Europe and a greater than twofold male predominance (Pexieder et al. 1995). It is characterized by a ventriculo-arterial discordance with the aorta arising from the right ventricle and the pulmonary artery arising from the left ventricle. In case of an atrioventricular concordance (with the right atrium connected to the right ventricle and the left atrium connected to the left ventricle) it is called dextro-TGA (d-TGA) due to the right-sided position of the ascending aorta. In case of an atrioventricular discordance (with the right atrium connected to the left ventricle and vice versa) it is called congenitally corrected-TGA (cc-TGA) or simplified levo-TGA (l-TGA) due to the mostly left-sided position of the ascending aorta. However, the use of the term "l-TGA" for this congenital heart disease (CHD) is unprecise as in cc-TGA with situs inversus the aorta is in "d"-position and there are also other CHD with "l"-position of the aorta like the double-outlet right ventricle (DORV).

Both forms of TGA have their own diagnostic and therapeutic challenges. In this chapter we focus on typical adult cardiac magnetic resonance (CMR) and computed tomography (CT) findings that result from the different types of surgical repair and which have a significant value for the early detection of typical long-term complications.

Med Radiol Diagn Imaging (2019)
https://doi.org/10.1007/174_2018_190, © Springer Nature Switzerland AG
Published Online: 31 January 2019

2 Etiology

The etiology of TGA is still not fully understood and there are two major theories trying to explain the altered morphologies (Ferencz et al. 1995).

One theory suggests that the underlying mechanism is an alteration of the normal clockwise rotation of the aorta towards the left ventricle caused by an abnormal persistence of the subaortic conus (Goor and Edwards 1973). Following this theory TGA can be interpreted as one end in the spectrum of dextroposition of the aorta (Unolt et al. 2013).

The second theory sees the underlying cause in a rather linear than normal spiral development of the aortopulmonary septum putting the future aorta in contact with the anterior conus, which is connected to the right ventricle (de la Cruz et al. 1981).

In epidemiologic studies, TGA showed a higher prevalence with maternal infection, maternal intake of pesticides and ibuprofen, and ionizing radiation and in infants with diabetic mothers, whereas the periconceptional intake of folic acid may have a protective effect (Loffredo et al. 2001).

D-TGA can be accompanied by additional cardiac anomalies of which a ventricular septal defect (VSD) is most common with almost 50%. Furthermore, right ventricular outflow tract (RVOT) obstruction, valvular stenosis, and, less commonly, coarctation of the aorta (5%) can be found. Extracardiac anomalies are rare and mostly include the kidneys and the brain.

In cc-TGA additional cardiac anomalies are very common (>95%) and determine the clinical course of the disease. Besides a VSD, which is present in about 25% of patients, stenoses of the left ventricular outflow tract (LVOT) and the pulmonary arteries, hypoplasia of the ventricles, and tricuspid insufficiencies can be found. Moreover, due to the atrioventricular discordance, also the cardiac conduction system is altered and up to 30% of the patients are diagnosed with an atrioventricular (AV) block (Warnes 2006).

3 Clinical Presentation

Unlike other congenital heart defects d-TGA does not present an alternative model of blood circulation. With the systemic and pulmonary circulation running in parallel there is no blood oxygenation after closure of the ductus arteriosus unless there is an additional shunt. If not treated, d-TGA is the leading cause of cardiac death in neonates and infants (Samanek 2000). The children develop progressive cyanosis and have an average life expectancy of 2 months.

In contrast to d-TGA there is a physiologic situation with the systemic and pulmonary circulation running in row in cc-TGA. However, in difference to normal hearts, the systemic ventricle is not the left, but the right ventricle.

The clinical presentation of cc-TGA shows a broad spectrum depending on the type and degree of additional anomalies. In the rare absence of additional cardiac anomalies (except of the cardiac conduction system) cc-TGA can remain undetected for a long time until it becomes clinically apparent in adulthood with the symptoms of systemic heart failure. Survival to the seventh and eighth decades has been reported. Although the right ventricle can compensate the systemic pressure for many years by hypertrophy, it is designed as a subpulmonary volume pump with a complex triangular shape and not as a concentric pressure pump like the left ventricle. Moreover the coronary artery anatomy is concordant and the hypertrophic RV is perfused by a single right coronary artery, which might cause an imbalance between oxygen demand and oxygen supply. Increasing tricuspid regurgitation is common in cc-TGA patients.

Pulmonary stenosis can be found in about 40% of patients and is mostly subvalvular, but also valvular stenosis occurs. In combination with a VSD varying degrees of cyanosis can be found.

4 Treatment Options and Prognosis

4.1 D-TGA

In the industrialized countries d-TGA can be determined during ultrasound screening in pregnancy in many cases and a precise prenatal diagnosis decreases both the infantile and the maternal risk and improves outcome. Still, d-TGA is one of the most difficult CHD to diagnose prenatally

because of the relatively normal appearance in the four-chamber view (Jouannic et al. 2004).

For patients without a prenatal diagnosis, CHD should be considered if there is cyanosis not responding to oxygen in the immediate newborn period. In fetal d-TGA diagnosis, birth should be planned in a center where a balloon atrial septostomy (BAS) can be performed.

Therapy of d-TGA consists of pharmacological therapy, initial palliative procedures to improve oxygenation by connecting the systemic and pulmonary circulations, and an early corrective surgery.

4.1.1 Prostaglandin and Balloon Atrial Septostomy

In hypoxic neonates prostaglandin is administered to maintain patency of the arterial duct. Additionally this large-volume shunt can cause left atrial hypertension and enlargement which is stretching the foramen ovale, resulting in improved mixing.

If prostaglandin therapy is insufficient a BAS has to be considered. Usually a BAS results in an acute and substantial improvement in oxygen saturation and can be performed under echocardiographic as well as fluoroscopic control. The benefits of a BAS have to be weighed against the rare but threatening risks like vascular trauma, arrhythmias, and atrial perforation.

4.1.2 Surgical Therapy

Corrective surgery of d-TGA is performed a few days after birth after transition from fetal to neonatal circulation and initiation of enteral nutrition. It is common to plan surgery within the first 2 weeks after diagnosis. This approach might avoid some adverse long-term effects of the unstable d-TGA circulation.

Before the anatomical correction became procedure of choice for surgical treatment of patients with d-TGA, the atrial switch operation was performed to achieve a physiological correction of blood flow since the 1960s. This type of correction involves the creation of a two-way systemic venous tunnel (baffle) at the atrial level to direct the deoxygenated systemic venous return towards the mitral valve, the LV, and eventually the pulmonary artery. Accordingly pulmonary venous blood is directed through the pulmonary venous baffle towards the tricuspid valve, the RV, and eventually the aorta. Depending on the used material for the baffle this procedure is also called Senning (use of autologous tissue) or Mustard (use of synthetic material) operation after the surgeons who described the procedures first. The long-term benefits of this procedure are moderate, and there are specific long-term complications that are associated with increased morbidity and mortality (Williams et al. 2003). In addition to the development of arrhythmias, systemic ventricular dysfunction is the most important sequela, being mainly caused by the nonphysiological systemic position of the right ventricle (RV). Moreover, hemodynamically relevant stenosis or leakage of the systemic venous baffle, particularly of the superior limb, can occur.

Since the late 1980s the arterial switch operation (ASO) has replaced the atrial switch procedure. The first successful ASO was performed in 1975 by Jatene and is now the procedure of choice in all centers (Jatene et al. 1976).

Although the concept of ASO is simply the restoration of the normal anatomic arrangement where the arteries are transferred to the proper ventricle, it is still one of the most complex and technically challenging operations in CHD. During this procedure the aorta and the pulmonary artery are transected above the sinuses and switched into their new position. The pulmonary trunk is hereby placed anterior to the ascending aorta (Lecompte maneuver) and the pulmonary arteries embrace the aorta (Fig. 1). The ASO includes the detachment of the coronary arteries along with a “button” from the aortic sinus and their transfer to the sinus of the neo-aorta.

The surgical technique of the ASO determines its potential short- and long-term complications. Particularly the meticulous reinsertion of the coronary artery origins is of highest importance for a successful procedure. Stenosis of the coronaries can result in immediate ischemia and early mortality is mostly due to difficulties with this transfer. However obstruction of the coronary arteries by growth can also be a long-term complication and visualization of the course of the proximal coronaries is an important component of lifelong follow-up care. Further potential long-term

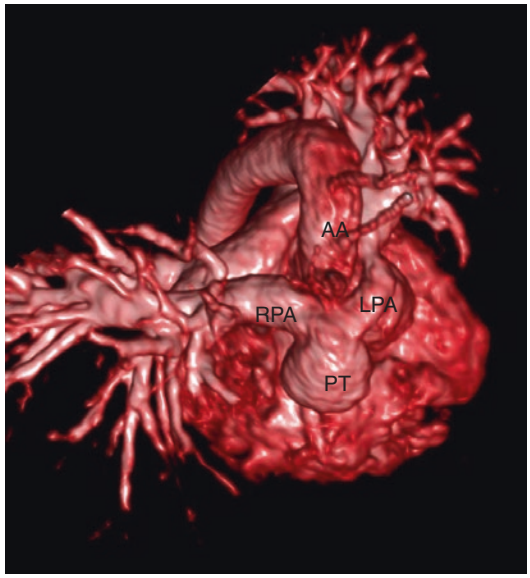

Fig. 1 3D volume rendering after arterial switch operation. The pulmonary artery branches are encompassing the ascending aorta. The pulmonary trunk is in anterior position after Lecompte maneuver. *AA* ascending aorta, *PT* pulmonary trunk, *RPA* right pulmonary artery, *LPA* left pulmonary artery

consequences are neo-pulmonary stenosis, neo-aortic regurgitation, and neo-aortic root dilatation.

Survival into adulthood is common and adults after ASO represent a large group in adult congenital heart disease clinics (Fricke et al. 2012).

When a d-TGA coexists with a pulmonary stenosis and a large subaortic VSD a Rastelli procedure can be performed. In this operation a patch is placed to conduct blood from the LV through the VSD to the aorta (Fig. 2). Additionally a valved conduit conducts blood from the RV to the pulmonary artery. The Rastelli procedure has the advantage that the LV is in systemic position. However, there are also typical long-term sequelae of which conduit degeneration and stenosis are of foremost importance.

4.2 CC-TGA

Therapy of cc-TGA depends on the type and severity of associated cardiac anomalies. If isolated, pharmacological therapy focuses on

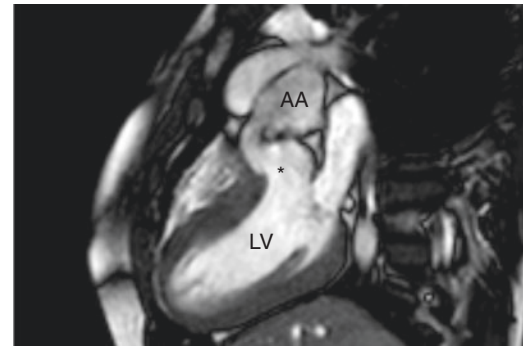

Fig. 2 Steady-state free-precession LVOT view after Rastelli procedure. A patch is placed to conduct blood through the VSD to the aorta (*asterisk*). *AA* ascending aorta, *LV* left ventricle

treatment and the prevention of RV failure. The basic principles do not differ from treatment of LV failure and focus on reduction of the pre- and afterload and improvement of ventricular contractility.

As the RV is in systemic position, systemic pressure causes hypertrophy which is followed by a dilatation of the RV as well as the tricuspid annulus. This mechanism causes the steady increase in tricuspid regurgitation over time. Long-term prognosis of adults with even mild systemic RV dysfunction or tricuspid regurgitation is poor and patients can develop severe tachyarrhythmia unpredictably (Filippov et al. 2016). In high-degree AV block the implantation of a pacemaker has to be considered.

As in many CHD surgical management of cc-TGA has evolved over the last decades. In the early 1960s the physiological repair was introduced. It consisted of repair of associated cardiac anomalies and surgical palliations to improve the prognosis. However in this type of repair the RV remains the systemic ventricle and long-term follow-up showed limited outcome in these patients.

During the 1990s the physiological repair was replaced by the double-switch operation. In this approach a Senning/Mustard repair is performed on the atrial level. In the rare cases in which the LV is in systemic or close to systemic pressures as a result of a VSD and

pulmonary stenosis, the atrial switch procedure can be combined with a Rastelli operation and an RV to PA conduit. More often, however, the LV has to be prepared for the systemic position before an additional arterial switch procedure can be performed. This preparation is achieved by a pulmonary artery banding procedure to induce LV hypertrophy. Perioperative mortality is reported to vary between 0 and 10% (Duncan et al. 2003). Late results after double-switch procedure are satisfactory and 10–20-year survival after surgery was reported as up to 85% with the majority of survivors in a good functional outcome (New York Heart Association functional class I or II) (Murtuza et al. 2011).

5 Imaging Goals

All patients with TGA are in need of regular follow-up examinations. Here, the knowledge of the type of surgical correction is crucial for postoperative imaging as each type of repair has its specific long-term complications and imaging protocols need to be adapted accordingly.

5.1 D-TGA After Atrial Switch

After atrial switch (Senning or Mustard) one imaging goal is to evaluate the status of the systemic right ventricle. This includes determination of RV size and function as well as the assessment of RV hypertrophy. It is known that a certain degree of RV hypertrophy is beneficial for maintaining RV systolic function (Grothoff et al. 2012). An excessive degree of hypertrophy, however, can deteriorate RV function as the single coronary artery is unable to provide a sufficient oxygen supply.

A second aim is to visualize the complex baffle anatomy. Shrinking and stenoses particularly of the superior limb of the systemic venous baffle can occur due to scarring and can cause upper venous congestion. Stenoses of the inferior limb are less common. Small baffle leaks are even more common than stenoses. Although hemodynamically insignificant in most cases they bear the risk of paradoxical embolus and stroke.

5.2 D-TGA After Arterial Switch

After arterial switch operation imaging has to focus on the reinserted coronary arteries as well as dilatation of the neo-aortic root with aortic regurgitation. Particularly the visualization of the proximal course of the coronaries using noninvasive cross-sectional imaging can avoid repeated diagnostic catheterization in this delicate patient group. Further attention has to be put on distortion of the RV outflow tract and stenoses of the pulmonary arteries that are encompassing the ascending aorta.

5.3 D-TGA After Rastelli

Besides the assessment of biventricular function imaging after Rastelli procedure has to exclude residual ventricular septal defects as well as subaortic stenosis. Furthermore the function of the ventriculo-pulmonary conduit has to be evaluated.

5.4 CC-TGA

If isolated, the diagnosis is often overlooked. Typical imaging findings of cc-TGA are the characteristics of the RV in the left position. These include the moderator band, the pronounced trabeculation of the myocardium, and the funnel-shaped muscular outflow tract (conus or infundibulum). Furthermore the parallel arrangement of the pulmonary trunk and the ascending aorta (side-by-side position) is common (Fig. 3). If surgically corrected the findings in cc-TGA depend on the type of repair (double switch or atrial switch with Rastelli procedure).

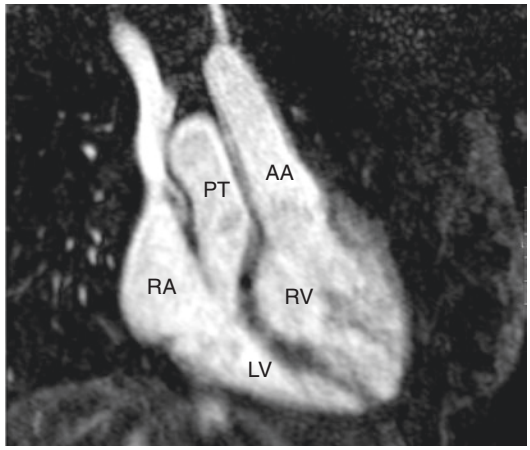

Fig. 3 MR angiography demonstrates the side-by-side position of the ascending aorta and the pulmonary trunk—here in cc-TGA with additional atrioventricular discordance. *RA* right atrium, *LV* left ventricle, *PT* pulmonary trunk, *AA* ascending aorta, *RV* right ventricle

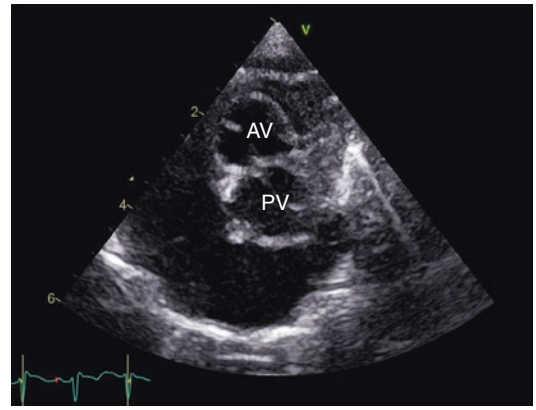

Fig. 4 Parasternal short-axis echocardiography showing the aortic valve anterior and rightward from the pulmonary valve. *AV* aortic valve, *PV* pulmonary valve

6 Noninvasive Imaging Techniques

6.1 Echocardiography

Echocardiography is the first-line imaging tool in CHD. In the hands of an experienced examiner it can provide a broad spectrum of morphological and functional information. Also in TGA it is used for the initial diagnosis and for surgical planning. In postoperative follow-up it should be complemented by cross-sectional imaging, predominantly by MRI.

In the preoperative assessment it is key to define the ventriculo-arterial connection. Here the subcostal imaging planes are particularly valuable. Sagittal imaging planes typically show the aorta positioned anterior to the pulmonary artery. In a short-axis orientation the aortic and the pulmonary valve can be visualized simultaneously, which confirms the ventriculo-arterial discordance (Fig. 4). Associated ventricular septal defects are best visualized by subcostal and parasternal short-axis planes. If the pressure in both ventricles is equal additional ventricular septal defects can be undetectable if only Doppler echocardiography is used. Therefore careful B-mode imaging is always required. For visualizing the aortic arch to exclude aortic coarctation (which is present in 5–10% of patients) a suprasternal approach is suitable. Preoperative visualization of the coronary arteries is challenging as there are numerous anatomic variations. Multiple imaging planes are required, of which the parasternal short-axis, the apical four-chamber, and the left oblique subcostal views are the most useful ones.

In postoperative imaging ultrasound has to address the complications that are inherent to the type of correction as mentioned above. These can occur immediately after correction or years later. After arterial switch, again, visualization of the coronary arteries is of great importance and should be performed with both two-dimensional B-mode and Doppler echocardiography. However, diagnostic imaging of the coronaries is not always possible due to acoustic window constraints. Assessment of myocardial contractility might be helpful but cannot differentiate whether a preserved contractility is caused by a normal coronary artery supply or by a collateral circulation (Taylor et al. 2005). Clearly, other imaging modalities are necessary to overcome these limitations in late follow-up examinations. As diagnostic cardiac catheterization is invasive and therefore not the ideal modality for regular follow-up examinations in adolescents and young adults, noninvasive coronary MR- or CT-angiography should be considered.

Besides stenoses of the coronaries also stenoses of the branch pulmonary arteries following the Lecompte maneuver have to be excluded in follow-up. In ultrasound these can be best visualized with a high parasternal short-axis view. In Doppler echocardiography gradients of >25 mmHg indicate a relevant stenosis and need further intervention.

After atrial switch (Senning or Mustard) systemic and pulmonary venous baffles have to be examined for obstruction or leaks. Here transesophageal echocardiography (TEE) is superior to transthoracic echocardiography (TTE). Midesophageal (ME) views using sweeps and particularly ME four-chamber views with flexion and rotation of the probe allow visualization of both baffles. Doppler echocardiography may determine the severity of stenoses, which mostly occur at the superior limb of the systemic venous baffle. Also injection of ultrasound contrast agent into an upper body peripheral vein can assess the function of the upper systemic venous limb. In the absence of an obstruction the contrast rapidly moves from the superior vena cava towards the tricuspid valve and no contrast can be seen in the inferior limb of the baffle. In the presence of a relevant baffle obstruction the contrast is also directed through collaterals to the lower limb of the baffle.

Assessment of systemic RV function, size, and hypertrophy can be difficult in echocardiography due to acoustic window constraints when the RV is in the right position. In TTE the most useful planes are the parasternal long-axis (PLAX) and parasternal short-axis (PSAX), subcostal long-axis, and parasternal RV inflow views. Accurate assessment of the systolic function of the RV is achieved by measuring one or many echocardiographic indices like the tricuspid annular plane systolic excursion (TAPSE), which is defined as the excursion of the tricuspid annulus from diastole to systole, and is measured typically at the lateral annulus using M-mode. For a better reproducibility of the RV status and imaging without limitations caused by the retrosternal position of the RV and patient constitution, MRI should be used in regular follow-up examinations to determine size and function.

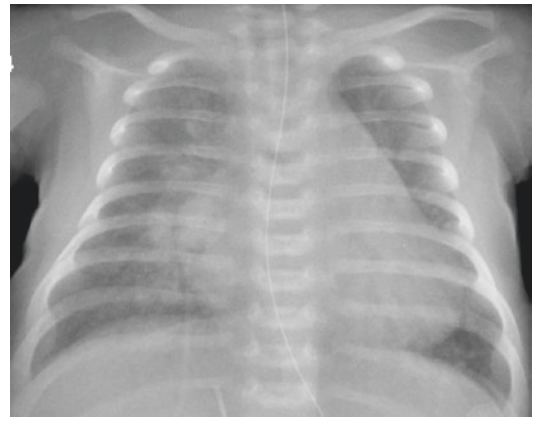

Fig. 5 Radiograph in uncorrected d-TGA. Note the absence of the ascending aorta on the right and the absence of the descending aorta on the left side

6.2 Radiography

With the advent of echocardiography and the cross-sectional imaging modalities the role of chest radiography in TGA has changed. It is no longer used for diagnosis purposes but to provide an overview over the general cardiopulmonary status. Typical findings in uncorrected TGA are an abnormally straight vascular pedicle caused by the loss of the normal arterial relationships. The ascending aorta is not visible on the right side and the aortic knob as well as the descending aorta is not visible on the left side (Fig. 5). In cc-TGA frequently dextrocardia can be found.

In the early postoperative period chest radiography is used for diagnosing early postoperative complications and is the method of choice for the close-meshed follow-up of the cardiopulmonary status. In late follow-up radiography is furthermore helpful in the evaluation of stent integrity after stent implantation in the superior limb of the systemic venous baffle.

6.3 Computed Tomography

In the era of low-dose computed tomography (CT) the spectrum of indications for this modality has extended, even in CHD. With prospective ECG-triggering techniques detailed morphologic information at reasonable radiation doses can be

obtained. Today the radiation dose in coronary computed tomography angiography (CCTA) is lower than that in standard percutaneous coronary angiography and the complication rate is lower (Meinel et al. 2015). A recent study showed that the high temporal and spatial resolution of CCTA can be used to reliably visualize the coronaries after arterial switch procedure in adolescents and young adults (Szymczyk et al. 2018). In knowledge of the great variance of the reimplanted coronaries and their importance for the individual outcome the visualization of the proximal course is part of most routine follow-up protocols.

Also after atrial switch CT can be helpful in long-term follow-up, particularly after stent implantation, e.g., in the upper limb of the systemic venous baffle. Here, MRI as the alternative cross-sectional modality has problems in visualizing the in-stent lumen due to susceptibility artefacts.

Independent of the type of surgery CT is the first-line modality in perioperative complications like hemothorax, pneumothorax, and venous thrombosis. These CT scans can be performed with low radiation exposures of approximately 0.5 mSv effective dose.

In complex vessel anatomy CT is also used for preoperative planning. The relationships of the arteries and the surrounding structures can be depicted in a submillimeter spatial resolution. A 3-dimensional volume rendering gives the surgeon an impression of the operative situs. Contrast agent is administered adapted to weight in a single bolus. The acquisition of a single phase with contrast in all major vessels is sufficient in most cases.

6.4 Magnetic Resonance Imaging

Cardiac MRI is the imaging modality that can acquire the widest range of information in children and adults with CHD. It is also the ideal method for regular follow-up examinations as it is free of ionizing radiation and not limited by patient constitution or a sufficient acoustic window. CMR is only rarely used for preoperative imaging. Without sedation it requires a certain degree of patient compliance over a time of at least 30–40 min. In children this is usually possible from the age of 8–9 years.

6.4.1 Morphology

In CHD, CMR imaging should start with an overview over the postoperative situs in a transverse orientation using black-blood or steady-state free-precession (SSFP) images. This gives a first impression of the dimensions of the chambers and great vessels as well as the degree of ventricular hypertrophy and reveals the type of repair and modifications. In a next step the direct acquisition of freely angulated planes in the three-dimensional space is possible. In d-TGA after atrial switch procedure, this is particularly helpful in visualizing the upper and lower limb of the systemic venous baffle. This is best achieved by a paracoronal view with an angulation from the superior to the inferior vena cava (Fig. 6a, b). If angulated properly, both limbs of the baffle can be visualized at once and obstructions can be detected. Implanted stents in the upper limb can cause susceptibility artifacts and make the assessment of stent patency impossible (Fig. 6c).

After arterial switch procedure the transverse imaging planes nicely demonstrate the anterior position of the pulmonary trunk after Lecompte maneuver (Fig. 7) and potential stenoses of the branch pulmonary arteries.

A substantial improvement in spatial resolution was the introduction of the three-dimensional whole-heart sequence. This ECG-gated sequence was developed to enable CMR coronary imaging and provides isotropic submillimeter voxels in free breathing. The use of acceleration techniques, of which parallel imaging is the most common one, results in acquisition times of about 10 min for a complete 3D dataset of the cardiovascular structures of the mediastinum during systole and/or diastole. In d-TGA after arterial switch 3D whole-heart imaging can reliably visualize the course of the proximal reinserted coronary arteries up to a heart rate of 100 beats/min and can replace the invasive and radiation-intense cardiac catheterization (Greil et al. 2017).

Furthermore, the 3D whole-heart sequence is usually performed without the administration of a contrast agent and may therefore replace the contrast-enhanced MR angiography (CE-MRA) as far as the central vessels, e.g., the pulmonary branches after Lecompte maneuver, are concerned. This is particularly helpful in an era of uncertainty regarding the possible deleterious effects of gadolinium deposition in the central nervous system (see also below).

6.4.2 Function

Functional assessment is one of the most important elements in follow-up examinations in patients with TGA. Impaired function in combination with other parameters may lead to an indication for reoperation or reintervention. Therefore the meticulous determination of ventricular size and ejection fraction and the early detection of tendencies are part of any CMR follow-up examination. Assessment of RV dimensions and function is

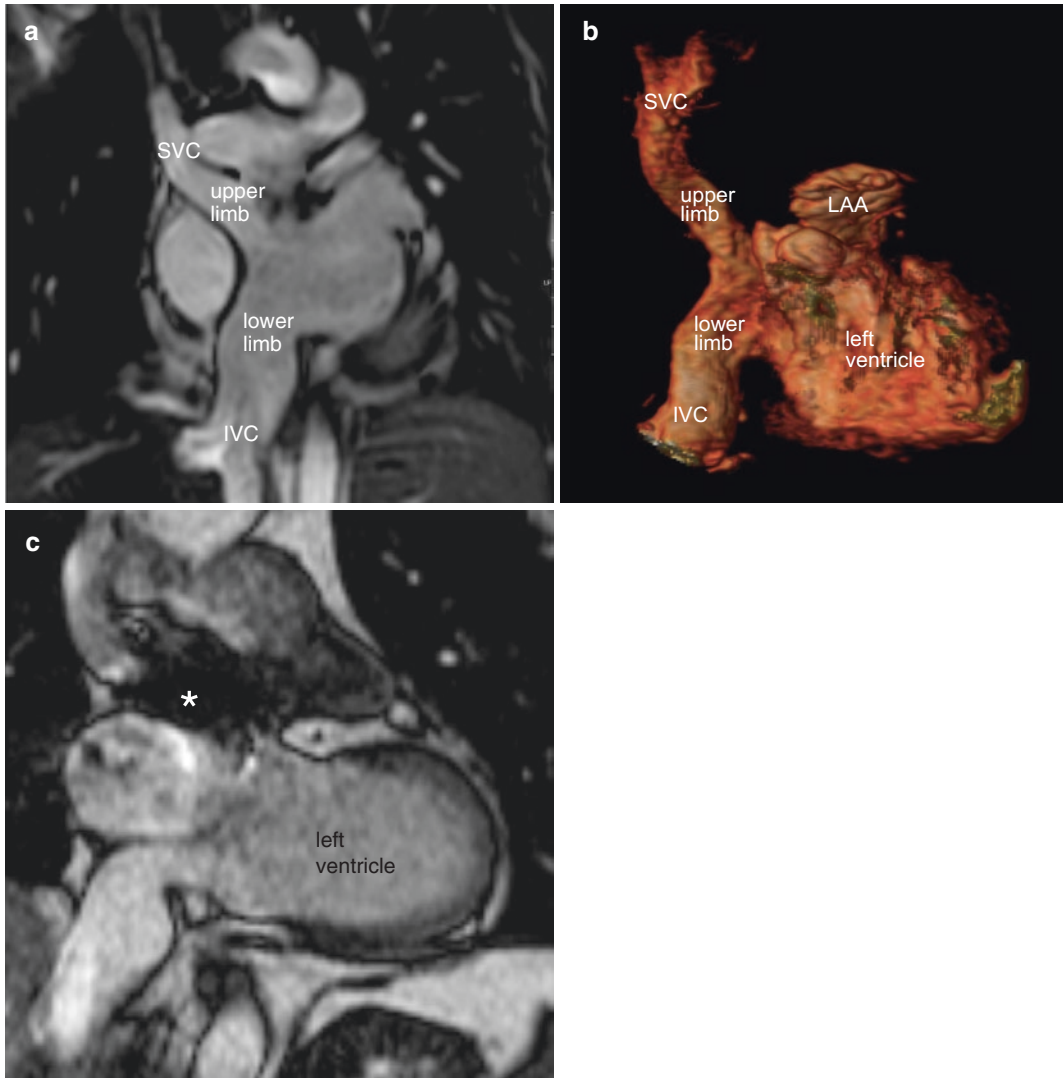

Fig. 6 (**a**) Steady-state free-precession paracoronal view after atrial switch operation shows the upper and lower limb of the systemic venous baffle conducting blood from the superior and inferior vena cava to the left ventricle. (**b**) 3D volume rendering of the same patient. (**c**) Stent in the upper limb of the systemic venous baffle after treatment of stenosis causing artefacts

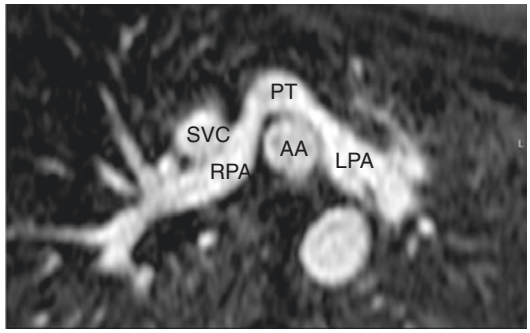

Fig. 7 MR angiography after arterial switch procedure. The proximal RPA and LPA are predilection sites for postoperative stenoses. *AA* ascending aorta, *PT* pulmonary trunk, *RPA* right pulmonary artery, *LPA* left pulmonary artery, *SVC* superior vena cava

difficult by echocardiography due to its retrosternal position and its complex chamber shape, which does not allow for application of an accurate geometric model. This is even truer for right ventricles after atrial switch procedure or in cc-TGA in which the systemic RV and its tricuspid valve are exposed to systemic arterial afterload. Therefore, the most commonly used two-dimensional echocardiography provides rather qualitative than quantitative information on RV dimensions and volume indices.

CMR has become the gold standard in the assessment of biventricular volume and mass. Mostly steady-state free precession (SSFP) sequences with a high contrast between myocardium and blood pool are used. Classical gradient echo sequences provide a lower contrast-to-noise ratio but can be helpful in reducing artifact, particularly banding artifacts in 3T imaging.

In the symmetrical LV CMR shows excellent reproducibility, and in the asymmetrical RV delineation of the contours is more challenging but reproducibility is still good (Kilner et al. 2010). For RV volume measurement various stack orientations can be used, each of them offering particular advantages and disadvantages. The short-axis orientation offers a good delineation between the diaphragm and the thin inferior wall of the RV but has problems with the delineation of the complexly shaped tricuspid valve. The four-chamber-view orientation can clearly depict the tricuspid valve, but lacks differentiation between inferior myocardium and diaphragm. A good compromise is the use of transversal slices, typically with a slice thickness of 6 mm without gap.

However, no matter what orientation is used, consistency in measurements is most important especially when RV parameters are assessed over many years in regular follow-up examinations and measurements are performed by various investigators. Consensus criteria and a training of postprocessing physicians and technicians are helpful in reaching consistency and a good interobserver variability at least within one institution. Commercially available automated or semiautomated contour detection programs for the geometrically complex RV still do not show satisfying results and time-consuming manual correction is mandatory.

When delineating the borders of the RV, the endocardial contour should be drawn along the compacted layer of the RV myocardium and exclude the trabeculations. Certainly this approach results in a systematic error namely an overestimation of the blood pool and an underestimation of the myocardial mass, particularly in hypertrophied systemic RVs in cc-TGA and d-TGA after atrial switch. However, it is impracticable and time consuming to delineate the numerous RV trabeculations and an attempt will result in lower intra- and interobserver reproducibility (Kilner et al. 2010). The myocardial mass is best assessed in end diastole as the hypertrophied trabeculations appear to merge in end systole and cannot be demarcated from the compacted layer.

In d-TGA after atrial switch procedure functional SSFP imaging can also be used for the detection of baffle leaks. With an adequate in-plane visualization the shunt jets can directly be visualized. Small leaks, however, may not be detectable and CMR is inferior to contrast-enhanced echocardiography in the detection of leaks (Lu et al. 2012).

6.4.3 Flow Measurement

Phase-contrast (PC) flow measurement is part of any CMR protocol in CHD. It is the only modality which can acquire quantitative hemodynamic

information noninvasively. In clinical routine mostly two-dimensional PC CMR is used to assess flow velocity and regurgitation. In TGA there are numerous applications for this method depending on the type of surgery: After arterial switch operation PC CMR is used to quantify stenoses of the branch pulmonary artery after Lecompte maneuver in a paraxial in-plane orientation. Furthermore PC flow can quantify the regurgitation fraction in neo-aortic insufficiencies. After atrial switch procedure flow measurement is helpful in quantifying stenoses of the upper limb of the systemic venous baffle and in quantifying shunts caused by baffle leaks by comparing the aortic and pulmonary forward flow. After Rastelli procedure PC CMR focuses on the assessment of stenoses or insufficiencies of the pulmonary conduit and obstructions of the left ventricular outflow tract.

A further development in PC flow measurement is time-resolved three-directional velocity encoding (4D PC CMR). Data acquisition can be performed in free breathing within 10–12 min. 4D flow provides full volumetric coverage of the great arteries and can improve hemodynamic evaluation in complex postsurgical anatomy. Postprocessing can be performed retrospectively and data quality is no longer dependent on correct pre-acquisition angulations as it is in 2D flow. Furthermore new flow parameters like helicity and vorticity of the flow can be visualized. Although robust and available for some years, 4D flow is still mostly used in scientific settings and reference values from larger cohorts are not available yet. Nevertheless, it will be the future of flow measurement in CHD.

6.4.4 Tissue Characterization

Systemic dysfunction is a common sequel in the long-term follow up of TGA patients with systemic RVs and there has been much debate for the reason of RV impairment. Tricuspid insufficiency, a complete atrioventricular block, and arrhythmias have been identified as risk factors. Also myocardial scarring assessed by late gadolinium enhancement (LGE) imaging can have a deleterious effect on RV function. Over the past years LGE techniques have evolved and been established as reliable and robust tools to visualize biventricular myocardial scars with high reproducibility. Phase-sensitive inversion-recovery (PSIR) DE sequences provide a better and more consistent image quality compared to DE sequences with magnitude detection. In d-TGA patients with atrial switch procedure performed in the late 1970s and the 1980s (before the arterial switch procedure became the method of choice) myocardial scars were found rarely in both the RV and the LV (Preim et al. 2013). Also in uncorrected cc-TGA scars are uncommon. In older patient cohorts after atrial switch scars were found more frequently, probably due to different surgical techniques, and also correlated with RV ejection fraction (Babu-Narayan et al. 2005). In this context it is important to notice that hyperenhancement adjacent to prosthetic patches, e.g., after closure of ventricular septal defects or Rastelli procedure, must not be considered as myocardial scar but rather as adhesion of contrast agent to the patch (Fig. 8).

LGE can only detect adjacent fibrosis with a volume of >0.5 mL but is unable to detect diffuse fibrosis. T1 mapping techniques might overcome this constraint as they are able to detect fibrosis by measuring tissue-specific relaxation times. After atrial switch diffuse fibrosis is more pronounced in the myocardium of the

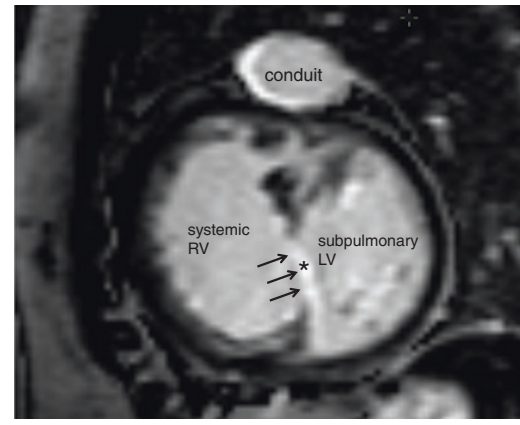

Fig. 8 Phase-sensitive inversion recovery (PSIR) late gadolinium enhancement image in d-TGA after atrial switch procedure with a conduit to the pulmonary trunk demonstrating adhesion of contrast (*arrows*) at a large VSD patch (*asterisk*). *LV* left ventricle, *RV* right ventricle

systemic RV of adults as compared with controls in equilibrium contrast mapping (Plymen et al. 2013). However, to quantify the extracellular volume, which is enlarged in diffuse fibrosis, the application of gadolinium is necessary. In our institution we try to avoid the repeated administration of gadolinium in regular follow-up examinations in children, adolescents, and young adults as it is unclear whether deposition in the central nervous system might have adverse long-term effects.

An overview over the key points in imaging is given in Box 1.

Box 1 Key Points in Imaging TGA

- Radiography:
  - Overview cardiopulmonary status and course
- Echocardiography:
  - First-line imaging modality, prenatal diagnosis, preoperative planning, follow-up examinations

Preoperatively:
- Detection of ventriculo-arterial discordance
- Parallel position of great arteries
- Detection of associated cardiac anomalies (e.g., VSD, pulmonary artery stenosis, coarctation of the aorta)

Postoperatively:
- Assessment of biventricular function
- *After arterial switch procedure*: detection of pulmonary branch artery stenoses
- *After atrial switch procedure (Senning/Mustard)*: evaluation of systemic RV (function and hypertrophy), detection of baffle stenoses and leaks, assessment of tricuspid insufficiency
- *After Rastelli procedure:* exclusion of residual VSD and subaortic stenosis, assessment of pulmonary conduit function

- Computed tomography
  - Imaging of perioperative complications, preoperative planning
- Cardiac magnetic resonance
  - Routine in follow-up examinations
  - Gold standard in evaluation of biventricular function and mass
  - Imaging of scar and fibrosis
  - Quantification of stenoses, insufficiencies, and shunts
  - *After arterial switch*: detection of coronary artery and pulmonary branch artery stenoses
  - *After atrial switch*: evaluation of systemic RV, detection of baffle stenoses and leaks, evaluation of tricuspid insufficiency
  - *After Rastelli:* exclusion of residual VSD and subaortic stenosis, assessment of pulmonary conduit function

Conclusion

Echocardiography is the first-line imaging modality in TGA and can already detect the ventriculo-arterial discordance during screening examinations in pregnancy. Also preoperative planning is mostly done by echo. After surgical correction imaging is an essential part of follow-up examinations for the detection of morphologic and hemodynamic changes. The postoperative imaging protocol strongly depends on the type of repair of which each has its specific long-term complications. Limitations in echocardiography in visualizing the RV and the coronary arteries can be overcome by CMR. This modality provides the most detailed information in morphology, function, and tissue characterization and is routinely performed in all tertiary care centers. Pathologies associated with a systemic RV can be imaged in freely angulated slices or in 3D without limitations by patient constitution. Modern imaging sequences like T1 mapping and 4D PC CMR may provide additional information but have to be evaluated in regard

to their clinical significance. Computed tomography can be valuable in detailed imaging of the morphology and is the first-line modality in perioperative complications.

References

Babu-Narayan SV, Goktekin O, Moon JC et al (2005) Late gadolinium enhancement cardiovascular magnetic resonance of the systemic right ventricle in adults with previous atrial redirection surgery for transposition of the great arteries. Circulation 111:2091–2098

Duncan BW, Mee RB, Mesia CI et al (2003) Results of the double switch operation for congenitally corrected transposition of the great arteries. Eur J Cardiothorac Surg 24:11–19

Ferencz C, Brenner JI, Loffredo C, Kappetein AP, Wilson PD (1995) Transposition of the great arteries: etiologic distinctions of outflow tract defects in a case control study of risk factors. In: Clark EB, Markwald RR, Takao A (eds) Developmental mechanism of heart disease. Futura, Armonk, pp 639–653

Filippov AA, del Nido PJ, Vasilyev NV (2016) Management of systemic right ventricular failure in patients with congenitally corrected transposition of the great arteries. Circulation 134:1293–1302

Fricke TA, d'Udekem Y, Richardson M et al (2012) Outcomes of the arterial switch operation for transposition of the great arteries: 25 years of experience. Ann Thorac Surg 94(1):139–145

Goor DA, Edwards JP (1973) The spectrum of transposition of the great arteries: with special reference to developmental anatomy of the conus. Circulation 48:406–415

Greil G, Tandon A, Vieira MS et al (2017) 3D whole heart imaging for congenital heart disease. Front Pediatr 5:36

Grothoff M, Hoffmann J, Abdul-Khaliq H et al (2012) Right ventricular hypertrophy after atrial switch operation: normal adaptation process or risk factor? A cardiac magnetic resonance study. Clin Res Cardiol 101:963–971

Jatene A, Fontes V, Paulista P et al (1976) Anatomic correction of transposition of the great vessels. J Thorac Cardiovasc Surg 72:364–370

Jouannic JM, Gavard L, Fermont L et al (2004) Sensitivity and specificity of prenatal features of physiological shunts to predict neonatal clinical status in transposition of the great arteries. Circulation 110:1743–1746

Kilner PJ, Geva T, Kaemmerer H et al (2010) Recommendations for cardiovascular magnetic resonance in adults with congenital heart disease from the respective working groups of the European Society of Cardiology. Eur Heart J 31:794–805

de la Cruz MV, Arteaga M, Espino-Vela J, Quero-Jimenez M, Anderson RH, Diaz GF (1981) Complete transposition of the great arteries: types and morphogenesis of ventriculoarterial discordance. Am Heart J 102:271–281

Loffredo CA, Silbergeld EK, Ferrencz C, Zhang J (2001) Association of transposition of the great arteries in infants with maternal exposures to herbicides and rodenticides. Am J Epidemiol 153:529–536

Lu JC, Dorfman AL, Attili AK et al (2012) Evaluation with cardiovascular MR imaging of baffles and conduits used in palliation or repair of congenital heart disease. Radiographics 32:E107–E127

Meinel FG, Henzler T, Schoepf UJ, Park PW, Huda W, Spearman JV et al (2015) ECG-synchronized CT angiography in 324 consecutive pediatric patients: spectrum of indications and trends in radiation dose. Pediatr Cardiol 36:569–578

Murtuza B, Barron DJ, Stumper O, Stickley J, Eaton D, Jones TJ, Brawn WJ (2011) Anatomic repair for congenitally corrected transposition of the great arteries: a single-institution 19-year experience. J Thorac Cardiovasc Surg 142:1348–1357

Pexieder T, Blanc O, Pelouch V, Ostadalova I, Milerova M, Ostadal B (1995) Late fetal development of retinoic acid-induced transposition of great arteries: morphology, physiology and biochemistry. In: Clark EB, Markwald RR, Takao A (eds) Developmental mechanism of heart disease. Futura, Armonk, pp 297–307

Plymen CM, Sado DM, Taylor AM et al (2013) Diffuse myocardial fibrosis in the systemic right ventricle of patients late after Mustard or Senning surgery: an equilibrium contrast cardiovascular magnetic resonance study. Eur Heart J Cardiovasc Imaging 14:963–968

Preim U, Hoffmann J, Lehmkuhl L et al (2013) Systemic right ventricles rarely show myocardial scars in cardiac magnetic resonance delayed-enhancement imaging. Clin Res Cardiol 102(5):337–344

Samanek M (2000) Congenital heart malformations: prevalence, severity, survival and quality of life. Cardiol Young 10:179–185

Szymczyk K, Moll M, Sobczak-Budlewska K et al (2018) Usefulness of routine coronary CT angiography in patients with transposition of the great arteries after an arterial switch operation. Pediatr Cardiol 39:335–346

Taylor AM, Dymarkowski S, Hamaekers P et al (2005) MR coronary angiography and late-enhancement myocardial MR in children who underwent arterial switch surgery for transposition of great arteries. Radiology 234:542–547

Unolt M, Putotto C, Silvestri LM et al (2013) Transposition of the great arteries: new insights into the pathogenesis. Front Paediatr 1:11

Warnes CA (2006) Transposition of the great arteries. Circulation 114:2699–2709

Williams WG, McCrindle BW, Ashburn DA, Jonas RA, Mavroudis C, Blackstone EH (2003) Outcomes of 829 neonates with complete transposition of the great arteries 12-17 years after repair. Eur J Cardiothorac Surg 24:1–9

Further Reading

Gutberlet M, Boeckel T, Hosten N, Vogel M, Kühne T, Oellinger H, Ehrenstein T, Venz S, Hetzer R, Bein G, Felix R (2000) Arterial switch procedure for D-transposition of the great arteries: quantitative mid-term evaluation of hemodynamic changes with cine MR imaging and phase-shift velocity mapping-initial experience. Radiology 214(2):467–475

Grothoff M, Fleischer A, Abdul-Khaliq H, Hoffmann J, Lehmkuhl L, Luecke C, Gutberlet M (2013) The systemic right ventricle in congenitally corrected transposition of the great arteries is different from the right ventricle in dextro-transposition after atrial switch: a cardiac magnetic resonance study. Cardiol Young 23(2):239–247. https://doi.org/10.1017/S1047951112000790 Epub 2012 Jun 14

Anomalies of the Systemic and Pulmonary Arteries

Arno A.W. Roest, Lucia J.M. Kroft, and Lars Grosse-Wortmann

Contents

Electronic supplementary material Supplementary material is available in the online version of this chapter at https://doi.org/10.1007/174_2017_165.

A.A.W. Roest, M.D., Ph.D. (✉)
Department of Paediatrics, Willem Alexander Children's Hospital, Leiden University Medical Center, Leiden, The Netherlands
e-mail: A.Roest@lumc.nl

L.J.M. Kroft, M.D., Ph.D.
Section Head of Cardiothoracic Radiology, Department of Radiology, Leiden University Medical Center, Leiden, The Netherlands

L. Grosse-Wortmann, M.D., F.R.C.P.S.C.
Section Head, Cardiovascular Magnetic Resonance, The Hospital for Sick Children, University of Toronto, Toronto, ON, Canada

Congenital abnormalities of the thoracic systemic and pulmonary arteries can occur in isolation or in the setting of a complex cardiovascular malformation. Severe or complex vascular defects are usually diagnosed and corrected in childhood. Infrequently, anomalies of the systemic and pulmonary arteries present during adulthood. After correction of a cardiovascular malformation most children survive into adulthood. In adults, the most common indication for imaging is to evaluate post-treatment sequelae. Understanding the underlying pathology and possible complications that may occur during follow-up is essential for planning imaging studies. Furthermore, knowledge on the different imaging modalities, including their strengths and limitations for assessing anomalies of the systemic and pulmonary arteries, is important.

This chapter discusses the role of the different imaging modalities for the assessment of congenital abnormalities of the thoracic systemic and pulmonary arteries both at diagnosis and during follow-up after treatment. As follow-up already starts directly after surgical correction this chapter includes images of both children and adults.

1 Overview of Imaging Techniques for the Systemic and Pulmonary Arteries

Chest radiography is usually the first imaging modality used in adults with suspected large vessel abnormalities. Chest radiographs may provide

Med Radiol Diagn Imaging (2018)
DOI 10.1007/174_2017_165, © Springer International Publishing AG
Published Online: 17 April 2018

clues to abnormalities of the thoracic vascular system. Signs that should raise suspicion of a vascular abnormality include abnormal location of the aortic knob, tracheal narrowing, rib notching, or an abnormal mediastinal silhouette (Ferguson et al. 2007).

Echocardiography is usually the next non-invasive imaging tool. In patients with favourable acoustic windows, echocardiography allows evaluation of the thoracic arterial vasculature in great detail and can detect abnormalities of the pulmonary and systemic arteries. Greyscale imaging in the parasternal short-axis view allows detailed depiction of the main pulmonary trunk and left and right pulmonary arteries. The aorta and its branching arch vessels are best visualised from the high parasternal and suprasternal views, allowing anatomical delineation to detect dilatation, narrowing or interruption of the aorta as well as an abnormal course of the aorta or its major branches. The descending and abdominal aorta can be appreciated from the subcostal views. Colour-Doppler flow shows the direction of blood flow and detects areas of turbulent flow, while pulsed-wave and continuous-wave Doppler assessment provides information on the location and severity of stenosis within the thoracic arteries. However, with increasing age and body mass index, echocardiographic evaluation of the thoracic vasculature is hampered by suboptimal acoustic windows. Furthermore, echocardiography cannot provide information on the surrounding structures, such as the trachea and oesophagus.

Oesophagography, using barium as a contrast medium, can be used to evaluate complaints of dysphagia, which is not infrequently the presenting symptom in adults with a vascular ring. Vascular rings cause a typical indentation on the oesophagus which give rise to the suspicion of the diagnosis (Berdon 2000). In clinical practice, however, this modality has been largely replaced by cross-sectional imaging modalities such as computed tomography (CT) and magnetic resonance imaging (MRI).

CT and MRI are the preferred non-invasive imaging modalities in adults for assessment of abnormalities of the systemic and pulmonary arterial system as well as for follow-up and assessing complications due to prior interventions.

The typical MRI examination starts with scout images in the three orthogonal planes, on which one can appreciate the large systemic and pulmonary arterial anatomy, and these scout views are used for planning dedicated MRI sequences. Targeted spin echo (‘black blood’) as well as gradient echo (‘white blood’) MRI sequences are used for anatomical evaluation. For evaluation of the aorta and branching vessels, the imaging planes are planned in at least two perpendicular directions when a two-dimensional (2D) technique is used, including the oblique sagittal plane along the long axis of the aorta. For imaging the right ventricular outflow tract (RVOT), the pulmonary valve and the proximal main pulmonary arteries planning along the long axis of the RVOT are recommended, whereas the right and left pulmonary arteries can be evaluated in an axial or oblique axial stack (Fratz et al. 2013). Isotropic three-dimensional (3D) imaging using contrast-enhanced or non-contrast-enhanced sequences can also be used to assess the thoracic vasculature.

Besides detailed anatomical evaluation, MRI also provides functional information on the hemodynamic consequences of vascular abnormalities. For example, phase-contrast flow velocity mapping is used to assess the shunt volume in extracardiac shunts, to quantify differential lung perfusion in the presence of branch pulmonary artery stenosis, and help gauge the hemodynamic severity of (re)coarctation of the aorta.

CT is especially useful to determine the relationship between the vessels and the airways for planning an intervention. Furthermore, CT is the preferred imaging modality in patients with contraindications to MRI or for stent evaluation. Correct contrast-bolus timing is essential and should be adjusted to the vasculature under investigation: CT pulmonary angiography, CT aortic angiography or both. Although radiation dose has been reduced considerably with new scan and reconstruction techniques (Xu et al. 2014; Kroft et al. 2010), the radiation burden of repeated CT scans is of concern and should be taken into account, especially in children and young adults

with congenital heart disease, making CT less attractive for serial follow-up (Baumgartner et al. 2010). Nuclear imaging techniques may be used to assess heterogeneity of pulmonary perfusion in patients with branch pulmonary artery stenosis and contraindications for MRI.

Cardiac catheterisation for diagnostic evaluation of systemic and pulmonary arteries is currently largely replaced by MRI and CT. However, fluoroscopic angiograms are still obtained prior to and during percutaneous interventions. Occlusion devices, balloons and stents are placed under fluoroscopy guidance. Furthermore, right-heart catheterisation is used in cases of suspected pulmonary hypertension in the rare adult patient with a long-standing unrepaired left-to-right shunt, such as septal defects, an aortopulmonary window or a patent arterial duct.

2 Development of the Systemic and Pulmonary Arterial System

The development from the embryological initial symmetrical cardiovascular system to a unilateral left-sided aortic arch and arterial duct is an intriguing and complex process that is not completely understood. The aortic and pulmonary vascular system develops from the aortic sac and the pharyngeal arch arteries (PAA) through extensive remodelling driven by flow-mediated mechanisms, with angiogenesis and apoptosis in a spatio-temporal pattern (Gittenberger-de Groot et al. 2006). In early embryonic stages, the aortic sac is divided by the aortopulmonary septum into ascending aorta and main pulmonary artery (Bartelings and Gittenberger-de Groot 1989). During cardiovascular morphogenesis five paired PAAs develop, numbered I–VI, with the fifth PAA never reaching full maturation. Eventually, the first and second PAAs contribute to the vasculature of the head, and the third forms the carotid artery system. During normal cardiovascular development the left fourth PAA forms the main part of the left-sided aortic arch and the left sixth PAA eventually connects the pulmonary artery system to the aorta through the arterial duct (Gittenberger-de Groot et al. 2006). Disruption of these complex events leads to a variety of abnormalities of the systemic and pulmonary arteries, occurring de novo or in the setting of known syndromes.

3 Individual Lesions

3.1 Coarctation of the Aorta

Coarctation of the aorta (CoA) accounts for 4.2% of all congenital heart diseases (Hoffman and Kaplan 2002) and most commonly occurs in a juxtaductal position distal to the origin of the left subclavian artery (Fig. 1) (Backer and Mavroudis 2000a). A clear association with bicuspid aortic valve (Fig. 2) exists with a reported prevalence as high as 85% in patients with coarctation (Roos-Hesselink et al. 2003). CoA is associated with Turner, Williams(−Beuren) and congenital rubella syndromes. CoA can be associated with intracardiac malformations including ventricular septal defects and left ventricular outflow tract obstruction. CoA may also develop secondary in Takayasu aortitis (Baumgartner et al. 2010).

Interrupted aortic arch (IAA) is a rare congenital cardiac defect. Given the near-universal mortality with closure of the arterial duct, presentations during adulthood are exceedingly rare (Knapper et al. 2014). After correction complications are similar to those after CoA correction and include aortic restenosis and aneurysm formation (Yang et al. 2008). Diagnosis and follow-up imaging are similar to CoA (Dillman et al. 2008; Yang et al. 2008).

3.1.1 Presentation and Diagnosis

Critical CoA presents at young age with signs of cardiac failure. In adults, CoA often presents inconspicuously with a murmur, hypertension, weak femoral pulses, headaches or, occasionally, claudication. Of note, in patients with extensive collateral circulation induced by a CoA, femoral pulses or lower extremity blood pressure may appear almost normal (Torok et al. 2015).

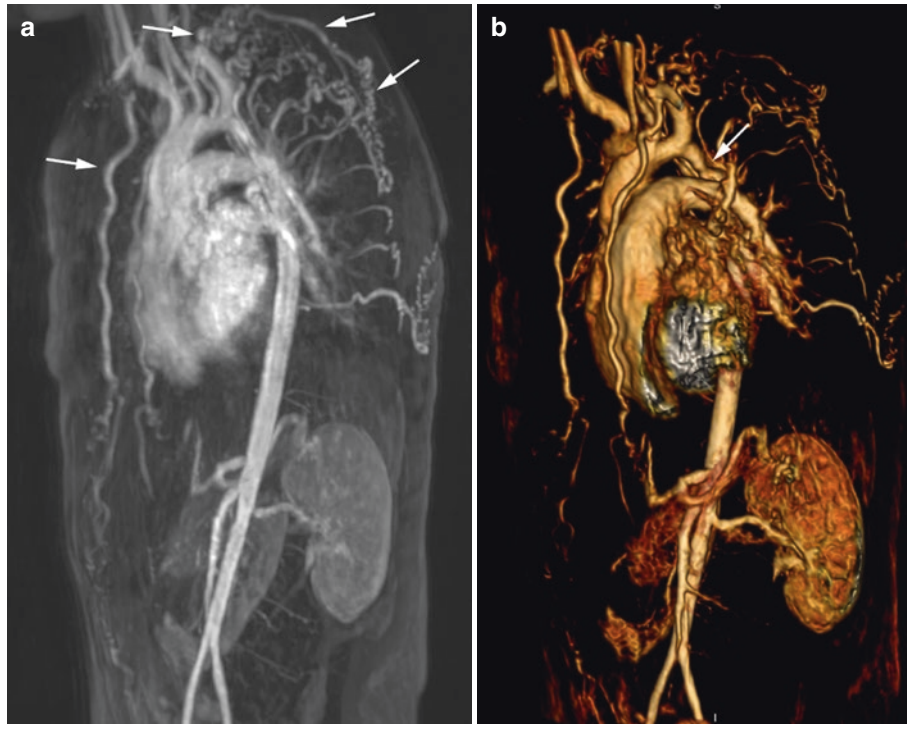

Fig. 1 Coarctation of the aorta. 9-year-old male with bicuspid aortic valve and coarctation of the aortic. Gadolinium-enhanced MR angiography. Parasagittal orientation showing the coarctation with collateral arteries. (**a**) Maximum intensity projection image demonstrating prominent intercostal- and internal mammary arteries (*arrows*). (**b**) Volume-rendering reconstruction of the aorta and collateral arteries showing the site of coarctation (*arrow*)

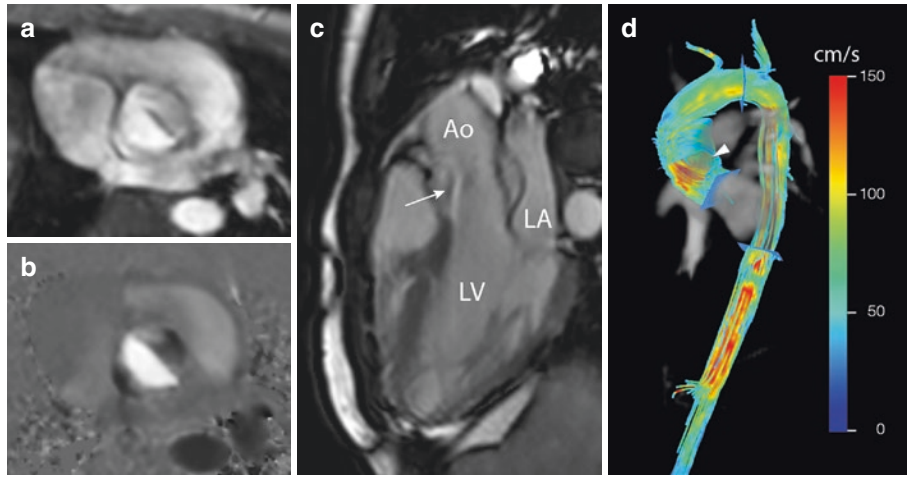

Fig. 2 Bicuspid aortic valve. 28-year-old male patient with bicuspid aortic valve and mild dilatation of the ascending aorta. Axial views of through-plane velocity-encoded phase-contrast MRI acquisition of the flow velocity through the valve ((**a**) magnitude image, (**b**) phase image). In (**c**) a double-oblique lateral view of the aortic outflow tract with the bicuspid aortic valve is presented with aortic regurgitation (*arrow*). (**d**) shows streamline visualisation with colour coding of systolic outflow, with abnormal circulating blood flow (*arrowhead*) and helical flow in the aortic arch. *LV* left ventricle, *LA* left atrium, *Ao* aorta. Figure from unravelling cardiovascular disease using four-dimensional flow cardiovascular magnetic resonance. (Adapted from Kamphuis et al. 2017)

Chest radiography may provide clues to the presence of CoA. In 50–66% of adults with CoA, a figure of three sign can be appreciated on the posterior-anterior chest radiograph, caused by dilatation of the aorta proximal to the stenosis, indentation at the site of stenosis and dilatation distal to the stenosis (Ferguson et al. 2007). Rib notching (deep grooves at the caudal part of the ribs, especially of the 4th–8th ribs) can sometimes be observed in adult patients with CoA, and is caused by collateral circulation via dilated intercostal vessels to bypass the site of stenosis. In patients with favourable windows, echocardiography has proved to be accurate in detecting aortic arch obstruction including CoA (Nihoyannopoulos et al. 1987; Tworetzky et al. 1999). In the suprasternal view, the aorta can be evaluated in its long-axis projection with special attention to the predilection site of CoA and diameters of all segments of the aortic arch. Doppler techniques are used to assess the velocities in the aorta, estimate the pressure gradient over the CoA site and evaluate the presence of the typical CoA flow pattern of antegrade diastolic forward flow. In adults with suspected CoA, CT and MRI are frequently used as the aortic arch, the site of coarctation and the collateral circulation can be appreciated in greater clarity and more detail (Karaosmanoglu et al. 2015). A standard MRI examination for the evaluation of a (re) CoA may include cine imaging in the long-axis plane of the aortic arch, contrast-enhanced MRA of the aorta (Fig. 1) and phase-contrast MRI at several sites within the aorta, including the aortic valve level, aorta just proximal to the CoA and distal to the CoA at the level of the diaphragm (Fratz et al. 2013). Based on the flow volume measurements just above the CoA site and at the level of the diaphragm the amount of collateral flow can be estimated (Fig. 3) (Steffens et al. 1994). Similar to echocardiography, phase-contrast MRI distal to the stenosis can reveal increased blood velocity and abnormal flow patterns. The combination of indexed minimal aortic cross-sectional area (derived from contrast-enhanced MRA) and heart rate-corrected deceleration time in the descending aorta at the level of the right pulmonary artery (derived from phase-contrast MRI) has been used to predict a transcatheter peak-to-peak pressure gradient of ≥20 mmHg with a sensitivity of 90% and a specificity of 76% in native as well as recurrent CoA (Muzzarelli et al. 2011).

Recently, 4D flow MRI has been introduced to assess flow patterns in patients with CoA (Fig. 4) and allows estimations of regional pressure differences within the aorta (Rengier et al. 2015). Although the clinical significance of this technique

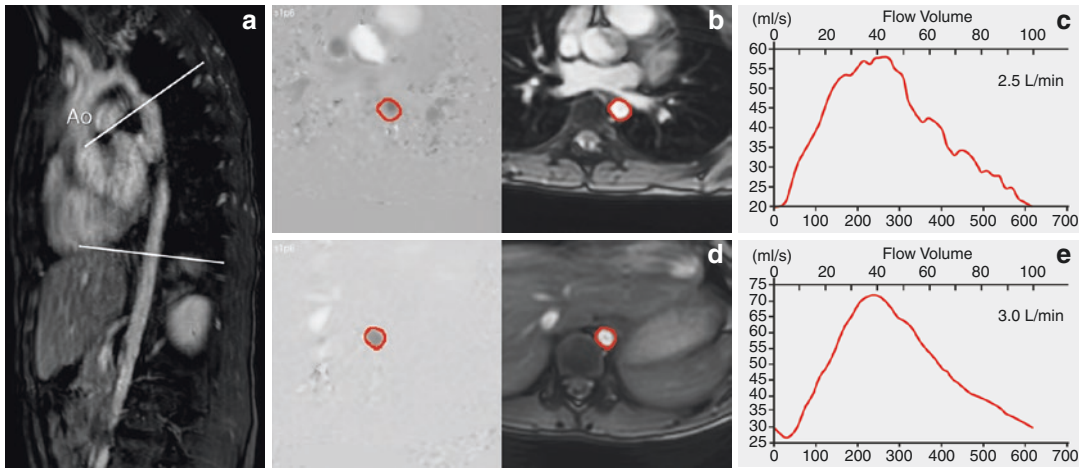

Fig. 3 Collateral flow quantification in coarctation of the aorta. Same patient as in Fig 1. MRI flow imaging with phase-contrast technique immediately distal to the coarctation (upper line in (**a**) and upper row (**b** and **c**)) and at diaphragm level (lower line in (**a**) and lower row (**d** and **e**)). Flow in the descending aorta is 2.5 L/min immediately distal to the coarctation (**c**), and 3.0 L/min at diaphragm level (**e**), indicating haemodynamically significant coarctation for the aorta. *Ao* aorta

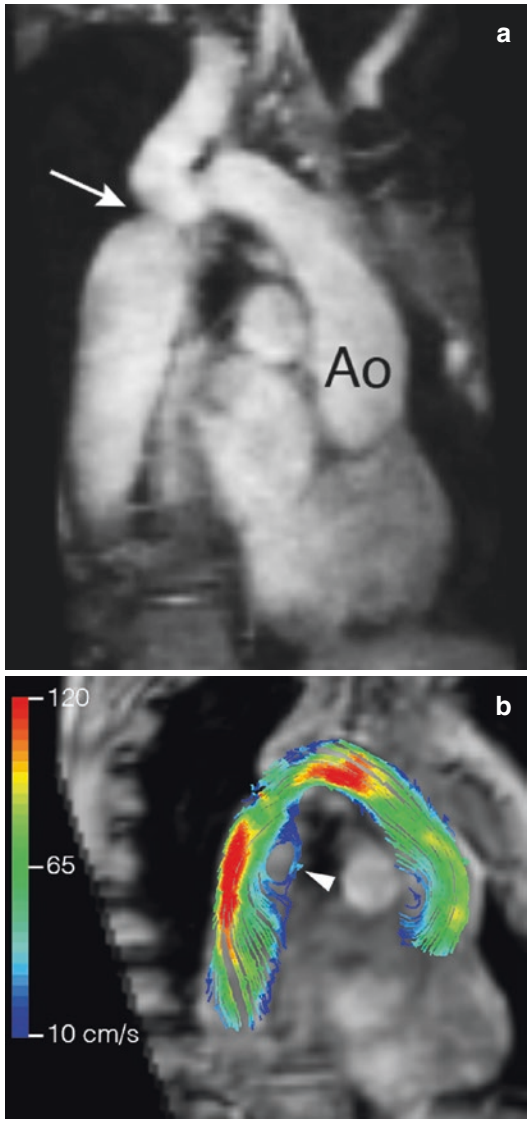

Fig. 4 4D flow MRI of coarctation of the aorta. 29-year-old male with a coarctation of the aorta. In (**a**) a bright blood image of the aortic arch and proximal descending aorta with coarctation of the aorta (*arrow*). (**b**) shows the streamline visualisation with colour coding. Distal to the coarctation site, abnormal circular flow is present (*arrowhead*). *Ao* aorta. Figure from unravelling cardiovascular disease using four-dimensional flow cardiovascular magnetic resonance. (Adapted from Kamphuis et al. 2017)

needs to be established, it has shown potential as a prognostic tool to assess the risk of aneurysms formation (Hope et al. 2010a, b, 2011).

CT evaluation of a (native) CoA can be performed with high diagnostic accuracy, but should be reserved for patients in whom echocardiography is insufficient and who cannot undergo an MRI examination (Nance et al. 2016).

3.1.2 Treatment

Critical CoA typically is corrected early in life with low mortality and morbidity (Ungerleider et al. 2013). In adults with CoA, intervention is recommended in patients with a peak-to-peak coarctation gradient greater than or equal to 20 mmHg or peak-to-peak coarctation gradient less than 20 mmHg in the presence of anatomic imaging evidence of significant coarctation and evidence of significant collateral flow (Warnes et al. 2008). Balloon angioplasty for treatment of native CoA shows less favourable outcomes compared to surgery and stent treatment of CoA (Forbes et al. 2011), but can be used as a treatment of recoarctation after previous surgical repair of CoA (Torok et al. 2015). Stent treatment of CoA has significant less acute complications compared to surgery or balloon angioplasty. Intermediate outcomes show that stent treatment is safe in children and adults with CoA with persistent relief of the obstruction (Meadows et al. 2015).

3.1.3 Follow-Up Imaging

Patients after treatment of CoA require lifelong follow-up with imaging of the aorta by CT or MRI at intervals of 5 years or less, according to current guidelines (Baumgartner et al. 2010; Warnes et al. 2008). Common complications after CoA treatment are recoarctation, aneurysm formation, hypertension and stent fracture. Special notice should be given to pregnant women with (treated) CoA, because hypertension-related adverse outcomes are common. Especially, smaller aortic dimensions, as assessed with MRI, are related to an increased risk of stroke, newly diagnosed hypertension and arrhythmias (Jimenez-Juan et al. 2014).

Restenosis after previous CoA treatment is common, especially in patients who underwent CoA repair within the first year of age (Brown et al. 2010; Chen et al. 2013). Although echocar-

diography is the first-line modality for the follow-up, many adults require cross-sectional imaging for adequate visualisation (Karaosmanoglu et al. 2015). According to the guidelines, MRI is the preferred imaging method (Fig. 5) (Baumgartner et al. 2010), and combined with clinical assessment proved to be cost effective in adults to identify complications, including recoarctation, after CoA repair (Therrien et al. 2000).

Serial follow-up with CT and MRI is mandatory in CoA patients after treatment, given the considerable incidence of aneurysm formation (Fig. 6), particularly in those whom patch aortoplasty was performed (Cramer et al. 2013). Many of these patients are asymptomatic (Hoffman et al. 2014; Tsai et al. 2011) and echocardiography is hampered by a poor sensitivity for aneurysm detection of only 24%.

Fig. 5 Follow-up imaging after coarctation repair with MRI. 11-year-old female patient after coarctectomy and end-to-end anastomosis. The non-contrast 3D steady-state free precession dataset and thick multiplanar reconstruction reveals no signs of re-coarctation (*). *Ao* aorta

Stent fracture or in-stent stenosis is a late complication after CoA treatment (Nance et al. 2016). Echocardiography can raise the suspicion of in-stent stenosis or fracture when increased velocity is encountered in the aorta distal to the stent. On MRI examination, metal stents lead to artefacts expanding beyond the immediate area around the stent. Spin-echo techniques and, to a lesser extent, gradient-echo techniques minimise the image degradation as compared to steady-state free precession pulse sequences, but in-stent stenosis remains impossible to be ruled out with MRI (Shepherd et al. 2015; Valsangiacomo Buechel et al. 2015). Therefore, CT is the modality of choice to assess stent patency and integrity (Fig. 7) (Nance et al. 2016).

3.2 Aortopulmonary Window

Aortopulmonary window, also known as aortopulmonary septal defect, is the rarest of the septal defects and accounts for 0.1% of all congenital cardiac anomalies (Jacobs et al. 2000). An AP window is usually diagnosed in infancy with signs of a large left-to-right shunt, such as respiratory distress, congestive heart failure or because of a murmur (Naimo et al. 2014). However, numerous case reports describe the primary diagnosis of an AP window in adulthood, often with concomitant pulmonary hypertension.

3.2.1 Diagnosis

Echocardiography is the principal method to evaluate an AP window (Mahle et al. 2010), although the diagnosis may be difficult even in experienced hands (Kiran et al. 2008). CT and MRI can aid in the diagnosis, particularly in adult patients with insufficient acoustic windows (Bobylev et al. 2014; Chattranukulchai et al. 2013; Rider et al. 2013; Wong et al. 2012). In addition, MRI allows quantification of the magnitude and net direction of the shunt. Cardiac catheterisation is recommended in adults with AP window to assess the pulmonary vasculature and pressure (McElhinney et al. 1998).

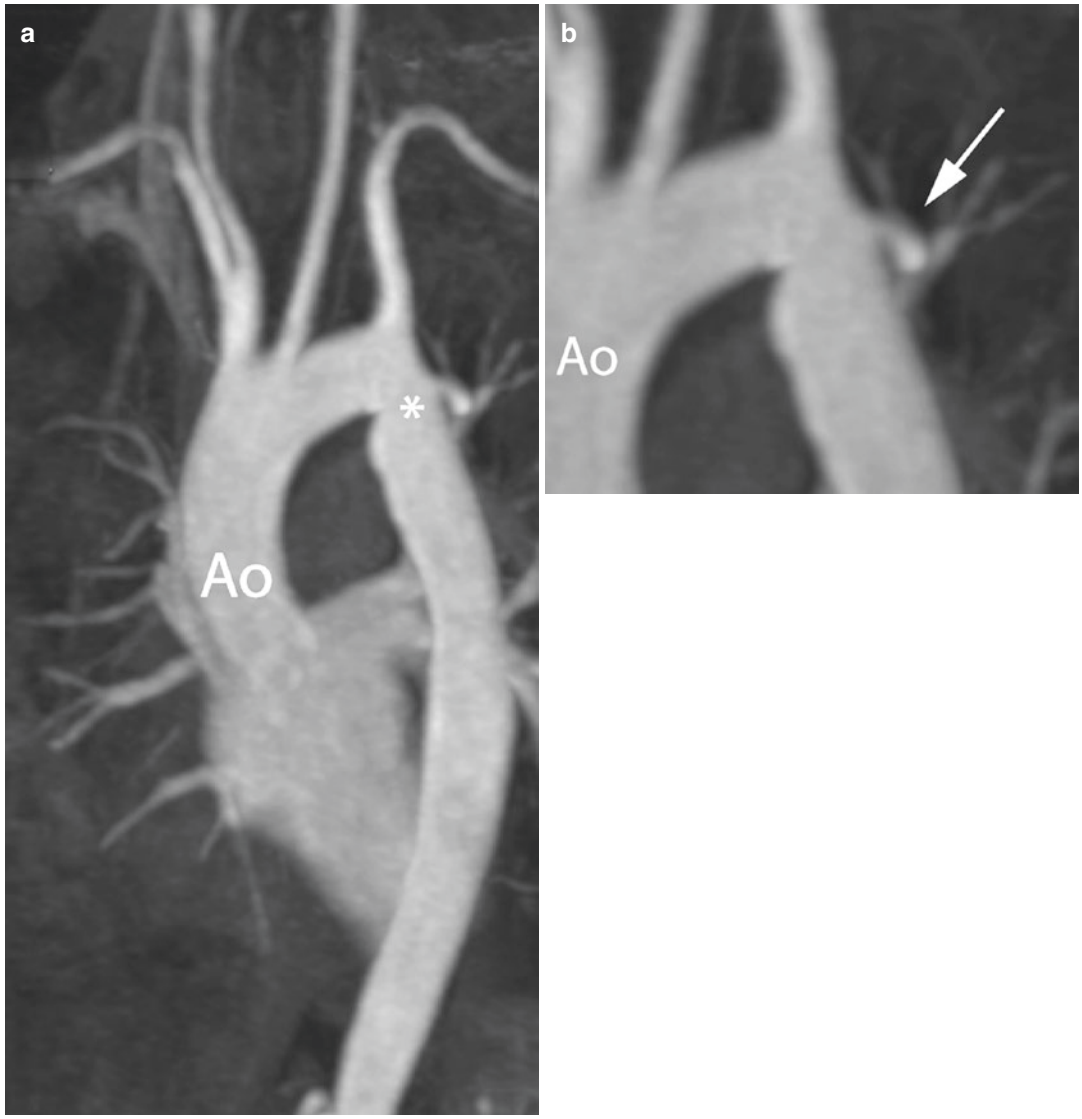

Fig. 6 Aneurysm after coarctation repair. CT angiography of a 35-year-old male after end-to-end anastomosis for coarctation of the aorta (**a**). A small aneurysm (*arrow* in panel **b**) is present at the site of coarctation repair (asterisk in **a**). *Ao* aorta. Courtesy Dr. AM Spijkerboer, Amsterdam, The Netherlands

3.2.2 Treatment and Follow-Up Imaging

Some types of AP windows are suitable for catheter intervention (Barnes et al. 2011), but most warrant surgical correction, especially in the presence of associated anomalies. Early and late outcomes of correction of simple AP window are excellent, approaching 0% mortality (Naimo et al. 2014). Main issues during follow-up are related to the associated anomalies. Especially in AP windows with interrupted aortic arch, recurrent aortic arch obstruction can develop. For follow-up of these patients echocardiography is the first-line imaging modality. When aortic arch obstruction is suspected or in patients with poor echocardiographic windows, CT and MRI are recommended with excellent visualisation of the aorta (Kimura-Hayama et al. 2010).

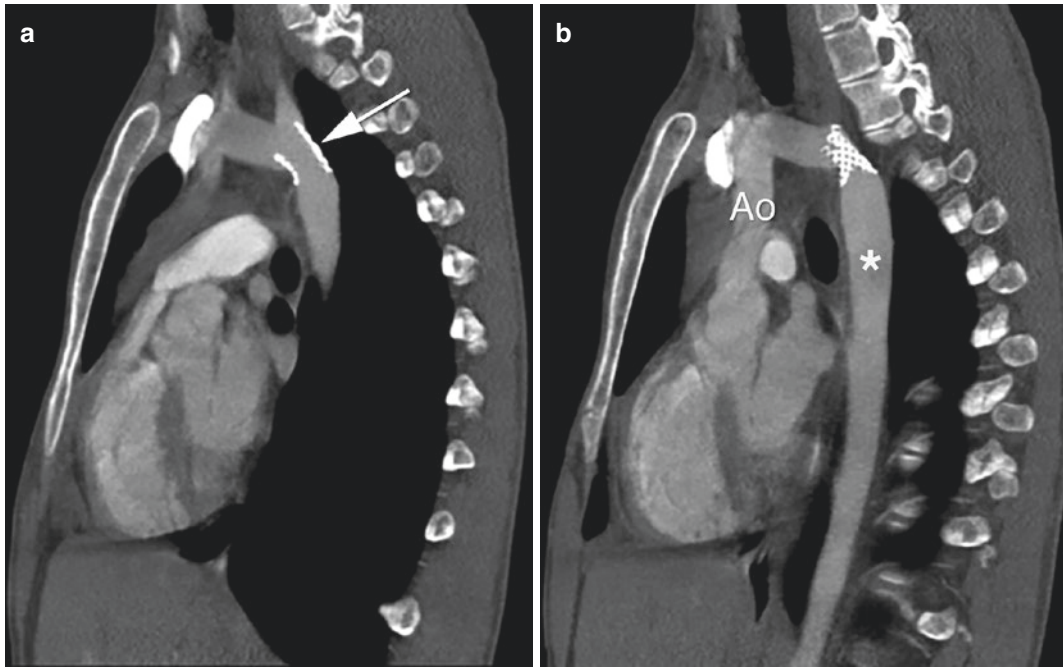

Fig. 7 Stented coarctation of the aorta. 26-year-old male after stent implantation for coarctation of aorta. The patency of the stent (*arrow*) is depicted in panel (**a**). Panel (**b**) distal to the stent the aorta is unobstructed (asterisk). *Ao* aorta. Courtesy Dr. AM Spijkerboer, Amsterdam, The Netherlands

3.3 Vascular Rings

Vascular rings refer to a group of thoracic vascular anomalies that encircle and may compress the oesophagus and trachea (Backer and Mavroudis 2000b). Vascular rings comprise 1.4% of all congenital heart diseases (Bjornard et al. 2013). The embryological development of vascular rings was proposed by Edwards (EDWARDS 1948) and is thought to be related to an abnormal sequence of regression of the individual components of the ventral and dorsal aorta and PAAs.

Double-aortic arch and right aortic arch with left ductal ligament are the classic complete vascular rings (Backer and Mavroudis 2000b). Other abnormalities that can cause compression of adjacent structures are innominate artery compression of the trachea and pulmonary sling (Backer and Mavroudis 2000b). The innominate artery compression syndrome is caused by a more distal and posterior take-off of the innominate artery, typically from a normal left-sided aortic arch. In pulmonary sling syndrome, the left pulmonary artery branches from the right pulmonary artery and courses between the trachea and the oesophagus on its way to the left lung (Fig. 8) (Backer and Mavroudis 2000b). Distal origin of the right subclavian artery from a left-sided aorta (lusoria artery) can cause dysphagia, referred to as dysphagia lusoria, because of the retro-oesophageal course of the right subclavian artery (Fig. 9) (Levitt and Richter 2007).

Abnormalities of the trachea are frequently seen in relation to vascular rings; especially pulmonary slings are associated with complete tracheal rings. Furthermore, associated congenital cardiac defects are reported and are risk factors for mortality in patients referred for correction of a vascular ring (Suh et al. 2012).

3.3.1 Presentation and Diagnosis

The presentation of vascular rings depends on the severity of tracheo-oesophageal compression. Respiratory symptoms include stridor, wheezing, cough and recurrent respiratory infections. In

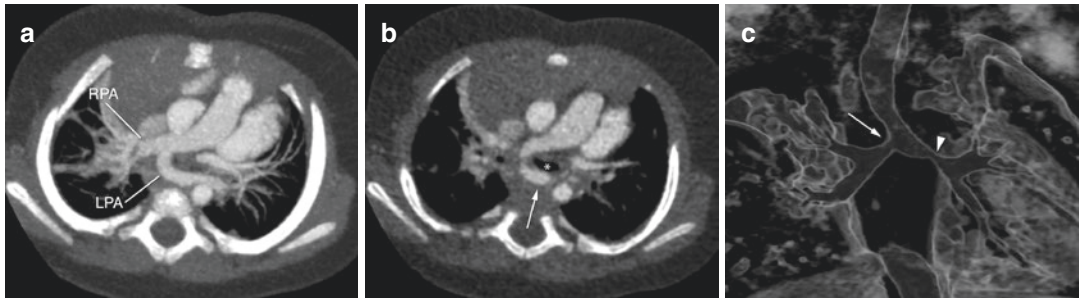

Fig. 8 Pulmonary artery sling. CT angiography in a 2-year-old boy with pulmonary artery sling. (**a**) The left pulmonary artery (LPA) originates distally from the right pulmonary artery (RPA). (**b**) The LPA (*arrow*) encircles the trachea (asterisks) and courses in front of the oesophagus. (**c**) The tracheobronchial tree is malformed with mild proximal right main bronchus stenosis (*arrow*), as well as narrowing and compression of the left main bronchus (*arrowhead*)

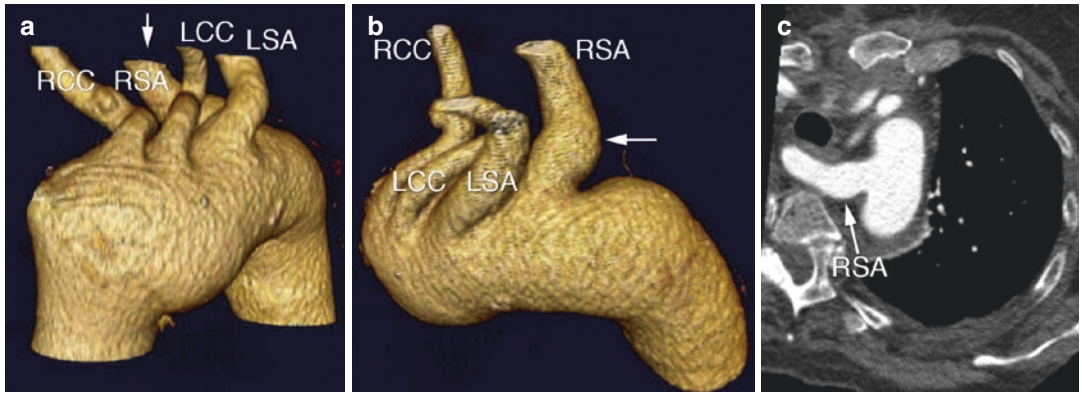

Fig. 9 Aberrant right subclavian artery. CT angiography in a 76-year-old female patient with aortic aneurysm after ascending aorta replacement. Aberrant right subclavian artery (RSA), also called lusoria artery as incidental finding (*arrow* **a** and **b**). The RSA artery arises as the last artery from the aortic arch, with a retro-oesophageal course to the right axilla (**c**). Lusoria artery is usually asymptomatic but may cause dysphagia. *RSA* right subclavian artery, *RCC* right carotid communis artery, *LCC* left carotid communis artery

adults, symptoms of oesophageal compression are more common. Regurgitation of indigested food, bloating and chest pain, especially with chunky foods, should trigger an evaluation for vascular rings and related disorders (Levitt and Richter 2007).

Chest radiographs may raise suspicion of a vascular ring as abnormalities are present in more than 95% of patients (Browne 2009). Double or right aortic arches are typically appreciated on the posterior-anterior projection. Tracheal narrowing in close relation to the aortic knob suggests airway compression. A pulmonary sling can cause tracheal hypoplasia as well as bronchial tree branching abnormalities (Browne 2009). Transthoracic echocardiography is frequently successful in the evaluation of vascular rings or related cardiac abnormalities. In the suprasternal views the aortic arch sidedness and all branching vessels need to be demonstrated. In the past, diagnosis of vascular ring was predominantly made with barium oesophagography. Posterior indentation suggested compression by an aberrant subclavian artery, with a left aberrant subclavian artery causing an indentation pointing towards the left shoulder. Anterior impression of the oesophagus can be caused by a pulmonary sling, while bilateral indentation on the anteroposterior view suggests double-aortic arch (Browne 2009). Currently barium oesophagography

has been largely replaced by tomographic techniques such as CT and MRI. Both MRI and CT have sensitivities approaching 100% to detect vascular rings. Some centres prefer MRI (Kir et al. 2012; Smith et al. 2015), while others advocate CT due to its superior spatial resolution and evaluation of the airways (Fig. 10) (Browne 2009; Etesami et al. 2014; Leonardi et al. 2015). The MRI protocol may encompass black-blood imaging in the axial or oblique coronal view to assess vascular anatomy, the tracheobronchial tree and the oesophagus. Contrast-enhanced 3D MRA or 3D SSFP sequences yield the anatomy of the vascular system (Dillman et al. 2011; Smith et al. 2015). If contrast-enhanced MR angiography or CT angiography is used, the contrast bolus must be adjusted for the suspected lesion, i.e. either the aortic arch or the branch pulmonary arteries in suspected pulmonary sling (Dillman et al. 2011).

In patients with a double-aortic arch it is important to identify the smaller arch as this dictates the surgical approach, with the smaller arch being ligated. The four-vessel sign refers to the symmetrical branching of the arch vessels from the aortic arch and is suggestive of a double-aortic arch (Fig. 11). If one of the arches is atretic or if a ductal ligament remains, diagnosis of vascular ring may be difficult. However, secondary signs may help diagnosing the vascular ring (Gould et al. 2015). Presence of a diverticulum in relation to the aortic arch or a right aortic arch with a left descending aorta should raise the suspicion of an atretic segment with double-aortic arch morphology (Fig. 12). The presence of a diverticulum of Kommerell, from which the subclavian artery arises, is also an indication for the presence of vascular ring with a ductal ligament connecting the diverticulum to the pulmonary artery, most commonly in the setting of a right aortic arch (Gould et al. 2015). Furthermore, a circumflex retro-oesophageal course of the aortic arch or the presence of a ductal dimple at the proximal descending aorta contralateral to the arch is an indicative of a vascular ring (Gould et al. 2015).

3.3.2 Treatment and Follow-Up Imaging

In symptomatic patients surgery is indicated (Backer et al. 2005; Slater and Rothenberg 2016). Long-term survival after vascular ring correction is excellent and comparable to the general population (Ruzmetov et al. 2009). However, recurrent compression symptoms either on the oesophagus or the trachea may occur. The diagnostic workup is similar to initial diagnosis of vascular ring.

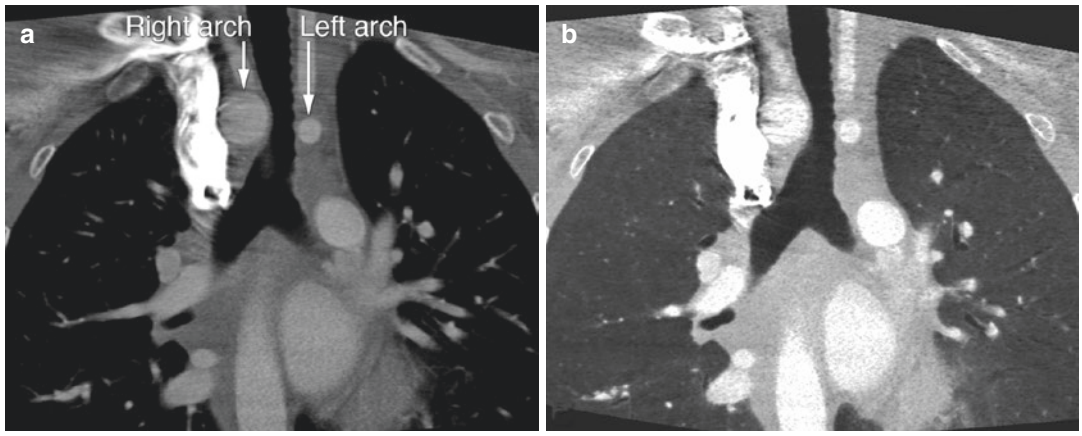

Fig. 10 Tracheal narrowing due to double-aortic arch. CT angiography in a 14-year-old male patient with double-aortic arch and recurrent pulmonary infections, coronal reconstructions. (**a**) Soft-tissue setting showing vascular ring with large right arch and small left arch. (**b**) Lung setting showing mild tracheal narrowing at the level of the vascular ring

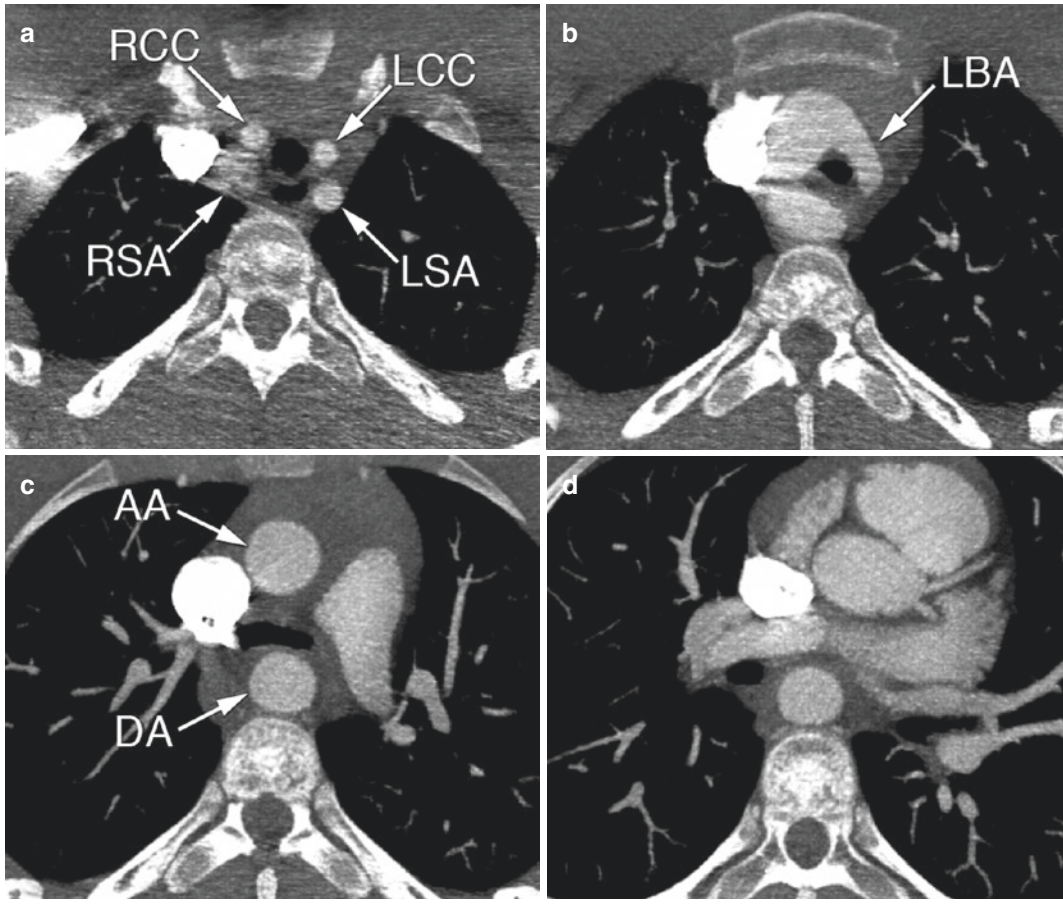

Fig. 11 Double-aortic arch with atretic segment. 14-year-old male patient with recurrent pulmonary infection. CT angiography showing complete vascular ring: Double-aortic arch with large right arch and small left arch with an atretic segment (fibrous strand) in connection to the descending aorta. The ring causes tracheal narrowing. Left upper panel above arch level with the typical four vessel sign (**a**), right upper panel at arch level and narrowing of trachea (**b**), left lower panel below arch level (**c**), right lower panel at descending aorta level that had median course (**d**). *AA* ascending aorta, *DA* descending aorta, *LBA* left brachiocephalic artery, *LCC* left carotid communis artery, *LSA* left subclavian artery, *RCC* right carotid communis artery, *RSA* right subclavian artery

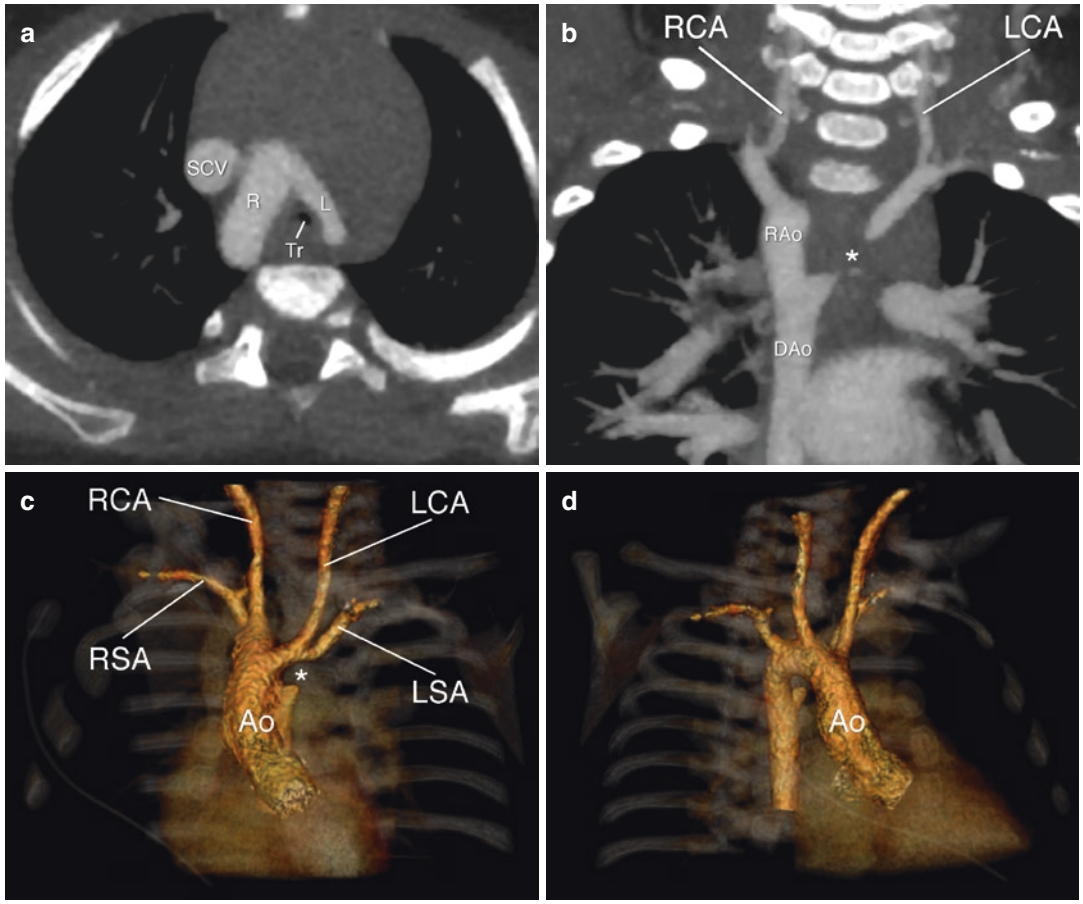

Fig. 12 Double-aortic arch with atretic segment. 7-month-old female patient, admitted to the intensive care unit with an upper airway tract infection and a history of multiple severe cyanotic incidents. CT angiography showing complete vascular ring: Double-aortic arch with large right arch and small left arch causing tracheal narrowing (**a**). An atretic segment (*, fibrous strand, confirmed at surgery) is connecting the left arch to the descending aorta (**b**). Panels (**c**) and (**d**): volume-rendered depictions of the double-aortic arch with symmetric branching of the arch vessels causing the typical four vessel sign. *Ao* aorta, *DAa* descending aorta, *L* left aortic arch, *LCA* left carotid artery; *LSA* left subclavian artery; *R and RAo* right aortic arch, *RCA* right carotid artery, *RSA* right subclavian artery; *SCV* superior caval vein, *Tr* trachea. *marks the location of the atretic segment closing the vascular ring. 14-year old male patient with recurrent pulmonary infection. Volume rendered movie of CT angiography showing a double aortic arch with large right arch and small left arch with an atretic segment (fibrous strand) in connection to the descending aorta. See chapter for further details.

4 Congenital Pulmonary Artery Abnormalities

4.1 Pulmonary Artery Stenosis

Congenital stenosis of the main pulmonary arteries may occur as isolated lesion or may be related to complex congenital heart defects, such as in tetralogy of Fallot (Fig. 13), or several other syndromes such as Williams(−Beuren), Noonan and Alagille (Pierpont et al. 2007). Pulmonary stenosis may also occur as important complication following congenital heart disease surgery, e.g. after arterial switch operation for transposition of the great arteries (Morgan et al. 2017).

At the most severe end of the spectrum of pulmonary artery obstruction is interruption of a pulmonary artery, where the lung is supplied with blood through collateral arteries or a persistent duct that connects to the hilar arterial vessels. This is a rare condition that may be found incidentally in adults, suspected on chest radiograph or found

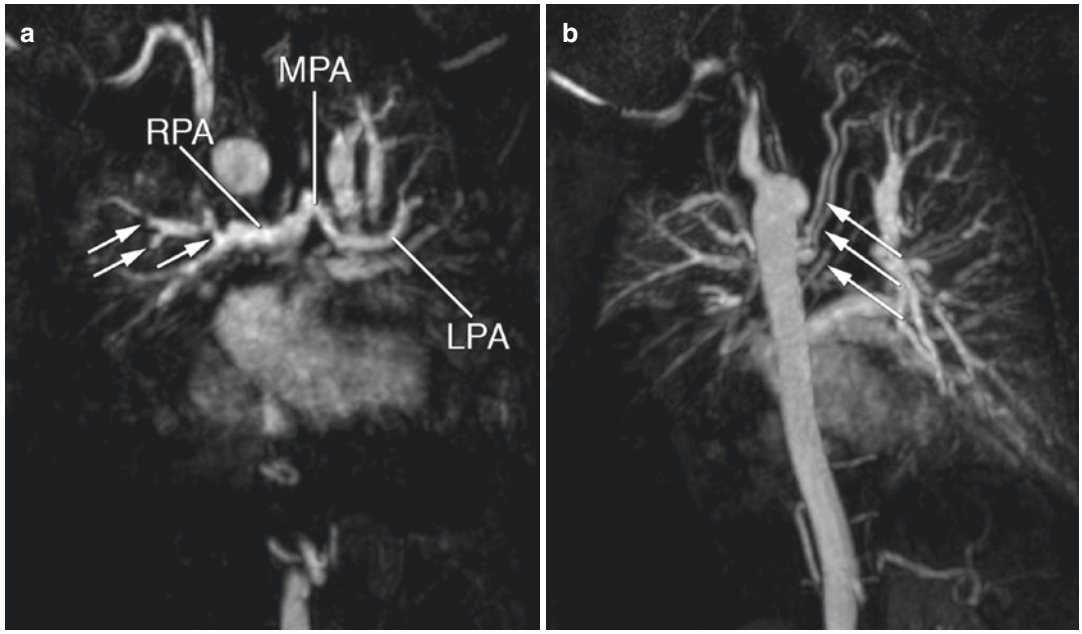

Fig. 13 Hypoplastic pulmonary arteries with stenoses. 26-year-old female patient with tetralogy of Fallot. Gadolinium-enhanced MR angiography, showing severely hypoplastic main and branch pulmonary arteries (**a**). Panel (**b**) demonstrates residual, non-unifocalised aorto-pulmonary collateral arteries (*arrows*). *MPA* main pulmonary artery, *LPA* left pulmonary artery, *RPA* right pulmonary artery

by cross-sectional imaging (Castaner et al. 2006). Patients with pulmonary valve atresia often are burdened with severe arborisation abnormalities and multiple peripheral pulmonary stenoses. Peripheral pulmonary artery stenosis, i.e. stenosis in the lobar or segmental/subsegmental pulmonary arteries, has been recognised in adults as a cause of pulmonary hypertension (Tonelli et al. 2015).

4.1.1 Presentation and Diagnosis

Primary presentation of an isolated pulmonary artery stenosis during adulthood is rare. Echocardiography allows evaluation of the main as well as the proximal left and right pulmonary arteries from the parasternal short axis. Luminal narrowing or interruption can be seen on greyscale imaging; turbulence on colour-Doppler imaging marks the location of stenosis, especially if the acoustic windows are limited. Using pulsed or continuous-wave Doppler and applying the modified Bernoulli equation an estimation of the gradient across the stenosis can be obtained. Both MRI and CT can evaluate the morphology of the pulmonary vasculature in great detail. MRI 3D SSFP techniques or 2D cine SSFP acquisitions in the (oblique) axial plane, or MR angiography (Fig. 13), can be used to image the pulmonary arteries. Phase-contrast velocity mapping can be used to quantify the flow velocities across a stenosis. It should be noted that the resultant velocities are lower than those obtained by pulsed-wave or continuous-wave Doppler ultrasound, unless the imaging slice is at the exact location of the fastest flow jet. This technique is also useful for the quantification of relative pulmonary blood flow, which is typically shifted towards the lung with the unobstructed arterial supply. In patients with severe pulmonary artery narrowing or with an arterial stent, flows in the pulmonary veins may more accurately represent the ipsilateral lung perfusion. Nuclear imaging can also be used to assess differential lung perfusion in case of branch pulmonary artery stenosis, although the technique is increasingly replaced by phase-contrast MRI (Sridharan et al. 2006). Some centres prefer detailed pulmonary fluoroscopic angiography for the planning of treatment, especially in the case of syndromal peripheral pulmonary stenosis (Monge et al. 2013).

4.1.2 Treatment and Follow-Up Imaging

Isolated pulmonary artery stenosis and even longer segment hypoplasia can be treated percutaneously, by either balloon angioplasty or stent placement, or surgically. Morbidity and mortality are low (Monge et al. 2013; van Gameren et al. 2006). Restenosis may occur and warrants close monitoring with echocardiography or cross-sectional imaging modalities. When stents are used for the relief of pulmonary stenosis, evaluation by echocardiography or MRI can be difficult, while CT can provide optimal information on stent integrity and in-stent stenosis (Fig. 14).

4.2 Pulmonary Arteriovenous Malformations

In adults, pulmonary arteriovenous malformations (PAVMs) are increasingly recognised with an estimated prevalence of 1 per 2630 in the general population (Nakayama et al. 2012). The most common cause of PAVMs is hereditary hemorrhagic telangiectasia. Also, AVMs may occur in complex congenital heart disease (Marianeschi et al. 1998). Furthermore, patients with cyanotic heart disease are at substantial increased risk of developing PAVMs, especially in lungs of a subset of patients with so-called single-ventricle circulations, that do not receive blood that has

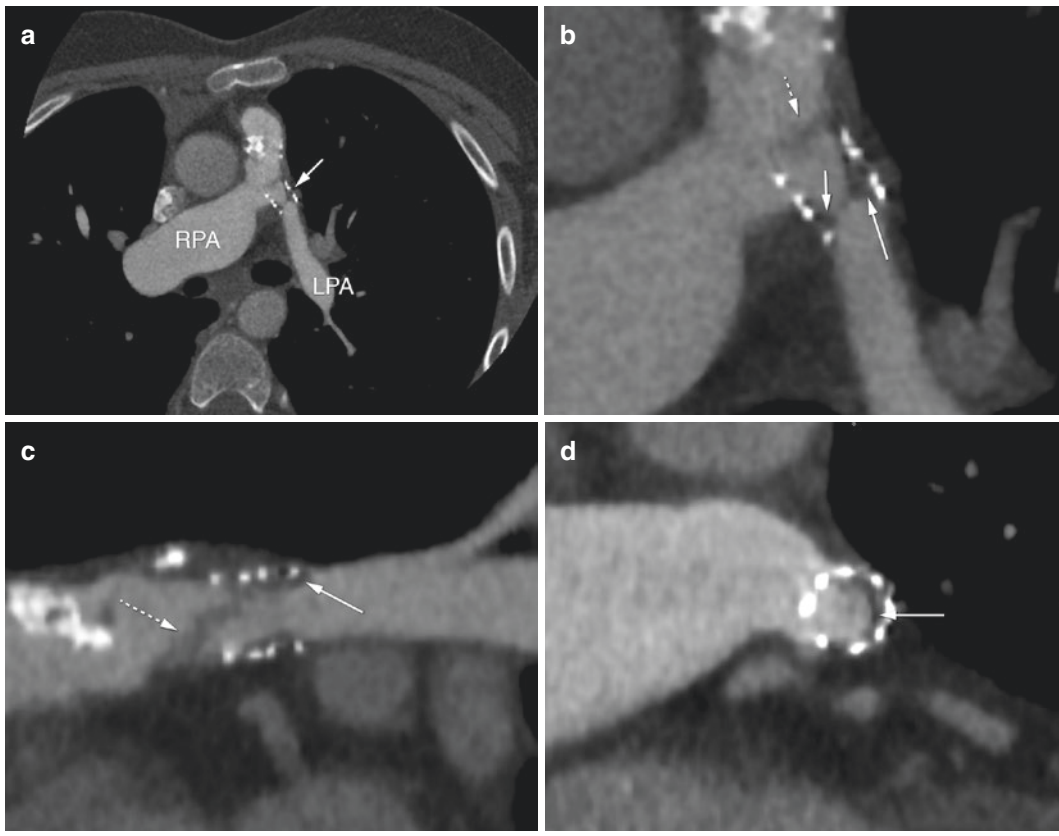

Fig. 14 Stented left pulmonary artery. CT angiography in an 11-year-old male patient with tetralogy of Fallot with pulmonary atresia and major aortopulmonary collateral arteries, after unifocalisation of the collaterals, insertion of pulmonary valve homograft and stent in the proximal left pulmonary artery. (**a**) The axial reconstruction shows a calcified homograft, a dilated right pulmonary artery (RPA) and stented LPA. (**c**) Long-axis view and (**d**) short-axis view of the LPA, showing intimal hyperplasia, creating in-stent obstruction (*arrows*). Also, presence of thrombus material (dotted *arrows* in **b**, and **c**)

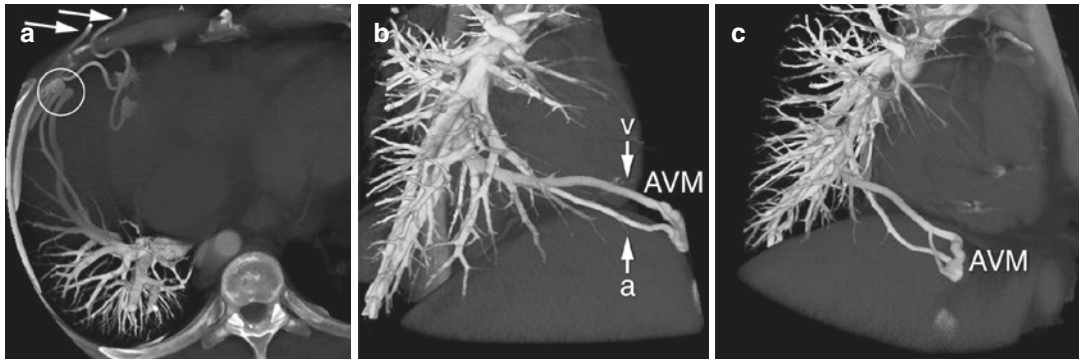

Fig. 15 Pulmonary arteriovenous malformation. 35-year-old patient with a Fontan-type circulation. Pulmonary arteriovenous malformation in the right lung (*circle* and *arrows* in **a**) in the anterobasal segment of the right lower lobe (**b**) and (**c**). *AVM* arteriovenous malformation, *a* artery, *v* vein

passed through the liver (Fig. 15), when the liver veins are not incorporated within the Fontan circulation.

Most PAVMs present in the lower lobes. A simple PAVM is fed by a single pulmonary artery, whereas in complex PAVMs more arteries are involved. The efferent vessels drain directly into the pulmonary veins (Cartin-Ceba et al. 2013).

4.2.1 Presentation and Diagnosis

PAVMs often become symptomatic in the first three decades of life, depending on their number and size (Cartin-Ceba et al. 2013). Symptoms and signs include dyspnoea, cyanosis, chest pain, haemorrhage (either hemoptesis or haemothorax) and stroke (Shovlin 2014). Of note, pregnancy is recognised as a period of increased risk for complications caused by PAVMs, such as haemorrhage, pulmonary emboli and myocardial infarction (Shovlin 2014). Chest radiography can reveal round or oval nodules especially in the lower lobes. Of course, nodules on the chest radiograph can have numerous causes and additional imaging is necessary for diagnosing PAVM. Echocardiography can be used to detect the right-to-left shunt via PAVMs with the use of contrast-enhanced echocardiography, either with agitated saline (gas microbubbles) or albumin. Arrival of any gas microbubbles on the left side of the heart, especially after only three to four cardiac cycles, indicates intrapulmonary shunting (Cartin-Ceba et al. 2013). However, this phenomenon can also be seen in normal lungs and in up to 8% of the general population at rest (Shovlin 2014). Radionuclide imaging, although not commonly used in patients with suspected PAVMs, can also be used to detect and approximate the right-to-left shunting (Cartin-Ceba et al. 2013; Shovlin 2014).

Currently, CT is considered the non-invasive reference standard for diagnosing PAVM, and to assess the localisation, number, size, extent and suitability for intervention (Gill et al. 2015). Both afferent and efferent vessels can be visualised. Imaging is timed when the contrast bolus is estimated to reach the pulmonary arteries. MRI has been used for the diagnosis of PAVMs, albeit with lower spatial resolution compared to CT. When using MR, contrast-enhanced MR angiography is the preferred technique, particularly using time-resolved approaches or ECG gated (Maki et al. 2001; Ohno et al. 2002; Schneider et al. 2008). Cardiac catheterisation is currently less frequently employed for diagnosing PAVMs, but is used for their percutaneous treatment.

4.2.2 Treatment and Follow-Up Imaging

Percutaneous embolisation is the treatment of choice in PAVMs with low morbidity and mortality. Occlusion is generally recommended, even in asymptomatic patients, to prevent complications. After embolisation, recanalisation and collateralisation can occur and current

guidelines recommend CT scans at 6–12 months post-intervention and subsequently at intervals of 1–5 years (Shovlin 2014).

Conclusions

Imaging of the thoracic systemic and pulmonary arteries in adults most commonly involves evaluation of post-treatment sequelae. Understanding the underlying pathology and possible complications that may occur during follow-up is essential for selecting the appropriate imaging modality and subsequent execution of the examination. Echocardiography is the first-line imaging modality to assess the vascular morphology, but for detailed assessment of the thoracic systemic and pulmonary arteries CT and MRI are often necessary. The main advantages of CT over MRI are the short acquisition times and the option to evaluate intravascular stent patency. MRI, on the other hand, does not depend on ionising radiation and offers functional information.

References

Backer CL, Mavroudis C (2000a) Congenital heart surgery nomenclature and database project: patent ductus arteriosus, coarctation of the aorta, interrupted aortic arch. Ann Thorac Surg 69.4(Suppl):S298–S307

Backer CL, Mavroudis C (2000b) Congenital heart surgery nomenclature and database project: vascular rings, tracheal stenosis, pectus excavatum. Ann Thorac Surg 69.4(Suppl):S308–S318

Backer CL et al (2005) Trends in vascular ring surgery. J Thorac Cardiovasc Surg 129(6):1339–1347

Barnes ME, Mitchell ME, Tweddell JS (2011) Aortopulmonary window. Semin Thorac Cardiovasc Surg Pediatr Card Surg Annu 14(1):67–74

Bartelings MM, Gittenberger-de Groot AC (1989) The outflow tract of the heart—embryologic and morphologic correlations. Int J Cardiol 22(3):289–300

Baumgartner H et al (2010) ESC guidelines for the management of grown-up congenital heart disease (new version 2010). Eur Heart J 31(23):2915–2957

Berdon WE (2000) Rings, slings, and other things: vascular compression of the infant trachea updated from the midcentury to the millennium—the legacy of Robert E. Gross, MD, and Edward B. D. Neuhauser, MD. Radiology 216(3):624–632

Bjornard K et al (2013) Patterns in the prevalence of congenital heart defects, metropolitan Atlanta, 1978 to 2005. Birth Defects Res A Clin Mol Teratol 97(2):87–94

Bobylev D et al (2014) Aortopulmonary window: a rare untreated adult case. Heart Lung Circ 23(10):e235–e236

Brown ML et al (2010) Late outcomes of reintervention on the descending aorta after repair of aortic coarctation. Circulation 122(11 Suppl):S81–S84

Browne LP (2009) What is the optimal imaging for vascular rings and slings? Pediatr Radiol 39(Suppl 2):S191–S195

Cartin-Ceba R, Swanson KL, Krowka MJ (2013) Pulmonary arteriovenous malformations. Chest 144(3):1033–1044

Castaner E et al (2006) Congenital and acquired pulmonary artery anomalies in the adult: radiologic overview. Radiographics 26(2):349–371

Chattranukulchai P et al (2013) Undetected large aortopulmonary window in an adult: a confluence of great vessels. J Am Coll Cardiol 62(19):e439

Chen PC et al (2013) Predictors of reintervention after repair of interrupted aortic arch with ventricular septal defect. Ann Thorac Surg 96(2):621–628

Cramer JW et al (2013) Aortic aneurysms remain a significant source of morbidity and mortality after use of Dacron((R)) patch aortoplasty to repair coarctation of the aorta: results from a single center. Pediatr Cardiol 34(2):296–301

Dillman JR et al (2008) Interrupted aortic arch: spectrum of MRI findings. Am J Roentgenol 190(6):1467–1474

Dillman JR et al (2011) Common and uncommon vascular rings and slings: a multi-modality review. Pediatr Radiol 41(11):1440–1454

Edwards JE (1948) Anomalies of the derivatives of the aortic arch system. Med Clin North Am 32:925–949

Etesami M et al (2014) Computed tomography in the evaluation of vascular rings and slings. Insights Imaging 5(4):507–521

Ferguson EC, Krishnamurthy R, Oldham SA (2007) Classic imaging signs of congenital cardiovascular abnormalities. Radiographics 27(5):1323–1334

Forbes TJ et al (2011) Comparison of surgical, stent, and balloon angioplasty treatment of native coarctation of the aorta: an observational study by the CCISC (congenital cardiovascular interventional study consortium). J Am Coll Cardiol 58(25):2664–2674

Fratz S et al (2013) Guidelines and protocols for cardiovascular magnetic resonance in children and adults with congenital heart disease: SCMR expert consensus group on congenital heart disease. J Cardiovasc Magn Reson 15:51

Gill SS et al (2015) Pulmonary arteriovenous malformations and their mimics. Clin Radiol 70(1):96–110

Gittenberger-de Groot AC, Azhar M, Molin DG (2006) Transforming growth factor beta-SMAD2 signaling and aortic arch development. Trends Cardiovasc Med 16(1):1–6

Gould SW et al (2015) Useful signs for the assessment of vascular rings on cross-sectional imaging. Pediatr Radiol 45(13):2004–2016

Hoffman JI, Kaplan S (2002) The incidence of congenital heart disease. J Am Coll Cardiol 39(12):1890–1900
Hoffman JL et al (2014) Screening for aortic aneurysm after treatment of coarctation. Pediatr Cardiol 35(1):47–52
Hope MD et al (2010a) Bicuspid aortic valve: four-dimensional MR evaluation of ascending aortic systolic flow patterns. Radiology 255(1):53–61
Hope MD et al (2010b) Clinical evaluation of aortic coarctation with 4D flow MR imaging. J Magn Reson Imaging 31(3):711–718
Hope MD et al (2011) 4D flow CMR in assessment of valve-related ascending aortic disease. JACC Cardiovasc Imaging 4(7):781–787
Jacobs JP et al (2000) Congenital heart surgery nomenclature and database project: aortopulmonary window. Ann Thorac Surg 69.4(Suppl):S44–S49
Jimenez-Juan L et al (2014) Cardiovascular magnetic resonance imaging predictors of pregnancy outcomes in women with coarctation of the aorta. Eur Heart J Cardiovasc Imaging 15(3):299–306
Kamphuis VP et al (2017) Unravelling cardiovascular disease using four dimensional flow cardiovascular magnetic resonance. Int J Cardiovasc Imaging (7):1069–81. doi: 10.1007/s10554-016-1031-9. Epub 2016 Nov 25
Karaosmanoglu AD et al (2015) CT and MRI of aortic coarctation: pre- and postsurgical findings. Am J Roentgenol 204(3):W224–W233
Kimura-Hayama ET et al (2010) Uncommon congenital and acquired aortic diseases: role of multidetector CT angiography. Radiographics 30(1):79–98
Kir M et al (2012) Vascular rings: presentation, imaging strategies, treatment, and outcome. Pediatr Cardiol 33(4):607–617
Kiran VS et al (2008) Lessons learned from a series of patients with missed aortopulmonary windows. Cardiol Young 18(5):480–484
Knapper JT et al (2014) Interrupted aortic arch in an active, asymptomatic adult. Eur Heart J Cardiovasc Imaging 15(10):1185
Kroft LJ, Roelofs JJ, Geleijns J (2010) Scan time and patient dose for thoracic imaging in neonates and small children using axial volumetric 320-detector row CT compared to helical 64-, 32-, and 16- detector row CT acquisitions. PediatrRadiol 40(3):294–300
Leonardi B et al (2015) Imaging modalities in children with vascular ring and pulmonary artery sling. Pediatr Pulmonol 50(8):781–788
Levitt B, Richter JE (2007) Dysphagia lusoria: a comprehensive review. Dis Esophagus 20(6):455–460
Mahle WT, Kreeger J, Silverman NH (2010) Echocardiography of the aortopulmonary window, aorto-ventricular tunnels, and aneurysm of the sinuses of Valsalva. Cardiol Young 20(Suppl 3):100–106
Maki DD et al (2001) Pulmonary arteriovenous malformations: three-dimensional gadolinium-enhanced MR angiography-initial experience. Radiology 219(1):243–246
Marianeschi SM, McElhinney DB, Reddy VM (1998) Pulmonary arteriovenous malformations in and out of the setting of congenital heart disease. Ann Thorac Surg 66(2):688–691
McElhinney DB et al (1998) Early and late results after repair of aortopulmonary septal defect and associated anomalies in infants <6 months of age. Am J Cardiol 81(2):195–201
Meadows J et al (2015) Intermediate outcomes in the prospective, multicenter coarctation of the aorta stent trial (COAST). Circulation 131(19):1656–1664
Monge MC et al (2013) Surgical reconstruction of peripheral pulmonary artery stenosis in Williams and Alagille syndromes. J Thorac Cardiovasc Surg 145(2):476–481
Morgan CT et al (2017) Understanding the mechanism for branch pulmonary artery stenosis after the arterial switch operation for transposition of the great arteries. Eur Heart J Cardiovasc Imaging 18(2):180–185
Muzzarelli S et al (2011) Prediction of hemodynamic severity of coarctation by magnetic resonance imaging. Am J Cardiol 108(9):1335–1340
Naimo PS et al (2014) Outcomes of aortopulmonary window repair in children: 33 years of experience. Ann Thorac Surg 98(5):1674–1679
Nakayama M et al (2012) Prevalence of pulmonary arteriovenous malformations as estimated by low-dose thoracic CT screening. Intern Med 51(13):1677–1681
Nance JW, Ringel RE, Fishman EK (2016) Coarctation of the aorta in adolescents and adults: a review of clinical features and CT imaging. J Cardiovasc Comput Tomogr 10(1):1–12
Nihoyannopoulos P et al (1987) Accuracy of two-dimensional echocardiography in the diagnosis of aortic arch obstruction. J Am Coll Cardiol 10(5):1072–1077
Ohno Y et al (2002) Contrast-enhanced MR perfusion imaging and MR angiography: utility for management of pulmonary arteriovenous malformations for embolotherapy. Eur J Radiol 41(2):136–146
Pierpont ME et al (2007) Genetic basis for congenital heart defects: current knowledge: a scientific statement from the American Heart Association Congenital Cardiac Defects Committee, Council on Cardiovascular Disease in the Young: endorsed by the American Academy of Pediatrics. Circulation 115(23):3015–3038
Rengier F et al (2015) Noninvasive 4D pressure difference mapping derived from 4D flow MRI in patients with repaired aortic coarctation: comparison with young healthy volunteers. Int J Card Imaging 31(4):823–830
Rider OJ, Bissell M, Myerson SG (2013) Congenital aortopulmonary window; an unusual cause of breathlessness. Heart 99(20):1546
Roos-Hesselink JW et al (2003) Aortic valve and aortic arch pathology after coarctation repair. Heart 89(9):1074–1077
Ruzmetov M et al (2009) Follow-up of surgical correction of aortic arch anomalies causing tracheoesophageal compression: a 38-year single institution experience. J Pediatr Surg 44(7):1328–1332
Schneider G et al (2008) MR angiography for detection of pulmonary arteriovenous malformations in patients

with hereditary hemorrhagic telangiectasia. AJR Am J Roentgenol 190(4):892–901
Shepherd B et al (2015) MRI in adult patients with aortic coarctation: diagnosis and follow-up. Clin Radiol 70(4):433–445
Shovlin CL (2014) Pulmonary arteriovenous malformations. Am J Respir Crit Care Med 190(11):1217–1228
Slater BJ, Rothenberg SS (2016) Thoracoscopic management of patent ductus arteriosus and vascular rings in infants and children. J Laparoendosc Adv Surg Tech A 26(1):66–69
Smith BM et al (2015) Rings and slings revisited. Magn Reson Imaging Clin N Am 23(1):127–135
Sridharan S et al (2006) Assessment of differential branch pulmonary blood flow: a comparative study of phase contrast magnetic resonance imaging and radionuclide lung perfusion imaging. Heart 92(7):963–968
Steffens JC et al (1994) Quantification of collateral blood flow in coarctation of the aorta by velocity encoded cine magnetic resonance imaging. Circulation 90(2):937–943
Suh YJ et al (2012) Clinical course of vascular rings and risk factors associated with mortality. Korean Circ J 42(4):252–258
Therrien J et al (2000) Repaired coarctation: a "cost-effective" approach to identify complications in adults. J Am Coll Cardiol 35(4):997–1002
Tonelli AR et al (2015) Peripheral pulmonary artery stenosis as a cause of pulmonary hypertension in adults. Pulm Circ 5(1):204–210
Torok RD et al (2015) Coarctation of the aorta: management from infancy to adulthood. World J Cardiol 7(11):765–775
Tsai SF et al (2011) Usefulness of screening cardiovascular magnetic resonance imaging to detect aortic abnormalities after repair of coarctation of the aorta. Am J Cardiol 107(2):297–301
Tworetzky W et al (1999) Echocardiographic diagnosis alone for the complete repair of major congenital heart defects. J Am Coll Cardiol 33(1):228–233
Ungerleider RM et al (2013) Contemporary patterns of surgery and outcomes for aortic coarctation: an analysis of the Society of Thoracic Surgeons Congenital Heart Surgery Database. J Thorac Cardiovasc Surg 145(1):150–157
Valsangiacomo Buechel ER et al (2015) Indications for cardiovascular magnetic resonance in children with congenital and acquired heart disease: an expert consensus paper of the imaging Working Group of the AEPC and the Cardiovascular Magnetic Resonance Section of the EACVI. Eur Heart J Cardiovasc Imaging 16(3):281–297
van Gameren M et al (2006) Early complications of stenting in patients with congenital heart disease: a multicentre study. Eur Heart J 27(22):2709–2715
Warnes CA et al (2008) ACC/AHA 2008 guidelines for the management of adults with congenital heart disease: a report of the American College of Cardiology/American Heart Association task force on practice guidelines (writing committee to develop guidelines on the management of adults with congenital heart disease). Circulation 118(23):e714–e833
Wong J et al (2012) Analysis of aortopulmonary window using cardiac magnetic resonance imaging. Circulation 126(15):e228–e229
Xu J et al (2014) Accuracy, image quality, and radiation dose of prospectively ECG-triggered high-pitch dual-source CT angiography in infants and children with complex coarctation of the aorta. Acad Radiol 21(10):1248–1254
Yang DH et al (2008) Multislice CT angiography of interrupted aortic arch. PediatrRadiol 38(1):89–100

Anomalies of the Systemic and Pulmonary Veins

Lars Grosse-Wortmann and Arno Roest

Contents

Abstract

The range of pathologies involving the systemic or pulmonary veins is wide. Many of these abnormalities are either clinically insignificant or have been surgically "corrected" during childhood. This chapter focuses on two types of clinical scenarios relevant to the care of adults with congenital heart disease: (1) Venous lesions that may present during or remain untreated until adulthood, and (2) those that are sequelae of previous interventions.

1 Overview of Imaging Techniques for Systemic and Pulmonary Venous Anatomy

In many adults with known congenital heart disease the anatomy of the systemic and pulmonary veins has been established through previous imaging and/or direct inspection at the time of prior operations.

L. Grosse-Wortmann (✉)
The Labatt Family Heart Centre, Department of Paediatrics, The Hospital for Sick Children, University of Toronto, Toronto, ON, Canada
e-mail: lars.grosse-wortmann@sickkids.ca

A. Roest
Department of Paediatrics, Willem Alexander Children's Hospital, Leiden University Medical Center, Leiden, The Netherlands
e-mail: A.Roest@lumc.nl

Med Radiol Diagn Imaging (2019)
https://doi.org/10.1007/174_2018_195, © Springer Nature Switzerland AG
Published Online: 31 January 2019

More than a century after the rays that Wilhelm Conrad Röntgen discovered were first used to image the thorax, chest X-ray remains an important imaging modality in congenital heart disease. To the trained eye, chest radiographs reveal many clues to systemic and pulmonary venous anomalies: For example, an abnormal caval vein may produce a characteristic shadow while pulmonary edema can suggest pulmonary venous obstruction. Furthermore, a chest X-ray can reveal important associated cardiac and extracardiac pathologies such as situs anomalies.

Echocardiography is often diagnostic for venous anomalies. It is important to interrogate the entire venous anatomy. On the systemic side, this includes the bridging (so-called innominate) vein and coronary sinus. Bilateral superior caval veins must be searched for routinely. On the pulmonary side, each pulmonary vein and its connection to the left atrium must be demonstrated. Anomalous pulmonary venous connections and obstructions within the left atrium must be carefully ruled out. Color Doppler maps the direction of blood flow and identifies areas of stenosis which are further evaluated by pulsed-wave Doppler.

If echocardiographic images are insufficient, or if information on blood flow is desired, cardiac magnetic resonance (CMR) is often the next applicable imaging modality. All cardiovascular acquisitions, except for conventional contrast-enhanced MR angiograms and some real-time applications, are electro- or vectorcardiogram-gated. Most centers have abandoned turbo-spin echo ("black blood") techniques in favor of gradient echo ("white blood") sequences. The latter are fast, offer excellent blood tissue contrast and can be performed in multiple phases per cardiac cycle, which are later arranged as cine clips. With a view to shorten scan time and increase signal-to-noise ratio steady-state-free-precession (SSFP) is the preferred pulse sequence for white blood imaging. However, spoiled gradient-echo sequences are occasionally preferred for their robustness towards field inhomogeneities and to visualize flow turbulence. Frequently, even static gradient echo sequences in the three orthogonal planes, obtained as "scouts" or "localizers" delineate the venous anatomy sufficiently. Information on ventricular volumes, which may be necessary to evaluate lesions that preload an atrial or ventricular chamber, is derived from multiphase ("cine") multislice sequences in the axial or short axis orientation. Three-dimensional (3D) contrast-enhanced magnetic resonance angiography provides a more detailed delineation of the luminal vascular anatomy. As mentioned, the conventional angiogram is a non-gated, either static or time-resolved, acquisition during breath-holding. The use of blood-pool contrast agent allows for a slower acquisition, using cardiac gating and diaphragm navigation to reduce blurring from pulsatility and respiration. The latter approach is also feasible with a non-enhanced 3D-SSFP-technique which can be employed when contrast is to be avoided. Phase-contrast flow velocity mapping is part of most protocols for patients with congenital heart disease, including those with venous pathologies. It clarifies the direction of blood flow, quantifies flow volume and maximum flow velocities, and depicts alterations of the expected flow velocity pattern. The use of 3D flow velocity mapping ("4D flow") in venous anomalies is hampered by the low signal-to-noise ratio and experimental at present. Computed tomography (CT) is used frequently in adults with congenital heart disease, particularly when CMR is contraindicated, poor CMR image quality is expected, or when pulmonary or mediastinal pathology is to be visualized. Electrocardiographic gating is employed when intracardiac or small vascular structures are the focus of the examination. Typically, CT is performed contrast-enhanced. For the systemic veins in particular, a CT angiogram must be carefully planned: First-pass imaging after injection into an upper-extremity vein often causes beam-hardening artifacts in the superior caval vein while delayed imaging may lead to subdiagnostic signal intensity in the veins (Choi et al. 2004). Careful selection of the injection site as well as adjustments to the concentration and timing of the contrast bolus help in minimizing artifacts. Cardiac catheterization is rarely necessary for the diagnosis of isolated venous anomalies, but the systemic and pulmonary veins are shown on

nearly all fluoroscopic angiographies. Changes in sampled blood oxygen saturations or pressure as the catheter passes through the heart are clues to shunts, including anomalous pulmonary or systemic venous connections. Of the nuclear imaging applications only lung perfusion scans for the quantification of pulmonary blood flow are employed with any frequency in congenital or postoperative venous pathologies. With the advent of phase contrast CMR lung perfusion scans have become an infrequently used tool at most centers.

2 Systemic Venous Abnormalities

When abnormalities of the systemic venous system occur in isolation they often cause minimal symptoms and are diagnosed coincidentally in later child- or even adulthood. Many patients do not require an intervention. Many complex types of congenital heart disease, on the other hand, are associated with systemic venous abnormalities. In these situations systemic vein anomalies can be a major determinant of surgical options and outcomes, as is the case in patients with heterotaxy syndrome and single ventricle circulations (Van Praagh and Van Praagh 1990). The development of the systemic veins is complex. As a result, the spectrum of possible deviations from the normal morphogenesis is wide and can not be covered in detail here. This chapter focuses on isolated systemic venous pathologies. Those that are part of complex congenital heart disease such as Fontan circulations are discussed in other chapters of this book.

2.1 Normal and Pathological Development of the Systemic Venous System

An understanding of the development aids in the understanding of pathologies of the systemic veins and, in many cases in the choice, acquisition, and interpretation of diagnostic studies. The precursors of the systemic veins are the cardinal veins, the umbilical veins, and the omphalomesenteric or vitelline veins. These develop as paired structures which drain into the horn of the sinus venosus on either side of the primitive heart. The cardinal veins eventually develop into the superior caval veins while the vitelline veins are the precursors of the hepatic veins and of the suprahepatic inferior caval vein (Smallhorn and Anderson 2010). Septation of the sinus venosus leads to a separation into right and left atrium and, in normal development, isolates the left atrium from the drainage of the cardinal, umbilical, and vitelline veins. The coronary sinus forms from the left horn of the sinus venosus and the left common cardinal vein. It drains the coronary venous blood and, if present, that from a persistent left superior caval vein, to the right atrium.

2.2 Persistent Left Superior Caval Vein and Anomalies of the Coronary Sinus

Of the initially paired superior caval veins the left one normally involutes around week seven of gestation. Persistence of the left superior caval vein occurs in 0.3% of the general population (Sanders 1946), but is much more frequent in individuals with congenital heart disease, particularly Tetralogy of Fallot, atrioventricular septal defect, and left-sided obstructive lesions (de Leval et al. 1975; Cochrane et al. 1994).

2.2.1 Anatomy

A persistent left superior caval vein always drains into the coronary sinus because both structures share a similar embryological origin: The left common cardinal vein. In approximately 10% of patients with a persistent left superior caval vein the coronary sinus is partially or completely unroofed, resulting in a right-to-left shunt (Meadows and Sharp 1965). Conversely, a completely or partially unroofed coronary sinus almost never occurs without a left superior caval vein. In rare instances the left may be the only superior caval vein present (Bartram et al. 1997). In patients with anomalies of the thoracic situs

the "morphologically right" superior caval vein may be on the patient's left.

2.2.2 Presentation

In isolated bilateral superior caval veins the presentation depends on whether or not the coronary sinus is intact, delivering the desaturated blood from the left superior caval vein to the right atrium. In severe cases an aneurysmally enlarged coronary sinus can cause obstruction to mitral inflow, leading to a clinical picture similar to cor triatriatum or pulmonary vein stenosis (below) (Agnoleti et al. 1999; Tham et al. 2007). A coronary sinus aneurysm is associated with Wolff–Parkinson–White syndrome (Guiraudon et al. 1988).

If the coronary sinus is deficient a bidirectional shunt results: Desaturated blood from the persistent left superior caval vein and the coronary veins enters the left atrium while pulmonary venous blood reaches the right atrium via the coronary sinus ostium. The degrees of heart failure (from the left-to-right shunt) and cyanosis (from the right-to-left shunt) depend on the presence and size of a left superior caval vein, on the presence or absence of bridging innominate (or left brachiocephalic) vein, and on the size of the coronary sinus defect. Rarely, the right-to-left shunt is sufficient to manifest in cyanosis.

2.2.3 Diagnosis

The majority of individuals with bilateral superior caval veins (and most other anomalies of the superior caval veins and coronary sinus) are asymptomatic. A persistent left superior caval vein must be differentiated from other veins in the left mediastinum, including anomalously connecting left pulmonary veins and a levoatrial cardinal vein. In contrast to a left superior caval vein, flow in these two situations is directed cephalad. A levoatrial cardinal vein is typically associated with left-sided obstructive lesions with restrictive atrial septae, providing an egress for pulmonary venous blood (Bernstein et al. 1995; Geva 2013). Its course is typically posterior to the left pulmonary artery while a left superior caval vein travels anterior to it (Lucas Jr. et al. 1962). Cephalad flow in the left superior caval vein itself occurs if the coronary sinus ostium into the right atrium is partially or completely occluded. In this situation, the only egress of coronary venous blood is via the superior caval vein and into the (bridging) innominate vein.

The presence of a left superior caval vein can be suspected on chest radiographs via a shadow along the left mediastinum. Echocardiography is typically sufficient to secure the diagnosis (Huhta et al. 1982). A left superior caval vein and a bridging innominate or left brachiocephalic vein are best seen from a high left parasternal or a suprasternal sagittal probe position. A dilated coronary sinus seen from a slightly lower right parasternal probe position or, in the rare adult with sufficient transhepatic windows, from subcostal, signifies a persistent left superior caval vein until proven otherwise. The integrity of the coronary sinus can be challenging to visualize conclusively by echocardiography. Imaging during injection of a bolus of agitated saline (so-called "bubble study") into a left arm vein is helpful in demonstrating a left superior caval vein: The bubbles will appear in the coronary sinus before the right atrium. If the coronary sinus is partially or completely unroofed the left atrium fills with bubbles before the right atrium. If these measures do not result in a definitive delineation of the caval and bridging venous as well as coronary sinus anatomy CMR establishes it with certainty. Contrast-enhanced angiography is usually not needed. Computed tomographic angiography accomplishes the same anatomical delineation as CMR. Catheterization may be obtained for reasons other than the systemic veins or with a view to occlude an abnormal vein.

2.2.4 Treatment

No treatment is necessary for isolated persistent left superior vena cava with an intact coronary sinus. If the coronary sinus is completely or partially unroofed with a small to moderate size left superior caval vein and good size bridging innominate vein the left caval vein can be ligated or occluded in the catheter laboratory with minimal penalty from drainage of coronary venous blood into the left atrium. A larger left superior caval vein without adequate connecting vein

needs to be baffled into the right atrium, a procedure that also directs coronary venous blood into the right atrium. Aneurysmal enlargement of the superior caval vein does not require surgery unless there is compression of neighboring structures, as the risk of rupture is exceedingly low (Geva 2013).

2.3 Connection of the Right Superior Caval Vein to the Left Atrium

In addition to an unroofed coronary sinus another, much more rare, route of systemic venous drainage into the left atrium is formed by an anomalously connected right superior caval vein (Van Praagh et al. 2003; Shapiro et al. 1981).

2.3.1 Anatomy

The right superior caval vein is partially or entirely committed to the left atrium, overriding an interatrial communication to varying degrees. This situation has been described as the systemic venous analogy of a sinus venosus atrial septal defect and anomalous pulmonary venous connection (Geva 2013).

2.3.2 Presentation

The cardinal sign, central cyanosis, depends on how much of the desaturated blood is directed towards the left atrium. Many patients are asymptomatic until late child- or well into adulthood. In addition to cyanosis patients are at risk for paradoxical emboli, resulting in cerebrovascular accidents and intracranial abscess formation.

2.3.3 Diagnosis

A high index of suspicion is key to making the diagnosis. While echocardiography can be sufficient to establish the anomalous venous connection the pathology is not infrequently missed (Chin 1994). This risk is greater in patients with absent subcostal windows as this is the best view to identify the roof of the atria. Parasternal and high parasternal views from both sides of the sternum are also helpful in this regard. Scanning during injection of agitated saline ("bubble study") may be useful in understanding the systemic venous drainage. Cross-sectional imaging with CMR or CT delineate the cavo-atrial connection with greater fidelity. The assessment includes a description of the degree of "overriding" of the interatrial communication by the superior caval and the presence of ostial venous stenosis. In addition, CMR phase-contrast flow measurements in the ascending aorta and the pulmonary artery permit a quantification of the right-to-left shunt in bi- or left atrial caval connection. Cardiac catheterization is usually not necessary and nuclear medicine techniques are not helpful.

2.3.4 Treatment

Management is surgical and consists of redirecting the right superior caval venous blood to the right atrium, either by dividing and anastomosing the vein to the right atrial appendage or by baffling it through the atrial communication, which may need to be enlarged, into the right atrium.

Complications consist of stenosis of the anastomosed vein or the baffle as well as baffle leaks.

2.4 Stenosis of the Systemic Veins

While primary stenosis of a major systemic vein is exceedingly rare and most often caused by expansive tumors of the mediastinum, like lymphoma, adults with congenital heart disease are predisposed to this complication of previous interventions: The most frequent mechanism is occlusion with a venous thrombus (Fig. 1). Clot formation is promoted by vessel wall injury through (a) instrumentation, (b) hypercoagulable states which occur during and after every surgery, (c) as side effects of cardiovascular pharmacotherapy, or (d) as a result of venous stasis.

2.4.1 Anatomy

The venous lumen is narrowed. Early in the disease process an intraluminal clot may be visible by imaging, which later becomes partially dissolved, organized, or integrated into the vessel wall.

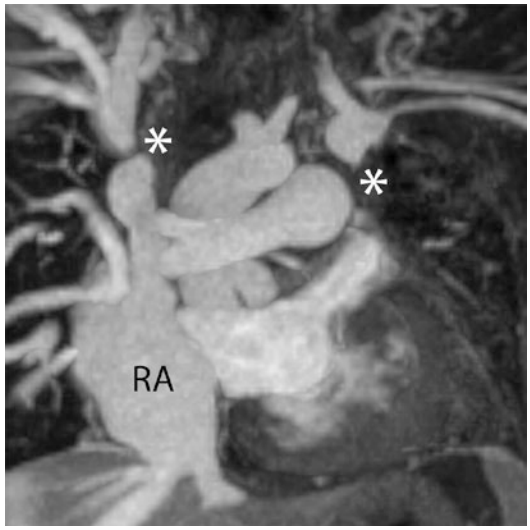

Fig. 1 CMR, bilateral superior vena cava occlusion. The patient was born with intracardiac total anomalous pulmonary venous connection and persistent left superior vena cava (LSVC) to the roof of the left atrium. Following the repair which included baffling of the LSVC to the right atrium, the patient developed occlusion of the left lower and severe stenosis of the left upper pulmonary vein. She also had complete thrombotic obstruction of her right and left superior vena cava (asterisks), with both veins draining via networks of venovenous collaterals. *RA* right atrium

2.4.2 Presentation

The venous drainage of the upper body is most often affected. The presence and extend of symptoms of superior vein stenosis depend on location and severity of the obstruction as well as the degree of collateralization. When severe narrowing develops rapidly before collaterals can form and there is only one superior caval vein, signs and symptoms are readily apparent: The most frequent presenting symptoms are dyspnea and headaches (Sharoni et al. 2001; Rice et al. 2006). Nasal congestion and nose bleeds are also common. Other symptoms include cough, arm swelling, hoarseness, and pleural effusions (Blalock et al. 1936).

2.4.3 Diagnosis

Echocardiography and Doppler ultrasound of the neck and mediastinum may show a narrowed lumen and flow acceleration by color and pulsed-wave Doppler. Computed tomography and CMR are the noninvasive methods of choice to visualize venous thrombi. The use of so-called blood pool contrast agents and electrocardiographic-gated inversion-recovery CMR sequences offers excellent visualization of thrombi. Invasive venography confirms the diagnosis but is typically reserved for cases in which a percutaneous treatment is planned in the same setting.

2.4.4 Treatment

Patients who are diagnosed acutely with a recently formed thrombus are treated with thrombolysis and anticoagulation. Surgical thrombectomy or percutaneous recanalization are sometimes undertaken. Percutaneous stent placement is the treatment of choice in patients with superior vena cava syndrome. Venous bypass grafts are rarely used. Lifelong follow-up is required to screen for recurrent obstruction.

2.5 Retroaortic Innominate Vein

Retroaortic innominate veins are found in ~0.5% of patients with congenital heart disease, most frequently tetralogy of Fallot (Kulkarni et al. 2008).

2.5.1 Anatomy

Normally, the bridging or innominate vein courses from left to right high in the mediastinum and anterior to the proximal aortic arch. In individuals with a retroaortic innominate vein the bridging innominate vein crosses the midline posterior to the ascending aorta and aortic arch and inserts into the right superior caval vein caudal, rather than cranial, to the azygos vein (Fig. 2) (Gerlis and Ho 1989; Choi et al. 1990; Smallhorn et al. 1985).

2.5.2 Presentation

Individuals are asymptomatic. The lesion is discussed here for its surgical implications during the repair of associated heart disease.

2.5.3 Diagnosis

A retroaortic innominate vein is typically diagnosed coincidentally by echocardiography or cross-sectional imaging. By ultrasound, a

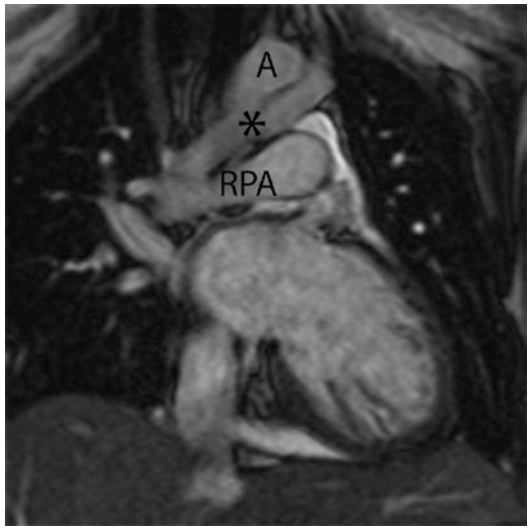

Fig. 2 CMR, retroaortic innominate vein. The coronal steady state free precession "localizer" image shows a left innominate vein (asterisk) beneath the aortic arch. *A* transverse arch, *RPA* right pulmonary artery

horizontal sweep from a high right parasternal probe position defines the relationship of the aortic arch to the innominate vein. The proximal portion of the innominate vein must not be mistaken for a persistent left superior caval vein.

2.5.4 Treatment

No treatment is indicated. However, the presence of a retroinnominate vein may necessitate alterations in surgical approach to associated lesions, for example during creation of a bidirectional cavopulmonary connection (Geva 2013). The superior caval vein cannula must be placed more caudally during cardiopulmonary bypass to avoid obstruction of the innominate vein (Chen et al. 2005). The anomalous innominate vein may cause technical difficulties during pacemaker insertion or central venous line placement through the left arm approach (Kulkarni et al. 2008).

2.6 Interrupted Inferior Caval Vein

Although interruption of the inferior caval vein can occur in isolation it should be viewed as a sign of anomalies of the visceral and thoracic situs until proven otherwise.

2.6.1 Anatomy

The inferior vena cava is interrupted along its abdominal course and an intrahepatic segment is absent. Venous blood from the extremities returns to the heart via a prominent azygos or hemiazygos vein (Fig. 3). In the abdomen, interruption of the inferior caval vein is associated with polysplenia, biliary atresia, and intestinal malrotation. In the thorax, it commonly indicates left isomerism of the atrial appendages, bronchi, and lungs. The left and right hepatic veins may drain via a common confluence to the same atrium or to different atria.

2.6.2 Presentation

Patients with isolated interruption of the inferior caval vein are asymptomatic because the azygos continuation ensures normal venous drainage despite an abnormal connection. The clinical importance of this anomaly is its frequent association with abdominal heterotaxy and left isom-

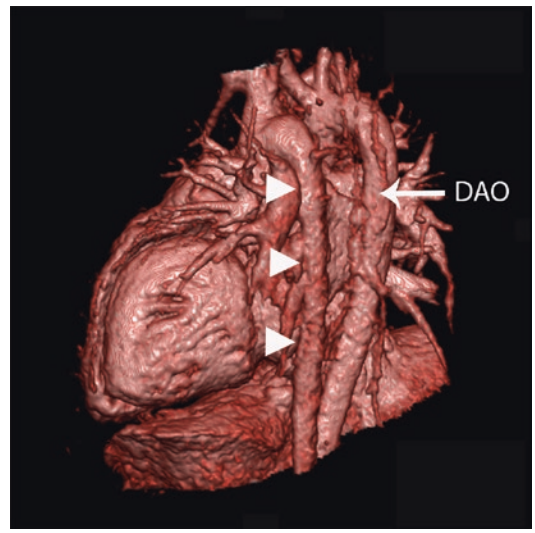

Fig. 3 CMR, absent infrahepatic inferior vena cava, large azygos vein. Volume rendered reformat of a magnetic resonance angiogram, seen from levo-posterior. This patient with "azygos continuation" (arrowheads) of the systemic venous return below the liver had a normal situs and tetralogy of Fallot with a right aortic arch. *DAO* descending aorta

erism of the atrial appendages. In this setting, congenital heart disease is common, most often in the form of left-sided obstructive lesions.

2.6.3 Diagnosis

In adults with significant congenital heart disease in the face of left isomerism of the atrial appendages the presence of an interrupted inferior caval vein with azygos continuation is known from previous diagnostic tests or surgery. Occasionally, it is diagnosed in adulthood. Chest plain films that show left isomerism of the main bronchi should prompt an echocardiogram to assess for interruption of the inferior caval vein and associated heart disease. Echocardiography shows a missing intrahepatic inferior vena cava segment and the dilated (hemi-)azygos vein as a prominent channel behind the liver in the paravertebral gutter (Huhta et al. 1984). In patients with sufficient acoustic windows the (hemi-)azygos vein can be shown in its entirety and connection with the superior caval vein. Cardiac magnetic resonance imaging and CT are definitive in the diagnosis. Cardiac catheterization is not needed except for in the diagnosis and treatment of associated heart disease. Imaging, preferably by abdominal ultrasound or CMR, delineates the abdominal situs, including the position of the stomach and liver; presence size, number, and position of the spleen(s), anatomy of the biliary system, and rotation of the intestine.

2.6.4 Treatment

When associated with complex congenital cardiac malformations which require a Fontan-type palliation the presence of an interrupted inferior caval vein changes the surgical strategy. At the time of the bidirectional cavopulmonary connection the blood from most of the lower body is diverted into the lungs via the azygos vein and its connection with the superior caval vein (Kawashima operation). At the time of the Fontan completion the hepatic venous flow is collected in a lateral tunnel or extracardiac conduit towards the pulmonary circulation.

Follow-up and life expectancy depend on the associated heart defects and their surgical palliation.

2.7 Anomalous Drainage of the Inferior Caval Vein

2.7.1 Anatomy

Whether a direct connection of the inferior caval vein to the morphological left atrium is embryologically possible is under debate (Smallhorn and Anderson 2010; Geva 2013). However, drainage of blood from the inferior caval vein into the left atrium via an atrial septal defect, particularly in a setting of a prominent persistent Eustachian valve, is a well-recognized occurrence (Lucas Jr. and Krabill 1995). Rarely, the inferior caval vein connects to the coronary sinus. Partial anomalous hepatic venous connection to the coronary sinus has also been described (Nabarro 1903). These anomalies are unlikely to occur in isolation and their discovery should prompt a search for other congenital heart disease.

2.7.2 Presentation

The anomalous drainage of desaturated blood to the left atrium results in cyanosis. The right-to-left shunt also carries the risk of paradoxical emboli.

2.7.3 Diagnosis

The diagnosis can usually established by transthoracic echocardiography. In patients with subdiagnostic acoustic windows cross-sectional imaging establishes the venous connections.

2.7.4 Treatment

Venous blood flow is surgically redirected to the right atrium.

2.8 Portosystemic Shunts

2.8.1 Anatomy

Congenital portosystemic shunts are divided into extra- and intrahepatic. In extrahepatic shunts the portal vein is either absent or part of the portal venous blood is diverted into the inferior caval vein. Intrahepatic portosystemic shunts are connections between branches of the portal vein and the hepatic veins.

2.8.2 Presentation

Ammonia and other toxins which are normally cleared by the liver result in hepatic encephalopathy, manifesting in tremors, seizures, and psychiatric symptoms. Other complications include failure to thrive, hepatopulmonary syndrome, and pulmonary hypertension. Patients may suffer from urate kidney stones because of increased amounts of uric acid in circulation which are excreted by the kidneys.

2.8.3 Diagnosis

Ultrasound with color Doppler imaging is the first-line imaging tool for the evaluation of portosystemic shunts (Franchi-Abella et al. 2010). Magnetic resonance imaging and CT angiography readily visualize the anatomy (Kakitsubata et al. 1996). Doppler ultrasound and magnetic resonance phase-contrast flow velocity mapping can be used to quantify the portovenous shunt ratio by dividing the total blood flow volume in the shunt by that in the portal vein (Kudo et al. 1993). Ratios <24–30% do not appear to result in hepatic encephalopathy while ratios >60% are an indication for intervention (Maeda et al. 1993). Nuclear medicine studies have also been used to quantify the magnitude of the shunt (Uchino et al. 1996).

2.8.4 Treatment

Asymptomatic patients do not require treatment. Percutaneous shunt occlusion or surgical closure of the shunt have been described. However, the portal venous system must be shown to be definitively intact before shunt occlusion to prevent mesenteric venous congestion and bowel ischemia.

2.9 Chiari Network

2.9.1 Anatomy

Chiari networks are the most frequent type of persistent embryonic valves within the right atrium. They consist of strands of tissue extending across the cavity of the right atrium from the terminal crest to the Thebesian or Eustachian valves (Smallhorn and Anderson 2010; Chiari 1897).

2.9.2 Presentation

Most patients are asymptomatic. Large Chiari networks can protrude through the tricuspid valves and cause obstruction to inflow. Endocarditis and thrombus formation within the network with embolization have also been described.

2.9.3 Diagnosis

Chiari networks are readily detected by echocardiography.

2.9.4 Treatment

Active management is usually not necessary. If there are complications resection may be considered.

3 Pulmonary Venous Abnormalities

3.1 Normal and Pathological Development of the Pulmonary Venous System

Around the fourth week in human development the blood from the primitive lung buds drains into the splanchnic plexus and from there into the paired common cardinal and umbilicovitelline veins (Lucas Jr. et al. 1963). A single primitive pulmonary vein develops shortly afterwards and fuses with the left atrium. For a short period of time, the pulmonary venous plexus is connected to both this early pulmonary vein and to the cardinal and umbilicovitelline veins. Soon afterwards, the connections to the latter two involute. These transient multiple connections of the pulmonary venous contributors serve to conceptualize all cases of anomalous pulmonary venous connection while an incomplete incorporation of the primitive pulmonary vein is the substrate for cor triatriatum: Anomalous connection to the systemic venous system are thought of as a result of the atresia of a pulmonary vein while pulmonary-to-systemic venous connections still exist. Cor triatriatum is the consequence of stenosis or incomplete fusion during the incorporation of the primitive single pulmonary vein into the left

atrium, after the pulmonary-to-systemic venous connections have been lost.

3.2 Partial Anomalous Pulmonary Venous Connection

Most people have two right- and two left-sided pulmonary veins, although a right middle pulmonary vein is not uncommon. In partial anomalous pulmonary venous connection (PAPVC) some, but not all, of the pulmonary veins connect to the systemic venous system instead of the left atrium. Usually, but not always, abnormal connection leads to abnormal drainage, and vice versa.

3.2.1 Anatomy

Anomalous pulmonary venous connection most often involves the right upper and middle pulmonary veins to the superior caval vein or right atrium (Fig. 4) as well as the left upper pulmonary vein to the left innominate vein (Fig. 5). Partial anomalous pulmonary venous connection of the right upper plus/minus right middle pulmonary vein(s) is often associated with a superior sinus venosus defect, a complex malformation involving the pulmonary veins, the superior caval vein/right atrium junction, and the superior wall between the right and left atria. An inferior sinus venosus defect constitutes an interatrial communication and anomalous drainage of the right lower pulmonary vein.

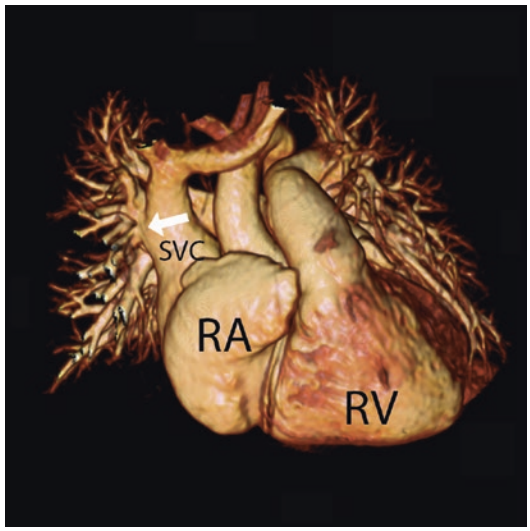

Fig. 4 CMR, partial anomalous pulmonary venous connection. This patient with multiple anomalously connected veins draining the right upper and part of the right middle lobe (arrow) also had a sinus venosus type interatrial communication. Together, the two left-to-right shunts amounted to a pulmonary to systemic blood flow ratio of 3.2, causing severe right atrial and right ventricular enlargement. The main pulmonary artery is also dilated. *RA* right atrium, *RV* right ventricle, *SVC* superior vena cava

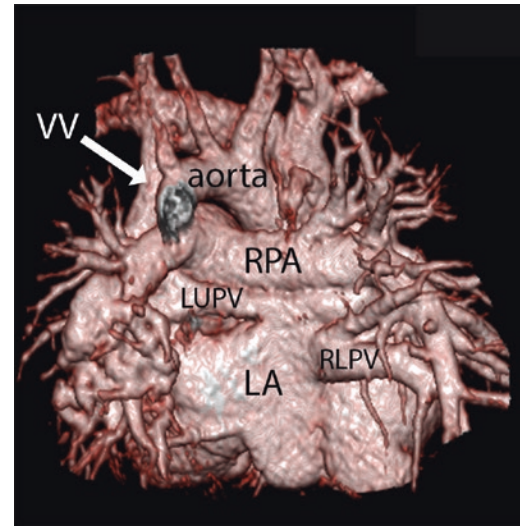

Fig. 5 CMR, repaired total anomalous pulmonary venous connection with residual left vertical vein. The volume rendered reformat of a magnetic resonance angiogram demonstrates a persistent left vertical vein in a patient who was born with total anomalous pulmonary venous connection. The connection of the left upper pulmonary vein to the left innominate vein was not corrected because the patient developed pulmonary hypertension during intra-operative test occlusion of the vertical vein. *LA* left atrium, *LLPV* left lower pulmonary vein, *RLPV* right lower pulmonary vein, *VV* vertical vein

3.2.2 Presentation

In many ways, the clinical picture of PAPVC is similar to that of an atrial septal defect. Both cause a left-to-right shunt which, if large enough, can lead to right heart dilatation, arrhythmias, and pulmonary arterial hypertension. Factors that influence the degree of left-to-right shunting include the number of anomalously connected pulmonary veins, the presence and size of any atrial septal defect (ASD), and the compliance of the right ventricle (Brown and Geva 2013; Seller et al. 2018).

3.2.3 Diagnosis

Patients with a significant shunt show increased pulmonary vascular markings and dilatation of the right ventricle and the pulmonary artery segment on chest X-ray. The X-ray may also provide clues to the type of PAPVC: In Scimitar syndrome, for example, the right lung is hypoplastic and the mediastinum shifted to the right, with elevation of the right hemidiaphragm (Yoo and Epelman 2010). There is retrosternal soft tissue density. The anomalously connected right-sided pulmonary veins are often recognized as a crescent-shaped shadow within the right mediastinum. With long-standing, unrepaired PAPVC pulmonary vascular disease can occur and manifest in "pruning" of the peripheral pulmonary arterial branches (Saalouke et al. 1977; Babb et al. 1981). Echocardiography is often, but not always, sufficient in the delineation of the pulmonary venous anatomy. The junction of the right upper pulmonary vein to the left atrium, in particular, can be difficult to ascertain. It is important that all pulmonary veins are detailed in their connection to either the left atrium or, anomalously, to a systemic venous structure, including the right atrium. Left and right parasternal, suprasternal, and apical acoustic windows are most useful to show the pulmonary veins. In slim individuals with favorable windows the subcostal approach may present another option. A complete echocardiography study also detects any associated lesions, most importantly an interatrial communication. The severity of left-to-right shunting can be gauged from the degree of right atrial and right ventricular enlargement. Flatting of the interventricular septum at end-diastole is an indicator of right ventricular volume overload. While transesophageal echocardiography can typically clarify the venous anatomy in patients with insufficient transthoracic windows this information can be obtained noninvasively and more comprehensively by CMR or CT. As mentioned in the imaging overview at the beginning of this chapter the CMR "localizer" or "scout" images are often sufficient to detail the pulmonary venous connections. However, contrast-enhanced angiography is beneficial, especially when more than one anomalously connected vein is suspected. When all of the right pulmonary veins are found to connect to the right atrium, inferior caval vein, or a hepatic veins the possibility of a Scimitar syndrome must be strongly considered (Fig. 6). Patients with Scimitar syndrome have other abnormalities, including, as mentioned, hypoplasia of the right lung and the right pulmonary artery, lung segmentation and bronchial branching abnormalities, and often a prominent aortopulmonary collateral artery from the abdominal aorta to the base of the right lung. Adults with this condition are usually symptomatic and a substantial proportion have pulmonary arterial hypertension. In addition to the anatomy, the degree of right ventricular dilatation and the magnitude of the left-to-right shunt is an important factor in surgical decision-making. Today's gold standard for ventricular volumetry and shunt quantification is CMR. Phase-contrast CMR allows for flow assessments in each individual pulmonary vein as well as across the atrial septum (Beerbaum et al. 2001; Goo et al. 2009; Grosse-Wortmann et al. 2007). Separating the contributions of shunt across the atrial communication and via the anomalously draining pulmonary vein is of clinical relevance in patients with

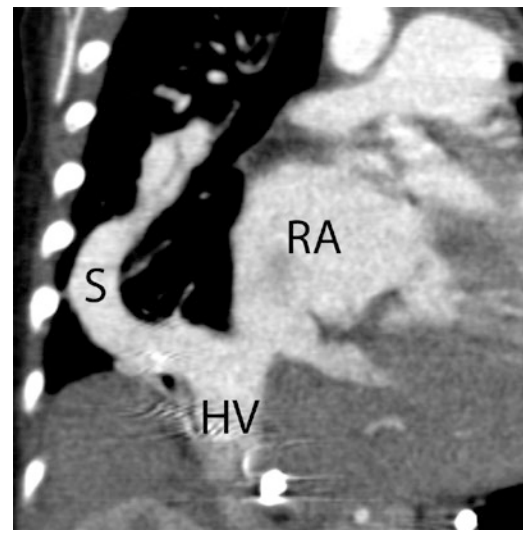

Fig. 6 CT, Scimitar syndrome. The computed tomography contrast-enhanced angiogram shows complete anomalous connection of the entire right lung via a scimitar vein to the suprahepatic inferior vena cava. *HV* hepatic vein, *RA* right atrium, *S* scimitar vein

PAPVC of the left upper pulmonary vein with secundum type atrial septal defect: If the shunt via the vein is minor percutaneous device closure of the atrial septal defect may be the preferred approach as opposed to a "full repair" on cardiopulmonary bypass. Given the performance of echocardiography and cross-sectional imaging cardiac catheterization is not routinely necessary in PAPVC, unless pulmonary arterial hypertension is suspected. The ratio of pulmonary (Qp) to systemic blood flow (Qs) is calculated via oximetry and the Fick principle. The levophase of a fluoroscopy after right ventricular or pulmonary arterial injection of contrast delineates the pulmonary venous drainage and connection. The anomalously connected vein may be entered retrogradely and injected selectively with dye.

3.2.4 Treatment

The natural history of PAPVC is not favorable in all cases. Anecdotal case reports of patients developing pulmonary vascular disease in the affected lung lobe in the presence of only one anomalously draining pulmonary vein document the risk of pulmonary hypertension in these patients (Saalouke et al. 1977; Babb et al. 1981). The indication for repair of PAPVC with or without atrial septal defect depends on symptoms, shunt magnitude, and degree of right ventricular dilatation. A pulmonary (Qp) to systemic flow (Qs) ratio ≥2.0 is widely used as a criterion for the operative repair of simple left-to-right shunt lesions, including atrial level shunts and PAPVC. Using CMR, we recently found that asymptomatic patients with isolated anomalous connection of the left upper pulmonary vein without an atrial septal defect are unlikely to have a significant left-to-right shunt and typically do not require surgery (Seller et al. 2018). On the other hand, the combination of right-sided PAPVC with (sinus venosus) atrial communication is routinely associated with a significant left-to-right shunt. The most important postoperative sequelae are pulmonary vein stenosis (see below) and atrial arrhythmias. The scimitar vein is typically baffled to the right atrium, either via route of an atrial septal defect, that can be associated with the Scimitar Syndrome or surgically created. Surgical indications and postoperative complications in patients with Scimitar syndrome are identical to other types of PAPVC, although Scimitar syndrome carries a worse prognosis, owing to the accompanying lung hypoplasia as well as bronchial branching and lung segmentation abnormalities, but also due to the higher prevalence of native pulmonary venous obstruction.

3.3 Total Anomalous Pulmonary Venous Connection

Anomalous connection of all pulmonary veins hardly ever presents in an adult and is only discussed superficially in this book (Cheng et al. 2015). However, the sequelae of surgical repair of total anomalous pulmonary venous connection (TAPVC), residual anomalous connection of one or more pulmonary veins or pulmonary vein stenosis, are not uncommon among adults.

3.3.1 Anatomy

The connection of the pulmonary veins to the systemic venous system may be at the supracardiac, (intra-)cardiac, or infracardiac level (Craig et al. 1957). Combinations of these three types are possible within the same patient.

3.3.2 Presentation

As mentioned, TAPVC typically manifests, and is repaired, in early childhood. The very few that survive to adulthood with this diagnosis have excellent atrial mixing and minimal obstruction of the pulmonary venous pathway. Given the propensity of obstruction in infracardiac TAPVC adult cases are invariably of the supracardiac, intracardiac, or mixed type. There is an obligatory left-to-right shunt and systemic cardiac output can only be maintained if there is also a right-to-left shunt, usually across the atrial septum. Consequently, patients present in heart failure with varying degrees of cyanosis.

3.3.3 Diagnosis

The chest X-ray shows cardiomegaly, increased pulmonary vascularity, and pulmonary edema. It is sometimes possible to detect dilated

pulmonary-to-systemic venous connections, such as in supracardiac TAPVC and the well-known "snowman sign" (Yoo and Epelman 2010). Echocardiography is often sufficient to define the pulmonary venous anatomy comprehensively in neonates. There are few lesions that produce an exclusive right-to-left shunt across the atrial septum. Total anomalous pulmonary venous connection is, one of them. The left ventricle in TAPVC is underfilled. With more advanced age at presentation cross-sectional imaging, i.e., CT or CMR, take on an increasingly important role in delineating the anatomy. It is imperative to define the anatomy of each pulmonary vein, the common pathway, if present, as well as any accompanying heart lesions. An important association exists between TAPVC and right isomerism of the atrial appendages so that the latter must be actively ruled out. Any obstruction within the pulmonary venous drainage or the obligatory right-to-left shunt at the atrial level must be assessed. Cardiac catheterization with assessment of pulmonary vascular resistance is advised prior to surgical correction in an adult patient.

3.3.4 Treatment

In the absence of prohibitive pulmonary vascular disease the pulmonary veins are anastomosed to the left atrium.

3.4 Cor Triatriatum

Cor triatriatum is the result of failure of incorporation of the primitive common pulmonary vein into the left atrium (Brown and Geva 2013).

3.4.1 Anatomy

The left atrium is divided into an upper and a lower chamber. The pulmonary veins enter the "upper chamber." Significant heterogeneity in presentation and management is introduced by the presence or absence of communications between either chamber and the right atrium and between the upper and lower left atrial compartments (Niwayama 1960). Cor triatriatum is commonly associated with PAPVC.

3.4.2 Presentation

The physiology and clinical presentation of Cor triatriatum varies widely according to atrial level shunts and associated PAPVC (47). If no communication between the upper chamber and the right atrium exists and the connection to the lower chamber is stenotic the clinical picture is that of mitral stenosis. If both left atrial chambers communicate with the right atrium and the connection between upper and lower chambers is either stenotic or atretic the physiology is that of TAPVC. (Brown 2009).

3.4.3 Diagnosis

It is important to delineate the membranous barrier between the upper and lower left atrial compartments. In contrast to supravalvar mitral stenosis the intraatrial membrane is situated above the left atrial appendage. All interatrial communications must be visualized in terms of size, estimated gradients, and flow directions. Given the common association with PAPVC all pulmonary veins must be interrogated. In many cases, transthoracic echocardiography visualizes the pertinent features with sufficient detail and certainty. The right ventricle is often dilated and hypertrophied. Depending on the physiology the chest X-ray shows evidence of pulmonary venous obstruction, with pulmonary edema and enlargement of the central pulmonary arteries. The assets of CMR and CT are the same as for TAPVC. The intraatrial membrane can be challenging to see by cross-sectional imaging, especially on an ungated CT angiogram. Invasive manometry during cardiac catheterization reveals pulmonary arterial hypertension unless the upper left atrial chamber has an unobstructed outlet, either into the right atrium or into the lower chamber. Selective injections into the pulmonary arteries opacify the pulmonary veins and the upper left atrial chamber. If there is a defect in the core membrane, the lower chamber and the left ventricle fill after a small delay and the membrane itself can be appreciated as a thin filling defect between the two chambers.

3.4.4 Treatment

The definite management is typically surgical and consists of resection of the intraatrial

membrane. Any associated PAPVC is corrected at that time, unless deemed to be hemodynamically insignificant. Percutaneous relief of obstruction with or without closure of unnecessary communications with the right ventricle is an alternative approach in select cases (Kerkar et al. 1996; Li et al. 2015). The prognosis in "uncomplicated" and repaired Cor triatriatum is good. Any associated PAPVC predisposes to postoperative pulmonary vein stenosis.

3.5 Pulmonary Vein Stenosis

Pulmonary vein stenosis manifests as a primary lesion or after pulmonary vein surgery. Primary pulmonary vein stenosis occurs as an isolated defect or associated with other types of congenital heart disease.

3.5.1 Anatomy

The morphology of pulmonary vein stenosis is either a discrete narrowing (Fig. 7) at the ostium into the left atrium or a diffuse, long-segment hypoplasia of the entire vein and often also its peripheral branches. Combinations of these two features are common as ostial stenosis often entails hypoperfusion which leads to shrinking of the contributing channels.

3.5.2 Presentation

Patients present with signs of pulmonary arterial hypertension, including tachypnea, reduced exercise tolerance and, sometimes, cyanosis. Recurrent pneumonia is a frequent complication; pulmonary hemorrhage occurs in advanced disease.

3.5.3 Diagnosis

In advanced disease the chest X-ray shows increased interstitial markings and dilation of the pulmonary lymphatic vessels with ground-glass changes (Yoo and Geoffray 2010). Long-standing pulmonary vein stenosis may lead to decreased ipsilateral pulmonary artery size and lung hypoplasia. The heart size is typically normal. Echocardiography is routinely used in the postoperative surveillance for obstruction following

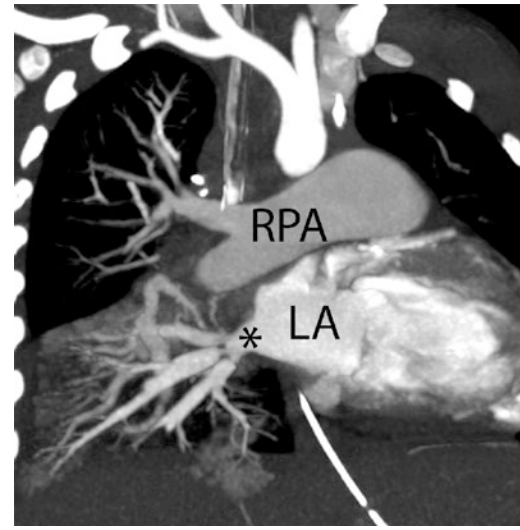

Fig. 7 CT, pulmonary vein stenosis. The coronal multiplanar reformat of the computed tomography angiogram demonstrates severe focal stenoses (asterisk) of all three contributors to the right lower pulmonary vein in a 3-year old. The right pulmonary artery is enlarged, secondary to pulmonary hypertension. The other three pulmonary veins were also obstructed. The stenoses recurred following surgical and catheter interventions and the patient eventually received a heart and lung transplant. *LA* left atrium, *RPA* right pulmonary artery

pulmonary vein repair. An unobstructed pulmonary vein has laminar flow by color Doppler and low velocity, phasic flow pattern with one or two systolic peaks, a diastolic peak and a brief nadir at the end of diastole (Grosse-Wortmann et al. 2007). A stenosed pulmonary vein lacks some or all of these features. An elevated mean gradient estimate by pulsed-wave Doppler confirms the stenosis. Relatively low velocity flow, however, does not rule out significant obstruction, especially if the classic phasic fluctuations across the cardiac cycle are attenuated, as flow redistribution away from the obstruction can mask a higher gradient. It has been shown repeatedly that echocardiography lacks sensitivity as well specificity in the detection of pulmonary vein stenosis, in comparison to CMR (Valsangiacomo et al. 2003a, b; Greenway et al. 2011). Magnetic resonance offers anatomical and functional delineation: In significant obstruction, the ipsilateral branch pulmonary artery is usually hypoplastic as a reflection of the decreased blood flow to the

lung with the affected vein (Roman et al. 2005). Diffusely small peripheral pulmonary venous contributors are a sign of severe obstruction and shunting of blood away from the stenosed vessel. This appearance may also reflect diffuse disease with so-called arterialization of long segments of the pulmonary veins. It is sometimes possible by CMR or CT to visualize venous collateral channels that deviate blood away from the obstructed egress (Grosse-Wortmann et al. 2007). Phase-contrast velocity CMR demonstrates the hemodynamic effects of the stenosis. This information aids in gauging the severity of obstruction and is particularly helpful in distinguishing compression of a vein (typically the left lower) between the descending aorta and the heart without obstruction to flow from significant stenosis. Flow mapping should be performed in the pulmonary arteries and in the pulmonary veins. Significant pulmonary vein obstruction often leads to redistribution of blood flow, away from the area drained by the obstructed lung. This redistribution can be seen at the arterial level as an imbalance of right vs. left pulmonary artery flow volume. It can also be observed at the venous level with a greater proportion of the ipsilateral pulmonary blood flow passing through the non-obstructed vein. The possibilities of multi-site and bilateral obstruction must be taken into consideration when interpreting flow data. The pulmonary arterial flow curve may show signs of pulmonary arterial hypertension, with an earlier systolic peak, diminished peak velocity, additional late systolic and diastolic peaks and a deep nadir in early diastole. The flow profile of the affected pulmonary vein is typically dampened with decreased amplitude. The average velocity of flow in the pulmonary vein is typically low when measured "upstream" of the stenosis and accelerated "downstream" from it (Grosse-Wortmann et al. 2007; Valsangiacomo et al. 2003b). Similar to phase-contrast CMR a lung perfusion scan with 99 m-technetium-labeled macroaggregated albumin shows reduced relative perfusion of the affected lung (Drubach et al. 2015). Cardiac catheterization is useful in the quantification of the severity of pulmonary arterial hypertension and in the anatomical delineation of the stenotic segment. When evaluating a fluoroscopic angiogram in the postero-anterior projection it should be remembered, however, that the cranio-caudal diameter in this view is often preserved despite significant narrowing in the antero-posterior dimension.

3.5.4 Treatment

In principle, two different surgical techniques are used to connect the pulmonary veins to the left atrium: With the "conventional repair," the pulmonary veins are directly sutured to the left atrium. In contrast, with the atriopericardial anastomosis, often referred to as "sutureless repair," a wide communication between the left atrium and the incised pulmonary veins is created using a pericardial patch. Both approaches are burdened with risks of restenosis (Greenway et al. 2011). Postoperative pulmonary venous obstruction manifests most commonly during the first year after surgery and can develop rapidly. Imaging surveillance consists out of a combination of echocardiography and cross-sectional imaging. Given the limitations of echocardiography in the diagnosis of pulmonary vein stenosis CT or CMR is recommended at least once or twice during the first postoperative year and in greater intervals thereafter. Percutaneous approaches to pulmonary vein obstruction with angioplasty and stenting have yielded disappointing results. Attempts at pharmacological interventions that target the fibrotic vascular remodeling give rise to optimism, but are experimental at the time of writing (Zhu et al. 2014).

References

Agnoleti G, Annecchino F, Preda L, Borghi A (1999) Persistence of the left superior caval vein: can it potentiate obstructive lesions of the left ventricle? Cardiol Young 9(3):285–290

Babb JD, McGlynn TJ, Pierce WS, Kirkman PM (1981) Isolated partial anomalous venous connection: a congenital defect with late and serious complications. Ann Thorac Surg 31(6):540–541

Bartram U, Van Praagh S, Levine JC, Hines M, Bensky AS, Van Praagh R (1997) Absent right superior vena cava in visceroatrial situs solitus. Am J Cardiol 80(2):175–183

Beerbaum P, Korperich H, Barth P, Esdorn H, Gieseke J, Meyer H (2001) Noninvasive quantification of left-to-right shunt in pediatric patients: phase-contrast cine magnetic resonance imaging compared with invasive oximetry. Circulation 103(20):2476–2482

Bernstein HS, Moore P, Stanger P, Silverman NH (1995) The levoatriocardinal vein: morphology and echocardiographic identification of the pulmonary-systemic connection. J Am Coll Cardiol 26(4):995–1001

Blalock A, Cunningham RS, Robinson CS (1936) Experimental production of chylothorax by occlusion of the superior vena cava. Ann Surg 104(3):359–364

Brown JW (2009) Pulmonary venous anomalies. In: Lai WW, Mertens L, Cohen M, Geva T (eds) Echocardiography in pediatric and congenital heart disease : from fetus to adult, 2nd edn. Wiley-Blackwell, London, United Kingdom, pp 119–142

Brown DW, Geva T (2013) Anomalies of the pulmonary veins. In: Allen HD, Driscoll DJ, Shaddy RE, Feltes TF (eds) Moss and Adams heart disease in infants, children, and adolescents: including the fetus and young adult, 8th edn. Lippincott Williams & Wilkins, Philadelphia, pp 809–839

Chen SJ, Liu KL, Chen HY, Chiu IS, Lee WJ, Wu MH et al (2005) Anomalous brachiocephalic vein: CT, embryology, and clinical implications. AJR Am J Roentgenol 184(4):1235–1240

Cheng C, Kuang LQ, Jiang MR, Hu YJ, Wang Y (2015) Mixed Supra- and intracardiac totally anomalous pulmonary venous connection in an adult female: pre- and postoperative evaluation with emphasis on MDCT angiographic advantages. Heart Lung Circ 24(11):e188–e192

Chiari H (1897) Über Netzbildungen im rechten Vorhof des Herzens. Beitr Pathol Anat 22:1–10

Chin AJ (1994) Subcostal two-dimensional echocardiographic identification of right superior vena cava connecting to left atrium. Am Heart J 127(4 Pt 1):939–941

Choi JY, Jung MJ, Kim YH, Noh CI, Yun YS (1990) Anomalous subaortic position of the brachiocephalic vein (innominate vein): an echocardiographic study. Br Heart J 64(6):385–387

Choi HS, Choi BW, Choe KO, Choi D, Yoo KJ, Kim MI et al (2004) Pitfalls, artifacts, and remedies in multidetector row CT coronary angiography. Radiographics 24(3):787–800

Cochrane AD, Marath A, Mee RB (1994) Can a dilated coronary sinus produce left ventricular inflow obstruction? An unrecognized entity. Ann Thorac Surg 58(4):1114–1116

Craig JM, Darling RC, Rothney WB (1957) Total pulmonary venous drainage into the right side of the heart; report of 17 autopsied cases not associated with other major cardiovascular anomalies. Lab Investig 6(1):44–64

de Leval MR, Ritter DG, McGoon DC, Danielson GK (1975) Anomalous systemic venous connection. Surgical considerations. Mayo Clin Proc 50(10):599–610

Drubach LA, Jenkins KJ, Stamoulis C, Palmer EL 3rd, Lee EY (2015) Evaluation of primary pulmonary vein stenosis in children: comparison of radionuclide perfusion lung scan and angiography. AJR Am J Roentgenol 205(4):873–877

Franchi-Abella S, Branchereau S, Lambert V, Fabre M, Steimberg C, Losay J et al (2010) Complications of congenital portosystemic shunts in children: therapeutic options and outcomes. J Pediatr Gastroenterol Nutr 51(3):322–330

Gerlis LM, Ho SY (1989) Anomalous subaortic position of the brachiocephalic (innominate) vein: a review of published reports and report of three new cases. Br Heart J 61(6):540–545

Geva T (2013) Abnormal systemic venous connections. In: Allen HD, Driscoll DJ, Shaddy RE, Feltes TF (eds) Moss and Adams heart disease in infants, children, and adolescents : including the fetus and young adult, 8th edn. Lippincott Williams & Wilkins, Philadelphia, pp 840–863

Goo HW, Al-Otay A, Grosse-Wortmann L, Wu S, Macgowan CK, Yoo SJ (2009) Phase-contrast magnetic resonance quantification of normal pulmonary venous return. J Magn Reson Imaging 29(3):588–594

Greenway SC, Yoo SJ, Baliulis G, Caldarone C, Coles J, Grosse-Wortmann L (2011) Assessment of pulmonary veins after atrio-pericardial anastomosis by cardiovascular magnetic resonance. J Cardiovasc Magn Reson 13:72

Grosse-Wortmann L, Al-Otay A, Goo HW, Macgowan CK, Coles JG, Benson LN et al (2007) Anatomical and functional evaluation of pulmonary veins in children by magnetic resonance imaging. J Am Coll Cardiol 49(9):993–1002

Guiraudon GM, Guiraudon CM, Klein GJ, Sharma AD, Yee R (1988) The coronary sinus diverticulum: a pathologic entity associated with the Wolff-Parkinson-White syndrome. Am J Cardiol 62(10 Pt 1):733–735

Huhta JC, Smallhorn JF, Macartney FJ, Anderson RH, de Leval M (1982) Cross-sectional echocardiographic diagnosis of systemic venous return. Br Heart J 48(4):388–403

Huhta JC, Smallhorn JF, Macartney FJ (1984) Cross-sectional echocardiographic diagnosis of azygos continuation of the inferior vena cava. Catheter Cardiovasc Diagn 10(3):221–232

Kakitsubata Y, Kakitsubata S, Kiyomizu H, Ogawa T, Kato K, Watanabe K (1996) Intrahepatic portal-hepatic venous shunts demonstrated by US, CT, and MR imaging. Acta Radiol 37(5):680–684

Kerkar P, Vora A, Kulkarni H, Narula D, Goyal V, Dalvi B (1996) Percutaneous balloon dilatation of cor triatriatum sinister. Am Heart J 132(4):888–891

Kudo M, Tomita S, Tochio H, Minowa K, Todo A (1993) Intrahepatic portosystemic venous shunt: diagnosis by color Doppler imaging. Am J Gastroenterol 88(5):723–729

Kulkarni S, Jain S, Kasar P, Garekar S, Joshi S (2008) Retroaortic left innominate vein - Incidence, association with congenital heart defects, embryology,

and clinical significance. Ann Pediatr Cardiol 1(2):139–141

Li WW, Koolbergen DR, Bouma BJ, Hazekamp MG, de Mol BA, de Winter RJ (2015) Cathether-based interventional strategies for cor triatriatum in the adult - feasibility study through a hybrid approach. BMC Cardiovasc Disord 15:68

Lucas RV Jr, Krabill KA (1995) Abnormal systemic venous connections. In: Emmanouilides GC, Reimenschneider TA, Allen HD (eds) Heart disease in infants, children and adolescents, 5th edn. Williams and Wilkins, Balimore, pp 874–902

Lucas RV Jr, Lester RG, Lillehei CW, Edwards JE (1962) Mitral atresia with levoatriocardinal vein. A form of congenital pulmonary venous obstruction. Am J Cardiol 9:607–613

Lucas RV Jr, Anderson RC, Amplatz K, Adams P Jr, Edwards JE (1963) Congenital causes of pulmonary venous obstruction. Pediatr Clin N Am 10:781–836

Maeda T, Mori H, Aikawa H, Komatsu E, Kagawa K (1993) Therapeutic embolization of intrahepatic portosystemic shunts by retrograde transcaval catheterization. Cardiovasc Intervent Radiol 16(4):245–247

Meadows WR, Sharp JT (1965) Persistent left superior vena cava draining into the left atrium without arterial oxygen unsaturation. Am J Cardiol 16:273–279

Nabarro D (1903) Two hearts showing peculiarities of the great veins. J Anat Physiol 37(Pt 4):382–391

Niwayama G (1960) Cor triatriatum. Am Heart J 59:291–317

Rice TW, Rodriguez RM, Light RW (2006) The superior vena cava syndrome: clinical characteristics and evolving etiology. Medicine 85(1):37–42

Roman KS, Kellenberger CJ, Macgowan CK, Coles J, Redington AN, Benson LN et al (2005) How is pulmonary arterial blood flow affected by pulmonary venous obstruction in children? A phase-contrast magnetic resonance study. Pediatr Radiol 35(6):580–586

Saalouke MG, Shapiro SR, Perry LW, Scott LP 3rd. (1977) Isolated partial anomalous pulmonary venous drainage associated with pulmonary vascular obstructive disease. Am J Cardiol 39(3):439–444

Sanders JM (1946) Bilateral superior vena cava. Anat Rec 94:657–662

Seller N, Yoo SJ, Grant B, Grosse-Wortmann L (2018) How many versus how much: comprehensive haemodynamic evaluation of partial anomalous pulmonary venous connection by cardiac MRI. Eur Radiol 28(11):4598–4606

Shapiro EP, Al-Sadir J, Campbell NP, Thilenius OG, Anagnostopoulos CE, Hays P (1981) Drainage of right superior vena cava into both atria. Review of the literature and description of a case presenting with polycythemia and paradoxical embolization. Circulation 63(3):712–717

Sharoni E, Erez E, Birk E, Katz J, Dagan O (2001) Superior vena cava syndrome following neonatal cardiac surgery. Pediatr Crit Care Med 2(1):40–43

Smallhorn J, Anderson RH (2010) Anomalous systemic venous return. In: Anderson RH, Baker EJ, Penny DJ, Redington AN, Rigby ML, Wernovsky G (eds) Paediatric cardiology, 3rd edn. Churchill Livingstone/ Elsevier, Philadelphia, PA, pp 485–496

Smallhorn JF, Zielinsky P, Freedom RM, Rowe RD (1985) Abnormal position of the brachiocephalic vein. Am J Cardiol 55(1):234–236

Tham EB, Ross DB, Giuffre M, Smallhorn J, Noga ML (2007) Images in cardiovascular medicine. Cardiac magnetic resonance imaging of a coronary sinus diverticulum associated with congenital heart disease. Circulation 116(21):e541–e544

Uchino T, Endo F, Ikeda S, Shiraki K, Sera Y, Matsuda I (1996) Three brothers with progressive hepatic dysfunction and severe hepatic steatosis due to a patent ductus venosus. Gastroenterology 110(6):1964–1968

Valsangiacomo ER, Levasseur S, McCrindle BW, MacDonald C, Smallhorn JF, Yoo SJ (2003a) Contrast-enhanced MR angiography of pulmonary venous abnormalities in children. Pediatr Radiol 33(2): 92–98

Valsangiacomo ER, Barrea C, Macgowan CK, Smallhorn JF, Coles JG, Yoo SJ (2003b) Phase-contrast MR assessment of pulmonary venous blood flow in children with surgically repaired pulmonary veins. Pediatr Radiol 33(9):607–613

Van Praagh R, Van Praagh S (1990) Atrial isomerism in the heterotaxy syndromes with asplenia, or polysplenia, or normally formed spleen: an erroneous concept. Am J Cardiol 66(20):1504–1506

Van Praagh S, Geva T, Lock JE, Nido PJ, Vance MS, Van Praagh R (2003) Biatrial or left atrial drainage of the right superior vena cava: anatomic, morphogenetic, and surgical considerations--report of three new cases and literature review. Pediatr Cardiol 24(4):350–363

Yoo SJ, Epelman M (2010) Partial and total anomalous pulmonary venous connections. In: Yoo SJ, MacDonald C, Babyn P (eds) Chest radiographic interpretation in pediatric cardiac patients. Thieme Medical Publishers, New York, NY, pp 206–214

Yoo SJ, Geoffray A (2010) Congenital stenosis and atresia of the individual pulmonary veins. In: Yoo SJ, MacDonald C, Babyn P (eds) Chest radiographic interpretation in pediatric cardiac patients. Thieme Medical Publishers, New York, NY, pp 206–214

Zhu J, Ide H, Fu YY, Teichert AM, Kato H, Weisel RD et al (2014) Losartan ameliorates "upstream" pulmonary vein vasculopathy in a piglet model of pulmonary vein stenosis. J Thorac Cardiovasc Surg 148(6): 2550–2557

Coronary Artery Anomalies

Andrew M. Crean

Contents

A.M. Crean, M.R.C.P., F.R.C.R.
Sanghvi Endowed Chair in Cardiovascular Imaging Professor of Cardiology and Pediatrics, University of Cincinnati Medical Center and Cincinnati Children's Hospital Medical Center, Cincinnati, OH, USA
e-mail: andrewcrean@gmail.com

1 Introduction

Coronary anomalies are uncommon yet occur not infrequently in the practice of any regular cardiac imager. They can be among both the most challenging and satisfying of lesions to investigate, and frequently noninvasive imaging represents the standard of reference for full description and understanding of the abnormality in question. This article uses a broad definition of coronary anomalies to include all non-atherosclerotic forms of coronary abnormality—not simply congenital anomalies, but also inflammatory anomalies (e.g., due to Kawasaki or Behcet disease) and postsurgical anomalies (e.g., after Ross, Bentall, or arterial switch procedure).

2 Prevalence of Congenital Coronary Anomalies

The prevalence of congenital coronary anomalies appears to have been rising in recent years, and yet this is almost certainly ascertainment bias due to the increased use of cardiac CT in particular which may identify anomalies without great clinical significance (as well as a much smaller number of prognostically important lesions). Most case series have reported a prevalence of around 1% when large cohorts of patients undergoing either coronary angiography or cardiac CT are examined (Table 1).

Med Radiol Diagn Imaging (2018)
DOI 10.1007/174_2017_170, © Springer International Publishing AG
Published Online: 09 March 2018

Table 1 Prevalence of congenital coronary anomalies in different series

First author	Country	Modality of diagnosis	Population size	Prevalence (%)	Commonest anomaly
Namgung (2014)	South Korea	Cardiac CT	8864	1.16	AORCA
Yuksel (2013)	Turkey	Coronary angiography	16,573	1.3	Separate origin LAD, Cx
Xu (2012)	China	Cardiac CT	12,145	1.02	AORCA
Sohrabi (2012)	Iran	Coronary angiography	6065	1.3	Separate origin LAD, Cx
Sivri (2012)	Turkey	Coronary angiography	12,844	0.74	AOLCx
Fujimoto (2011)	Japan	Cardiac CT	5869	1.52	AORCA
Erol (2011)	Turkey	Cardiac CT	2096	1.96	AORCA and separate origin LAD, Cx
Garg (2000)	India	Coronary angiography	4100	0.95	AORCA
Graidis (2015)	Greece	Cardiac CT	2572	2.33[a]	Separate origin LAD, Cx
Yamanaka (1990)	USA	Coronary angiography	126,595	1.3[a]	Separate origin LAD, Cx
Yildiz (2010)	Turkey	Coronary angiography	12,457	0.9	Separate origin LAD, Cx
Tongut (2016)	Turkey	Cardiac CT	2401	9.37[b]	Separate origin LAD, Cx
Shabestari (2012)	Iran	Cardiac CT	2697	3.1	Separate origin LAD, Cx
Eid (2009)	Lebanon	Coronary angiography	4650	0.73	AOLCx

LAD left anterior descending, *Cx* circumflex, *AORCA* anomalous origin of the right coronary artery (from the opposite sinus), *AOLCx* anomalous origin of the left circumflex

[a]Did not exclude abnormalities of high takeoff which are excluded a priori in most other series

[b]Did not exclude myocardial bridges which are relatively common in the general population—exclusion of these 100 patients reduced their overall prevalence to 5.7%. A further 85 patients were said to have coronary aneurysm or ectasia (no definition provided in methods) which could well have been atherosclerotic (mean age 56 years) or due to prior Kawasaki disease. Exclusion of these patients reduces the prevalence of "true" congenital coronary anomalies to 2.1% which is closer to most other published series

3 Classification of Coronary Anomalies?

Coronary anomalies may initially be subdivided into those present at birth and those which develop at some point after birth because of inflammation or vasculitis (Kawasaki disease, Behcet disease, etc.) or secondary to an operation which involves detachment and reimplantation of the coronary arteries. This chapter is principally concerned with the former, although the latter two categories will be touched upon briefly.

After this basis subdivision, congenital coronary anomalies are best broken down further by the simple classification of:

(a) Abnormalities of origin
(b) Abnormalities of course
(c) Abnormalities of termination

Examples of each are provided in Table 2. These categories are not always totally discrete—abnormalities of origin and proximal course, for example, may accompany one another. Most of the abnormalities in categories a and b are benign, although a few are not. The most significant abnormalities in this regard are the origin of the left or

Table 2 Examples of the most common coronary anomalies and their relative clinical significance (in the author's opinion)

Congenital	Anomaly	Clinical importance
Abnormalities of origin	Anomalous aortic origin from the opposite coronary sinus	High (especially if proximal intramural course)
	Ectopic origin above aortic sinus	Low
Abnormalities of course	Transseptal/infundibular left coronary	Low
	Retro-aortic circumflex	Low
	Pre-pulmonic LAD	Low
	Myocardial bridging	Low
Abnormalities of termination	Circumflex to coronary sinus/right atrial fistula	Intermediate
	Anomalous left coronary artery draining to the pulmonary artery (ALCAPA)	High
	Anomalous right coronary artery draining to the pulmonary artery (ARCAPA)	Intermediate/low
Inflammatory or Vasculitic	Kawasaki disease	High (if aneurysms)
	Behcet disease	High (if aneurysms)
	Takayasu arteritis	High (if stenoses)
Postoperative	Post-arterial switch	Intermediate/low
	Post-Ross procedure	Low
	Post-Bentall procedure	Low

right coronary artery from the opposite sinus of Valsalva. Anomalous origin of the right coronary artery is being seen increasingly frequently due to rapid uptake of cardiac CT and often generates management dilemmas, particularly when a patient presents with symptoms that *might* represent angina but where no objective evidence of ischemia can be found.

Abnormalities of termination generally involve fistulation into another vascular structure or a cardiac chamber. They range from the trivial to the significant.

4 Are All Coronary Anomalies Equally Dangerous?

Table 2 suggests that the answer to this question is no. A more difficult question, however, is *which* anomalies may be life-threatening and how do we identify them. Our knowledge of the natural history of coronary anomaly lesions is incomplete and inadequate. Most of our data is derived from selected pathologic series of civilian deaths or deaths of military recruits during training. In these samples the larger denominator—the numbers of people with identical anomalies but who do *not* die—is unknown.

4.1 Anomalies of Origin

Awareness of the potential for cardiac mortality was raised almost 50 years ago following review of the exhibits at the Armed Forces Institute of Pathology (Cheitlin et al. 1974). This series was among the first to suggest that origin of the left main or left anterior descending (LAD) coronary artery from the right sinus appeared to be disproportionately associated with sudden cardiac death in the setting of exercise. Although not clearly described, the implied mechanism was that of ostial narrowing of the vessel as it emerged obliquely through the aortic wall (Fig. 1). They further suggested that as aortic pressure increases with exercise, there could be a "flap-valve" effect whereby the ostial abnormality

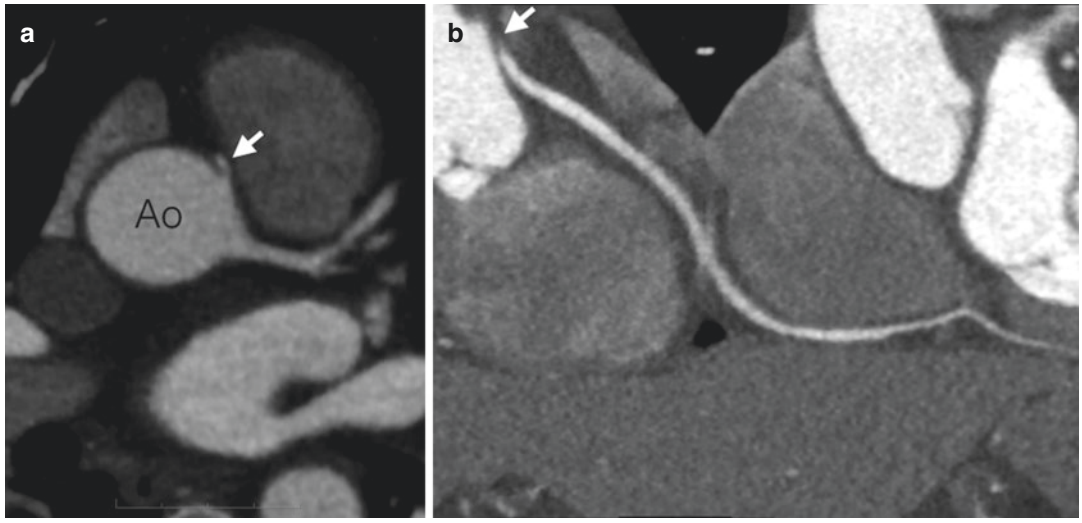

Fig. 1 Intramural right coronary artery (RCA) arising from the left coronary sinus. (**a**) Gated axial CT image at the level of the aortic root (Ao). The RCA arises from the left coronary cusp, and in its most proximal portion, it takes an intramural course through the aortic wall (arrow). (**b**) The effect of intramural passage in creating a slit-like orifice is better appreciated on this curved multiplayer reformat where the ostial portion of the vessel (arrow) appears tightly stenosed compared to its more distal caliber

transiently worsens. Interestingly they saw no cases where an anomalous right coronary artery (RCA) arising from the left sinus of Valsalva led to sudden death; however, it is worth noting that this anomaly—which they display in Fig. 2 of their original publication—does *not* demonstrate the slit-like intramural course which we know to be present from cardiac CT data in this era. Therefore we must question whether their data on this lesion can really be applied to the patient population we see increasingly.

A similar review was performed by the Pathology branch of the National Heart Lung and Blood Institute (Kragel and Roberts 1988). In this series five out of seven cases where the left main (LM) coronary artery arose from the opposite sinus resulted in sudden death. Outcome for patients where the RCA arose from the opposite sinus was more variable with only 8 out of 25 dying as a result of their coronary lesion. In this paper great attention was paid to morphology of the coronary ostia. Out of the 25 cases of RCA from the opposite sinus, 14 were shown to have slit-like morphology of whom only 6 were believed to have died because of the anomaly itself (clear alternative causes of death in the remaining 8 patients). Interestingly, however, two of the patients with RCA from the opposite sinus but *without* a slit-like origin were also classified as having died suddenly and presumably related to their anomaly as no other cause was determined. Overall then, eight patients were presumed to have died from their RCA abnormality; however, the body of the paper goes on to mention that three of these eight had evidence of at least one 75% stenosis in an epicardial coronary vessel and one out of the eight had evidence of hypertrophic cardiomyopathy. So in effect four of the eight sudden deaths may have had an alternative explanation. A further possible confounder is whether or not an anomalous RCA provides the posterior descending artery (i.e., shows right coronary dominance) since this determines the extent of myocardium at risk.

A third necropsy series considered ten patients with RCA from the opposite sinus, three of whom died presumably due to acute ischemia caused by the lesion (each case related to exercise) and seven in whom the abnormality was an incidental finding after death from another cause (Roberts et al. 1982). Interestingly each one of the ten cases had a slit-like RCA ostium, but what

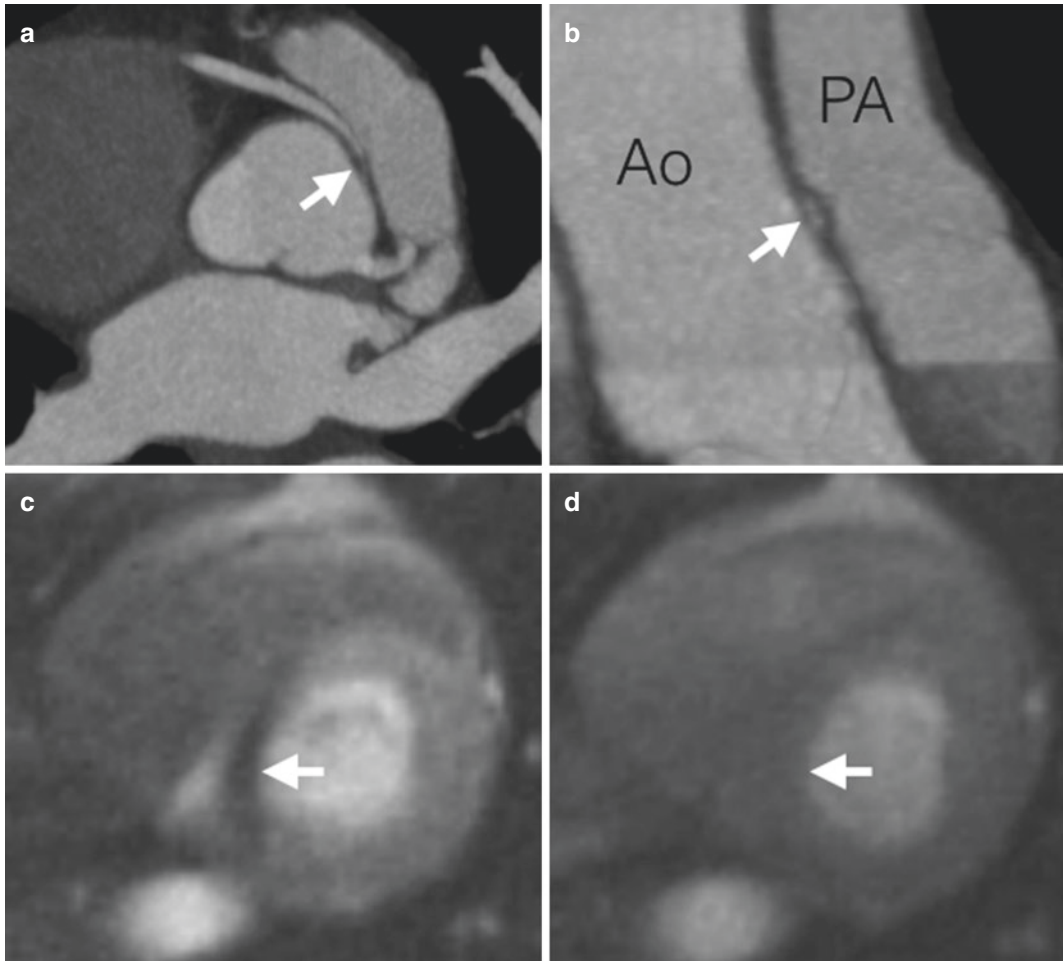

Fig. 2 Anomalous RCA from the left coronary sinus with evidence of ischemia. (**a**) Axial slice from gated CT at the level of the aortic root demonstrates that the RCA arises from the left coronary cusp and has a slit-like origin in its proximal portion (arrow). (**b**) Sagittal oblique reconstruction from gated CT to show the relationship between the aortic root (Ao) and main pulmonary artery (PA). The slit-like ostium can be appreciated in cross section (arrow) as the vessel runs through the aortic wall. (**c**) Basal slice from dipyridamole stress perfusion CMR. A low-signal perfusion defect is present in the inferior septum (arrow). (**d**) Basal slice from dipyridamole stress perfusion CMR 6 months after unroofing surgery which alleviated the patient's symptoms. No evidence of a perfusion abnormality is seen on stress imaging

seemed to be more significant was the presence of macroscopic left ventricular scarring which was present in all three of the sudden death cases but only one out of seven of the noncardiac death cases (and this is in a patient with severe atherosclerotic disease). The same four patients also were the only ones to have evidence of myocardial interstitial fibrosis at histopathology.

At the current time the general consensus is that when the left main or LAD coronary artery arises from the opposite sinus, the patient should be offered surgical repair. Given the rare occurrence of this pathology, no survival or outcome data are available. Anomalous origin of the RCA does not necessarily require repair, particularly when an incidental finding. Patients, however, who have anginal symptoms or evidence of ischemia on testing (Fig. 2) should be considered for repair on a case-by-case basis.

4.2 Anomalies of Termination

This kind of anomaly includes coronary fistulae and anomalous left coronary artery from the pulmonary artery (ALCAPA) which in a way may also considered to be a special kind of fistula. The frequency of congenital coronary fistulae is roughly 0.2% (Gillebert et al. 1986). If fistulae are large in size, they may lead to progressive volume loading of a ventricular chamber with the risk for gradual deterioration in myocardial function (Lee and Chen 2009). Large fistulae may also be associated with a risk of myocardial ischemia (see ALCAPA, below). Another risk which has been associated with fistulae is that of bacterial endocarditis (Said 2016). Finally—although underappreciated—there is a mortality risk associated with long duration fistulae, particularly if untreated (Nakahira et al. 2007; Rajs et al. 2001; Dichtl et al. 2005; Lau 1995; Bartoloni et al. 2012; Lozano et al. 2008). It has been suggested that the risk of rupture associated with fistulae may be higher in women than men (Said et al. 2008) (Fig. 3).

Anomalous left coronary artery from the pulmonary artery (ALCAPA) is a particularly important type of fistulous lesion since it can be associated with sudden cardiac death in both children and adults. This is assumed to be secondary to ischemia and arrhythmia occurring as a result of myocardial steal, as coronary flow is exposed to low-pressure runoff into the pulmonary artery which invariably has a lower diastolic pressure than the aorta. Although the majority of such lesions are detected in early childhood, there are regular reports of first detection of ALCAPA in adulthood (Basha et al. 2016; Hofmeyr et al. 2009; Sajjadieh Khajouei et al. 2016; Toumpourleka et al. 2015; Liu and Miller 2012; Lopes et al. 2011) and in rare cases, even in the elderly (Sadanandan et al. 2012; Fierens et al. 2000). As with other kinds of fistula, there may be aneurysmal dilatation of either left or right coronary artery (Bajona et al. 2007), and this can occur even *after* surgical repair (Bravo-Valenzuela and Silva 2015). On occasion the initial presentation in adult life may be with heart failure or cardiac arrest (Safaa et al. 2013; Quah et al. 2014; Krexi and Sheppard 2013; Kristensen et al. 2008; Pachon et al. 2015; Ripley et al. 2014; Raghuram et al. 2004; Kang et al. 2007; Frapier et al. 1999). For a comprehensive review of ALCAPA imaging in adults, see Pena et al. (2009).

5 Structured Imaging of Coronary Anomalies

Patients are generally sent for imaging with varying degrees of prior knowledge about their lesion. In some cases the provided information may be misleading or frankly incorrect. It is important

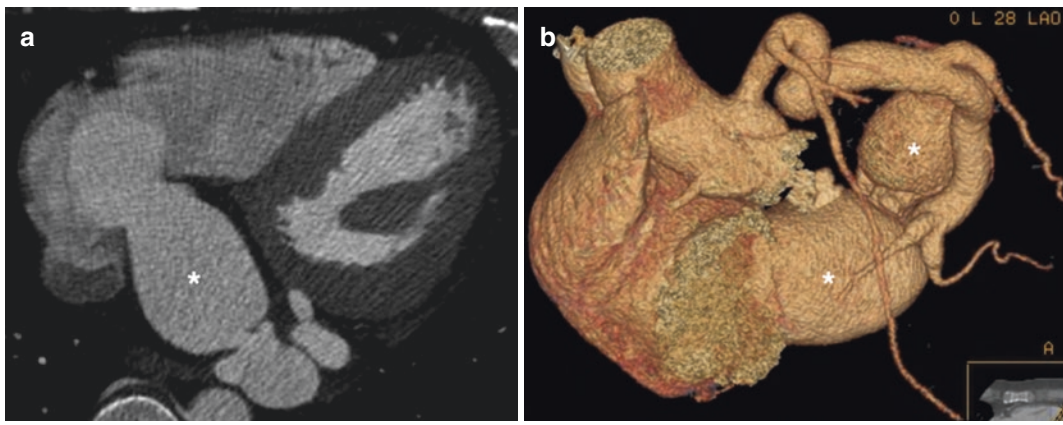

Fig. 3 Left circumflex artery to coronary sinus fistula. (**a**) Gated axial CT image demonstrating a very dilated coronary sinus (asterisk) draining into the right atrium. (**b**) Volume-rendered CT image of the same patient showing more clearly the fistulous communication between the circumflex artery and the coronary sinus

therefore to consider a structured and comprehensive imaging approach for imaging coronary anomalies. The key issues to be addressed by imaging are coronary anatomy, myocardial ischemia, myocardial scar, and the presence or absence of coronary thrombus.

5.1 Anatomic Imaging

Any assessment of a coronary anomaly necessitates a clear understanding of the entire course of the vessel in question—from origin to termination. Although some patients may be sent to the noninvasive lab *after* coronary angiography, invasive angiography is rarely the best method to appreciate the three-dimensional relationship between the coronary artery and surrounding structures. Cardiac MR has been touted as a reliable method for assessing coronary anomalies and certainly can provide a level of information about the vessel's course. However the most frequently used technique for coronary imaging by CMR is a free-breathing navigated steady-state free precession (SSFP) approach which is very dependent upon both heart rate and respiratory pattern for data acquisition. A complete axial 3D volume may therefore take 10–15 min to acquire. Since the quality of the volume stack of images can not be assessed until the last slice is acquired, it unfortunately happens on occasion that the overall image quality is inadequate and up to 10-15 minutes of imaging time will have been wasted acquiring. Nonetheless if a CMR study is planned, we usually attempt coronary imaging and often find it helpful. In situations where the right coronary artery is suspected to arise from the left coronary sinus, or where there is concern for a slit-like origin, then our experience has been that coronary imaging by CMR is often insufficient for diagnostic certainty, and we proceed to cardiac CT in those circumstances.

Cardiac CT is an excellent modality for anatomic coronary imaging, facilitating visualization of coronary origin, course, termination (Su et al. 2010), as well as luminal remodeling, stenosis, and aneurysm. Modern scanners invariably permit prospectively triggered acquisition which limits radiation exposure to a small portion of the cardiac cycle. Overall doses for coronary CT are usually in the range of 1–3 mSv which compares very favorably with invasive angiography and SPECT imaging. In thin patients it is possible to perform sub-millisievert studies through judicious reduction in tube kilovoltage (kV). As a result cardiac CT is now a reasonable option in children (Shen et al. 2016) although historical concerns regarding dose have limited its usage (which is ironic considering how widespread the use of SPECT imaging is in many pediatric institutions).

The isotropic spatial resolution of a modern CT scanner is in the region of 0.5 mm^3, which is 2–3 times better than that achieved by standard CMR angiography and is the reason why the potential proximal intramural portion of a coronary anomaly is better assessed by CT than CMR. The other benefit of CT is its ability to detect atherosclerotic coronary disease which—in patients who present at an older age—may be the real reason for symptoms rather than the coronary anomaly, accused but an innocent bystander (Keir et al. 2017; Crean et al. 2008).

5.2 Ischemia Imaging

The single biggest concern for most anomalies is whether or not they have the potential to result in myocardial ischemia and, subsequently, arrhythmic sudden cardiac death. There is no consensus in the literature or among experts as to how coronary anomalies should be investigated—as a result most groups work toward their own internal consensus (Keir et al. 2015; Gräni et al. 2017). In many centers, myocardial perfusion stress/rest SPECT imaging is utilized to stratify risk. However the larger cohort studies all contain individuals who dropped dead at some time point after a previously normal perfusion study which is hardly reassuring (Basso et al. 2000). More pertinent perhaps is the frequency of false positive results, both before and *after* surgical repair (Brothers et al. 2007).

Stress echo with exercise or dobutamine for wall motion assessment may be a reasonable choice for the assessment of ischemia given its

widespread availability. Myocardial contrast perfusion echo on the other hand is much less practiced, and its use is only very rarely described in the setting of coronary anomalies (Rana et al. 2009). As with all other forms of noninvasive imaging, evidence supporting the diagnostic and prognostic power of stress echo is lacking in this population (Thompson 2015).

Stress perfusion CMR has been shown to have a substantially higher diagnostic *and* prognostic accuracy than SPECT imaging for obstructive atheromatous coronary artery disease (Greenwood et al. 2012, 2016). Conflicting nuclear data suggest that triage by either technique is reasonable with similar medium-term outcomes (Sharples et al. 2007; Thom et al. 2014). There are few corresponding data for congenital heart disease patients, although one study which directly compared isotope perfusion to CMR perfusion in an adult arterial switch population demonstrated a high false positive rate for the nuclear technique (Tobler et al. 2014). Coronary stenosis after coronary reimplantation is relatively rare but is seen on occasion (Fig. 4). We have now studied over 100 patients with stress perfusion CMR in the Toronto Coronary Anomaly Clinic, and our experience is described elsewhere (Deva et al. 2014; Crean et al. 2016). Briefly, among those where a formal reference standard was available for comparison, stress perfusion cardiovascular magnetic resonance demonstrated a sensitivity of 82% and specificity of 100%. Of the 34 studies, two were false negatives, in which the etiology of ischemia was extrinsic arterial compression rather than intrinsic coronary luminal narrowing.

We and others have found that the ALCAPA lesions invariably show evidence of myocardial perfusion abnormality (Nony et al. 1992) but that anomalies of coronary origin—particularly the right coronary from the left cusp with proximal intramural course—are much more variable. Our approach has been to seek to confirm either a positive or negative vasodilator stress CMR study with a second modality, usually stress echocardiography. This latter is chosen because of persistent concerns in some quarters that physiologic stress which raises the blood pressure and dilates the aortic root may promote ischemia to a greater extent than simple drug-induced coronary vasodilatation.

Any anomaly which is demonstrated to generate ischemia is usually subjected to surgical repair. The more difficult scenario arises when stress CMR and stress echo are both negative but the patient continues to complain of symptoms. In this situation we take an aggressive approach with coronary catheterization combined with intravascular ultrasound (IVUS) and measurement of fractional flow reserve (FFR). A 50% reduction in vessel cross-sectional origin at the ostium or an FFR < 0.8 generally results in a decision to proceed with surgical repair. If both

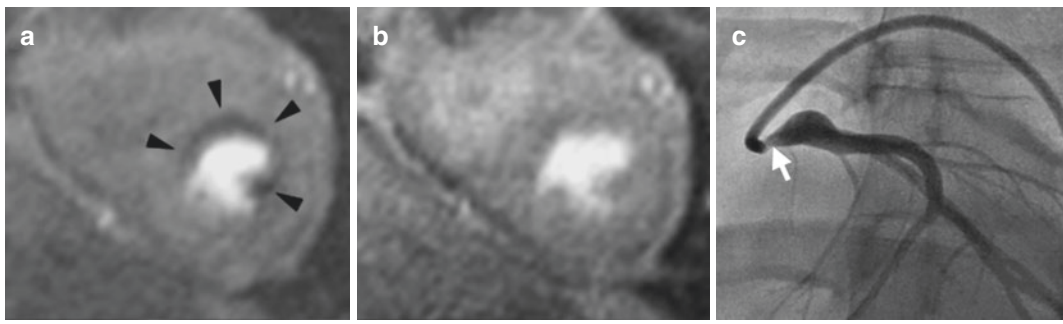

Fig. 4 Ischemia as a long-term complication of the arterial switch procedure. (**a**) Still frame from dipyridamole stress perfusion CMR study demonstrating subendocardial ischemia (arrowheads) in the left coronary territory. (**b**) Rest perfusion image shows normal perfusion. (**c**) Invasive angiogram depicting a significant left main stem coronary artery stenosis (arrow)

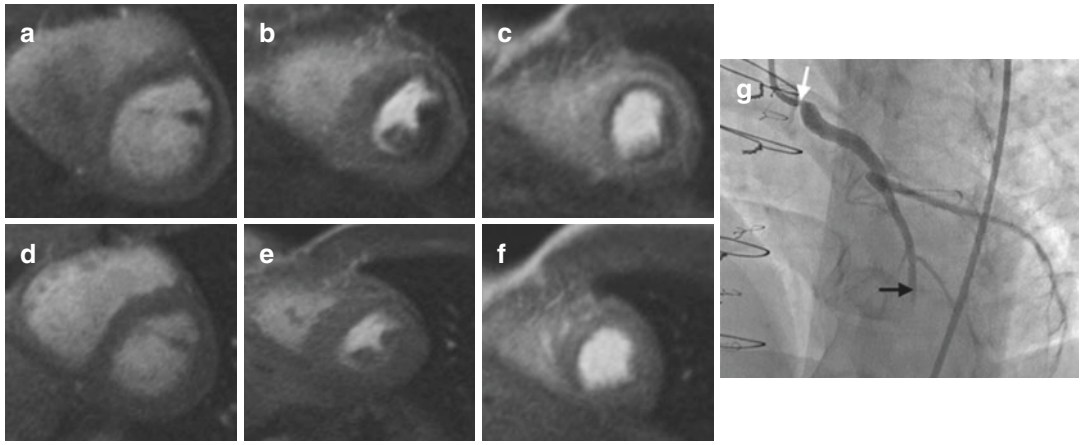

Fig. 5 Tight stenosis of reconstructed left main coronary artery following ALCAPA repair. (**a–c**) Basal, mid, and apical short axis slices from dipyridamole stress CMR study. There is an extensive low-signal defect throughout the left coronary territory. (**d–f**) The defect appears full reversible in matching locations at rest. (**g**) Invasive angiogram several days later. There is an extremely tight focal stenosis at the site of implantation of the left main coronary (arrow). Note also incomplete LAD filling due to competitive retrograde flow (black arrow) which still exists from the right coronary collateral network. The patient subsequently underwent left main stem stenting

IVUS and vasodilator FFR are normal, it may be reasonable to repeat FFR measurements with full dobutamine stress to mimic exercise (Angelini and Flamm 2007; Angelini 2014; Angelini et al. 2015; Lee et al. 2016).

Consideration should always be given to an early postoperative CMR study in order to establish a new baseline appearance should symptoms recur in the future. This is particularly important for ALCAPA patients in whom perfusion may not entirely normalize post repair (Seguchi et al. 1990) or where occlusion at the reimplantation site is suspected (Secinaro et al. 2011) (Fig. 5).

5.3 Scar Imaging

Patients with coronary anomalies are at risk of coronary thrombosis or, occasionally, coronary thromboembolism—both potentially resulting in myocardial infarction. There is little doubt that CMR is the gold standard for detection of myocardial scar, and late gadolinium enhancement (LGE) should be included in every CMR protocol when assessing coronary anomalies (Fig. 6). In patients with prior cardiac surgery (e.g., Ross, Bentall, or arterial switch procedure), it should be borne in mind that scar is not always due to the anomaly itself and that prior cardiopulmonary bypass may result in small areas of scarring. Patients who have had VSD patch closure may demonstrate an LGE signal in the region of repair due to overlying fibrotic tissue, and this needs to be distinguished from true myocardial damage. Genuine scar is a risk factor for adverse remodeling and arrhythmogenesis as it is in the noncongenital population and ideally should be quantitated in the imaging report. There is also increasing research interest in subclinical fibrosis in congenital cardiology using techniques such as T1 and ECV mapping (de Meester de Ravenstein et al. 2015; Burchill et al. 2017).

A small number of patients are unable to undergo LGE imaging due to claustrophobia or other CMR contraindications. In these cases SPECT imaging may substitute although it is insensitive for small amounts of scar (Wagner et al. 2003). However, if cardiac CT is planned, then a second study some minutes after contrast injection may be considered to demonstrate infarction by the technique of late iodine enhancement (Kramer et al. 1984) which is

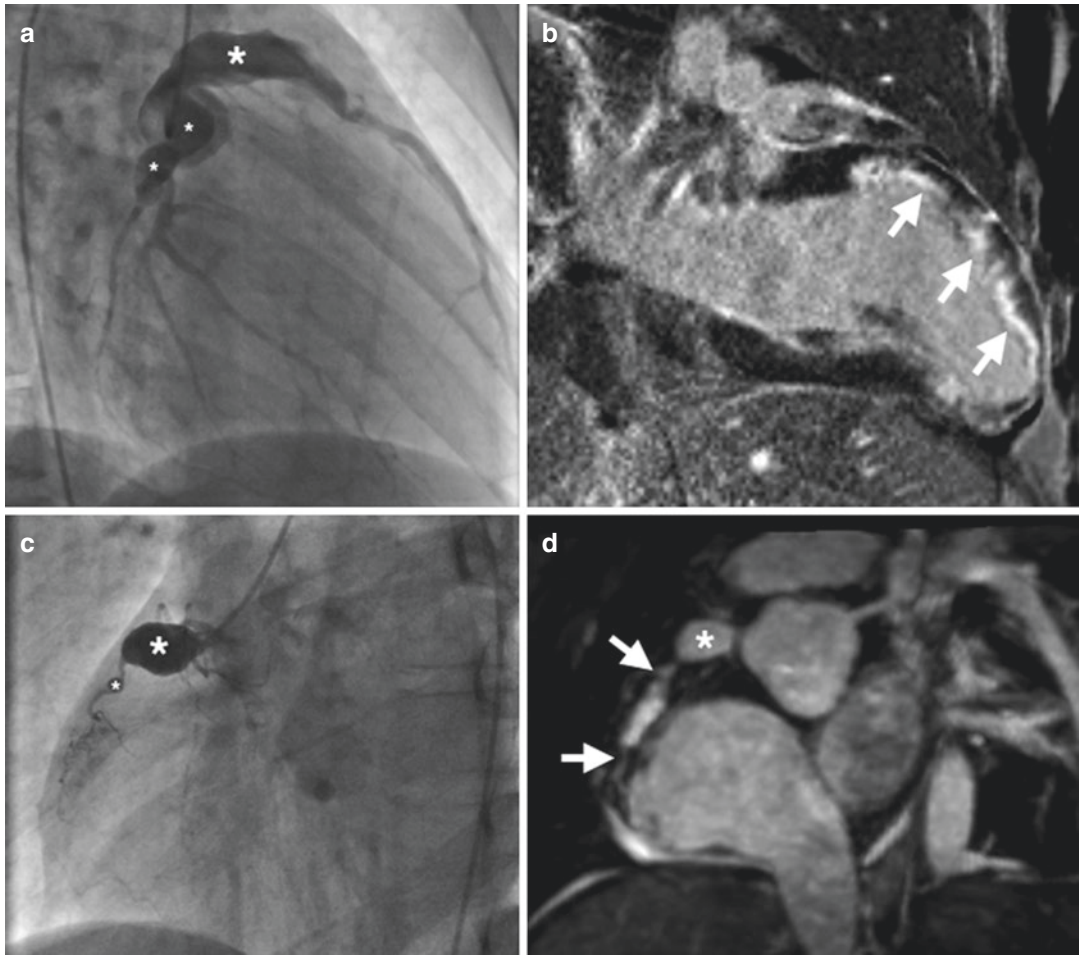

Fig. 6 Kawasaki disease complicated by myocardial infarction. (**a**) Invasive angiogram with injection into the left coronary system. There is a large tubular LAD aneurysm (asterisk) and two smaller sequential circumflex artery aneurysms (smaller asterisks). (**b**) Two chamber late gadolinium enhancement CMR image demonstrating an extensive subendocardial infarct (arrows) in the LAD territory. This occurred in adolescence in association with acute aneurysm thrombosis after the patient self-discontinued anticoagulation therapy. (**c**) Invasive angiogram in the same patient shows a large proximal RCA aneurysm (large asterisk) together with a much smaller one more distally (smaller asterisk). (**d**) Short axis reformat from whole-heart navigated free-breathing CMR coronary angiogram. The aneurysms in the RCA are clearly appreciated, but note that delineation of the intervening vessel segments (arrows) is inferior compared to invasive angiography (prior frame)

analogous to LGE imaging albeit with lower contrast and signal to noise (Jacquier et al. 2008). This has been validated in animals (Baks et al. 2006; Buecker et al. 2005; Burk et al. 2015; Lardo et al. 2006; Crean et al. 2013) and in humans by CMR (Deux et al. 2013; Habis et al. 2009), electroanatomic mapping (Esposito et al. 2016), and positron emission tomography (Dwivedi et al. 2013). The technique is less robust than LGE imaging, and neither the optimal dose of contrast nor the delay prior to image acquisition is well validated. Anecdotal reports indicate that intracoronary injection of contrast may help visualization of thin rims of scar (Baks et al. 2006; Buecker et al. 2005; Burk et al. 2015; Lardo et al. 2006; Crean et al. 2013), but this seems insufficiently pragmatic to become a mainstream approach.

5.4 Thrombus Imaging

The risks of thrombus formation relate to perturbations of Virchow's triad as much for a coronary anomaly as anywhere else in the cardiovascular system. Thus all three aspects—altered vessel, altered flow, altered coagulability—need to be considered (Lowe 2003). Vascular and flow aspects can be determined by CMR/CT, and knowledge of the patient's coagulation status (medications, pregnancy, smoking, obesity, cancer, etc.) is valuable when interpreting these studies.

Thrombus is only rarely a consideration in large fistulae where flow is brisk. However the circumflex artery to coronary sinus fistula has been associated with myocardial infarction (Dichtl et al. 2005; Al-Turki et al. 2015). In our clinic we have seen one such case arising in a young woman after several weeks of immobilization post orthopedic surgery, presumably reflecting reduced flow due to a much lower basal cardiac output than usual.

The most concerning coronary anomaly where thrombus should be actively excluded is in the setting of Kawasaki disease with giant coronary aneurysms (Patil et al. 2008; El-Segaier and Galal 2013; Ghosh and Agarwala 2011; Mendiola Ramírez et al. 2011; Okura et al. 2013). Aneurysm formation leads to abnormal shear stress and abnormal flow patterns within the ectatic vessel components (Kuramochi et al. 2000). Here there is a real risk of thrombus formation which may lead to distal embolization or acute closure of the vessel (Rizk et al. 2015; Argo et al. 2016; Teo and Paul 2005). Acute Kawasaki disease in children is a diffuse inflammatory state, and care should be taken to exclude thrombi elsewhere within the heart also (Song et al. 2015). Recognition of thrombus is important as aggressive therapy with warfarinization or even thrombolysis needs to be considered (Harada et al. 2013).

Thrombus may be recognized in children by 2D echocardiography as an echogenic mass within the coronary lumen. However in adults cross-sectional imaging is usually required. Both cardiac CT and CMR are believed to be accurate for this purpose, but regardless of which modality is chosen, it is usually necessary to adopt a late enhancement strategy to maximize the low attenuation/signal of the thrombus against the luminal background (Fig. 7). In practical terms this means either using LGE imaging after a standard 10 min delay or alternatively acquiring gated CT images roughly 60–90 s after either a bolus or infusion of iodine (Figs. 8 and 9). CT images acquired in the standard coronary arterial phase (used for routine atherosclerotic CT coronary angiography) may be unreliable as swirling flow within the larger aneurysms often leads to a mixture of opacified and unopacified blood within the aneurysm in the early arterial phase—with the unopacified portion mimicking thrombus.

5.5 Flow Imaging

Flow assessment is generally not a major part of coronary anomaly imaging although on occasion it may be used to help ascertain the point of termination of a fistula when the anatomy is unclear. Flow imaging in order to assess shunt size is important primarily in the setting of coronary fistula. Phase-contrast CMR is used to measure both aortic and pulmonary flow for calculation of shunt ratio—large shunts will often be associated with chamber enlargement, and this in itself is often an adequate reason for surgical repair. Shunt ratio may also be formally estimated by cardiac catheterization, and there is reasonably good correlation between this modality and CMR estimation of shunt (Hundley et al. 1995).

In the specific setting of ALCAPA/ARCAPA, the dilated collateral network between the right and left coronary systems gives rise to a number of echocardiographic features (Courand et al. 2013; Silverman 2015; Yang et al. 2007) including systolic coronary flow predominance which has not been reported in any other coronary anomaly (Ghaderi et al. 2014). Three-dimensional echo may be useful intraoperatively for demonstrating the site of connection of the left coronary artery to the surgeon in real time (Jin et al. 2011).

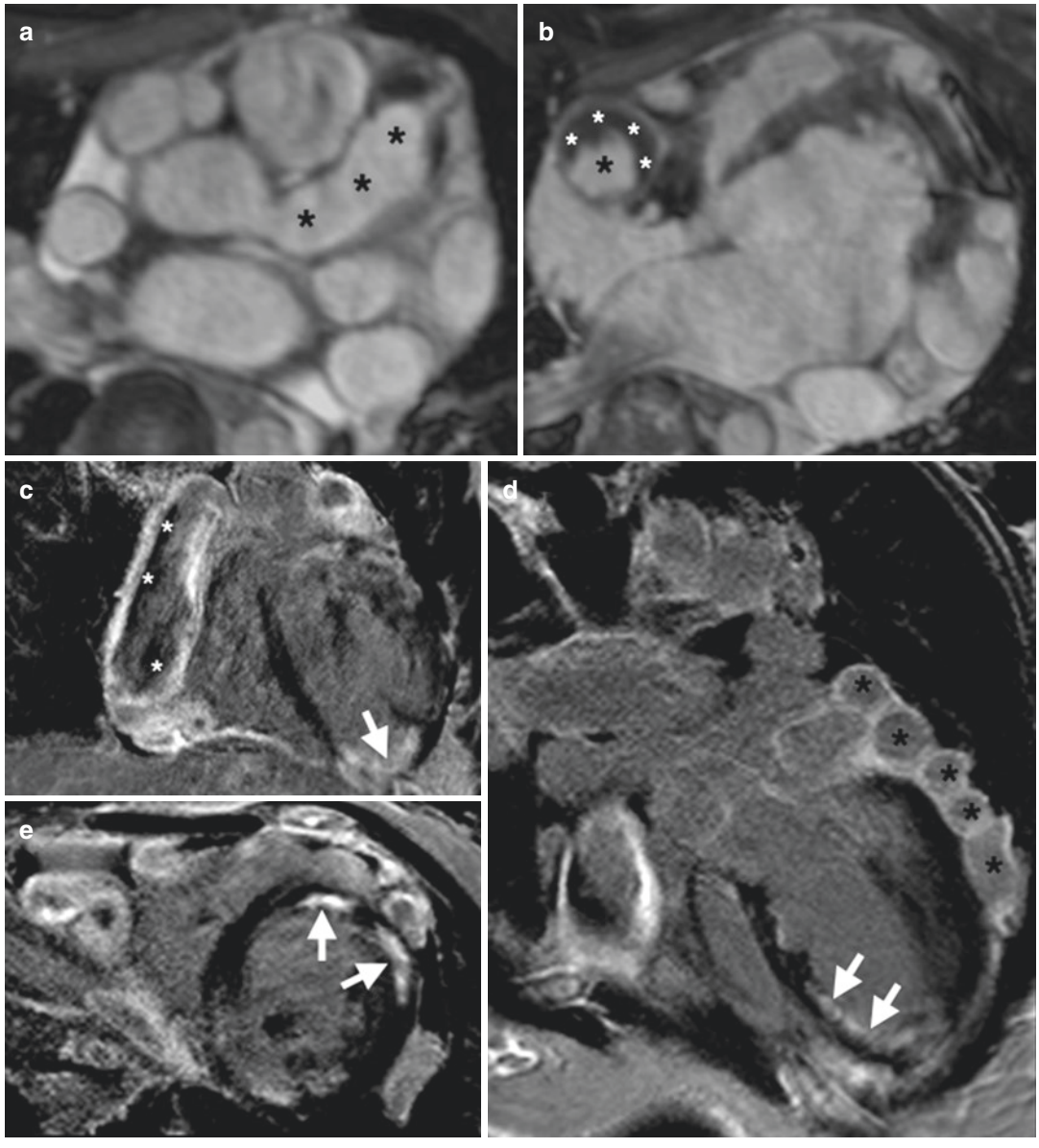

Fig. 7 Noonan syndrome with diffuse severe coronary ectasia, thrombus, and embolic infarction. (**a**) Axial image from whole-heart coronary CMR angiogram. There is severe ectasia of the left main coronary artery (asterisks) up to around 15 mm (normal <5 mm). (**b**) CMR whole-heart angiogram demonstrating a rim of thrombus (white asterisks) in a severely dilated right coronary artery (black asterisk). (**c**) Coronal late gadolinium enhancement image demonstrates low-signal mural thrombus (asterisks) in the RCA which measures up to 20 mm in diameter (normal 2–4 mm). (**d**) Four-chamber LGE image demonstrates subendocardial infarction (arrows) in the mid to distal septum. In addition the bizarrely dilated circumflex artery is seen as a "string of beads" along the left lateral aspect of the ventricle (black asterisks). (**e**) Short axis LGE view demonstrates additional scar (arrows) in the mid-anterior wall

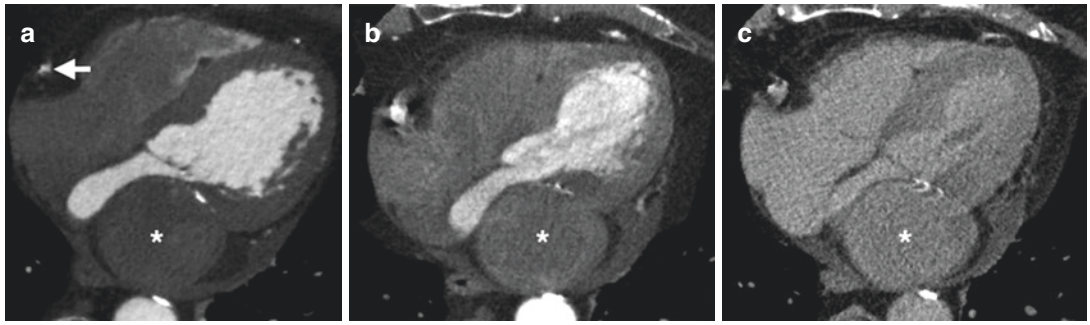

Fig. 8 Cardiac CT in a Kawasaki patient with a giant circumflex artery aneurysm. (**a**) Coronary arterial phase—there is no enhancement of the circumflex artery aneurysm (asterisk) although note that contrast has already enhanced the right coronary artery (arrow). (**b**) Late arterial phase—uneven attenuation is present throughout the aneurysm which could be due to the presence of thrombus. (**c**) Extended venous phase—these images were acquired at 6 min from injection, and this was the first time point at which uniform enhancement was seen throughout the aneurysm. There is no evidence of thrombus (but see Fig. 9)

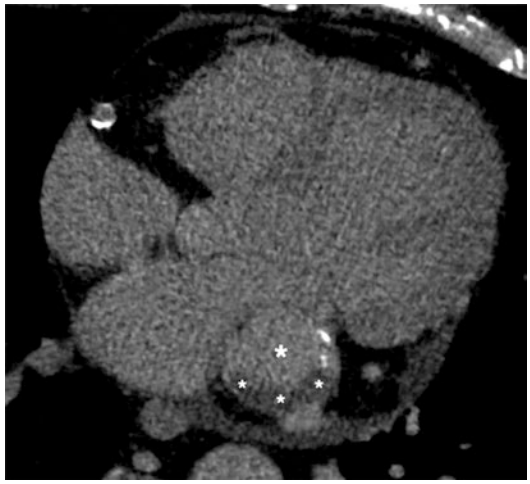

Fig. 9 Cardiac CT demonstrating thrombus in a Kawasaki aneurysm. Same patient as Fig. 8 but at a different place in the circumflex artery. The images have been acquired in a late venous phase at 6 min after contrast, although it is unusual to have to wait this long. The aneurysm (larger asterisk) is uniformly enhanced except for a posterior low attenuation crescentic rim (smaller asterisks) which represents chronic mural thrombus

6 Summary

Coronary imaging is often required for non-atherosclerotic congenital anomalies as well as for inflammatory/vasculitic conditions and in the setting of postoperative coronary repair. No single form of imaging is universally applicable, and complicated cases are likely to require a multimodality approach. Every attempt should be made to demonstrate ischemia in order to justify surgery. On rare occasions, however, there may still be circumstances where surgery can be justified even in the absence of a positive study. Close collaboration between imagers, cardiologists, and cardiac surgeons is vitally important in these cases.

References

Al-Turki MA, Patton D, Crean AM, Horlick E, Dhillon R, Johri AM (2015) Spontaneous thrombosis of a left circumflex artery fistula draining into the coronary sinus. World J Pediatr Congenit Heart Surg 6(4):640–642

Angelini P (2014) Novel imaging of coronary artery anomalies to assess their prevalence, the causes of clinical symptoms, and the risk of sudden cardiac death. Circ Cardiovasc Imaging 7(4):747–754

Angelini P, Flamm SD (2007) Newer concepts for imaging anomalous aortic origin of the coronary arteries in adults. Catheter Cardiovasc Interv 69(7):942–954

Angelini P, Uribe C, Monge J, Tobis JM, Elayda MA, Willerson JT (2015) Origin of the right coronary artery from the opposite sinus of Valsalva in adults: characterization by intravascular ultrasonography at baseline and after stent angioplasty. Catheter Cardiovasc Interv 86(2):199–208

Argo A, Zerbo S, Maresi EG, Rizzo AM, Sortino C, Grassedonio E et al (2016) Utility of post mortem MRI in definition of thrombus in aneurismatic coronary arteries due to incomplete Kawasaki disease in infants. J Forens Radiol Imag 7:17–20

Bajona P, Maselli D, Dore R, Minzioni G (2007) Anomalous origin of the left main artery from the

pulmonary artery: adult presentation with systemic collateral supply and giant right coronary artery aneurysm. J Thorac Cardiovasc Surg 134(2):518–520
Baks T, Cademartiri F, Moelker AD, Weustink AC, van Geuns R-J, Mollet NR et al (2006) Multislice computed tomography and magnetic resonance imaging for the assessment of reperfused acute myocardial infarction. J Am Coll Cardiol 48(1):144–152
Bartoloni G, Giorlandino A, Calafiore AM, Caltabiano R, Cosentino S, Algieri G et al (2012) Multiple coronary artery-left ventricular fistulas causing sudden death in a young woman. Hum Pathol 43(9):1520–1523
Basha KMS, Vaijyanath P, Thomas S (2016) Adult type ALCAPA–A rare presentation. J Indian Colleg Cardiol
Basso C, Maron BJ, Corrado D, Thiene G (2000) Clinical profile of congenital coronary artery anomalies with origin from the wrong aortic sinus leading to sudden death in young competitive athletes. J Am Coll Cardiol 35(6):1493–1501
Bravo-Valenzuela NJM, Silva GRN (2015) Aneurysm of the left coronary artery in postoperative bland-white-garland syndrome. Case Rep Cardiol 2015:568014
Brothers JA, McBride MG, Seliem MA, Marino BS, Tomlinson RS, Pampaloni MH et al (2007) Evaluation of myocardial ischemia after surgical repair of anomalous aortic origin of a coronary artery in a series of pediatric patients. J Am Coll Cardiol 50(21):2078–2082
Buecker A, Katoh M, Krombach GA, Spuentrup E, Bruners P, Günther RW et al (2005) A feasibility study of contrast enhancement of acute myocardial infarction in multislice computed tomography: comparison with magnetic resonance imaging and gross morphology in pigs. Investig Radiol 40(11):700–704
Burchill L, Huang J, Tretter J, Khan A, Crean A, Veldtman G et al (2017) Noninvasive imaging in adult congenital heart disease. Circ Res 120:995–1014
Burk LM, Wang K-H, Wait JM, Kang E, Willis M, Lu J et al (2015) Delayed contrast enhancement imaging of a murine model for ischemia reperfusion with carbon nanotube micro-CT. PLoS One 10(1):e0115607
Cheitlin MD, De Castro CM, McAllister HA (1974) Sudden death as a complication of anomalous left coronary origin from the anterior sinus of Valsalva, a not-so-minor congenital anomaly. Circulation 50(4):780–787
Courand P-Y, Bozio A, Ninet J, Henaine R, Veyrier M, Bakloul M et al (2013) Focus on echocardiographic and Doppler analysis of coronary artery abnormal origin from the pulmonary trunk with mild myocardial dysfunction. Echocardiography 30(7):829–836
Crean AM, Kilcullen N, Younger JF (2008) Arrhythmic acute coronary syndrome and anomalous left main stem artery: culprit or innocent bystander. Acute Card Care 10(1):60–61
Crean AM, Spears DA, Suszko AM, Chauhan VS (2013) High-resolution 3D scar imaging using a novel late iodine enhancement multidetector CT protocol to guide ventricular tachycardia catheter ablation. J Cardiovasc Electrophysiol 24(6):708–710
Crean AM, Deva DP, Wald R (2016) Emerging role of stress perfusion cardiovascular magnetic resonance in the patient with congenital heart disease. In: da Cruz EM, Ivy D, Hraska V, Jaggers J (eds) Pediatric and congenital cardiology, cardiac surgery and intensive care. Springer, London, pp 1–22
Deux J-F, Potet J, Lim P, Teiger E, Mayer J, Bensaid A et al (2013) Is multidetector computed tomography a suitable alternative to MR imaging for the assessment of myocardial necrosis after alcohol septal ablation? Int J Cardiol 164(3):306–311
Deva DP, Torres FS, Wald RM, Roche SL, Jimenez-Juan L, Oechslin EN et al (2014) The value of stress perfusion cardiovascular magnetic resonance imaging for patients referred from the adult congenital heart disease clinic: 5-year experience at the Toronto General Hospital. Cardiol Young 24(5):822–830
Dichtl W, Waldenberger P, Pachinger O, Müller S (2005) An uncommon coronary artery fistula causing survived sudden cardiac death in a young woman. Int J Card Imaging 21(4):387–390
Dwivedi G, Al-Shehri H, deKemp RA, Ali I, Alghamdi AA, Klein R et al (2013) Scar imaging using multislice computed tomography versus metabolic imaging by F-18 FDG positron emission tomography: a pilot study. Int J Cardiol 168(2):739–745
Eid AH, Itani Z, Al-Tannir M, Sayegh S, Samaha A (2009) Primary congenital anomalies of the coronary arteries and relation to atherosclerosis: an angiographic study in Lebanon. J Cardiothorac Surg 4:58
El-Segaier M, Galal M (2013) Intracoronary thrombus in an infant with Kawasaki disease and giant coronary aneurysm. Acta Paediatr 102(5):e227–e228
Erol C, Seker M (2011) Coronary artery anomalies: the prevalence of origination, course, and termination anomalies of coronary arteries detected by 64-detector computed tomography coronary angiography. J Comput Assist Tomogr 35(5):618–624
Esposito A, Palmisano A, Antunes S, Maccabelli G, Colantoni C, Rancoita PMV et al (2016) Cardiac CT with delayed enhancement in the characterization of ventricular tachycardia structural substrate: relationship between CT-segmented scar and electro-anatomic mapping. JACC Cardiovasc Imaging 9(7):822–832
Fierens C, Budts W, Denef B, Van De Werf F (2000) A 72 year old woman with ALCAPA. Heart 83(1):E2
Frapier JM, Leclercq F, Bodino M, Chaptal PA (1999) Malignant ventricular arrhythmias revealing anomalous origin of the left coronary artery from the pulmonary artery in two adults. Eur J Cardiothorac Surg 15(4):539–541
Fujimoto S, Kondo T, Orihara T, Sugiyama J, Kondo M, Kodama T et al (2011) Prevalence of anomalous origin of coronary artery detected by multi-detector computed tomography at one center. J Cardiol 57(1):69–76
Garg N, Tewari S, Kapoor A, Gupta DK, Sinha N (2000) Primary congenital anomalies of the coronary arteries: a coronary: arteriographic study. Int J Cardiol 74(1):39–46
Ghaderi F, Gholoobi A, Moeinipour A (2014) Unique echocardiographic markers of anomalous origin of the left coronary artery from the pulmonary

artery (ALCAPA) in the adult. Echocardiography 31(1):E13–E15
Ghosh A, Agarwala BN (2011) Kawasaki disease: giant aneurysm with a large thrombus of the left coronary artery. Clin Pract 1(2):e23
Gillebert C, Van Hoof R, Van de Werf F, Piessens J, De Geest H (1986) Coronary artery fistulas in an adult population. Eur Heart J 7(5):437–443
Graidis C, Dimitriadis D, Karasavvidis V, Dimitriadis G, Argyropoulou E, Economou F et al (2015) Prevalence and characteristics of coronary artery anomalies in an adult population undergoing multidetector-row computed tomography for the evaluation of coronary artery disease. BMC Cardiovasc Disord 15:112
Gräni C, Buechel RR, Kaufmann PA, Kwong RY (2017) Multimodality imaging in individuals with anomalous coronary arteries. JACC Cardiovasc Imaging 10(4):471–481
Greenwood JP, Maredia N, Younger JF, Brown JM, Nixon J, Everett CC et al (2012) Cardiovascular magnetic resonance and single-photon emission computed tomography for diagnosis of coronary heart disease (CE-MARC): a prospective trial. Lancet 379(9814):453–460
Greenwood JP, Herzog BA, Brown JM, Everett CC, Nixon J, Bijsterveld P et al (2016) Prognostic value of cardiovascular magnetic resonance and single-photon emission computed tomography in suspected coronary heart disease: long-term follow-up of a prospective, diagnostic accuracy cohort study. Ann Intern Med 165(1):1–9
Habis M, Capderou A, Sigal-Cinqualbre A, Ghostine S, Rahal S, Riou JY et al (2009) Comparison of delayed enhancement patterns on multislice computed tomography immediately after coronary angiography and cardiac magnetic resonance imaging in acute myocardial infarction. Heart 95(8):624–629
Harada M, Akimoto K, Ogawa S, Kato H, Nakamura Y, Hamaoka K et al (2013) National Japanese survey of thrombolytic therapy selection for coronary aneurysm: intracoronary thrombolysis or intravenous coronary thrombolysis in patients with Kawasaki disease. Pediatr Int 55(6):690–695
Hofmeyr L, Moolman J, Brice E, Weich H (2009) An unusual presentation of an anomalous left coronary artery arising from the pulmonary artery (ALCAPA) in an adult: anterior papillary muscle rupture causing severe mitral regurgitation. Echocardiography 26(4):474–477
Hundley WG, Li HF, Lange RA, Pfeifer DP, Meshack BM, Willard JE et al (1995) Assessment of left-to-right intracardiac shunting by velocity-encoded, phase-difference magnetic resonance imaging. A comparison with oximetric and indicator dilution techniques. Circulation 91(12):2955–2960
Jacquier A, Revel D, Saeed M (2008) MDCT of the myocardium: a new contribution to ischemic heart disease. Acad Radiol 15(4):477–487
Jin YD, Hsiung MC, Tsai SK, Chang C-Y, Wei J, Ou C et al (2011) Successful intraoperative identification of an anomalous origin of the left coronary artery from the pulmonary artery using real time three-dimensional transesophageal echocardiography. Echocardiography 28(7):E149–E151
Kang WC, Chung W-J, Choi CH, Park KY, Jeong MJ, Ahn TH et al (2007) A rare case of anomalous left coronary artery from the pulmonary artery (ALCAPA) presenting congestive heart failure in an adult. Int J Cardiol 115(2):e63–e67
Keir M, Wald RM, Roche SL, Oechslin EN, Horlick E, Osten MD et al (2015) Does a dedicated subspecialty ACHD coronary clinic result in greater consistency in approach and reduced loss to follow-up? An evaluation of the first 3years of the Toronto congenital coronary Clinic for Adults. Prog Pediatr Cardiol 39(2):145–150
Keir M, Spears D, Caldarone C, Crean AM (2017) Proving the innocence of a “malignant” coronary artery: calling dobutamine stress CT for the defence. J Cardiovasc Comput Tomogr 11(1):68–69
Kragel AH, Roberts WC (1988) Anomalous origin of either the right or left main coronary artery from the aorta with subsequent coursing between aorta and pulmonary trunk: analysis of 32 necropsy cases. Am J Cardiol 62(10 Pt 1):771–777
Kramer PH, Goldstein JA, Herkens RJ, Lipton MJ, Brundage BH (1984) Imaging of acute myocardial infarction in man with contrast-enhanced computed transmission tomography. Am Heart J 108(6):1514–1523
Krexi L, Sheppard MN (2013) Anomalous origin of the left coronary artery from the pulmonary artery (ALCAPA), a forgotten congenital cause of sudden death in the adult. Cardiovasc Pathol 22(4):294–297
Kristensen T, Kofoed KF, Helqvist S, Helvind M, Søndergaard L (2008) Anomalous origin of the left coronary artery from the pulmonary artery (ALCAPA) presenting with ventricular fibrillation in an adult: a case report. J Cardiothorac Surg 3:33
Kuramochi Y, Ohkubo T, Takechi N, Fukumi D, Uchikoba Y, Ogawa S (2000) Hemodynamic factors of thrombus formation in coronary aneurysms associated with Kawasaki disease. Pediatr Int 42(5):470–475
Lardo AC, Cordeiro MAS, Silva C, Amado LC, George RT, Saliaris AP et al (2006) Contrast-enhanced multidetector computed tomography viability imaging after myocardial infarction: characterization of myocyte death, microvascular obstruction, and chronic scar. Circulation 113(3):394–404
Lau G (1995) Sudden death arising from a congenital coronary artery fistula. Forensic Sci Int 73(2):125–130
Lee M-L, Chen M (2009) Diagnosis and management of congenital coronary arteriovenous fistula in the pediatric patients presenting congestive heart failure and myocardial ischemia. Yonsei Med J 50(1):95–104
Lee SE, CW Y, Park K, Park KW, Suh J-W, Cho Y-S et al (2016) Physiological and clinical relevance of anomalous right coronary artery originating from left sinus of Valsalva in adults. Heart 102(2):114–119
Liu Y, Miller BW (2012) ALCAPA presents in an adult with exercise intolerance but preserved cardiac function. Case Rep Cardiol 2012:471759

Lopes R, Almeida PB, Amorim MJ, Magalhães D, Silva JC, Pinho P et al (2011 Aug) Anomalous origin of the left coronary artery from the pulmonary artery in an asymptomatic adult. Congenit Heart Dis 6(4):366–369

Lowe GDO (2003) Virchow's triad revisited: abnormal flow. Pathophysiol Haemost Thromb 33(5–6):455–457

Lozano I, Batalla A, Rubin J, Avanzas P, Martin M, Moris C (2008) Sudden death in a patient with multiple left anterior descending coronary artery fistulas to the left ventricle. Int J Cardiol 125(3):e37–e39

de Meester de Ravenstein C, Bouzin C, Lazam S, Boulif J, Amzulescu M, Melchior J et al (2015) Histological validation of measurement of diffuse interstitial myocardial fibrosis by myocardial extravascular volume fraction from modified look-locker imaging (MOLLI) T1 mapping at 3 T. J Cardiovasc Magn Reson 17:48

Mendiola Ramírez K, Osorio Díaz JO, Maldonado Velázquez Mdel R, Faugier Fuentes E (2011) Kawasaki's disease in remission with cardiac involvement: intrasacular thrombus in a giant aneurism of both coronary arteries. Case report. Reumatol Clin 7(5):329–332

Nakahira A, Sasaki Y, Hirai H, Fukui T, Motoki M, Takahashi Y et al (2007) Rupture of aneurysmal circumflex coronary artery into the left atrium after ligation of its arteriovenous fistula. Circ J 71(12):1996–1998

Namgung J, Kim JA (2014) The prevalence of coronary anomalies in a single center of Korea: origination, course, and termination anomalies of aberrant coronary arteries detected by ECG-gated cardiac MDCT. BMC Cardiovasc Disord 14:48

Nony P, Beaune J, Champsaur G, Bozio A, Age C, Fontana J et al (1992) Anomalous origin of left coronary artery from the pulmonary artery: evolution of left ventricular function and perfusion after surgery in a 44-year-old man. Clin Cardiol 15(6):466–468

Okura N, Okuda T, Shiotani S, Kohno M, Hayakawa H, Suzuki A et al (2013) Sudden death as a late sequel of Kawasaki disease: postmortem CT demonstration of coronary artery aneurysm. Forensic Sci Int 225(1–3):85–88

Pachon R, Bravo C, Niemiera M (2015) Sudden cardiac death as a presentation of anomalous origin of the left coronary artery from pulmonary artery in a young adult. Eur Heart J Acute Cardiovasc Care 4(6):589–590

Patil S, Shirodkar S, Pinto R, Dalvi B (2008) Giant coronary artery aneurysm with a thrombus secondary to Kawasaki disease. Ann Pediatr Cardiol 1(1):59–61

Peña E, Nguyen ET, Merchant N, Dennie C (2009) ALCAPA syndrome: not just a pediatric disease. Radiographics 29(2):553–565

Quah JX, Hofmeyr L, Haqqani H, Clarke A, Rahman A, Pohlner P et al (2014) The management of the older adult patient with anomalous left coronary artery from the pulmonary artery syndrome: a presentation of two cases and review of the literature. Congenit Heart Dis 9(6):E185–E194

Raghuram AR, Krishnan R, Kumar S, Balamurugan K, Anand ND (2004) Anomalous left coronary artery from pulmonary artery (ALCAPA) in an adult. Indian J Thorac Cardiovasc Surg 20(4):213–215

Rajs J, Brodin LA, Hertzfeld I, Larsen FF (2001) Death related to coronary artery fistula after rupture of an aneurysm to the coronary sinus. Am J Forensic Med Pathol 22(1):58–61

Rana O, Swallow R, Senior R, Greaves K (2009) Detection of myocardial ischaemia caused by coronary artery-left ventricular fistulae using myocardial contrast echocardiography. Eur J Echocardiogr 10(1):175–177

Ripley DP, Gosling OE, Harries S, Spurrell PA, Bellenger NG (2014) Multimodality imaging in bland-White-Garland syndrome in an adult with a left dominant coronary artery system. Congenit Heart Dis 9(4):E110–E112

Rizk SRY, El Said G, Daniels LB, Burns JC, El Said H, Sorour KA et al (2015) Acute myocardial ischemia in adults secondary to missed Kawasaki disease in childhood. Am J Cardiol 115(4):423–427

Roberts WC, Siegel RJ, Zipes DP (1982) Origin of the right coronary artery from the left sinus of valsalva and its functional consequences: analysis of 10 necropsy patients. Am J Cardiol 49(4):863–868

Sadanandan R, Thankappan A, Jacob B, Kuriakose KM (2012) Anomalous left coronary artery from pulmonary artery (ALCAPA) repair and mitral valve replacement with bioprosthetic valve with in a 62 year old lady. Indian J Thorac Cardiovasc Surg 28(2):146–147

Safaa AM, LL D, Batra R, Essack N (2013) A rare case of adult type ALCAPA syndrome: presentation, diagnosis and management. Heart Lung Circ 22(6):444–446

Said SA (2016) Characteristics of congenital coronary artery fistulas complicated with infective endocarditis: analysis of 25 reported cases. Congenit Heart Dis 11(6):756–765

Said SAM, Schroeder-Tanka JM, Mulder BJM (2008) Female gender and the risk of rupture of congenital aneurysmal fistula in adults. Congenit Heart Dis 3(1):63–68

Sajjadieh Khajouei A, Samie-Nasab M, Behjati M, Biederman RW (2016) Cardiac computed tomography of an asymptomatic 48-year-old woman with ALCAPA syndrome. Echocardiography 33(12):1923–1925

Secinaro A, Ntsinjana H, Tann O, Schuler PK, Muthurangu V, Hughes M et al (2011) Cardiovascular magnetic resonance findings in repaired anomalous left coronary artery to pulmonary artery connection (ALCAPA). J Cardiovasc Magn Reson 13:27

Seguchi M, Nakanishi T, Nakazawa M, Doi S, Momma K, Takao A et al (1990) Myocardial perfusion after aortic implantation for anomalous origin of the left coronary artery from the pulmonary artery. Eur Heart J 11(3):213–218

Shabestari AA, Akhlaghpoor S, Tayebivaljozi R, Fattahi Masrour F (2012) Prevalence of congenital coronary artery anomalies and variants in 2697 consecutive patients using 64-detector row coronary CT angiography. Iran J Radiol 9(3):111–121

Sharples L, Hughes V, Crean A, Dyer M, Buxton M, Goldsmith K et al (2007) Cost-effectiveness of functional cardiac testing in the diagnosis and management of coronary artery disease: a randomised controlled trial. The CECaT Trial Health Technol Assess 11(49):iii–iiv, ix

Shen Q, Yao Q, Hu X (2016) Anomalous origin of the left coronary artery from the pulmonary artery in children: diagnostic use of multidetector computed tomography. Pediatr Radiol 46(10):1392–1398

Silverman NH (2015) Echocardiographic presentation of anomalous origin of the left coronary artery from the pulmonary artery. Cardiol Young 25(8):1512–1523

Sivri N, Aktoz M, Yalta K, Ozcelik F, Altun AA (2012) Retrospective study of angiographic ally determined anomalous coronary arteries in 12,844 subjects in Thrace region of Turkey. Hippokratia 16(3):246–249

Sohrabi B, Habibzadeh A, Abbasov E (2012) The incidence and pattern of coronary artery anomalies in the north-west of iran: a coronary arteriographic study. Korean Circ J 42(11):753–760

Song G, Ren W, Liu Z, Wu D (2015) Incomplete Kawasaki disease with coronary artery aneurysm and coronary sinus thrombus. Pediatr Cardiol 36(5):1097–1099

Su C-S, Tsai I-C, Lin W-W, Lin F-Y, Ting C-T, Wang K-Y (2010) Usefulness of multidetector-row computed tomography in diagnosis of anomalous origin of left coronary artery arising from the pulmonary artery. J Chin Med Assoc 73(9):492–495

Teo CHY, Paul G (2005) An uncommon cause of death in an older child part 1. Pathology 37(2):172–173

Thom H, West NEJ, Hughes V, Dyer M, Buxton M, Sharples LD et al (2014) Cost-effectiveness of initial stress cardiovascular MR, stress SPECT or stress echocardiography as a gate-keeper test, compared with upfront invasive coronary angiography in the investigation and management of patients with stable chest pain: mid-term outcomes from the CECaT randomised controlled trial. BMJ Open 4(2):e003419

Thompson WR (2015) Stress echocardiography in paediatrics: implications for the evaluation of anomalous aortic origin of the coronary arteries. Cardiol Young 25(8):1524–1530

Tobler D, Motwani M, Wald RM, Roche SL, Verocai F, Iwanochko RM et al (2014) Evaluation of a comprehensive cardiovascular magnetic resonance protocol in young adults late after the arterial switch operation for d-transposition of the great arteries. J Cardiovasc Magn Reson 16:98

Tongut A, Özyedek Z, Çerezci İ, Erentürk S, Hatemi AC (2016) Prevalence of congenital coronary artery anomalies as shown by multi-slice computed tomography coronary angiography: a single-centre study from Turkey. J Int Med Res 44(6):1492–1505

Toumpourleka M, Belitsis G, Alonso R, Rubens M, Moat N, Gatzoulis M (2015) Late presentation and surgical repair of ALCAPA. Int J Cardiol 186:207–209

Wagner A, Mahrholdt H, Holly TA, Elliott MD, Regenfus M, Parker M et al (2003) Contrast-enhanced MRI and routine single photon emission computed tomography (SPECT) perfusion imaging for detection of subendocardial myocardial infarcts: an imaging study. Lancet 361(9355):374–379

Xu H, Zhu Y, Zhu X, Tang L, Xu Y (2012) Anomalous coronary arteries: depiction at dual-source computed tomographic coronary angiography. J Thorac Cardiovasc Surg 143(6):1286–1291

Yamanaka O, Hobbs RE (1990) Coronary artery anomalies in 126,595 patients undergoing coronary arteriography. Catheter Cardiovasc Diagn 21(1):28–40

Yang Y-L, Nanda NC, Wang X-F, Xie M-X, Lu Q, He L et al (2007) Echocardiographic diagnosis of anomalous origin of the left coronary artery from the pulmonary artery. Echocardiography 24(4):405–411

Yildiz A, Okcun B, Peker T, Arslan C, Olcay A, Bulent Vatan M (2010) Prevalence of coronary artery anomalies in 12,457 adult patients who underwent coronary angiography. Clin Cardiol 33(12):E60–E64

Yuksel S, Meric M, Soylu K, Gulel O, Zengin H, Demircan S et al (2013) The primary anomalies of coronary artery origin and course: a coronary angiographic analysis of 16,573 patients. Exp Clin Cardiol 18(2):121–123